



JULY 1984

ENVIRONMENTAL SCIENCE & TECHNOLOGY

ES&T



FORMALDEHYDE:
Assessing the risk
Page 216A

INTRODUCING
NEW STATE-OF-THE-ART INSTRUMENTATION:
"The SEASTAR IN SITU WATER SAMPLER"



Uses microprocessor control and extraction columns to make the most significant advance in water sampling technology since the Nansen bottle.

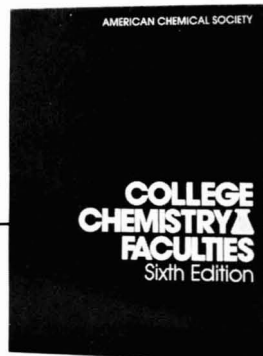
FEATURES:

- Capable of large volume ultra-trace water sampling
- Equally useful for organic and inorganic applications
- Utilizes a variety of types of extraction columns, each with guaranteed blank levels
- Microprocessor-controlled for unprecedented flexibility of sampling, and precise control of flow rate and sample volume
- Can be moored (for days or weeks) or triggered with a messenger from a hydrowire
- Totally self-contained, powered by D-cell batteries

BUILT WITH PRIDE BY
 **SEASTAR INSTRUMENTS LTD**

2045 MILLS ROAD, SIDNEY, B.C. CANADA V8L 3S1 (604) 656-0891 TELEX 049-7526
 CIRCLE 2 ON READER SERVICE CARD

The most complete listing of college chemistry faculties in the U.S. and Canada



College Chemistry Faculties

Sixth Edition

Covering 2,400 two-year and four-year colleges and universities in the U.S. and Canada, COLLEGE CHEMISTRY FACULTIES lists the current affiliations and major teaching fields of over 18,000 faculty members.

A multi-purpose reference, COLLEGE CHEMISTRY FACULTIES is an important tool for researchers, recruiters, industrial chemistry labs, students and teachers as well as college and high school counselors and libraries. It provides:

1. State-by-state listings of institutions showing degrees offered, staff members and their major fields, department address and phone number.
2. Index of faculty members' names.
3. Index of institutions.


Soft cover, 8½" × 11". 204 pages...\$34.00

Call Toll Free
1-800-424-6747

(for credit card orders),

Or mail your order to:
 American Chemical Society
 Distribution Office
 1155 Sixteenth Street, N.W.
 Washington, DC 20036

FREE! 1984 Books & Journals Catalog from the American Chemical Society



- More than 400 books, including 39 new ones listed for the first time
- All ACS periodical publications
- Royal Society of Chemistry books

Use the coupon below or call the ACS Sales Office toll free 800-424-6747 to request your free 1984 catalog today.

Rush me a free copy of the **1984 American Chemical Society Books and Journals Catalog.**

Name _____
 Address _____
 City _____ State _____ Zip _____

Mail coupon to: **Sales Office**
 American Chemical Society
 1155 Sixteenth Street, NW
 Washington, DC 20036

Editor: Russell F. Christman
Associate Editor: John H. Seinfeld
Associate Editor: Philip C. Singer

ADVISORY BOARD:

Julian B. Andelman, Kenneth L. Demerjian,
Steven Eisenreich, William H. Glaze, Glenn R.
Hilst, Michael R. Hoffmann, Lawrence H.
Keith, Donald Mackay, Leonard Newman,
Eugene B. Welch

WASHINGTON EDITORIAL STAFF
Managing Editor: Stanton S. Miller
Associate Editor: Julian Josephson
Associate Editor: Bette Hileman

MANUSCRIPT REVIEWING
Manager: Janice L. Fleming
Associate Editor: Monica Creamer
Assistant Editor: Yvonne D. Curry
Editorial Assistant: Mary Ellen Provencher

MANUSCRIPT EDITING
Assistant Manager: Mary E. Scanlan
Assistant Editor: Ruth A. Linville

GRAPHICS AND PRODUCTION
Production Manager: Leroy L. Corcoran
Art Director: Alan Kahan
Staff Artist: Julie Katz
Production Editor: Gail Mortenson

BOOKS AND JOURNALS DIVISION
Director: D. H. Michael Bowen

Head, Journals Department: Charles R. Bertsch
Head, Production Department: Elmer M. Pusey
Head, Research and Development Department:
Lorin R. Garson

ADVERTISING MANAGEMENT
Centcom, Ltd.

For officers and advertisers, see page 226A.

Please send *research* manuscripts to Manuscript Reviewing, *feature* manuscripts to Managing Editor. For author's guide and editorial policy, see the February 1984 issue, page 69A, or write Janice L. Fleming, Manuscript Reviewing Office, *ES&T*. A sample copyright transfer form, which may be copied, appears on the inside back cover of the February 1984 issue.

Environmental Science & Technology
© Copyright 1984 by the American Chemical Society

Environmental Science & Technology ES&T (ISSN 0013-936X) is published monthly by the American Chemical Society at 1155 16th Street, N.W., Washington, D.C. 20036; 202-872-4600, TDD 202-872-8733. Second-class postage paid at Washington, D.C. and at additional mailing offices. POSTMASTER: Send address changes to Membership & Subscription Services, PO Box 3337, Columbus, OH, 43210.

SUBSCRIPTION PRICES 1984: Members, \$22 per year; nonmembers (for personal use), \$25 per year; institutions, \$121 per year. Foreign postage, \$8 additional per year/Air freight add \$33; multiple year rates available on request. Single issues \$10.50 for current year; \$12.50 for prior years. Back volumes \$146. Rates above do not apply to nonmember subscribers in Japan, who must enter subscription orders with Maruzen Company Ltd., 3-10 Nihonbashi 2-chome, Chuo-ku, Tokyo 103, Japan. Tel: (03) 272-7211.

COPYRIGHT PERMISSION: An individual may make a single reprographic copy of an article in this publication for personal use. Reprographic copying beyond that permitted by Section 107 or 108 of the U.S. Copyright Law is allowed, provided that the appropriate per-copy fee is paid through the Copyright Clearance Center, Inc., 21 Congress St. Salem, Mass. 01970. For reprint permission, write Copyright Administrator, Books & Journals Division, ACS, 1155 16th St., N.W., Washington, D.C. 20036.

REGISTERED NAMES AND TRADEMARKS, etc., used in this publication, even without specific indication thereof, are not to be considered unprotected by law.

SUBSCRIPTION SERVICE: Orders for new subscriptions, single issues, back volumes, and microfiche and microform editions should be sent with payment to Office of the Treasurer, Financial Operations, ACS, 1155 16th St., N.W., Washington, D.C. 20036. Phone orders may be placed, using Visa, Master Card, or American Express, by calling toll free (800) 424-6747 from anywhere in the continental U.S. Changes of address, subscription renewals, claims for missing issues, and inquiries concerning records and accounts should be directed to Manager, Membership and Subscription Services, ACS, P.O. Box 3337, Columbus, Ohio 43210. Changes of address should allow six weeks and be accompanied by old and new addresses and a recent mailing label. Claims for missing issues will not be allowed if loss was due to insufficient notice of change of address, if claim is dated more than 90 days after the issue date for North American subscribers or more than one year for foreign subscribers, or if the reason given is "missing from files."

The American Chemical Society assumes no responsibility for statements and opinions advanced by contributors to the publication. Views expressed in editorials are those of the author and do not necessarily represent an official position of the society.

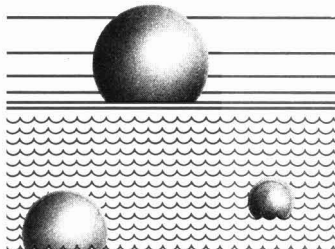
ES&T CONTENTS

Volume 18, Number 7, July 1984

FEATURE

207A

Evaluating chemical fate models. One approach involves heterogeneous spatial distribution. Donald Mackay and Sally Paterson, University of Toronto, Ontario, Canada



207A

REGULATORY FOCUS

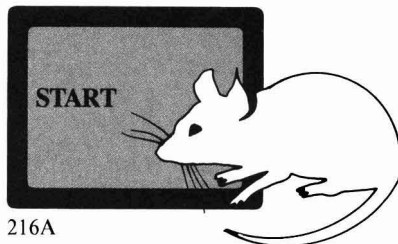
215A

Biomonitoring. Richard Dowd explains the use of this technique in developing regulations.

OUTLOOK

216A

Formaldehyde. Risk assessments are clouded by conflicting scientific data.



216A

222A

Hazardous waste research. The emphasis will most likely be on thermal destruction.

DEPARTMENTS

203A Editorial

204A Currents

224A Products

225A Literature

226A Classified

226A Consulting Services



204A

ESTHAG 18(7) 201A-226A
491-570 (1984)
ISSN 0013-936X

Credits: 223A, *ES&T's* Julian Josephson
Cover: Photo by Chris Kuhn © 1984 American Chemical Society

RESEARCH

491

Copper and cadmium uptake by estuarine sedimentary phases. Robert J. Davies-Colley, Peter O. Nelson,* and Kenneth J. Williamson

In this study, the behavior of copper and cadmium is predicted on the basis of adsorption experiments used to calibrate a simple distribution model.

500

On-road emission rates of carbon monoxide, nitrogen oxides, and gaseous hydrocarbons. Robert A. Gorse, Jr.

These on-road results are compared with predictions from the EPA computer model MOBILE 2 and with other vehicle emissions studies.

507

Nonsingle-valued adsorption-desorption of bromacil and diquat by freshwater sediments. Dennis L. Corwin* and Walter J. Farmer

Simple multiple regression models are developed from an adsorption-desorption study of two chemically dissimilar herbicides.

514

Persistence of pesticides in surface soil and relation to sublimation. Charles A. Sleicher* and John Hopcraft

A model and field tests with DDT support direct sublimation as a principal mechanism of disappearance of pesticides from soil surfaces.

518

Henry's law constants for the trihalomethanes: Effects of water composition and temperature. Brenton C. Nicholson,* Brian P. Maguire, and Donald B. Bursill

Henry's law constants for THMs in potable waters are independent of water composition and approximately double for each 10 °C rise in temperature.

521

Optimal sampling geometry for hazardous waste sites. David F. Parkhurst

This work demonstrates that triangular grids are preferable to square grids when searching for toxic materials buried in abandoned dumps.

523

Mutagenic changes in dilute wood smoke as it ages and reacts with ozone and nitrogen dioxide: An outdoor chamber study. Richard M. Kamens,* Glenn D. Rives, Jean M. Perry, Douglas A. Bell, R. Flynn Paylor, Jr., Randall G. Goodman, and Larry D. Claxton

Reacting dilute wood smoke in outdoor Teflon film chambers with sub-ppm levels of O₃ + NO₂ resulted in large mutagenic increases.

530

Effect of censoring trace-level water-quality data on trend detection capability. Robert J. Gilliom,* Robert M. Hirsch, and Edward J. Gilroy

Not reporting trace-level measurements that are below laboratory detection limits may eliminate valuable information even when these data are highly unreliable.

535

Determination of subnanogram per liter levels of earthy-musty odorants in water by the salted closed-loop stripping method. Cordelia J. Hwang*, Stuart W. Krasner, Michael J. McGuire, Margaret S. Moylan, and Melissa S. Dale

This method provides improved sensitivity and reduced stripping time in determining geosmin, 2-methylisoborneol, and other odorants in water.

540

Organic Photochemistry. 19. Quantum yields for *O*,*O*-diethyl *O*-(3,5,6-trichloro-2-pyridinyl) phosphorothioate (chlorpyrifos) and 3,5,6-trichloro-2-pyridinol in dilute aqueous solutions and their environmental phototransformation rates. Wendell L. Dilling,* Lori C. Lickly, Tim D. Lickly, Patrick G. Murphy, and Richard L. McKellar

The calculated quantum yields and the measured absorption spectra are used to estimate the photochemical half-lives of the studied compounds.

544

Comparison of micron and submicron fly ash particles using scanning electron microscopy and X-ray elemental analysis. N. Kaufherr and David Lichtman*

Both the micron and submicron particles studied were found to be spherical and to contain Si, Al, K, Fe, Ti, and S as main components.

548

Analysis of coal fly ash properties of importance to sulfur dioxide reactivity potential. Gregory D. Reed,* Wayne T. Davis, and Randal E. Pudelek

The SO₂ removal efficiency of a fly ash slurry in a spray dryer-baghouse system is a function of surface area and slurry alkalinity.

■ 552

Mercury in recent and century-old deep-sea fish. Richard T. Barber,* Patrick J. Whaling, and Daniel M. Cohen

Analysis of the length vs. concentration relationship indicates there has not been an increase in mercury concentration in deep-sea fish during the past century.

556

Effects of temperature and pressure on the photochemical reactivity of a representative aviation fuel. William P. L. Carter,* Roger Atkinson, and Arthur M. Winer

The data address the photochemical reactivity of the fuel relative to ozone formation and NO oxidation rates.

561

Avoidance responses of estuarine fish exposed to heated-dechlorinated power plant effluents. Lenwood W. Hall, Jr.,* Dennis T. Burton, William C. Graves, and Stuart L. Margrey

Striped bass and Atlantic menhaden showed little avoidance to dechlorinated estuarine water (no ΔT) at acclimation temperatures ranging from 15 to 30 °C.

NOTES

566

Decay rates of nitrogen oxides in a typical Japanese living room. Shin'ichi Yamanaka

The decay process of NO₂, which includes homogeneous and heterogeneous processes as well as air exchange, follows approximately first-order kinetics.

* To whom correspondence should be addressed.

■ This article contains supplementary material in microform. See ordering instructions at end of paper.

Editorial policy changes

The meanings of the terms originality and significance have been under discussion by the editors, staff, and Advisory Board of *ES&T* for the past year. From the perspective of those responsible for the management of a current research journal, the criteria by which originality and significance are judged change as knowledge advances. The changes we are adopting in *ES&T* most directly involve current research papers on routine monitoring studies.

The following statement will become our policy as of July 1984 and will appear in the Editorial Policy Statement printed in each January issue: *Environmental Science & Technology* seeks to publish papers of an original and significant nature. Originality should be evidenced by new experimental data, new interpretations of existing data, or new theoretical analysis of environmental phenomena. Significance will be interpreted with respect to the breadth of impact of the reported findings. Manuscripts reporting data of a routine nature that do not offer heretofore unavailable important information or do not substantially augment already available data will be declined publication in *ES&T*. The scope of the reported data in ambient monitoring studies should be such that broad conclusions applicable to more than the particular local scale are possible.

In the March 1982 editorial (*Environ. Sci. Technol.* **1982**, *16*, 143A), the desirability of criteria was discussed for confidence levels behind GC/MS data used to claim structural identifications. Comments received on this issue led me to decide that these criteria would most appropriately be used as guidelines to authors and reviewers (November 1982 editorial, p. 594A). Subsequently, two Advisory Board members (Drs. Glaze and Keith) drafted a guideline statement that we will begin sending to reviewers of relevant manuscripts in the near future.

These guidelines offer the following definitions regarding the use of spectroscopic and chromatographic properties for identification of unknown analytes.

Confirmed Identification (Level 3)

General: An identification based on sufficient spectral and/or chromatographic data so as to show that the unknown analyte and an authentic standard of a compound are identical, within instrumental measurement variations in the same laboratory.

Example (GC/MS): The data may include appropriate combinations of low- or high-resolution mass spectra obtained, using one or more ionization techniques in conjunction with chromatographic retention times or retention volumes.

Confident Identification (Level 2)

General: An identification based on sufficient spectral and/or chromatographic data of an unknown analyte and of an authentic compound from the literature (including spectral libraries) obtained under similar experimental conditions, so as to obtain a match with a high level of confidence.

Example (GC/MS): The data may include appropriate combinations of spectral and chromatographic properties as in Level 3; literature values may be taken from mass spectra data bases, lists of retention indices, and other appropriate sources.

Tentative Identification (Level 1)

General: An identification based on spectral and/or chromatographic data of quality and/or quantity less than that required for level 2 or level 3 identification; but indicative of a specific molecular structure for the analyte. This category may include the situation where no authentic standard or literature data are available for comparison and the identification is based on a priori spectral identification.

Example (GC/MS): the data may include mass spectra that do not match with reference data to a high level of confidence, but interpretation of the mass spectra suggests a specific molecular structure. Analyte with compounds of similar structure and interpretations based on known fragmentation patterns are examples of relevant information of interest.

In general, stating that an analyte has been identified at a certain level of confidence should not substitute for an appropriate description of how and on what basis the identification was made.

The editors believe that adherence to these two new policy definitions will make the research contributions more meaningful.

R.F. Christman

ES&T CURRENTS

INTERNATIONAL

Canada has asked the U.S. to withdraw from a proposed settlement with Occidental Chemical Corporation for cleaning up the S-area landfill in Niagara Falls, N.Y. According to Canadian Environment Minister Charles Caccia, thousands of tons of toxic chemicals will be left in the ground only a few feet from the Niagara River under this settlement and there is no assurance that leakage from the site will be stopped. Environment Canada has found persistent leaks of toxic chemicals from the site into the river. Water samples taken upstream and downstream of the S-area landfill show up to 20-fold increases in the concentrations of many chemicals.

WASHINGTON

The EPA refused to allow additional burnings of hazardous waste by ocean incineration ships off the Gulf of Mexico. Regular permits were denied in April, but it was expected that special research permits would be granted for burning 3.3 million gallons of waste that contains PCBs and DDT. In May, Assistant EPA Administrator Jack E. Raven denied the research permits saying that the proposed permits "have not been subject to procedures . . . to ensure that all legal, technical, and operational issues are addressed." For the past three years, Chemical Waste Management has been trying to obtain licenses for two incinerator ships, Vulcanus I and II.

There is "very solid" evidence that second-hand smoke has caused lung disease in nonsmokers, according to U.S. Surgeon General C. Everett Koop. Until now, this phenomenon, called passive smoking, has not been designated a serious health hazard by the Surgeon General. In a new report on the health consequences of smoking, he said that in pulmonary function tests, children

of smokers show small but measurable differences compared with children of nonsmokers. Children of smokers also are more susceptible to respiratory infections. The report provides a detailed biological explanation of how cigarette smoke damages lung cells.



Train: Chairman of Clean Sites

A new nonprofit corporation called Clean Sites, Inc., was formed May 31 to facilitate the cleanup of hazardous waste sites. Russell E. Train, president of World Wildlife Fund-U.S., serves as chairman of the board. The corporation was created to "bring new, additional resources to the battle now being waged by Superfund," Train said. According to present plans, work will begin on 20 sites by the end of the corporation's first year and on 60 sites annually in the third year. Industry contributions and foundation grants will provide the operating funds for the corporation, which is a cooperative venture between several industries and environmental groups that was formed under the auspices of the Conservation Foundation. Clean Sites will not supplant EPA work under Superfund, but will augment and accelerate cleanup.

Proposed standards for three industrial sources of benzene have been withdrawn by EPA. These include regulations proposed for maleic anhydride plants, ethylbenzene and styrene plants, and benzene storage tanks. EPA has decided that the benefits of the rules are not worth

the cost. At the same time, final regulations were issued for benzene fugitive emissions from 229 refineries and chemical plants, and regulations were proposed for 42 coke by-product plants. At press time, a spokesman for the Natural Resources Defense Council said the organization will probably sue to overturn the EPA decision to withdraw the proposed regulations.

Federal agency guidelines for the regulation of cancer-causing substances have been issued by the White House Office of Science and Technology. Principles for assessing and regulating risks are included in the report, which states that a substance that causes cancer in animals should be considered a "suspected human carcinogen." It also assumes that any exposure to a carcinogen, no matter how small, poses a measurable risk of cancer. In addition, it does not distinguish between initiators and promoters of cancer. The report has been praised by environmentalists and public health scientists.

Nine cancer deaths were caused by radioactive fallout from above-ground nuclear tests that the government conducted in a negligent manner, according to the ruling of a federal district judge in Salt Lake City. The tests were run between 1951 and 1962 at the Nevada Test Site. This is the first case in which a major federal activity involving radiation has been judged harmful to civilians. The ruling states that residents who lived in the path of the tests' fallout were not warned about the dangers of radioactive contamination. The federal government will be appealing the case. This ruling is likely to affect other cases that arose from the atomic tests.

In 1984 businesses in the U.S. plan to spend 5.5% more on pollution control equipment than they spent in 1983, according to a recent report by the Department of Commerce. The report states that in-

vestments in pollution control equipment will increase for the first time since 1980 if businesses spend as planned. More will be spent for air pollution and solid waste control, whereas in real terms less will be spent for water pollution control. The paper industry, operators of blast furnaces, and the nonferrous metals industry will increase spending for pollution abatement. The chemical industry, petroleum industry, and electric utilities are among those planning to decrease outlays.

STATES

Florida is working hard to combat water pollution, which is posing a serious threat to the state's ability to accommodate rapid growth. A new water quality law sets up a pesticides review council, requires local governments to identify all sources of hazardous waste, and establishes a central data bank to record information about all chemicals used in the state. In the past 10 months, 642 of 4978 wells tested have been closed by state officials because of EDB contamination. Under the new law, septic tank regulations also have been tightened and new rules for underground storage tanks have been promulgated.

The EPA has taken tentative action to prohibit New York City and other communities in the New York area from dumping sewage sludge at a site 12 miles off the New Jersey coast. The EPA calls the current site "heavily degraded." The agency may require dumping at a site 106 miles off the coast. The agency also said it will try to halt all ocean dumping at the 106-mile site after five years. During a series of hearings about the new plan held in June, New York City claimed it would cost an additional \$20 million per year to haul the sludge to the 106-mile site. At present it costs \$3.6 million annually to dump the sludge.

The state of New Jersey is suing the EPA for refusing to grant 26 claims against Superfund for natural resource damages. The claims were filed before the statutory deadline in December. EPA denied the claims because New Jersey had failed to submit a plan for spending the recovered money and had also failed to obtain preauthorization

from EPA to spend the money. New Jersey believes that Superfund does not contain such requirements and that EPA's dismissal of the 26 claims is arbitrary and capricious.

Tree damage has been reported in the Indiana and Wisconsin regions of the Ohio Valley

by Orle L. Loucks, director of the Holcombe Research Institute of Butler University (Indianapolis, Ind.). Both severely impaired tree foliage and declining tree growth were observed at 22 sites in the region. Loucks has hypothesized that the damage is caused by high sulfate aerosol concentrations, by high levels of ozone, or both. According to Loucks, sulfate concentrations are up to 100% higher in the Ohio Valley than in New York, Chicago, Detroit, and Boston. John W. Winchester of Florida State University has taken air samples while flying over the Ohio Valley and has found pHs ranging from 1.2 to -0.8 with an average reading of 0.1.

State officials are charging that the low level of state grants under the Reagan administration may be eroding environmental progress. Federal grants to states for environmental programs dropped from \$269 million in fiscal year 1981 to \$230 million in 1983. In 1984 they rose to \$242 million and requests for 1985 have fallen to \$237.7 million. At the same time, EPA has asked that the states implement more regulations, standards, and programs. EPA Administrator William Ruckelshaus counters the charges by saying that nearly all federal programs have been cut in the past few years and that state grants are therefore diminished. State officials contend that unless more funds are appropriated for 1985, the states will be forced to abandon some environmental goals.

There may be a link between marine pollution and diseases of clams, according to Carol Reinisch of Tufts University (Medford, Mass.). The clam diseases occur in the form of tumors. For example, Reinisch has seen tumors in nearly 80% of clams collected in the harbor of New Bedford, Mass., during the past year. By comparison, 10-27% of the clams from the cleaner western

Cape Cod area suffered tumors. But these diseases "may be accelerating. Nowhere along the New England Coast have we been able to find soft-shelled clams that are totally free of this disease," Reinisch said.

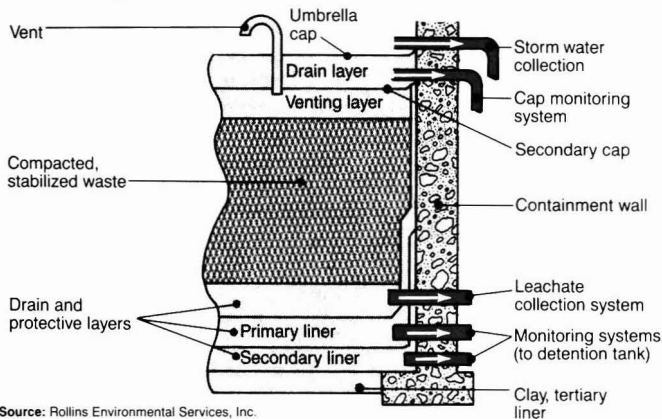
Can knowledge of how crystals grow help to solve disposal problems

of environmentally undesirable materials? George Nancollas of the State University of New York at Buffalo believes so, and is studying the precipitation of radioactive strontium, a fission by-product, as a fluoride. Precipitation would not reduce radioactivity, but it would eliminate the by-product's ability to contaminate groundwater through leaching. Likewise, crystal studies could help to make SO₂ capture by calcium, and conversion into gypsum, more efficient. However, care must still be taken to avoid tainting surrounding areas.

A multicomponent emission monitoring system will be set up in the Federal Republic of Germany's highly industrialized state of Saarland. The system will measure SO₂, NO_x, carbon monoxide, ozone, dust, methane, and methane-free total hydrocarbons. Dust samples will be further analyzed. The key will be the Immesa telemetric system, developed by Siemens AG, which consists of three multicomponent measuring stations, six single-component measuring stations, and a monitoring center with a process computer. Meteorological data also will be obtained. Air pollution will be recorded continuously and classified according to scope and type, as provided by German anti-pollution laws.

A new hazardous waste landfill design "virtually eliminates any chance of groundwater or surrounding land contamination," says Rollins Environmental Services, Inc. (Wilmington, Del.), its developer. Known as the Environmental Vault, the design employs a reinforced concrete base and walls. Multiple protective layers "insulate" wastes from the environment. Any leachate that may escape from the containment structure is collected and analyzed. The wastes and vault are capped with a double seal through which gas and other contents can be monitored. If waste

Landfill design



Source: Rollins Environmental Services, Inc.

reclamation is indicated, it can be removed with no degradation of the vault.

Volatile organic compounds (VOCs) in groundwater are being removed by a stripping tower with a packed-column unit. The tower and unit, located in Zanesville, Ohio, were designed by Malcolm Pirnie, Inc., of Columbus. VOC concentrations can run as high as 50 000 parts per billion. The packed column was designed for a 99.0% VOC removal efficiency at 600 gpm, but according to Malcolm Pirnie, it operates at a 99.7% efficiency, "exceeding expectations." Contaminants at an industrial complex included trichloroethylene and *trans*-1,2-dichloroethylene.

An inexpensive way of producing ammonia with solar energy is being developed by the Southwest Research Institute (SwRI, San Antonio, Tex.). Air is saturated with water and, under solar light, is pumped through activated silicate foam "doped" with a trace metal catalyst. The moisture is converted to hydrogen and oxygen, the hydrogen combines with nitrogen to form ammonia or one of its derivatives, and the ammonia is collected by an aqueous acid scrubbing process. SwRI says that 5-10 mg/h of ammonia can be produced from 0.25 ft³/h of air, and that the silicate is available for about \$30/ft³. Further test on light, apparatus, and other areas will be aimed at increasing ammonia output.

Hospital and industrial wastes might be converted to energy efficiently with the SynchroFire Sys-

tem developed by Kelley Co., Inc. (Milwaukee, Wis.). This base-load boiler system employs automatic controls to use heat from waste incineration, conventional fuels, or both, to make steam or hot water. Calling the system pollution-free, Kelley engineers explain that it combines a single-stack configuration and innovative flue gas flow controls with a rear-entry, three-pass boiler and a boiler burner. Flow controls for the stack are non-mechanical, and the system can withstand flue gases reaching temperatures of 2000 °F, according to Kelley.

Simultaneous removal of SO_x and NO_x from power plant flue gas might be accomplished by a zinc oxide process, says Harvey Rosenberg of Battelle's Columbus Laboratories (Ohio). Battelle has a \$195,000 contract to evaluate the process on a bench scale and, if the test succeeds, to "cost out" the process for a 500-MW power plant. Optimal removal methods will be sought, as will ways of regenerating zinc oxide. The advantage of such a process would be combining the now-separate processes of removing SO_x and NO_x. It is hoped that costs could be lowered in this way.

BUSINESS

Where does the Great Plains Coal Gasification Project (Beulah, N.D.) stand? As of Nov. 30, 1983, it was 95% complete and only about two weeks behind schedule, according to the U.S. General Accounting Office. Moreover, cumulative project costs were less than originally estimated. Still, the company con-

sortium building Great Plains wanted to withdraw from the project because of forecasted drops in energy prices. For that reason, the U.S. Synthetic Fuels Corporation (Washington, D.C.), a government concern, is considering assistance in the form of price guarantees for the plant's synthetic natural gas.

Du Pont (Wilmington, Del.) has unveiled two new agricultural research facilities to help the company develop products to improve crop yields and to control weeds, insects, and plant diseases. One is at the Stine-Haskell Research Center near Newark, Del.; the other is the Experiment Station near Wilmington. Built at a cost of more than \$60 million, these facilities represent Du Pont's largest single capital investment in agricultural research. The new facilities include greatly expanded laboratories, greenhouses, plant growth chambers, and test farms.

An industrial market research survey, "Water & Wastewater Treatment—Pulp & Paper Industry," has been completed as part of the WaterMark 84 program of the Water and Wastewater Equipment Manufacturers Association (WWEMA). Covering 674 mills, the survey is aimed at assisting senior marketing executives with selling their products to this fourth-largest industrial water user. WWEMA also has completed a comprehensive analysis of the petroleum industry for the WaterMark 84 program. Among the survey's features are outlines of historical and present capital expenditures and predicted spending outlays for 10 industries in 1984.

To improve the outlook for nuclear power, more stable construction costs and better management by many utilities will be needed, Norman Rasmussen of the Massachusetts Institute of Technology told the American Nuclear Insurers. An increasing demand for electricity also would be important, said Rasmussen, who pointed out that U.S. electric power demand actually declined by 2% in 1982. He ascribed part of the cost instability to rising interest rates and to the long amount of time—12 years, now—that it takes to complete nuclear plant construction. Rasmussen also cited "unanticipated revisions in federal regulations" as a factor.

Spatial concentration distributions

These can be used to describe concentration variations in actual environmental data and in evaluative models of chemical fate in the environment

**Donald Mackay
Sally Paterson**

*Department of Chemical
Engineering
and Applied Chemistry
University of Toronto
Toronto, Ontario M5S 1A4, Canada*

When one assesses the environmental behavior of new and existing chemicals, it is instructive to calculate the partitioning, reaction, and inter-phase transport characteristics of the chemical in a hypothetical or evaluative environment or "unit world." This concept, originally suggested by Baughman and Lassiter (1), has been used by others, notably Mackay (2), Mackay and Paterson (3, 4), Neely (5), Neely and Mackay (6), Klöpffer et al. (7), and Hushon et al. (8). A common assumption in such assessments is that each environmental compartment, medium, or phase, such as water, air, or soil, is homogeneous. Some heterogeneity can be in-

troduced, however, by considering multiple compartments of similar material, as for example the troposphere and stratosphere, or the epilimnion and hypolimnion.

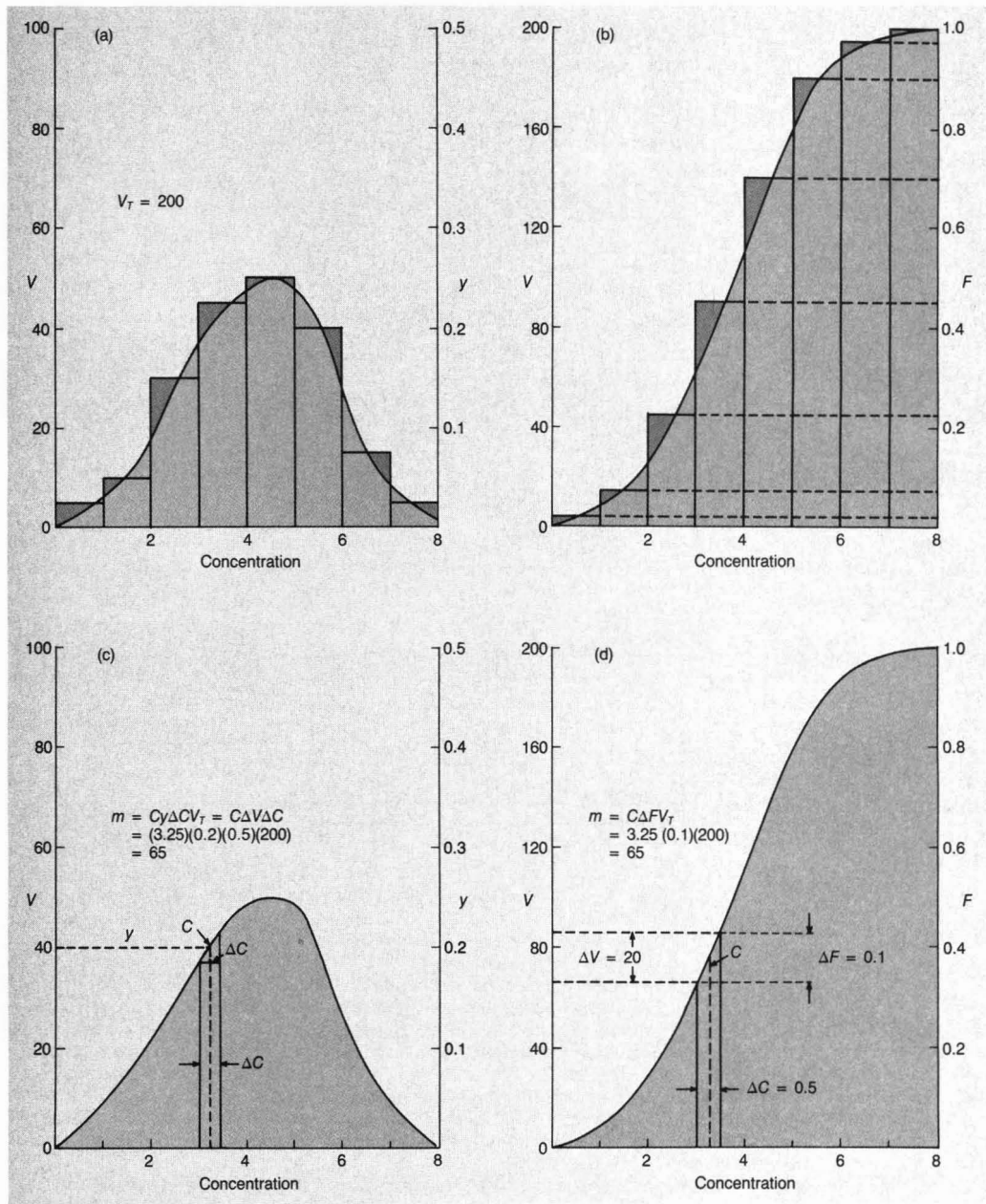
In this article, we address the issue of characterizing the heterogeneous spatial distribution of a chemical within a compartment using a probability density function. The advantage of this approach is that rather than merely stating that "the mean chemical concentration in the water (or fish, or air) is 1.0 mol/m^3 ," it is possible to add that "approximately 10% of the volume may experience a concentration in excess of 10 mol/m^3 and 1% may experience a concentration in excess of 50 mol/m^3 ." Although a mean concentration may be judged to be "acceptable," it is likely that a small fraction of the environment experiences an "unacceptable" concentration. It is useful to know if this small fraction is 1% or 0.0001%.

A chemical in the environment also varies in concentration temporally,

especially in the atmosphere; thus there is a dual variability. In this discussion, however, we assume a steady-state condition—that is, concentrations do not change with time, or at least the spatial distribution is constant, although the locations subject to a given concentration range may change with time. This steady-state assumption is most valid for relatively immobile compartments such as sediments or soils. The issue of the spatial statistical distribution of pollutant concentrations has many features in common with the issue of the temporal distribution, which has been reviewed recently for air by Georgopoulos and Seinfeld (9) and for water by Dean (10).

In evaluative environmental calculations, the information provided is usually the compartment volume and the amount of chemical present, often in the form of the mean concentration or fugacity. The task that we address here is to convert this data into a distribution of concentrations, which

FIGURE 1
Distribution and cumulative functions



when integrated, corresponds to the same total amount of chemical.

Distribution functions

We assume that an environmental compartment has a total volume V_T m³ and contains M mol of chemical; thus the mean concentration C_M is M/V_T mol/m³. If representative

samples of the entire volume could be taken and analyzed, the data could be categorized according to the concentration range in which each sample lies, and a histogram could be prepared of volume vs. concentration as shown in Figure 1a. The total volume—that is, the total heights of the rectangles—must equal V_T . The

number of moles in each rectangle m_i can be calculated as C_iV_i (where C_i is the mean concentration in the rectangle), and when totaled, $\sum m_i$ must yield M .

It is also possible to present these data in cumulative distribution form in which the total volume experiencing a concentration less than C is plot-

ted against C . This is shown in Figure 1b, which is obtained simply by adding each rectangle to all those of lower concentrations. The cumulative curve shows immediately the fraction of the volume (F) experiencing concentrations of less than or greater than a given value. In the example given, half the volume has a concentration above 3.8 mol/m^3 , and 10% is in excess of 5.5 mol/m^3 .

It is useful and instructive to fit equations to these distributions so that changes with time or space can be ascertained rigorously. The selection of the equation ideally should be based on an understanding of the fundamental causes of the variation, but at the present state of the art we are unable to justify any particular equation. Our present selection is thus based entirely on trial and error and convenience, but it is hoped that future selections will be more soundly based. This "curve-fitting" procedure can be viewed as fitting an equation to the distribution or cumulative distribution curves, or (equivalently) redrawing the axes to linearize the cumulative distribution curve. The curve obtained is in principle a continuous distribution function or probability density function as reviewed in the texts by Aitchison and Brown (11), Hahn and Shapiro (12), Johnson and Kotz (13), and Elderton and Johnson (14).

Each function has two forms: the bell-shaped distribution function corresponding to the continuous line in Figure 1c in which the ordinate is designated y , and the cumulative function (Figure 1d) with ordinate F . The

function should have the properties that

when $C \rightarrow \infty$, $F \rightarrow 1.0$, and $y \rightarrow 0$,

and when $C = 0$, $F = 0$ (1)

It is worth considering the significance of F and y in the present context. F is the fraction of the total volume (V/V_T) experiencing less than a given concentration and is dimensionless, ranging from zero to unity. The derivative of F with respect to C is y and is thus the incremental change in volume fraction per concentration increment. It is the slope of the F curve and has units of reciprocal concentration. The volume V , which has a concentration between, for example, 3.0 and 3.5 mol/m^3 (i.e., ΔC), can thus be determined either from the F curve as $V_T \Delta F$ or from the y curve as $V_T y \Delta C$. As illustrated in Figures 1c and 1d, the y value is read at a C value of 3.25 mol/m^3 , and ΔC is 0.5 mol/m^3 . The amount of chemical in this volume is thus $3.25 V_T \Delta F$ or $3.25 V_T y \Delta C$ mol or 65 mol , as calculated in the figures. The total amount of chemical in V_T is M , which is thus $\sum C V_T \Delta F$ or $\sum C V_T y \Delta C$, or in differential form

$$V_T \int_0^{\infty} (Cy) dC = V_T C_M \quad (2)$$

where C_M is the mean concentration. This relationship generally determines one parameter in the empirical equation relating y to C . A second parameter usually determines the degree of spread on either side of C_M . When a third parameter is introduced, it may provide a constraint on the minimum value of C .

Of the numerous functions that can satisfy these constraints, we consider here the normal, lognormal, and Weibull functions and suggest that the Weibull function is particularly suitable for this situation because of its versatility. Indeed, it can closely reproduce both normal and lognormal distributions. Figure 2 lists the three functions and some of their properties. Georgopoulos and Seinfeld have listed and discussed others (9).

Data treatment

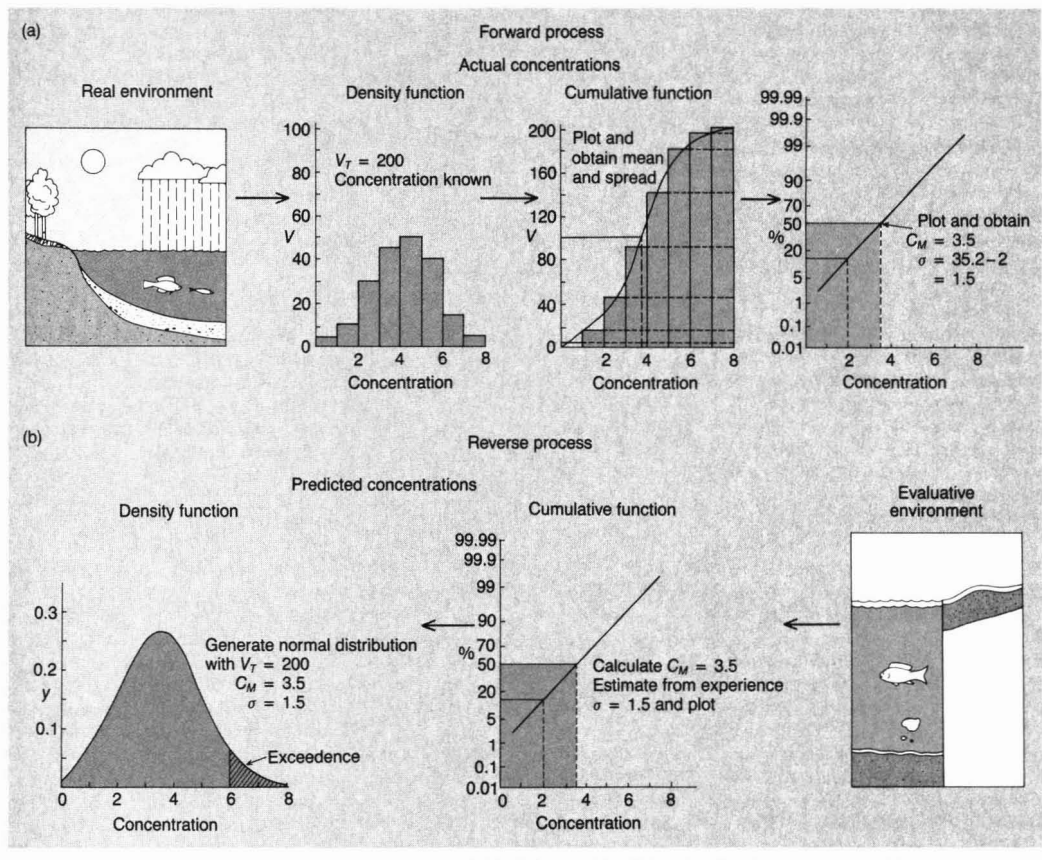
Two data treatment or calculation directions may be encountered. First is the usual "forward" direction in which we process environmental concentration data obtained from a monitoring program for a known V_T to obtain M , C_M , and an equation with fitted parameters. Second is the "reverse" process in which V_T , M , and C_M are obtained from "evaluative" calculations and the aim is to devise a suitable distribution equation and its parameters. These processes are shown schematically in Figure 3. The reverse process requires some additional information in the form of, for example, the likely "spread" of the data, which can be obtained only from environmental measurements for the compound of interest or *similar compounds* in the environment of interest or from measurements in *similar environments into which the compound was similarly introduced*.

If we can build up, from experience, information about the likely values of the other parameters and the factors that control these values, we may be able to make useful statements about

FIGURE 2
Distribution functions and their properties

	Distribution function	Cumulative function	Properties		
			Mean	Median	Mode
Normal	$\frac{1}{\sigma\sqrt{2\pi}} \exp\left[-\frac{(C-C_M)^2}{2\sigma^2}\right]$	$\frac{1}{\sqrt{2\pi}} \int_{-\infty}^z \exp\left[-\frac{C^2}{2}\right] dC$ where $Z = \frac{C-C_M}{\sigma}$	C_M	C_M	C_M
Lognormal	$\frac{1}{C \ln S \sqrt{2\pi}} \exp\left[-\frac{(\ln C - \ln C_G)^2}{2(\ln S)^2}\right]$	$\frac{1}{\sqrt{2\pi}} \int_{-\infty}^z \exp\left[-\frac{C^2}{2}\right] dC$ where $Z = \frac{\ln C - \ln C_G}{\ln S}$	$C_G \exp\left[\frac{(\ln S)^2}{2}\right]$	C_G	$\frac{C_G}{\exp[(\ln S)^2]}$
Weibull	$\frac{\lambda}{C_W} \left[\frac{C}{C_W}\right]^{\lambda-1} \exp\left[-\left[\frac{C}{C_W}\right]^\lambda\right]$	$1 - \exp\left[-\left[\frac{C}{C_W}\right]^\lambda\right]$	$C_W \Gamma(1 + 1/\lambda)$	$C_W (0.693)^\lambda$	$C_W \left[\frac{\lambda-1}{\lambda}\right]^{1/\lambda}$ for $\lambda > 1$

FIGURE 3
Forward and reverse processes for treatment of real and evaluative concentration data



exceedences—that is, the fractions of the environment that have “excessive” concentrations. This will greatly enhance the usefulness of evaluative environmental calculations. It could provide a method by which monitoring data can be examined to check consistency with evaluative estimates.

We will examine first the mathematics of the forward and reverse processes and then illustrate the overall process for mirex in the sediments of Lake Ontario. It is suggested that a graphical technique is the best way to treat data because it provides a direct, visual impression of the goodness of fit. Other more rigorous techniques can be used, but at the present state of the art their accuracy is rarely justified.

Normal distribution

This function has two adjustable parameters, the mean C_M and the spread parameter or standard deviation σ . Unfortunately the cumulative function cannot be expressed ana-

lytically. Thus, error function tables must be used or values must be computed by numerical integration.

In the normal distribution function, the concentrations are symmetrically distributed about the mean, C_M , which is also the median. That is, at $F = 0.5$, C is C_M and the mode or concentration at which the maximum value of y occurs. Sixty-eight percent of the concentrations lie between $(C_M - \sigma)$ and $(C_M + \sigma)$ and 95% lie between $(C_M - 2\sigma)$ and $(C_M + 2\sigma)$. One undesirable property of this function is that it can yield negative concentrations, especially if σ is an appreciable fraction of C_M . However, this problem can be overcome by truncating the distribution at zero concentration or “folding” the negative values back into the positive region. It is thus most likely to be used if C_M greatly exceeds σ . In this situation, which occurs when the chemical is well mixed in the medium, the distribution is very “tight” about the mean. Heterogeneities are therefore

slight and the incentive for calculating their magnitude may also be slight.

The graphical fitting technique is to plot concentration vs. F on probability paper in which the ordinate scale is adjusted to linearize F by using a scale of

$$\frac{1}{\sqrt{2\pi}} \int_0^z \exp\left(-\frac{C^2}{2}\right) dC$$

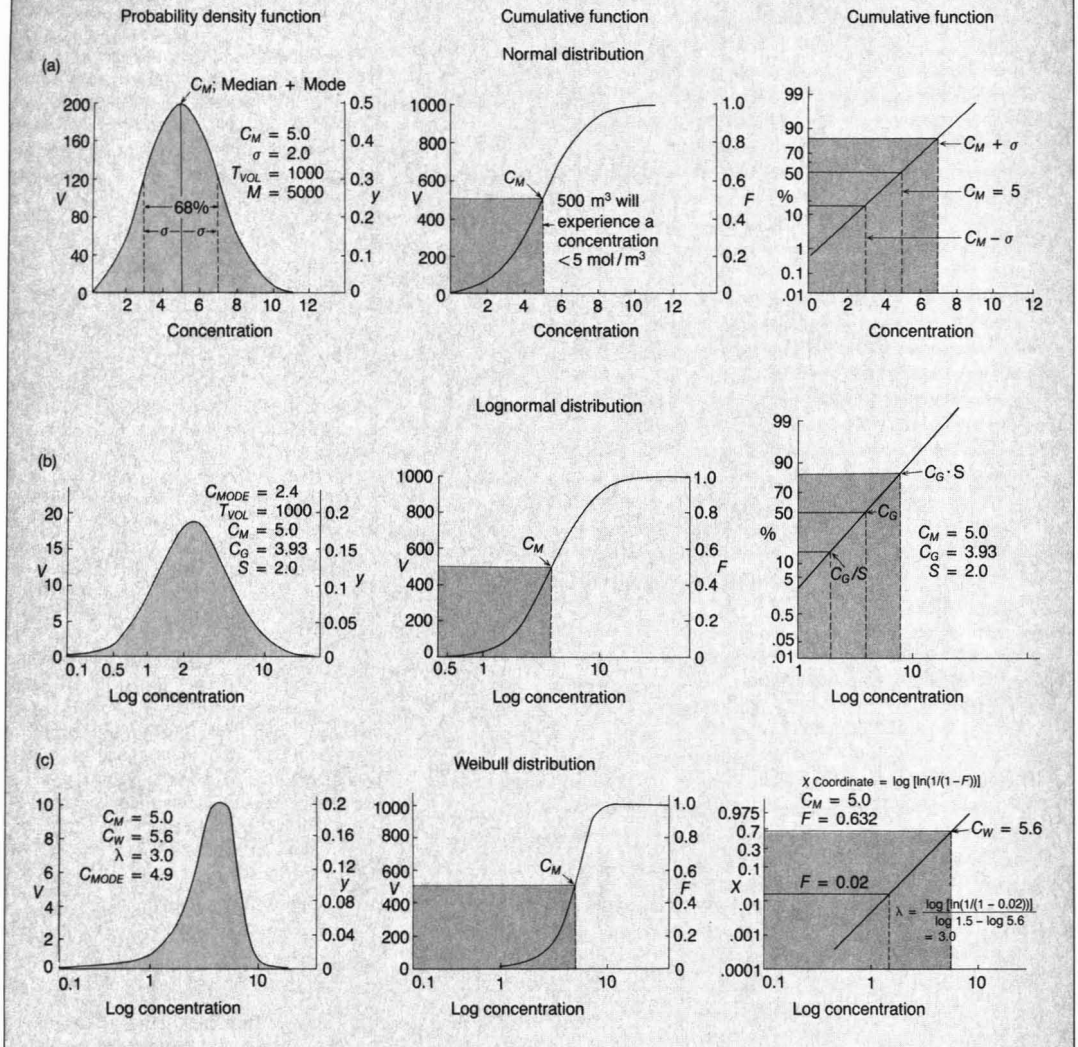
where $z = (C - C_M)/\sigma$ (3)

A straight line is then drawn through the data.

The parameters can be read from the graph easily, as is shown in Figure 4a, where C_M is $C_{0.5}$ and σ is $(C_{0.84} - C_{0.16})/2$ or $(C_{0.84} - C_{0.5})$. The subscripts refer to the values of F .

The reverse process gives C_M directly. The spread factor is best expressed as a fraction of C_M (actually the coefficient of variation) in a statement of the type “ σ/C_M is typically 0.1 for chemical A in environment B.”

FIGURE 4
Three distribution functions



From this estimate of σ , the F - C line can be drawn on probability paper from which the exceedences may be read directly.

Lognormal distribution

The advantage of this function, which is the most widely used environmental distribution expression, is that it always yields positive concentrations and gives distributions in which the concentration values are low except for a small fraction or "tail" of high values corresponding to polluted environments. C_G and S are distribution parameters, and the function is symmetrical when y is plotted against $\ln C$.

Unfortunately, y cannot be integrated analytically. The cumulative function is given in Figure 2 and can be obtained from error function tables.

The graphical data-fitting technique used in Figure 4b is to plot log concentration vs. F on probability paper with the same ordinate as in the normal distribution, and to read C_G where F is equal to 0.5. From a straight line through the data, S can be read as

$$\ln S = (\ln C_{0.84} - \ln C_{0.16}) / 2$$

$$\text{or } S = \sqrt{C_{0.84} / C_{0.16}}$$

$$= C_{0.84} / C_{0.5} = C_{0.5} / C_{0.16} \quad (4)$$

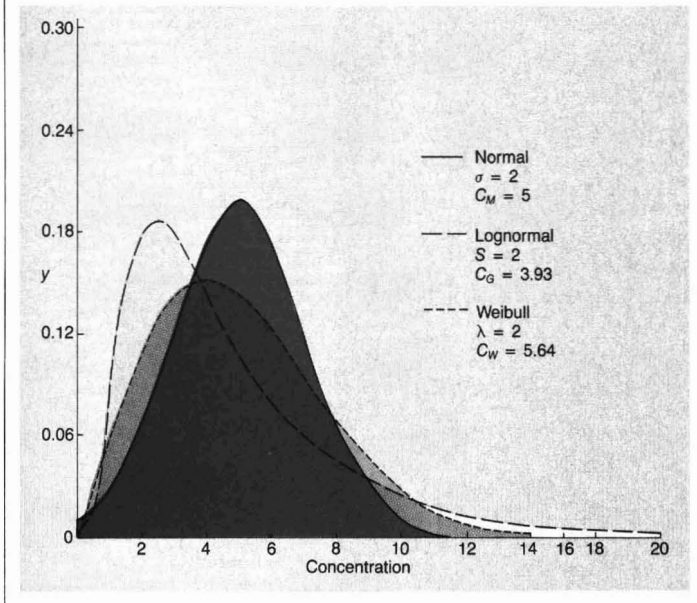
The dimensionless spread factor S has the following significance: If, for example, the geometric mean or median C_G is 3.93 units and S is 2, then the mean is 5.0 [i.e., $3.93 \exp((\ln 2)^2 / 2)$], 16% of the volume will exceed 3.93×2 , or 7.9; about 5% will exceed 3.93×2^2 , or 16; and 0.1% will exceed 3.93×2^3 , or 31 units.

The reverse process gives C_M but not C_G , unless there is information about S in a statement of the type, "S is typically 5 for chemical A in environment B." Then C_G can be evaluated from

$$\ln C_G = \ln C_M - (\ln S)^2 / 2 \quad (5)$$

and the F - $\ln C$ curve drawn by locat-

FIGURE 5
Three distribution functions with a spread factor of two and an arithmetic mean of five



ing log concentration points at 0.84 or 0.16, these values being a factor S greater than and less than C_G , respectively.

Weibull distribution

This function was introduced by Weibull in 1951 (15) and was applied first to the variation in steel and cotton strength and to the size of fly ash, planktonic protozoa, beans, and British males.

It has two parameters, a dimensionless factor, λ , which controls the spread, and a concentration, C_W . It cannot give negative values and has the advantage that it can be integrated to give

$$F = 1 - \exp(-(C/C_W)^\lambda) \text{ or } C = C_W[\ln(1/(1-F))]^{1/\lambda} \quad (6)$$

It can yield curves similar to the lognormal function with a small fraction of high values. When λ is less than or equal to 1.0, the y - C curve ceases to be bell-shaped and there is an intercept on the y axis at zero C . To fit data to the function and obtain λ and C_W , it is convenient to plot log concentration vs. X where

$$X = \log[\ln(1/(1-F))] \quad (7)$$

It can be shown that

$$X = \lambda(\log C - \log C_W) \quad (8)$$

A straight-line plot of this type on "extreme value graph paper" (see Figure 4c) yields values of C_W equal

to C when F is 0.632 (i.e., X is zero). The spread factor can be obtained from another point. For example, when F equals 0.02, X is -1.69 and

$$\lambda = -1.69/(\ln C_{0.02} - \ln C_W) \quad (9)$$

The mean concentration C_M is given by

$$C_M = C_W \Gamma(1 + 1/\lambda) \quad (10)$$

where Γ is the gamma function and is available in tables.

Again, in the reverse process, some information about the likely or typical values of λ is required from experience before C_W can be estimated from C_M . The advantage of the Weibull function is that F can be expressed analytically as a function of C . In other words, the fraction of exceedence can be calculated for any desired concentration as, for example, 0.1% of the volume may exceed 10 units. The explicit nature of the cumulative equation enables one to calculate the minimum concentration of a given fraction. Such statements as "the 'worst' 1% will exceed 5 mol/m³" can be made.

Figure 5 illustrates a normal, lognormal, and Weibull distribution, each with a spread factor of two and an arithmetic mean of five.

Illustration

Thomas and Frank reported data for the concentration of various con-

taminants in Great Lakes sediments and prepared isopleths showing the regions of high concentration (16). Such surveys provide an invaluable assessment of the condition of the sediments and of the location of various depositional regimes. We examine here the data for mirex in Lake Ontario. These data were provided by Thomas in detailed concentration-location form. Some additional data reported by Scudato and DelPrete have been added (17). A total of 280 samples were taken, of which only 74 had concentrations above the detection limit of 1.0 ng/g. Because samples were taken on a regular grid, each sample corresponds to a constant and different sediment volume of approximately 8200 m × 8200 m × 3 cm deep or 2.0 × 10⁶ m³. If a density of 1500 kg/m³ is assumed, this volume has a mass of 3 × 10⁹ kg. The data were sorted into order according to concentration and the cumulative curve established with F as a function of C . Of course no information can be deduced for concentrations below 1.0 ng/g. Thus the experimental curve extends from an F of 1.0 down to only 0.75 or 206/280.

A normal distribution is clearly inappropriate since the standard deviation exceeds the mean. In Figures 6 and 7 lognormal and Weibull cumulative plots are shown. The lines are drawn by eye, and the parameters are indicated. The mean concentrations and total amounts for the total sediment volume of 560 × 10⁶ m³, or mass of 840 × 10⁹ kg, are

$$\text{Lognormal } C_M = 2.5 \text{ ng/g, mass} = 2100 \text{ kg} \quad (11)$$

$$\text{Weibull } C_M = 1.8 \text{ ng/g, mass} = 1500 \text{ kg} \quad (12)$$

If, for example, concentrations in excess of 2 ng/g are judged to be of particular concern, the distributions predict that 22% (lognormal) and 18% (Weibull) experience this exceedence.

It is apparent from the isopleths (16) that the principal sources of mirex are the Niagara and Oswego rivers, although offshore spillage also may have occurred. It is likely that other contaminants with sedimenting characteristics similar to those of mirex, and with similar sources, would display generally similar values. Two interesting classes of compounds in this regard are the PCBs and the chlorodibenzodioxins (CDDs), which are also highly hydrophobic organic contaminants. The PCB distribution (16) is more homogeneous than that of mirex and shows

FIGURE 6
Lognormal distribution fitted to sediment concentration data for mirex in Lake Ontario

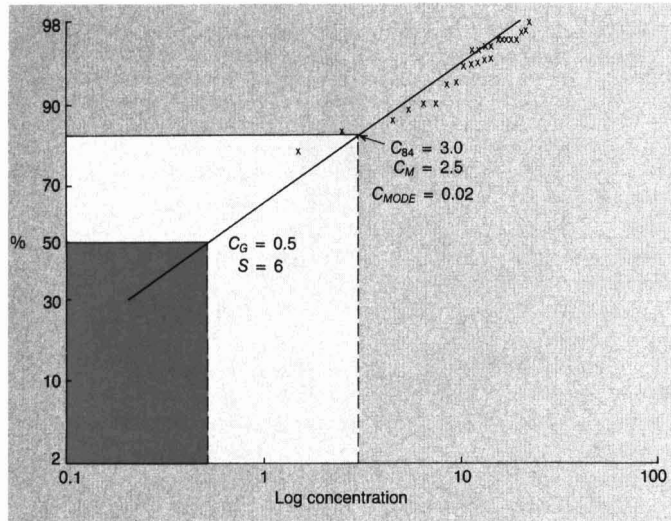
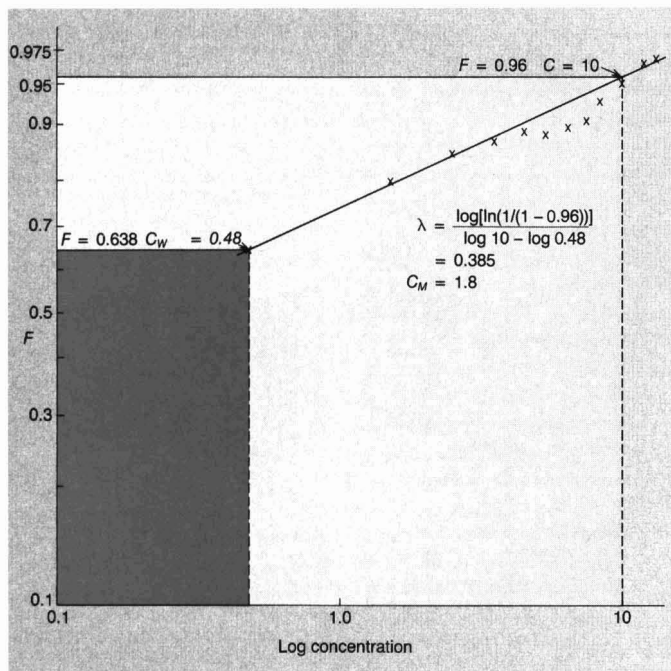


FIGURE 7
Weibull distribution fitted to sediment concentration data for mirex in Lake Ontario



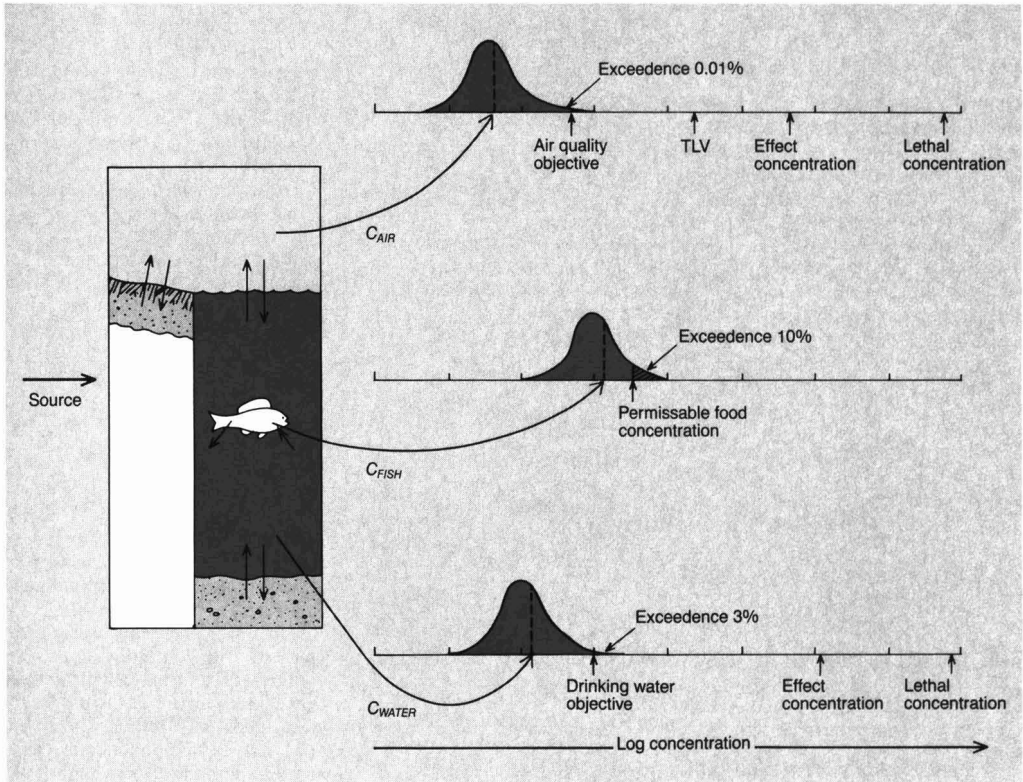
some high concentrations on the Canadian side, indicating the presence of Canadian sources and possibly atmospheric sources as discussed by Eisenreich et al. (18). The S value for PCBs thus appears to be low (i.e., the spread is less) with a value of approximately three. No data are available for the CDDs, but it seems likely that the Niagara River is a major source; thus a high value of S is probable. The conclusion is that by assembling such data and experience about the likely magnitudes of λ or S in sediments, water, air, and soil, some useful information can be obtained about likely exceedences. In this way, the severity of highly polluted environments or "hot spots" can be better assessed and even may be predicted.

In an earlier paper we presented some examples of output from fugacity level III calculations for a hypothetical chemical in the form of predicted concentrations in various environmental media (19). If environmental distribution data become available, it will be possible to extend these diagrams, as illustrated in Figure 8, to give ranges of predicted concentrations. These ranges can be juxtaposed with concentrations that are judged to be of toxicological significance—for example, effect or no-effect levels or threshold limit values (TLVs)—and conclusions can be drawn about the severity of the risk by viewing the proximity of these levels to the predicted concentration ranges. While it may be concluded that the mean concentration of a certain chemical in water is acceptable when it is smaller than a certain effect level, it may transpire that the concentrations are unacceptable for 1% or 0.1% of the water environment and thus presumably for the 1% or 0.1% of the population who rely on that water.

This approach may also assist in the "validation" of evaluative environmental models. If a model is assembled to describe a region approximately, giving mean concentrations and, as discussed here, distributions of concentration, it then becomes possible to compare real monitoring data with the distribution given by the model. Monitoring data may or may not be inconsistent with the concentration distributions in the model. This comparison is not strictly validation; rather it is a test of possible mutual consistency. But if this can be done successfully for several chemicals and environments, confidence will grow that the models are describing real physical-chemical phenomena with appropriate parameters.

FIGURE 8

Relationship of predicted environmental concentration distributions to toxic effect concentrations



Consequently, the use of the models for assessing the environmental fate of chemicals will be increasingly justified.

Acknowledgment

The authors are grateful to the Ontario Ministry of the Environment for financial support given for this work.

Before publication, this article was reviewed for suitability as an *ES&T* feature by George Baughman, EPA Research Laboratory, Athens, Ga. 30613; and by Philip M. Gschwend, Department of Civil Engineering, MIT, Cambridge, Mass. 02139.

References

(1) Baughman, G.; Lassiter, R., "Prediction of Environmental Pollutant Concentration," ASTM STP 657; American Society for Testing and Materials: Philadelphia, Pa., 1978, p. 35.
 (2) Mackay, D. *Environ. Sci. Technol.* **1979**, *13*, 1218.
 (3) Mackay, D.; Paterson, S. *Environ. Sci. Technol.* **1981**, *15*, 1006.
 (4) Mackay, D.; Paterson, S. *Environ. Sci. Technol.* **1982**, *16*, 654A.
 (5) Neely, W. B. *Environ. Toxicol. Chem.* **1982**, *1*, 259.

(6) Neely, W. B.; Mackay, D. In "Modeling the Fate of Chemicals in the Aquatic Environment"; Dickson, K. L.; Maki, A. W.; Cairns, S., Eds.; Ann Arbor Science: Ann Arbor, Mich., 1982.
 (7) Klöpffer, W.; Rippen, G.; Frische, R. *Ecotoxicol. Environ. Safety* **1982**, *6*, 294.
 (8) Hushon, J. M. et al. *Chemosphere* **1983**, *12*, 887.
 (9) Georgopoulos, P. G.; Seinfeld, J. H. *Environ. Sci. Technol.* **1982**, *7*, 401A.
 (10) Dean, R. B. In "Chemistry in Water Reuse"; Cooper, W. J., Ed.; Ann Arbor Science: Ann Arbor, Mich., 1981; Vol. 1
 (11) Aitchison, J.; Brown, J.A.C. "The Log-normal Distribution"; Cambridge University Press: Cambridge, Mass., 1966.
 (12) Hahn, G. J.; Shapiro, S. S. "Statistical Models in Engineering"; Wiley: New York, N.Y., 1967.
 (13) Johnson, N. L.; Kotz, S. "Continuous Univariate Distribution"; Houghton-Mifflin: Boston, Mass., 1970; Vol. 2.
 (14) Elderton, W. P.; Johnson, N. L. "Systems of Frequency Curves"; Cambridge University Press: Cambridge, Mass., 1969.
 (15) Weibull, W. "A Statistical Distribution Function of Wide Applicability"; Presented to the American Society of Mechanical Engineers, Atlantic City, N.J., 1951.
 (16) Thomas, R. L.; Frank, R. In "Physical Behavior of PCBs in the Great Lakes"; Mackay, D. et al., Eds.; Ann Arbor Science: Ann Arbor, Mich., 1983, pp. 245-67.
 (17) Scudato, R. J.; DelPrete, A. *J. Great Lakes Res.* **1982**, *8*, 695.
 (18) Eisenreich, S. J.; Loones, B. B.; Hollod,

G. J. In "Physical Behavior of PCBs in the Great Lakes"; Mackay, D. et al., Eds.; Ann Arbor Science: Ann Arbor, Mich., 1983; pp. 115-26.

(19) Mackay, D.; Paterson, S.; Joy, M. In "Fate of Chemicals in the Environment"; Swann, R. L.; Eschenrocher, A., Eds.; ACS Symposium Series 225; American Chemical Society: Washington, D.C., 1983.



Donald Mackay is a professor and Sally Paterson is a research associate in the Department of Chemical Engineering and Applied Chemistry at the University of Toronto. Their research interests are the environmental fate and effects of toxic substances, especially modeling, studies of volatilization of organic contaminants from water, and measurement of physical chemical properties.

Biological monitoring



Richard M. Dowd

Biological monitoring—evaluating the health or condition of an organism or ecosystem through biological measurements—is being used increasingly to develop data for environmental regulations. This trend is attributable in part to improvements in analytical chemistry: Our ability to measure traces of chemicals at ever-lower concentrations increases the number of chemicals identifiable in the environment. As a result, interest has renewed in the possibility of directly measuring the integrated effects of chemicals through biological measurements in humans and in ecological systems. In some cases, data on biological monitoring may eliminate the need for chemical measurement; in others, the data may reproduce the same ambient air or water measurements in organic tissue or fluids.

Biological monitoring can be characterized in two ways. The first indicates levels of human exposure to certain substances and the resultant effects; the second way measures non-human exposure and the effects attributable to certain substances.

Measurements of nonhuman exposure, specifically those done on aquatic life, have a relatively long history in the development of regulations. For some time in its long-term ambient water quality monitoring program, EPA has employed strategies that include the biological monitoring of aquatic species. This program consists of three different activities: traditional field surveys of the health of aquatic ecosystems; bioassays of effluents and in some cases of receiving

waters; and detailed examinations of the levels of toxic substances in fluid, tissues, and other organs.

Bioassays of effluents

Bioassays of effluents may be required for discharge permits, either to monitor and report results or to achieve certain required levels of effluent concentration; bioassays also can be used to indicate of the effectiveness of pollution controls. Typically, EPA or a state water quality agency asks a permittee to conduct an LC₅₀ test, in which a sample of fish or another species is exposed to a measured quantity of effluent to determine at what concentration 50% of the species will die. Most often, this LC₅₀ bioassay requirement is satisfied by reporting the test results; sometimes the test data are required to demonstrate achievement of specified permit limits.

The agency has recently refined the use of chronic aquatic toxicity tests by which stream or effluent waters are tested on fast-growing water species to determine their effects on reproduction. There have been some reports of success in correlating the results of such tests with changes in the observed population of certain organisms in river segments. This past February, EPA's Water Quality Office announced a policy that allows the incorporation of water-quality-based limits in NPDES permits, using either chemical concentrations or biologically based limits.

A third area of activity would measure physiological subcellular effects of chemicals in aquatic organisms. EPA is developing tests for such effects, and these tests could be used in the future as indicators of the healthfulness of receiving waters.

Human health effects

Many of the reasons EPA is interested in a human biological monitoring program stem from the increased emphasis on the use of risk assess-

ment. The agency has acknowledged the difficulty of obtaining definitive estimates of human exposure to harmful substances on the basis of monitoring dosages or exposure levels alone. Much of the interest in human biological monitoring is relatively new, and nearly all of it is centered in the Office of Research and Development (ORD).

In its operating guidance for fiscal years 1985-86, the agency cited a "new biomonitoring policy [that] will receive wide-range ORD support by providing the Regions and States with field-validated bioassay techniques, monitoring protocols, toxic wasteload allocation models, toxic treatability evaluations of specific industries, and assessments of generic toxicity reduction of various municipal and industrial wastewater treatment processes." This has led to research initiatives in the area of biological monitoring for effects on human health. Allocation of funding for such efforts could approach \$7 million in the agency's fiscal year 1986 budget.

The goal of this effort is to establish the ability within EPA to measure concentrations of various chemical species in biological tissues and fluids and to perform related metabolic studies. While this is obviously a long-term research strategy, it is also a clear attempt to relate the ambient level of substances in the environment or a particular medium—such as food, air, or water—to which people are exposed, to the amounts that may be concentrated in human organs and tissues. This initiative includes an effort to develop new measurement techniques using biological indicators that will detect and quantify exposure levels. In addition, EPA plans to integrate epidemiological studies with such exposure assessments.

Richard M. Dowd, PhD, is a Washington, D.C., consultant to Environmental Research and Technology, Inc.

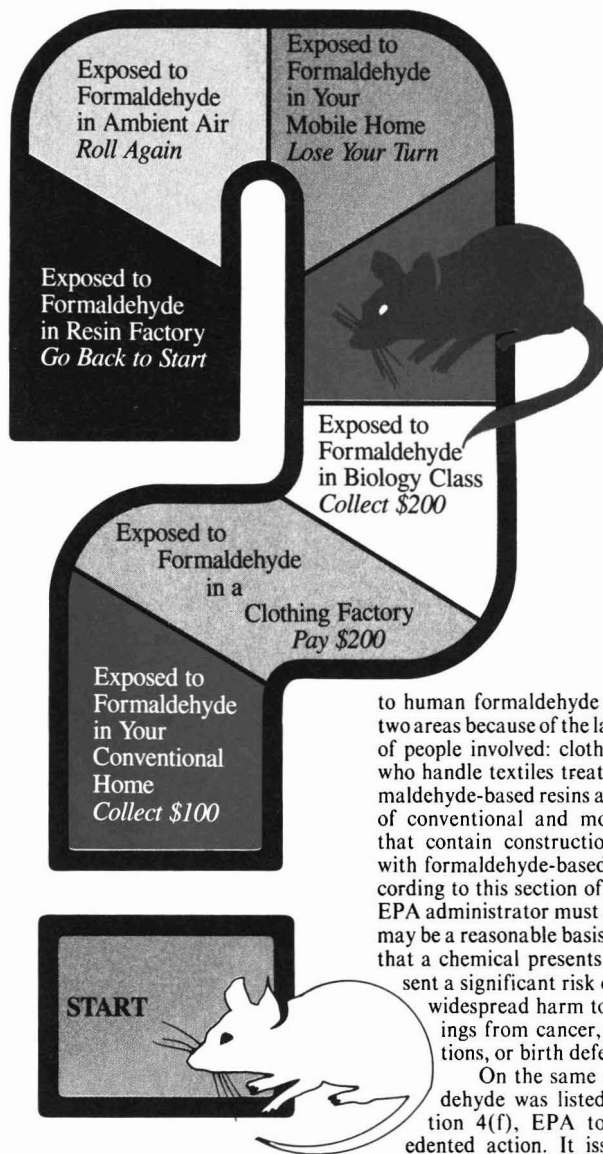
Formaldehyde: Assessing the risk

Much of the scientific data for determining risks associated with this chemical is conflicting and ambiguous

Formaldehyde is a substance to which each of us is exposed every day. Unlike most carcinogens identified in animal cancer tests, formaldehyde is also a normal metabolite in human biochemistry. It is contained in cigarette smoke at levels as high as 40 ppm and in ambient air even in remote areas. It can be found as a residual in a large variety of consumer products from permanent press fabrics to cosmetics. But the strongest sources of exposure for the nonsmoking general population are particle board, plywood, and urea formaldehyde foam insulation. When new, these emit formaldehyde and can cause the levels in indoor air to become relatively high. Despite the fact that formaldehyde is ubiquitous in the environment, emotionalism and controversy surround the discussion of every aspect of this chemical.

As much is known about formaldehyde as is known about almost any other chemical that has been studied for possible carcinogenicity to humans. But when these facts are examined, they do not point unequivocally in one direction in any area, and sometimes an individual finding or study can be interpreted as pointing in two directions simultaneously. The example of formaldehyde and the controversy that surround it also raise interesting science policy questions that can be applied to many other cancer-causing or potentially cancer-causing chemicals.

Right now, formaldehyde is more controversial than ever. On May 18 the EPA decided to list it as a priority chemical for regulatory assessment under section 4(f) of the Toxic Substances Control Act (TSCA), reversing an earlier decision of the agency in February 1982 (see *ES&T*, Oct. 1982, p. 543A). Under section 4(f), EPA will give priority consideration



to human formaldehyde exposure in two areas because of the large number of people involved: clothing workers who handle textiles treated with formaldehyde-based resins and residents of conventional and mobile homes that contain construction materials with formaldehyde-based resins. According to this section of the act, the EPA administrator must act if "there may be a reasonable basis to conclude that a chemical presents or will present a significant risk of serious or widespread harm to human beings from cancer, gene mutations, or birth defects . . ."

On the same day formaldehyde was listed under section 4(f), EPA took unprecedented action. It issued an ad-

vance notice of proposed rulemaking to initiate a full regulatory investigation concerning formaldehyde exposure of workers in apparel manufacture and of people who live in mobile and conventional housing. For other chemicals listed under section 4(f), the advance notice of proposed rulemaking was issued some time later.

The actions of May 18 are not a definite indication that formaldehyde will be regulated. In the decision to regulate, the economic costs will be weighed against the benefits provided by the substance. Also, EPA may eventually refer some, or all, aspects of the regulation of formaldehyde exposure to other federal agencies such as the Occupational Safety and Health Administration or the Department of Housing and Urban Development (HUD).

Two kinds of risk

For humans and animals, airborne formaldehyde seems to be far more of a problem than ingested formaldehyde. Even when animals are fed rather large doses, they seem to suffer no ill effects. Formaldehyde gas presents two major possible forms of risk to humans—an irritating and possible sensitizing effect, and cancer. Sensory irritation of the eyes, nose, and throat is the primary response. Irritation has been noted at levels as low as 0.25 ppm in chamber studies, and at levels of 1 ppm or higher under normal conditions. Other acute symptoms such as coughing, diarrhea, nausea, vomiting, dizziness, and lethargy have been reported after prolonged exposure at home or at work.

Formaldehyde in aqueous solution can be a cause of skin irritation in sensitive individuals. In the work population, the rate of dermal sensitization has been reported to be between 4% and 6%.

It is also well established that "some individuals are hypersensitive to formaldehyde," John J. Clary of the Celanese Corporation reported at the recent ACS symposium on formaldehyde in St. Louis. These individuals "respond to formaldehyde by showing dermal irritation or irritation of the eyes, nose, and throat at lower levels than a normal individual."

The irritant and sensitizing effects of formaldehyde seem less important than the possible carcinogenicity. These irritant effects are, however, important in the overall picture because they are the primary reason, or one of the primary reasons, for many complaints about urea formaldehyde foam insulation or mobile homes with

higher than average indoor levels of formaldehyde. Richard B. Gammage of Oak Ridge National Laboratory noted at the ACS symposium that complaints about formaldehyde he had heard from homeowners were related to the acute health symptoms, not the possible cancer risk. HUD has recently proposed changes in its manufactured-housing regulations that would limit indoor ambient levels to 0.4 ppm. This proposed regulation is designed to reduce acute reactions to formaldehyde.

Carcinogenicity in animals

The question of whether formaldehyde is a human carcinogen at levels normally found at home or in the



EPA will give priority consideration to formaldehyde exposure in two areas because of the large number of people involved.



workplace is far more controversial. All observers agree that formaldehyde induces nasal cancer (squamous cell carcinoma) in rats. In a study sponsored by the Chemical Industry Institute of Toxicology (CIIT), squamous cell carcinomas were observed in approximately 50% of the rats in the 14.3-ppm exposure group and 1% of the rats in the 5.6-ppm exposure group, when rats were exposed for six hours per day, five days per week, for 24 months. Another study, at New York University, confirmed the finding in rats, showing 50% incidence in the exposure group receiving ~14 ppm formaldehyde.

Formaldehyde has also been associated with nasal cancer in mice. In a CIIT study, two of the male mice out of a study group of 119 exposed to 14.3 ppm formaldehyde developed squamous cell carcinomas, whereas the female group remained cancer free. The cancer incidence might have been higher if more mice had lived until the end of the two-year experiment. Eighty-two of the male mice in this group died before the end of the exposure period, many from fighting.

In the CIIT rat study, benign tumors called polypoid adenomas were

also seen in both treated and control rats; 3.4%, 2.6%, and 2.2% of the animals exposed to 2.0, 5.6, and 14.3 ppm formaldehyde, respectively, developed polypoid adenomas, while the incidence was only 1% in the control group. There is disagreement about whether these tumors are permanently benign or whether a certain percentage progress to become cancers.

An independent review of CIIT's findings concluded that "there was no morphological evidence that these lesions progressed to squamous cell carcinomas." Other scientists would argue, however, that they are precancerous lesions that can progress to squamous cell carcinomas. The interpretation of the data about polypoid adenomas is important because if they are considered precancerous lesions, then it could be argued that a certain small percentage of the rats exposed at 2 ppm would develop nasal cancer, if enough rats could be tested for a long enough time. If this were true, it would be less likely that a threshold below which formaldehyde is safe for rats lies near 2 ppm, but it does not eliminate the possibility that a threshold does exist at some concentration below 2 ppm.

Some scientists believe that because formaldehyde is a natural metabolite, a human threshold for this chemical would have to be greater than the level of exposure provided naturally by the human body itself. Normal endogenous tissue levels of formaldehyde produced by metabolism range from 3 to 12 ng/g of tissue (3–12 ppm). About 10–40% of this exists as free formaldehyde.

Others argue that our bodies are not necessarily capable of handling formaldehyde safely even if the external exposure level does not exceed the amount the body itself manufactures. Nicholas A. Ashford and colleagues wrote in a letter to *Science* magazine (May 11, 1984) that some fraction of the formaldehyde that enters the body will reach DNA and react with it because "there is a finite concentration of enzyme molecules that can metabolize formaldehyde and a finite series of membranes providing barriers to diffusion." Subsequently, the limited number of DNA repair enzymes may not be able to repair all the DNA lesions before the next cell replication. Even without formaldehyde exposure from the external environment, the natural formaldehyde concentration could cause damage by this mechanism in the same way that natural radiation within the body may sometimes cause cancer. Ashford

therefore believes that natural levels of a substance do not necessarily constitute a harmless level and that small increments above the natural level cause "additional biological cost and risk."

Ambivalent findings

Mutagenicity tests on formaldehyde show mixed results. In general, most of the *in vitro* tests, including the Ames test, are positive, but the *in vivo* tests, those carried out on living organisms, show mixed results, evenly divided between positive and negative. Formaldehyde has been shown to bind covalently to DNA. In tests to determine whether formaldehyde causes birth defects in animals, the results to date have been negative.

Conflicting results

The epidemiological studies also show results that can be interpreted in a variety of ways. In general, it can be said that the data are sparse and conflicting and that currently there is no strong evidence of a causal relationship between formaldehyde and cancer. However, no human studies thus far exclude the possibility that formaldehyde is a human carcinogen.

Studies have been carried out on basically two groups: workers in plants where formaldehyde is used or produced, and professional groups who are exposed to formaldehyde in their work—*anatomists, pathologists, embalmers, and morticians*. Not a single case of nasal cancer has been found in any group studied, except for a slight excess in workers at one particle board factory in Sweden. Nasal

cancer is a very rare form of cancer, however, and is therefore difficult to detect by epidemiological methods.

In a number of the four professional groups exposed to formaldehyde, though not in the industrial workers, an excess of brain cancer and leukemia were noted. In some professional groups, the brain cancer incidence was twice that seen in the general population. Also, for U.S. morticians there was a highly significant excess of colon cancer.

But several factors make it difficult to attribute these excesses to formaldehyde. All of these professionals work with a number of chemicals in addition to formaldehyde as well as with human tissue. Moreover, many scientists believe that formaldehyde can react only at the site of contact. Mechanistic studies suggest that it may be nearly impossible for formaldehyde to reach the brain or the blood because it is metabolized quickly to formic acid and then to carbon dioxide and water. Others believe that even if a large proportion of formaldehyde is metabolized, a small fraction of it, perhaps as little as 1%, may escape metabolism and diffuse through the cell membrane to cause DNA lesions as explained previously.

It can take years for a carcinogen to be detected with epidemiological studies, if it is detected at all. Usually the cancer risk level from a certain chemical must be at least twice as high as that seen in the general population for the carcinogenic effect to be clearly discernible. In May 1982, Norton Nelson, former director of the New York University Institute of En-

vironmental Medicine, said in testimony before a congressional subcommittee that "Epidemiological studies must be regarded as a crude and insensitive tool. Only the most violent and intense carcinogens are likely to be detected by epidemiological techniques as normally conducted." He noted that if, for example, formaldehyde causes a 2% excess in lung cancers over the 100 000 fatal cancers a year caused by smoking, these ~2000 cancers from exposure to formaldehyde would be virtually impossible to detect with epidemiological techniques because the background level of cancers from smoking is so high.

A proliferation of possibilities

The dose-response data from the CIIT-sponsored experiment showing that formaldehyde causes nasal cancer in rats are used as the primary basis in constructing risk assessments for the human population. It is here that the possibilities for disagreement proliferate almost exponentially. First of all, a number of different models are employed for estimating risk. Second, different assumptions may be used when choosing the input data for these models. Third, some argue that since we know so little about the biological processes of carcinogenesis, there is no valid reason for choosing one model over another.

As Philippe Shubik, professor at Green College at the Radcliffe Observatory in England, said at the ACS meeting, "It is unequivocally the case that all data in chemical carcinogenesis fit at least several of the mathematical models so far produced.

EPA risk assessment models for formaldehyde give vastly different estimates^a

Exposed population	Number of individuals exposed	Predicted additional cancers/100 000 population ^b						
		Less stringent models			More stringent models			
		Gamma multihit	Additive probit	Multistage 5-stage	Additive logit	Additive Weibull	Multistage 3-stage	"Linearized" multistage ^c
Industrial workers^d								
Manufacturers of:								
Abrasives	7 000	<1(<1)	<1(4)	<1(169)	2(24)	6(47)	12	104
Particle board	4 000	<1(<1)	<1(<1)	<1(49)	<1(4)	<1(11)	<1	27
Resins	6 025	<1(<1)	<1(9)	<1(229)	3(41)	9(71)	29	153
Apparel	777 000	<1(<1)	<1(2)	<1(97)	<1(10)	3(23)	3	56
Residents of:								
New mobile homes	4 200 000	<1(<1)	<1(<1)	<1(25)	<1(2)	<1(5)	<1	14
Conventional homes (non-UFFI) ^e	>100 000 000	n/a	n/a	n/a	n/a	<1(4)	<1	11
Urban areas exposed to ambient air	162 000 000	<1(<1)	<1(<1)	<1(7)	<1(<1)	<1(2)	<1	4
High school students	3 834 000	<1(<1)	<1(<1)	0	<1(<1)	<1(<1)	<1	<1

^a One excess cancer per 100 000 people is equivalent to a risk of 10⁻⁵.

^b The boldfaced numbers in parentheses are the upper 95% confidence limit of the lifetime risk.

^c This model is the upper 95% confidence level of the 3-stage multistage.

^d Only a small sample of the various categories of industrial workers is given.

^e Non-urea-formaldehyde foam insulation.

These different models can result in projected 'safe levels' varying by several orders of magnitude. None of the mathematical models has a sound biological foundation because so much of the biology is inadequate as a basis for detailed mathematical examination."

Those who subscribe to this view, however, could draw two very different conclusions from it. One is that we should choose the most conservative model—the one that provides results that are most protective of the human population—because we do not know enough about carcinogenesis to confidently choose any of the others. The other is that the models are all practically meaningless and that we should therefore employ other evidence to evaluate risk.

A new risk assessment

EPA has prepared a quantitative risk assessment of formaldehyde that is, like most risk assessments of this chemical, based on the dose-response findings obtained by CIIT. Five of the seven models employed in this assessment provide good fits to the rat data. Results from the "3-stage multistage" model do not fit the rat data well, and a goodness-of-fit test is inappropriate for the "linearized multistage" model (which is in fact the upper bound for the 3-stage multistage model). However, some scientists argue that even when a model does not fit the data well at high concentrations, it may at low concentrations, where the data must be extrapolated. In general, the linearized multistage, which is a linear low-dose extrapolation model, provides the highest estimates of risk and can therefore be considered the most stringent model, or the model whose results are most protective of the human population.

When the rat data were used in these models, the average level of formaldehyde exposure was adjusted downward, according to the fraction of the day and the number of days per week the rats were exposed. Therefore, an exposure level of 5.6 ppm was multiplied by 6 h/24 h and by 5 days/7 days, causing 5.6 ppm to equal 1.0 ppm in the models. This calculation could be criticized because there is biological evidence that the effects of formaldehyde depend more on the concentration than on the total dose. For example, a dose of 6 ppm for six hours seems to have much more of an effect on rats than a dose of 1 ppm for 36 hours. Perhaps the most persuasive evidence is a new CIIT study showing that cell replication in rats is nonlinear at different concentrations of for-

maldehyde.

In the EPA risk assessment, risk was estimated for 38 groups, including a number of classifications of workers subject to industrial exposures, residents of new mobile homes, and persons exposed to ambient urban air. The outside observer who happens to read the risk assessment might decide that there are several ways to interpret it. One approach might be to take what are called point estimates of risk (or median estimates) for all seven models and average these. Another might be to consider only the models that provide a good fit to the rat data. A third might be to look only at the median estimates. A final

When the results of the linearized multistage model are examined, most of the groups studied are subject to an unacceptable risk.

method of interpretation might be to look only at the results for the most stringent model—the linearized multistage. Each of these methods of interpretation would produce very different assessments of the risks posed by formaldehyde.

However, the carcinogen assessment group at EPA believes that none of the models is precise enough to be relied on alone. Since the linearized multistage gives an upper bound on the risk, the EPA group has decided that this one is the most appropriate. Therefore, the results of this model were given the most attention in the decision to list formaldehyde as a 4(f) chemical.

To interpret the formaldehyde risk assessment adequately, an upper level of acceptable risk must be defined. EPA does not have a definite cutoff point above which risk is always considered unacceptable, but the agency has a kind of track record. Usually a lifetime cancer risk of less than one excess cancer per 100 000 people is considered acceptable if benefits accrue from incurring this risk. The agency tends to be ambivalent about the region between one and 10 cancers per 100 000 people, though for

most chemicals, risks in this region have been considered unacceptable. Cancer risks greater than 10 cancers per 100 000 have generally prompted regulations.

In the determination of unreasonable risk, EPA considers the number of people at risk as well as the absolute level of the risk. Very large groups with relatively lower risks are usually given more attention than small groups with relatively higher risks.

When the results of the linearized multistage model are examined, most of the groups studied are subject to an unacceptable risk. The risk to manufacturers of resins is the highest—153 additional cancers per 100 000 workers—while the risks for many of the other industrial groups are also quite high. (The additional cancer occurrences for the industrial groups range from seven to 153 per 100 000 people.) High school biology students are subject to the lowest excess risk—less than one in 100 000; residents of new mobile homes and conventional houses are subject to risks generally considered unacceptable—13 per 100 000 (excess risk for an exposure period of ten years) and 11 per 100 000 (for an exposure period of 70 years), respectively.

The risks for each group are very different if the results from most of the other models are examined. Many of the groups that are subject to unacceptable risks with the linearized multistage model are subject to acceptable risks with most of the other models. The upper 95% confidence limit of the Weibull model is the only model that produces results similar to the linearized multistage.

In summary, the new risk assessment offers ample material for controversy. Those who favor the linearized multistage model and the upper 95% confidence limit of the Weibull model could argue that formaldehyde needs to be regulated to protect nearly all groups included in the risk assessment. Those who believe that these models are invalid could argue that formaldehyde presents a significant risk primarily to certain industrial workers.

Others may quarrel with the methods used to derive input data for the assessment or deny the meaning of any of it by arguing that the rat is not a good biological model for man. Clearly, the matter is still not settled. The EPA ultimately will have to decide various science policy questions that cannot at present be answered solely on a technical basis.

—Bette Hileman

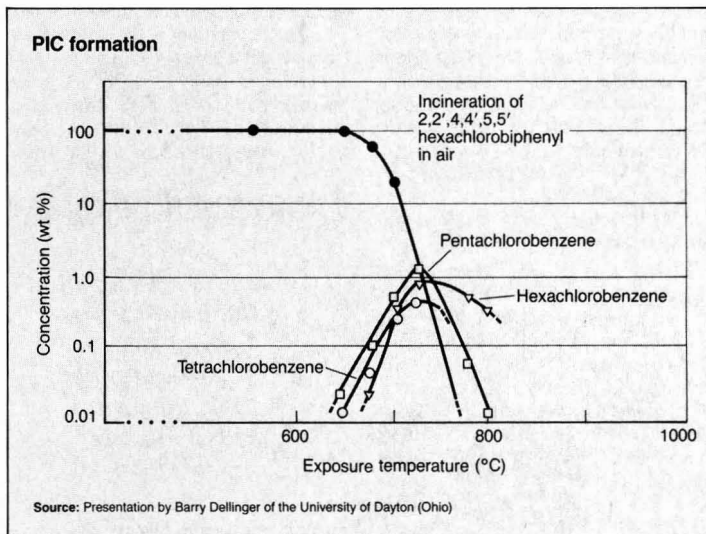
Hazardous waste research

*The present emphasis is on thermal destruction;
other approaches will also be studied*

Where will hazardous waste research take us in the next several years? "Research is called for in the existing law [Resource Conservation and Recovery Act of 1976 (RCRA)], and will certainly be included in any RCRA reauthorization. Amendments to RCRA could determine future directions of hazardous and non-hazardous waste research," predicted Francis Mayo, director of EPA's Municipal Environmental Research Laboratory (MERL, Cincinnati, Ohio). This research might entail safer bulk liquids handling; managing highly hazardous wastes in ways that exclude land disposal; and risk analysis.

David Stephan, director of EPA's Industrial Environmental Research Laboratory (IERL), also in Cincinnati, considered it very important to develop "more cost-effective [management] techniques," if, as appears likely, the upper limit of small-quantity hazardous waste generation is lowered from 1000 to 100 kg/mo. Smaller businesses would need this help. Stephan also saw research increasing in pretreatment before land disposal and various alternatives to land disposal. In the future, attention will be given to more efficient incineration, chemical detoxification processes, and even genetically engineered microbes that could attack specific substances.

These possibilities were discussed at the Tenth Annual Research Symposium on Land Disposal, Remedial Action, Incineration and Treatment of Hazardous Waste. Organized by MERL and IERL, the symposium was held at Fort Mitchell, Ky., in April. It dealt exclusively with EPA-supported activities. One message that seemed to be conveyed to the nearly 1000 participants was that public fears of land disposal—and a mood in Congress sympathetic to those fears—could well lead to a mandated deemphasis on this method and



a greater stress on alternative approaches. Where land disposal is practiced, research would emphasize stronger—perhaps double—site linings and better techniques for groundwater monitoring and protection and leachate sampling and analysis.

The possibility that amendments to RCRA might put more weight on alternatives to land disposal was discussed further by Donald Ehreth, EPA's deputy assistant administrator for research and development. "There will be strong pressures to move from landfilling and surface impoundments to incineration, chemical treatment, and other detoxification approaches. We are proposing to spend \$35 million on hazardous waste research during fiscal year 1985, on top of the \$35 million planned for 1984," he said.

"Four nines"

"The most logical alternative to land-based options in the near future will be combustion," Ehreth observed. "Incinerability of a waste and the efficiency of the burn will be the principal focus of combustion research," because at least "four nines"—99.99%—in the way of destruction and removal efficiency

(DRE) is required. In order to achieve a "four nines" DRE, research addresses two main questions: Exactly what destruction goes on in the flame (the "D" portion of DRE), and how does one ensure that no undesirable materials are emitted (the "R" portion) through the stack to the atmosphere?

Incineration research will be directed toward improving destruction efficiency, even, where possible, when the hazardous wastes are used as a fuel to produce energy while they are being destroyed. Nevertheless, "I hope we don't completely rule out land disposal options, especially where other approaches could pose even greater risks," Ehreth said. "We still need answers on what can and cannot be landfilled, and how to dispose of what can be landfilled properly," he added.

What assures destruction of the hazardous waste material are the "three Ts"—incinerator temperature and turbulence, and residence time. Experiments will be conducted to find what combination of these or other combustion variables will provide the minimum amounts of each necessary to achieve "four nines"; anything in excess of those minima can adversely



Ehreth: "Combustion is the most logical alternative"

affect the economics of a destruction and removal system.

IERL has begun an in-house research program on flame and non-flame thermal destruction at an EPA facility at Center Hill in Cincinnati, Ohio. One objective is to find out how major process variables affect DRE and the formation of unwanted combustion by-products. Another is to test various incineration techniques to determine which improved combustion technologies would be reasonable candidates for upgrading.

George Huffman of IERL mentioned pilot tests about to start at Center Hill. "These include flame mode tests with a 'turbulent-flame reactor' and with a 'controlled-temperature tower' [a refractory-lined reactor providing for turbulence, secondary combustion, and simulated cold walls]. We are running scrubber tests to study the removal part of DRE," he said. "They are being conducted in a packed-bed scrubber for hydrogen chloride control, with activated carbon to ascertain pollutant removal. Gas phase analyses are done with a gas chromatograph-mass spectrometer (GC/MS)."

Another EPA establishment for studying thermal destruction, which reports to IERL, is the Combustion Research Facility (CRF) at Jefferson, Ark., a large pilot-scale facility. Richard Carnes, who manages the facility, said that a principal effort at the CRF is to conduct research to gain a better understanding of residence time and its bearing on permit compliance.

POHCs and PICs

One of the more vexing questions concerning hazardous waste incineration is what to do about the principal organic hazardous constituents (POHCs) in the feedstream, and products of incomplete combustion (PICs). Huffman said that the aim of incineration is not only to destroy all POHCs, but to try to make sure that no harmful levels of PICs result from or are formed during the burn to sub-

sequently escape to the atmosphere. PICs, the more troublesome of the two, are defined as organic compounds *not* in the original waste feed that show up at 100 $\mu\text{g/g}$ of feed or more during and after an incineration run. Andrew Trenholm of Midwest Research Institute (Kansas City, Mo.) told *ES&T* that a problem in determining PICs is that sampling methods "are not yet cast in concrete."

Trenholm described PICs detected during burns at 110–13 000 lb/h of feed at 1400–2650 °F, with a residence time of 0.07–6.5 s, and 60–130% excess air. He noted that the incineration of aniline, for example, could form *o*-nitrophenol, and that a hexachlorobenzene burn produced chlorophenols. Sometimes the total amount of hazardous PICs can exceed the total of the original POHCs, Trenholm warned. He added that PICs can be identifiable fragments of feed constituents; products of complex recombination or substitution reactions *in the flame or the post-flame zone*; or even compounds that enter the incineration process through, say, a leak from the outside, such as ambient air; internal sources, such as auxiliary fuel; or scrubbing liquids.

Barry Dellinger of the University of Dayton (Ohio) addressed research aimed at quantifying and graphically displaying POHC destruction and PIC formation. Gas phase destruction data were obtained in flowing air, with high-temperature zone residence times of 1–6 s. Temperature data were then mathematically adjusted to be expressed in terms of $T_{99.99}(2)$; that is, the temperature at which 99.99% of a substance is destroyed after a 2-s residence time. The analysis was done by GC.

What a graphic display of PIC formation might show is that at a $T_{99.99}(2)$ of 770 °C, the remaining fraction of, say, 2,2',4,4',5,5'-hexachlorobiphenyl would drop abruptly from a given level to zero. But one or more new hazardous compounds could show up, whose "remaining fraction" curves would be shaped like parabolas whose peaks coincide approximately with the temperature at which the original compound disappeared. Apparently, it would take more residence time, higher temperatures, or both to break down these more refractory "daughter" compounds. Dellinger noted that laboratory data indicating PICs should be addressed when the establishment of an incinerator's operating conditions is being considered.

There are other problems with fine particulate matter, hydrogen halide gases, metal aerosols, and the like, which escape the incineration process. Wayne Westbrook of Research Triangle Institute (RTI, Research Triangle Park, N.C.) observed that presently available air pollution control devices cannot handle these materials. He said that RTI and Engineering-Science, Inc., are conducting field tests of new methods such as supersonic steam injection, ionizing wet scrubbers, "advanced" electrostatic precipitation methods, and other such systems. Pilot units are being tested on a slip-stream from ENSCO, Inc.'s, incinerator in El Dorado, Ark.

Biological and chemical methods

The search is on for microbes that can break down hazardous wastes—chlorinated organics are but one example—and then, ideally, "self-destruct" after they have consumed their "food," according to P. R. Sferra of IERL. Gene splicing, plasmid transfer, and selective breeding are some of the ways to develop these microorganisms. Certain modified species of *Pseudomonas*, for instance, seem to show potential as organochlorine compound detoxifiers; that is, they cleave the chlorine from the rest of the molecule at specific positions.

Chemical treatment methods are also being studied. Possibilities include uses of alkalis or glycols that can destroy toluene solutions of polychlorinated biphenyls (PCBs) and dioxins under ambient conditions, according to IERL's Charles Rogers. He added that while such reagents can break down free contaminants, by dehalogenation, for example, it is also necessary to find reliable chemical means of destroying pollutants bound to materials such as soils.

Anil Mehta of the Montana College of Mineral Science and Technology (Butte) noted that toxic electroplating waste sludges that contain heavy metal hydroxides or cyanides can be detoxified with metal recovery. He added that this technique has been demonstrated at the college and is now being tested at a plant in California. Neutralization and oxidation remove the cyanide. Metals can be recovered through solvation and concentration by solvent extraction or anodic stripping reactions. Recovery of metals such as cadmium, chromium, copper, iron, nickel, and zinc may be achieved with the metal in ionic or elemental form.

—Julian Josephson

ES&T PRODUCTS

FT-IR accessory starter kit

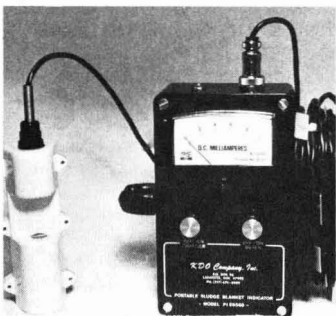
Kit contains all accessories needed for FT-IR sampling of gases, liquids, and solids by pollution control chemists. The accessories include two FT-IR demountable holders, 12 KBR windows, KBR handi-press and three dies, KBR die pellet holder, magnetic pellet holder, and a number of other items. Spectra-Tech **101**

Countertop baths and circulators

Microprocessor-controlled countertop baths and circulators are available in three sizes. The temperature range and ramping increments are selected on the push-button control panel. The ramp rate is programmable in increments of 1 °C/h. Forma Scientific **102**

In situ water sampler

Sampler concentrates organics and heavy metals in situ from fresh and seawater onto specially designed extraction columns. It can be moored for days or weeks to obtain an integrated sample. The sampler is totally self-contained and microprocessor controlled. Seastar Instruments **103**



Sludge blanket indicator

This unit provides quick and accurate measurements of sludge depths and volumes in settling and flotation tanks. The indicator is hand-held and measures a resistance drop across a photo-sensitive cell. It has a wide sen-

Need more information about any items? If so, just circle the appropriate numbers on one of the reader service cards bound into this issue and mail in the card. No stamp is necessary.

sitivity range so that it can be used both in clear and in turbid waters. KDO Company **104**

Closed-loop stripping analysis

System rapidly analyzes purgeable organics in drinking and wastewater. It incorporates capillary GC and GC/MS and is ultrasensitive, especially in the 1–10 ng/L range. Charcoal is used as an absorbent instead of Tenax. Erba Instruments **105**

Mini bore-hole water sampler

Water quality sampler was designed for the International Atomic Energy Agency to monitor groundwater pollution. It can be used in bore holes with diameters as narrow as 2 in. and can obtain a 1-L sample of liquid without contaminating it. Kahl Scientific Instrument **106**

Continuous monitoring system

Instrument monitors steel underground storage tanks with secondary containment. It consists of an automatic leak alarm and a remote monitor that connects to the tank's secondary containment system. The system may also include an optional liquid level gauge and a corrosion potential meter for measuring the tank's protective coating. Clawson Tank Company **107**

Chemistry measurement system

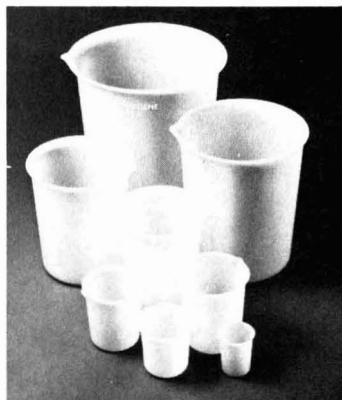
By changing plug-in modules, the microprocessor-based mainframe becomes a pH meter, a dissolved-oxygen meter, a conductivity meter, or an ion concentration meter. Plug-in module 2007 measures pH with a resolution of 0.01 and an accuracy of ± 0.005 pH. Module 2008 measures dissolved oxygen in percent saturation or ppm. Other modules measure conductivity and ion concentration. Solomat **108**

Monochromator and filter holder

A new filter holder has been added to Kratos's monochromator to eliminate higher order wavelengths that are multiples of the selected wavelengths. Optical filters can be placed in the filter holder to block off interfering wavelength regions. Kratos Analytical Instruments **109**

Underground tank

Fiberglass tank collects surface water from landfills and stores it until the leachate can be pumped out and discharged properly. It has a 10 000 gal capacity and is equipped with a 22-in. manway, an internal ladder, and an internal fill tube. Lifetime Fiberglass Tank **110**



ECTFE beakers

Beakers made of ethylene-chlorotrifluoroethylene (ECTFE) copolymer have a chemical resistance nearly identical to those made of Teflon. They are durable, rigid, and resistant to strong oxidizing acids and a wide range of organic solvents. They can be used at temperatures from -100 °C to $+150$ °C and can be autoclaved repeatedly. Nalge **111**

Portable sample generator

Parts-per-million sample generator provides a continuous gas sample of $\pm 2\%$ accuracy. It can be used with any gas or combination of gases. It operates by volumetric dilution, using a sample injection valve with a fixed port size. Unaffected by temperature changes, it has no decay factor and allows no sample deterioration resulting from pre-preparation. Tracor Atlas **112**

Companies interested in a listing in this department should send their resumes directly to Environmental Science & Technology, Attn: Products, 1155 16th St., N.W., Washington, D.C. 20036

ES&T LITERATURE

Water and wastewater filtration. Bulletin HC-100 describes the Hydro-Clear pulsed-bed, single-medium, shallow profile design filter for water and wastewater filtration. The filter can handle high solids loadings. Zimpro 151

PCB screening. Brochure describes a kit that can screen for the presence of polychlorinated biphenyls on-site, within 4 min. It is normally used to assure the presence of <50 ppm PCBs. Dexsil Chemical 152

Chlorine detector. Brochure PDS-5300AUX describes Model 5324 analyzer and transmitter system, which detects ambient chlorine. The system is equipped with a multiplexer. Delta Analytical 153

Environmental standards. Catalog lists kits that contain standards and standard mixtures for performing analyses according to EPA methods and consent decree protocols. PCBs, pesticides, dioxins, furans, and other standards are available. Ultra Scientific 154

Respirators. Guide contains the latest technical and TVL/TWA information on more than 500 airborne contaminants. These data aid in the selection of the correct respirator for a given situation. HSC 155

Groundwater cleanup. Brochure sets forth company services for evaluating and abating groundwater contamination, including risk management, hydrocarbon stripping, and other clean-up procedures. Oil Recovery Systems 156

Groundwater technology. Brochure outlines a field practice program in groundwater technology entailing a full five-day course and a 17-member instructional staff. Department of

Need more information about any items? If so, just circle the appropriate numbers on one of the reader service cards bound into this issue and mail in the card. No stamp is necessary.

Geological Sciences, Wright State University, Dayton, Ohio 45435 (write direct)

Hazardous waste. Article by EPA Region 3 Administrator Thomas Eichler is entitled "The Status of the Hazardous Waste Management Program in the Middle Atlantic States." George V. Bochanski, Jr., Office of Public Affairs, U.S. EPA Region 3, 6th and Walnut Sts., Philadelphia, Pa. 19106 (write direct)

The water industry. Brochure announces survey of how exhibitors at the Water Pollution Control Federation's 56th Annual Conference and Exposition (Atlanta, Ga., Oct. 2-5, 1983) fared in developing markets. Water Pollution Control Federation, 2626 Pennsylvania Ave., N.W., Washington, D.C. 20037 (write direct)

Waste site liners. Brochure describes Poly-Flex, a line of polyethylene geomembranes for lining hazardous waste sites. The membranes feature high chemical resistance. Wynn Alterman, Poly-America Inc., 23 Dellforest Court, The Woodlands, Tex. 77380 (write direct)

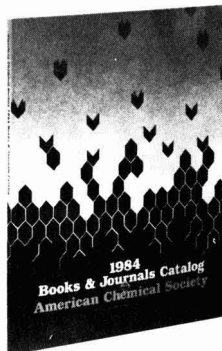
Standard reference materials. Catalog SP260 lists more than 900 standard reference materials, many environmental, Office of Standard Reference Materials, B311 Chemistry Bldg., National Bureau of Standards, Washington, D.C. 20234 (write direct)

Indoor air quality. Information sheet announces "Manual on Indoor Air Quality," available for \$13 (\$26 overseas). EPRI publication EM-3469. Research Reports Center, Electric Power Research Institute, P.O. Box 50490, Palo Alto, Calif. 94303 (write direct)

Companies interested in a listing in this department should send their releases directly to Environmental Science & Technology, Attn: Literature, 1155 16th St., N.W., Washington, D.C. 20036

FREE! FREE! FREE! 1984 Books & Journals Catalog

from the
**American
Chemical Society**



- More than 400 books, including 39 new ones listed for the first time
- All ACS periodical publications
- Royal Society of Chemistry books

Use the coupon below or call the ACS Sales Office toll free 800-424-6747 to request your free 1984 catalog today.

Rush me a free copy of the **1984 American Chemical Society Books and Journals Catalog.**

Name _____

Address _____

City _____ State _____ Zip _____

Mail coupon to:

Sales Office
American Chemical Society
1155 Sixteenth Street, NW
Washington, DC 20036

Cenref Labs

P.O. BOX 68, BRIGHTON, CO 80601
(303) 659-0497

ENVIRONMENTAL TESTING

GC/MS • PSD • PCB'S
RCRA • NPDES
STACK TESTING



nanco labs, inc.
"The Complete Testing Laboratory"

**Nation's Best Price/Performance
GC/MS Facility**

Unity Street at Route 376, P.O. Box 10
Hopewell Junction, NY 12533
NY Phone (914) 221-2485
Elsewhere (800) 22NANCO

Clayton Environmental Consultants

- Industrial Hygiene Surveys
- AIMA - Accredited and CDC - Licensed Laboratories
- GC/MS, HPLC, X-Ray Diffraction, AA, and Electron Microscopy (SEM/EDS)
- Hazardous Waste Management
- Emission and Ambient Air Surveys
- Engineering Design
- Environmental Audits
- Materials and Material Safety Data Sheets
- Expert Testimony

25711 Southfield Rd • Southfield, MI • 48075 • 313 424 8860

Atlanta, GA • Edison, NJ • Windsor, Ont.
(404) 952-3064 • (201) 225-6040 • (519) 255-9797

A Technical Service of Marsh & McLennan

Complete Analytical Services

SINCE 1919

- Screening of Industrial Waste for EPA Priority Pollutants using Finnigan OWA-30 GC/MS
- NPDES & SPDES Organic & Inorganic Testing
- Drinking Water Analysis to EPA Standards
- Bioassay, Bioaccumulation & Toxicity Studies of Industrial Waste, Municipal Sludge & Dredge Spoils
- Leachate Potential Studies & Analysis
- Total Instrumental Analysis: A.A., GC/MS, G.C., I.R., TOC & TOD
- RCRA Hazardous Waste Testing

NEW YORK TESTING LABORATORIES
81 Urban Avenue, Westbury, N.Y. 11590
(516) 334-7770

ENVIRODYNE ENGINEERS

a consulting engineering and sciences firm

- environmental engineering
- analytical chemistry
- priority pollutant analyses
- environmental monitoring and assessment
- hazardous waste monitoring
- hazardous waste management
- transportation engineering
- energy engineering
- construction management

12161 Lackland Road
St. Louis, Missouri 63141
(314) 434-6960

Baltimore / Chicago / New York

MAIN 1893

Complete Environmental and Engineering Services

THE C.T. MAIN CORPORATION

OFFICES WORLDWIDE
CORPORATE HEADQUARTERS
PRUDENTIAL CENTER, BOSTON, MA 02199
617-262-3200

Scott Environmental Technology, Inc.

COMPREHENSIVE
AIR POLLUTION SERVICES

- ★ Source and Ambient Monitoring
- ★ Hazardous Incinerator Testing
- ★ Continuous Monitor Certification
- ★ Dispersion Modeling
- ★ Auto Emissions Testing

Route 611, Plumsteadville, PA 18949
(215) 766-8861

CONSULTING GROUND-WATER GEOLOGISTS

ROUX ASSOCIATES INC

- RCRA Monitoring
- Superfund Response
- Site Evaluation
- Aquifer Clean-Up
- Resource Development

50 NORTH NEW YORK AVENUE
HALESITE, NEW YORK 11743 516 673-4921

500 PURDY HILL ROAD
MONROE, CONNECTICUT 06468 203 268-2846

The Professionals

ENTROPY

Environmentalists Inc.
Leaders in Source Testing, Continuous Monitor
Certification, and Hazardous Waste Testing
P.O. Box 12291 Research Triangle Park, NC 27709
In NC 919-781-3550 Outside NC 1-800-ENTROPY

DUNN GEOSCIENCE

Albany, New York 518/783-8102
Harrisburg, Pennsylvania 717/761-6710
New York, New York 212/772-0651
Buffalo, New York 716/884-1500

GEOLOGIC AND HYDROLOGIC CONSULTANTS

- Ground Water Assessment & Supply
- Solid & Hazardous Waste Site Studies

Laboratories

EPA Drinking Water Stds. & Priority Pollutants
Haloforms, PCB's—Gases, TOC, Solid Waste
Extractions, Heavy Metals

4100 Pierce Road (805) 327-4911
Bakersfield, California 93308

ENVIRONMENTAL SCIENCE, TECHNOLOGY, AND ENGINEERING.

ECOLOGICAL ANALYSTS

Hunt Valley Loveton Center, 15 Loveton Circle, Sparks, MD 21152 • 301-771-4959
Baltimore • Chicago • Cincinnati • Lincoln • New York • San Francisco

Classified Section HAZARDOUS WASTE OPPORTUNITIES

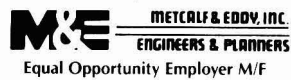
Metcalf & Eddy, Inc., a leading environmental engineering firm, has immediate and future openings for Engineers and Scientists in the following disciplines:

- Environmental Engineering
 - Groundwater/Geology
 - Risk Endangerment
 - Chemical Engineering
 - Industrial Safety Engineering
- Metcalf & Eddy offers a salary commensurate with experience and a comprehensive benefits package which includes profit sharing, stock ownership and a thrift plan.

If you are interested in joining an established firm that is developing a leadership position in a challenging new market, please send your resume to:

East Coast Address:
Metcalf & Eddy, Inc.
Judith April Horgan
50 Staniford Street,
Boston, MA 02114

West Coast Address:
Metcalf & Eddy, Inc.
Edward T. Burns
1029 Corporation Way
Palo Alto, CA 94303



FACULTY POSITION IN ENVIRONMENTAL SCIENCE

Applications are invited for a tenure-track research/teaching position for the Fall of 1984. A Ph.D. is required. The successful candidate is expected to teach one graduate environmental science course per semester while serving as Principle Investigator on a two-year research grant performing water quality analyses for a River/Estuarine complex environmental assessment study. Following completion of the research phase, the individual will become a full-time member of the faculty. Appointment rank and salary are negotiable and commensurate with experience and qualifications. Available August 1, 1984. Send resume and letters of recommendation to Dr. L. Harold Stevenson, Department of Biological and Environmental Sciences, McNeese State University, Lake Charles, Louisiana 70609. McNeese is an Affirmative Action, Equal Opportunity Employer.

ENVIRONMENTAL SCIENTIST/ENGINEER

Candidates for this position must have a PhD degree in Environmental Sciences/Engineering and demonstrated experience in atmospheric pollutant transport and transformations, hazardous substances disposal practices, multimedia environmental monitoring methods (including geophysical methods), and health physics (radiation).

Send resume and salary history to:

**Dr. David N. McNelis, Director
Environmental Research Center
University of Nevada
Las Vegas, Nevada 89154**

Closing Date: July 15, 1984.
The University of Nevada is an EOE.

GRADUATE FELLOWSHIPS AND ASSISTANTSHIPS

— Appointments for engineers and scientists as M.S. candidates in our Environmental Engineering Science Master's Program (Hazardous & Toxic Waste Option). Starting September 1984 at stipends of \$6000-10,000 including summer and tuition remission. For further information, contact Dr. Richard Trattner, Director of Academic Programs, Institute for Hazardous and Toxic Waste Management, New Jersey Institute of Technology, Newark, New Jersey, 07102 (201-396-3555).

Copper and Cadmium Uptake by Estuarine Sedimentary Phases

Robert J. Davies-Colley,[†] Peter O. Nelson,* and Kenneth J. Williamson

Civil Engineering Department, Oregon State University, Corvallis, Oregon 97331

■ An understanding of the distribution of toxic trace metals and other materials of environmental interest among the different sedimentary phases is necessary to assess the hazard associated with pollution of aquatic sediments. A simple model, analogous to speciation in solution among soluble ligands, was developed to enable the distribution of metals within sediments to be estimated. The model requires the conditional metal binding constants (slopes of the linear portions of the adsorption isotherms) to be evaluated for a small number of model sedimentary phases in isolation, as well as knowledge of the composition of the sediment and water. The model has been applied to the distributions of copper and cadmium in estuarine sediments and predicts that iron and organic matter are the sedimentary constituents of greatest importance for these metals. Manganese phases may contribute to cadmium binding, but clay minerals and (probably) aluminosilicates are insignificant sinks for both copper and cadmium. The model predictions for copper and cadmium in estuarine sediments are in good semi-quantitative agreement with the results of selective extraction studies on natural sediments reported in the literature and studies reported here of cadmium uptake by natural sediments.

Introduction

Sediments are the major compartment in the estuarine environment for trace metals and other toxic materials. Thus, an understanding of the interaction of such materials with sedimentary phases is necessary to assess ecological impacts. The most common approach to examining the phase associations of metals in aquatic environments is by application of so-called "selective extraction" sequences (1-3) to sediments and associated waters. The sediment samples are subjected to a sequence of physical or chemical procedures that extract one or more sedimentary components (or the materials bound to those components) at each step. Severe problems are encountered with the use of chemical extraction schemes with natural sediments for examining trace metal distributions because there is always a tradeoff between *selectivity* (for the target phase) and *efficiency* (proportion of metals extracted from that phase) at each selective extraction step (1, 4). Furthermore, metals extracted from one phase may adsorb on the other phases present (4, 5).

A more useful approach to the problem of phase association of metals in sediments may be to estimate metal distribution from the known composition of the sediments and the measured affinity of each of the constituent phases for the metals (6). This was the approach adopted in the present study for examining the behavior of the toxic metals copper and cadmium in estuarine environments. The study was confined to consideration of surface (adsorption) reactions since that fraction of the total metal which is incorporated into mineral lattices is most unlikely to have any ecological significance. The study involved performing simple adsorption experiments with model sedimentary phases in order to calibrate a model (outlined below) for metal partitioning among competing constituent phases in (aerobic) sediments. Predicted copper and cadmium distributions in aerobic estuarine sediments are then compared with the general pattern of results of reported selective extraction studies (1-8) and with some direct measurements of uptake by natural sediments reported here.

Model for Trace Metal Distribution in Estuarine Sediments

Since "trace" metals (by definition) are present at low concentrations, binding sites on surfaces of sedimentary phases are in great excess, and adsorption is independent of metal concentration. This greatly simplifies analysis of metal distributions since the mass balance for all the surfaces and ligands can be neglected and only the mass balance on the metal need consideration.

Oakley et al. (9) have presented a simple model for the partitioning of a trace metal among a number of different phases comprising an aerobic sediment. The model is analogous to solution phase metal speciation in a single-metal multiple monodentate ligand system. It is assumed that all the sedimentary phases behave independently; i.e., metal uptake by each phase depends only on mass concentration of that phase and not on state of dispersion or interaction with other phases.

Consider a sediment comprised of N phases at any degree of dispersion (whether settled or suspended). The dimensionless concentration of the n th phase, F_n , is given as

$$F_n = \frac{\{S_n\}}{TS} = \frac{\{S_n\}}{\sum_{n=1}^N \{S_n\}} \quad (1)$$

where TS is the total solids content of the sediment slurry

[†]Present address: Water and Soil Division, Ministry of Works and Development, Hamilton, New Zealand.

Table I. Ranges of Concentration of Selected Sedimentary Phases in Aerobic Estuarine Sediments

component	concentration, % dry weight		model phase
	typical range	average	
(1) hydrous iron oxides (as iron)	1-5	2	synthetic ferrihydrite
(2) hydrous manganese oxides (as manganese)	0-0.2	0.02	synthetic birnessite
(3) clay minerals (<2- μ m fraction)	0-30...70?	5?	Wyoming montmorillonite
(4) "extractable" SiO ₂ + Al ₂ O ₃	?	?	synthetic aluminosilicate
(5) organic matter (about 50% humic)	0-10	4	estuarine humic substances (EHS)

and $\{S_n\}$ is the concentration of the n th phase. The metal binding constant for the total sediment is defined as

$$K_{tot} = \frac{[Sed-M]}{M_{TS} \sum_{n=1}^N \{S\}} \quad (2)$$

where $[Sed-M]$ represents the concentration of total sediment-bound metal and M_{TS} is the total solution phase metal. The metal binding constant for the n th individual phase is defined as

$$K_{p,n} = \frac{[S_n-M]}{M_{TS}\{S_n\}} \quad (3)$$

Since $[Sed-M]$ is the sum of the concentration of metal bound to the N individual phases comprising the sediment, we can restate eq 2 as

$$K_{tot} = \frac{\sum_{n=1}^N K_{p,n} M_{TS} \{S_n\}}{M_{TS} \sum_{n=1}^N \{S_n\}} = \sum_{n=1}^N K_{p,n} F_n \quad (4)$$

Equation 4 allows the binding constant for adsorption on the total sediment to be predicted from data for isolated model phases and also permits a comparison of the proportional contribution of the different phases to the total sediment capacity for uptake of trace metals.

Selection of Model Sedimentary Phases

Aerobic sediments are composed of a number of geochemical phases all of which are possible sinks for trace metals and other materials of environmental concern (10). These phases include metal oxides, phyllosilicates (clays), other aluminosilicates, organic matter, and metal carbonates. The selection of model geochemical phases for experimentation is summarized below and detailed elsewhere (19).

Of the metal oxides occurring in estuarine sediments, the poorly ordered, amorphous forms of iron and manganese are typically present in the greatest quantities and are likely to be involved in metal binding (10). Poorly crystallized hydrous oxides of iron referred to as "ferrihydrite" (12), and manganese, referred to as "birnessite" (13), were synthesized in the laboratory for use in adsorption experiments.

The crystalline clay minerals, especially of the smectite group, have often been suggested as important sinks for trace metals because of their high cation-exchange capacity and high specific surfaces (10). Wyoming Montmorillonite (SW-1) obtained from the Clay Mineral Society (14) was used as a model phase.

The contribution of sand or coarse, silt-sized, silicate grains of relatively low specific surface area to metal binding per se is minimal. Of greater importance may be aluminosilicate gel coatings of clay minerals similar to allophane (10). To model such materials, an amorphous aluminosilicate was synthesized in the laboratory (15).

The largest single component of organic matter in aquatic sediments is the brown-colored, high molecular weight, polymeric, and acid humic material (16, 17). To model the organic metal-binding capacity of estuarine sediments, humic substances were directly obtained from natural estuarine sediments by base extraction (16).

The metal carbonates were not considered because in estuarine sediments this fraction is mostly biogenic in origin and occurs as relatively large shell fragments with low specific surface areas which are commonly coated with organic matter (11) and thus are unlikely to be available for metal binding.

Table I lists the model sedimentary phases chosen to represent various estuarine sediment components and also indicates ranges and approximate average concentrations of sediments components reported in the literature (19).

Sedimentary phases, particularly where present in colloidal-sized particles, tend to occur in intimate association. Hydrous iron and aluminum oxides are often close to their isoelectric points at environmental pHs and act as bridges in binding together the other negatively charged and mutually repelling phases (20).

Association of two solid phases might be expected to reduce the availability of metal-binding sites on both surfaces. To gain some insight into this possibility, adsorption experiments were performed with three types of solid phase complexes: (i) iron-hydroxy interlayered montmorillonite; (ii) humic-coated ferrihydrite; (iii) a ternary clay-iron-humic complex.

Methods

Preparation and Characterization of Model Phases.

A synthetic ferrihydrite phase was manufactured by the slow neutralization with stirring of a 5×10^{-3} M Fe(III) solution in 0.1 M NaNO₃ with 0.1 M NaOH, largely following the procedure of Davis & Leckie (21). The synthetic birnessite was produced by combination of stoichiometric quantities of reactants to give a final 5×10^{-3} M Mn(IV) suspension according to the reaction (22)



A BET analysis applied to water adsorption data on freeze-dried preparations (19) gave specific surfaces of 250 ± 30 m²·g⁻¹ for birnessite and 300 ± 50 m²·g⁻¹ for ferrihydrite. Both preparations were X-ray amorphous, lacked definite morphology under the electron microscope, and were totally extractable in acid ammonium oxalate reagent (12). The synthetic birnessite was found to have a non-integral stoichiometry, MnO_{1.96}, similar to results of other studies (22).

The Wyoming Montmorillonite (SWy-1) (14) was saturated with Na⁺ and then dialyzed against distilled water to remove salt. The <2- μ m equivalent spherical diameter clay fraction was obtained by allowing coarser material to settle from a dispersed, 2% suspension. The synthetic aluminosilicate gel was manufactured by a method similar to that of Hem et al (23). A 3×10^{-2} M Al(III) solution

as nitrate was combined with a stoichiometrically equivalent quantity of silicate solution at a pH of 2.3. This solution was then neutralized slowly with NaOH while being stirred continuously. The suspension of white flocs was aged with intermittent agitation for 1 month before use. The resulting X-ray amorphous gel had a Si:Al molar ratio of 0.83:1.

Humic material was extracted from an estuarine sediment sample obtained from a tidal flat in Yaquina Bay on the Oregon Coast (19). Six 24-h extractions with 0.5 M NaOH under N₂ were performed (16, 24). The combined raw extractants were then acidified to pH 2.2 and run through columns of Amberlite XAD-8 resin (Rohm and Haas, Philadelphia). Purified humic material was eluted with 3 bed volumes of 0.1 M NaOH and then batch reacted with 3 times with strong acid ion-exchange resin in the H⁺ form (to remove sodium) before being concentrated further on a rotary evaporator at 35 °C and freeze-dried. The resulting material, henceforth referred to as estuarine humic substances (EHS), was a dark brown, fluffy solid with a 49% carbon content. The infrared spectrum was typical for a humic substance (16). Ultrafiltration experiments suggested that 50% of the material was nominally above 30 000 in molecular weight.

Hydroxy-iron interlayered montmorillonite complexes were synthesized at three different iron:clay ratios corresponding to 1, 4, and 16 m mequiv of Fe(III)/g of clay by using the method of Tullock and Roth (25). The continuously stirred montmorillonite suspension was titrated to pH 2.5, combined with a standard solution of Fe(III) also at pH 2.5, and then slowly neutralized. The presence of poorly ordered iron-clay complexes was demonstrated by X-ray diffraction following Carstea et al. (26). Iron-organic complexes of 1:12, 1:2, and 3:1 organic carbon to iron ratios (by weight) were synthesized in seawater, allowing EHS to adsorb onto preformed synthetic ferrihydrite. The EHS solution was observed to become rapidly decolorized when added to (unstirred) ferrihydrite. Experiments utilizing the "soluble" (not sedimented after 20 min of centrifuging at 20000g at near-neutral pHs) fraction of the EHS demonstrated that the ferrihydrite could adsorb more than its own weight of humic matter (19). A ternary clay-iron-organic complex was also synthesized for use in metal uptake experiments by simply adding EHS to a previously reacted mixture of iron and montmorillonite. In this complex which mimics the likely phase association of organics, iron, and clay minerals in sediments, the humic macromolecules are probably adsorbed onto the external iron-coated clay mineral surfaces.

Adsorption Experiments with Inorganic Phases.

The prepared solids were dispersed in artificial seawater, usually of either 35 or 5‰ salinity. The suspensions were dispensed volumetrically into Oak Ridge type centrifuge tubes, and pH was adjusted in the range 6–8.5 with microliter additions of NaOH or HCl. Known volumes of copper or cadmium solutions prepared from analytical standards and spiked with the γ -emitting tracers ⁶⁴Cu and ¹⁰⁹Cd were then added. Final concentrations of metal in the reaction tubes were in the range 2.8–140 $\mu\text{g}\cdot\text{L}^{-1}$. Thermodynamic calculations confirmed that fresh precipitates of copper and cadmium solid phases would not be supersaturated under the experimental conditions.

The capped centrifuge tubes were shaken in a constant temperature room (20 °C) for 20 h. After equilibrium the pH was measured with a Corning semimicroelectrode connected to an Orion 701A meter. The tube contents were then stirred with a vortex mixer, and a subsample was dispensed by volumetric pipet into counting vials for

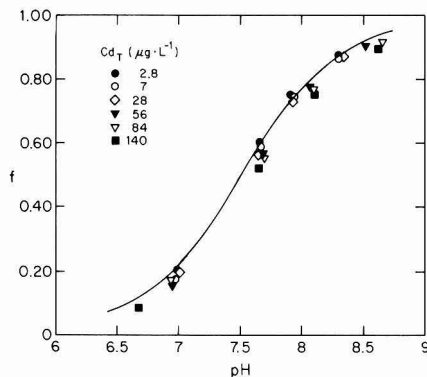


Figure 1. Fractional adsorption vs. pH for cadmium uptake by hydrous iron oxide in artificial seawater.

assay of total tracer activity. The solid phase was separated by centrifuging for 20 min at 20000g, and a subsample of the supernatant (same volume as taken for total activity) was taken for assay of solution-phase activity. The tracer activities in the subsamples were counted with a Picker Autowell II gamma detector, and fractional adsorption, f , was calculated as the ratio $(N_T - N_S)/N_T$ where N_T is the total activity and N_S is the solution phase activity, both counts being corrected for background. The binding constant at the measured pH in each tube is then given as

$$K_p = \frac{f}{(1-f)\{S\}} \quad (5)$$

where $\{S\}$ is the solid phase mass concentration.

An essentially identical procedure was used for measurement of metal uptake by natural sediment suspensions.

Metal Binding Experiments with EHS. The EHS could not be satisfactorily separated from seawater by centrifuging so other methods of measuring metal binding by organics were employed. A techniques similar to that used for inorganic phases was applied to cadmium binding by EHS except that the humic material was separated from seawater by ultrafiltration. The method did not work for copper because of sorption losses on the membrane.

Copper binding by the EHS was studied by using a potentiometric titration method. The EHS sample (in seawater) was contained in a polyethylene beaker immersed in a thermostated water bath (20 °C). Magnetic stirring of the sample was maintained throughout the titration, and the pH was kept constant (± 0.1 unit) by microliter additions of acid or base. The potential of an Orion 94-29 cupric ion electrode relative to an Orion double junction reference electrode was used to measure total solution phase ("unbound") copper by reference to potentials generated in a 100 $\mu\text{g}\cdot\text{L}^{-1}$ copper standard made up in seawater at pH 5. After each addition of a microliter quantity of copper, at least 20 min was allowed for reaction before potential readings were taken on an Orion 701A digital voltmeter. The binding appeared to be a very fast reaction (minutes), but the electrode response was sluggish at low copper concentrations, and at least 40 min was required for stabilization of drift below 40 $\mu\text{g}\cdot\text{L}^{-1}$ Cu_T.

Results of Metal Uptake Experiments with Model Sedimentary Phases

Adsorption Experiments with Isolated Solid Phases. Figure 1 shows typical results of an adsorption experiment with inorganic phases. Fractional adsorption, f , of cadmium on ferrihydrite in 35‰ seawater is plotted

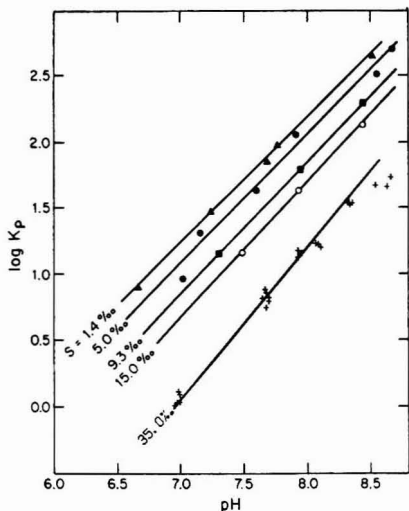


Figure 2. $\log K_p$ vs. pH for cadmium uptake by hydrous iron oxide in artificial seawater at different salinities.

vs. pH for a range of total cadmium concentrations. The adsorption curve has the typical S shape (27, 28) and rises steeply from 10 to 90% over only 2 pH units. Fractional adsorption is nearly independent of cadmium concentration over the range investigated.

To test the possibility that salinity may influence adsorption of cadmium, an experiment was performed with ferrihydrite in artificial seawater diluted to give a range of salinities. Figure 2 shows adsorption data for a range of salinities, including the 35‰ salinity data from Figure 1, plotted as $\log K_p$ vs. pH ($[S]$ is expressed as Fe in $g \cdot L^{-1}$). The adsorption data at a given salinity fall on a straight line with a slope of approximately unity. Evidently salinity has a pronounced effect on cadmium sorption such that there is more than a 10-fold decrease in K_p going from 5 to 35‰ salinity. Since cadmium is strongly complexed by the chloride ion while there is ample evidence that chloro complexes of metals have very little if any tendency to adsorb to oxidic surfaces (21), it seems probable that the effect of salinity on cadmium adsorption is largely the effect of chloride competing with the surface for available cadmium. Indeed speciation calculations (19) suggested that concentrations of free cadmium ion (Cd^{2+}) as a proportion of total solution cadmium changed from about 2.8% at 35‰ to about 21% in 5‰ salinity seawater which is sufficient to explain most of the salinity effect on adsorption. (Other consequences of salinity change may also have an effect: change in ionic strength and thus ionic activities and change in surface charge.)

Figure 3 shows results of copper titration experiments with $20.03 \text{ mg} \cdot L^{-1}$ EHS in 35‰ salinity seawater plotted according to the (modified) Scatchard equation

$$[EHS-Cu]/Cu_{TS} = K_i(n_i[EHS] - [EHS-Cu])$$

where $[EHS]$ is the concentration of humic material ($mg \cdot L^{-1}$), $[EHS-Cu]$ is humic-bound copper (μg of $Cu \cdot L^{-1}$), K_i is the binding constant of the i th site type, and n_i is the total copper binding capacity of the i th site type in milligrams of copper per gram of EHS. The Scatchard plots at the three different experimental pHs are highly nonlinear, indicating the presence of more than one type of copper binding site as has been observed for humic materials by other workers (29, 30). The first two binding constants K_i ($i = 1, 2$) at each pH were estimated by the

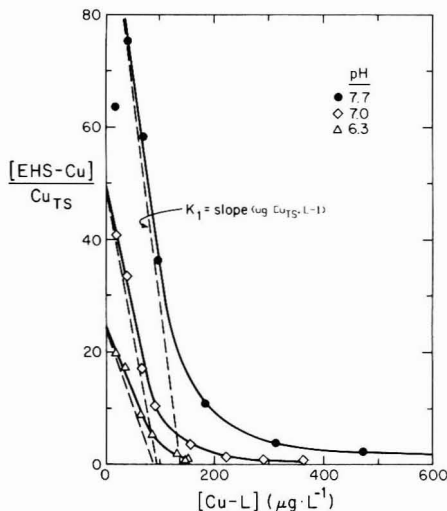


Figure 3. Scatchard plots of Cu electrode titration data for copper binding by EHS.

Table II. Summary of Scatchard Analyses for Copper Binding by EHS in Artificial Seawater^a

pH	$\log K_1^b$	$\log K_{p1}$	n_1 , mg· g^{-1}	$\log K_2^b$	$\log K_{p2}$	n_2 , mg· g^{-1}
6.3 ± 0.1	7.24	3.09	4.51	5.94	1.64	3.17
7.0 ± 0.1	7.53	3.40	4.62	5.75	1.92	9.27
7.7 ± 0.1	7.68	3.71	6.80	5.56	2.15	24.5

^aRegression lines: $\log K_{p1} = 0.443 \text{ pH} + 0.30$; $\log K_{p2} = 0.364 \text{ pH} - 0.65$. ^bExpressed in terms of total solution phase copper, Cu_{TS} , rather than free copper ion, $[Cu^{2+}]$. The $\log K$ values would be higher by the value of $p\alpha_0$ at the given pH if they were expressed in terms of free copper.

method of Bresnehan et al. (30) and are given in Table II. Also given in this table are the values of $\log K_p$ corresponding to the two site types and calculated from $K_{p,i} = n_i K_i$. $\log K_p$ appears to be a linear function of pH, and regression lines in Table II give the calculated relationship. The $\log K_i$ values obtained in this study are about average compared with reported values (usually in the range 7–9 log units (31)), and the pH trend is also consistent with other studies.

Cadmium adsorption experiments were performed with phases other than ferrihydrite (discussed above) at 5‰ and 35‰ salinity, and plots similar to Figure 2 were prepared for the range of metal concentrations over which the adsorption isotherm was linear. Copper adsorption was found to be rather insensitive to salinity, and experiments were confined to 35‰ artificial seawater with the exception of the synthetic birnessite. Figures 4 and 5 present the regression lines for all the metal binding experiments with isolated phases in 35‰ salinity seawater and serve to summarize the results. The figures allow comparisons between the phases as to their specific affinities for cadmium and copper (measured by K_p) and the pH dependence of this affinity (measured by the slope of the lines). The regression lines for cadmium uptake in 5‰ salinity seawater are not presented since the pattern is very similar to that in Figure 4 but with all lines shifted upward (K_p higher by a factor of approximately 10). The order of specific affinity for cadmium remains as hydrous manganese oxide > hydrous iron oxide > estuarine humic sub-

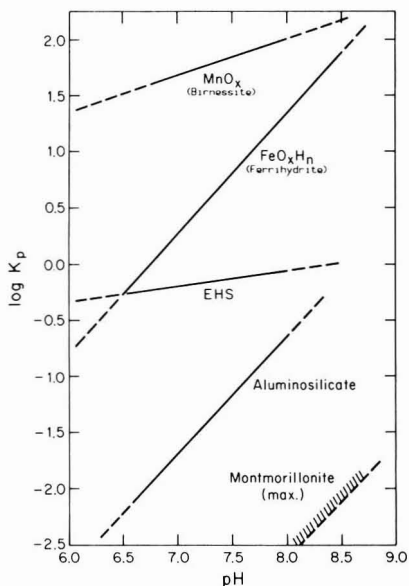


Figure 4. Comparison of the specific affinity of model solid phases for cadmium in 35‰ artificial seawater.

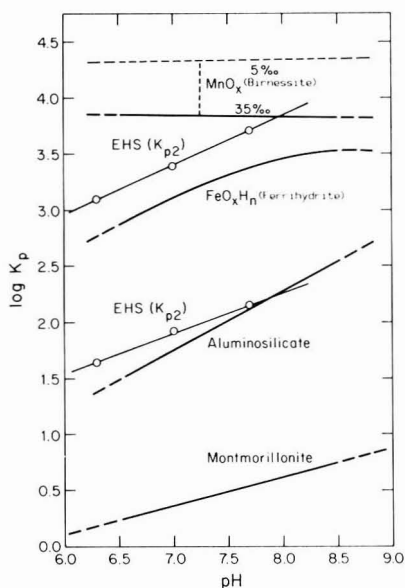


Figure 5. Comparison of the specific affinity of model solid phases for copper in 35‰ artificial seawater.

stances > aluminosilicate > montmorillonite. Only an approximate upper bound can be given for montmorillonite in 35‰ seawater (Figure 4) since the cadmium uptake by this phase was barely measurable even in a solid suspension at a solid concentration of 35 g·L⁻¹ in which the viscosity was too great to be sure that mixing was achieved. The specific affinity of the five phases for cadmium varies over more than 4 orders of magnitude.

The pH dependence of adsorption of cadmium varies markedly among the five model phases. The slopes of the lines for the synthetic ferrihydrite, the aluminosilicate gel, and the montmorillonite are approximately unity (one

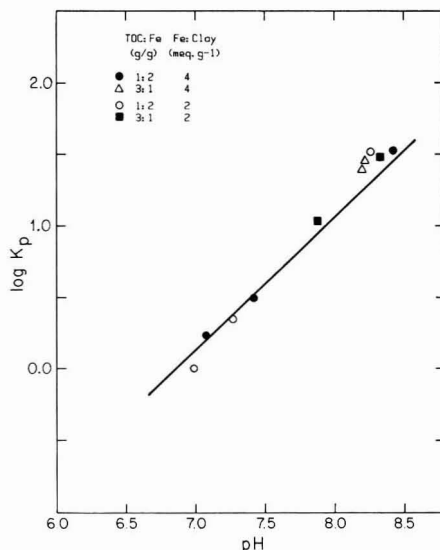


Figure 6. Cadmium uptake by ternary clay-iron-organic complexes in artificial seawater. Regression line is for uncoated iron-clay complexes.

proton released per cadmium ion adsorbed) while the slope of the line for the synthetic birnessite is lower at about 0.33. The very low level of adsorption observed with the montmorillonite is highly pH dependent and may be due to traces on the clay surface of hydrous oxide coatings (which exhibit pH-dependent adsorption). Cadmium binding by the EHS is almost independent of pH.

The specific affinities of the model phases for copper also range over 4 orders of magnitude (Figure 5), but the K_p values are approximately 100 times higher than for cadmium. Copper binding was insensitive to salinity except in the case of the synthetic birnessite which underwent a factor of 3 change over the salinity range 5–35‰. The relative order of the specific affinities for copper is similar to that for cadmium with the exception of the EHS. The highest energy binding site on the EHS has a higher specific affinity for copper than does the synthetic ferrihydrite although the second site type has a much lower specific affinity. While still the strongest binding phase, synthetic birnessite binds copper less strongly than cadmium relative to the other phases.

Generally the pH dependence of copper binding was lower than for cadmium. However, copper binding by the EHS was more dependent on pH than was cadmium. Adsorption of copper by the birnessite was almost independent of pH while the regression lines for the other inorganic phases had similar, rather low, slopes.

Experiments with Combined Phase Complexes. Adsorption experiments with the solid-phase complexes failed to detect any attenuation of metal binding which could be attributed to the interactions involved (19). That is, the combined model phases acted independently toward copper and cadmium such that metal uptake by a phase complex was equal to the sum of the contributions calculated for the isolated phases. This somewhat surprising result was obtained for both the clay-iron complexes (hydroxy interlayered clay) and the iron-organic complexes (humic-coated ferrihydrite) and was also observed for a series of ternary clay-iron-organic complexes.

By way of example, Figure 6 shows cadmium uptake by ternary complexes (data points) compared with that by

Table III. Predicted Cadmium Distribution in a Model Sediment of "Average" Composition at pH 8 and 5‰ Salinity^a

model phase	F_n , %	$K_{p,n}$, L·g ⁻¹	$K_{p,n}F_n$	P_n , %
(1) synthetic ferrihydrite (as Fe)	2	130	2.6	80
(2) synthetic birnessite (as Mn)	0.02	1500	0.3	9
(3) montmorillonite	<100	0.1	<0.1	<3
(4) aluminosilicate (as SiO ₂ + Al ₂ O ₃)	?	3.3	low?	
(5) humic substances	2	17	0.34	10

^a $K_{tot} = \sum K_{p,n}F_n \approx 3.24 \text{ L}\cdot\text{g}^{-1} (100\%)$

uncoated iron-clay complexes (regression line). The data points have been corrected for the contribution of the EHS to cadmium uptake (the contribution of the clay was negligible), assuming this phase *does*, in fact, act independently. The close agreement of the data points and regression line suggests that the iron and organic matter in the phase complexes do indeed act independently toward cadmium. That is, the occurrence of the organic coating on the iron particles does not result in occlusion of adsorption sites on either phase's surface.

The independent binding of trace metals by interacting phases involved in solid-phase complexes may be explained if the hydrous iron oxide (the key phase in the formation of solid complexes) is viewed as a highly porous gel consisting of an open structure produced by aggregated, subspherical, hydroxy-ferric polycations (21). Such a conceptual model would explain both the free movement of solute species, including trace metal ions, to adsorption sites and the lack of attenuation of metal binding when the iron phase interacts with other solid phases. Interaction of another solid with the open iron structure may negligibly affect the total surface area or the available binding sites. The laboratory experiments which demonstrated the independent functioning with regard to metal binding of combined solid phases suggest that the phases comprising complex natural assemblages known as "sediments" will also have behave independently. This should certainly be the case in the common situation in which hydrous iron oxides occur in poorly ordered open structures rather than in crystalline forms (19).

Metal Partitioning in Model Estuarine Sediments

The results of the adsorption studies with model sediment phases summarized in Figures 4 and 5 can now be used to predict partitioning in idealized estuarine sediments that simulate natural sediments over the typical compositional ranges indicated in Table I. The method of calculation is illustrated in Table III for cadmium uptake by a model sediment of "average" composition at pH 8 in 5‰ seawater. It is assumed that about 50% of the total sediment organic content is "humic" in character (a typical value for base-extractable organics) and that the remainder of the organic content has a negligible capacity for metal binding. Alternatively we could assume that all the average sediment organic fraction had the same affinity for metals as humic substances and thus double the predicted contribution of organics to total binding capacity. The sum of the products, $K_{p,n}F_n$, gives K_{tot} (L·g⁻¹), the total sediment binding constant according to eq 4 above. The percent of sediment-bound cadmium associated with each phase is given in the last column (P_n values).

The analysis predicts that hydrous iron oxides should dominate the binding capacity of oxidized estuarine sediments for cadmium under the stated conditions. Manganese oxides and organic matter are associated with about 10% each of the total cadmium content. The clay contribution is negligible since, even if 100% of the sediment was montmorillonite, it would bind only 3% of the cad-

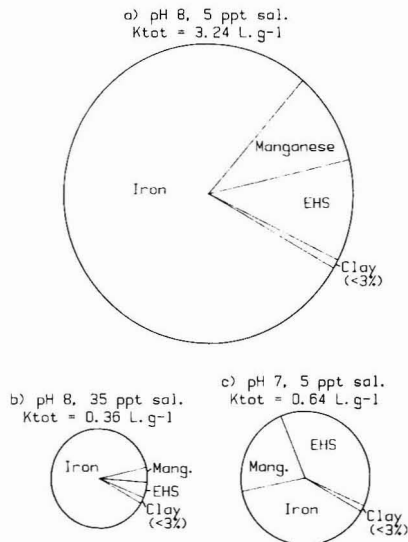


Figure 7. Cadmium distribution in a model estuarine sediment of average composition.

mium. The aluminosilicate was neglected in Table III because of the lack of any good means of weighting this phase in regard to its metal-binding capacity. However, to be of equal importance to the organic matter and manganese compartments, the aluminosilicate would have to be present at a concentration of 10% by weight. It seems unlikely that extractable Al₂O₃ + SiO₂ would approach 10% with the exception of those sediments containing large quantities of recent volcanic ash.

Figure 7 shows data obtained by the method in Table III plotted as a pie graph in which segment area represents metal-binding capacity. The capacity of the total sediment for cadmium binding changes by a factor of 10 with change in salinity from 5 to 35‰ (at constant pH 8), but the relative importance of the contributing phases changes only slightly. The effect of a pH change from 8 to 7 (constant salinity = 5‰) significantly decreases the total sediment capacity for cadmium and also decreases the relative importance of the iron phase.

Figure 8 shows the variation of cadmium distribution with change in sediment composition over the range of concentrations in Table I (5‰ salinity, pH 8). Iron was selected as the independent variable since it dominates cadmium uptake in an average model sediment while four different combinations of manganese and EHS concentrations were represented. The organic and manganese phases only become dominant cadmium compartments when present at very high concentrations with concomitant low iron content.

A number of selective extraction studies on natural sediments suggest that cadmium is mostly associated with the oxides and organic-plus-sulfide phases (1-3). The

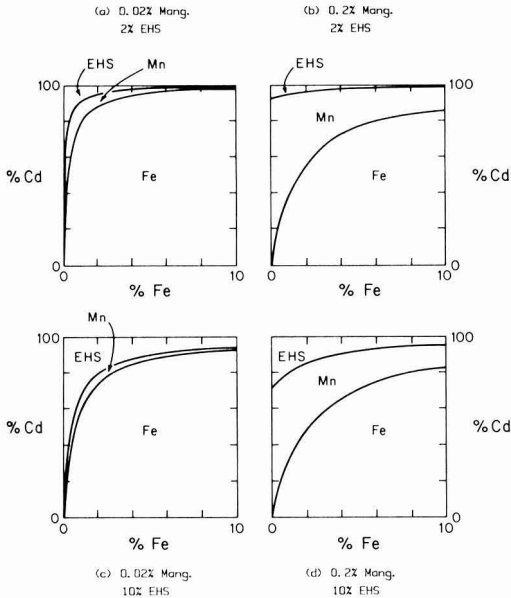


Figure 8. Cadmium distribution in model estuarine sediment as a function of sediment composition (pH 8, 5‰ salinity).

“easily reducible” oxides (usually extracted with hydroxylamine hydrochloride (3) and associated with manganese oxides and poorly crystalline iron oxides) usually contain more cadmium than the “moderately reducible” oxides (mostly crystalline detrital iron oxides). The anaerobic sediments almost all cadmium is found in the sulfide-plus-organic fraction (extracted by peroxide) and is probably present as solid sulfides since the presence of free sulfides depresses free metal concentrations to very low levels, thus effectively suppressing adsorption.

The selective extraction study of Luoma and Bryan (6) gave distributions of metals in oxidized surface sediments that are in substantial agreement with those predicted in this study. Cadmium was found to correlate significantly with HCl- and oxalate-extractable iron but not total iron. Cadmium also correlated with organic carbon, particularly the humic fraction, and with total manganese content and grain size. Since iron, organic carbon, and grain size were all covariant, it was not possible to unequivocally separate the relative importance of these parameters.

Figure 9 shows the predicted distribution of copper in an estuarine sediment. The distribution of copper and the total copper uptake do not change greatly with reduction in salinity although birnessite increases in relative importance. The organic fraction of the sediment is the dominant compartment for copper provided that high energy binding sites are not depleted. Iron is of slightly lesser significance while the contribution of manganese is relatively much lower than in the case of cadmium. Copper binding capacity of the model sediment falls somewhat with decrease in pH from 8 to 7, but the total capacity changes only by a factor of 2.6 compared with a factor of 5.1 for cadmium. Decrease in pH slightly increases the relative contribution of iron. As in the case of cadmium, the contribution of montmorillonite to total copper binding is negligible. The contribution of the aluminosilicate was neglected in Figure 9 for lack of a suitable weighting factor. However, this contribution, similarly to the case for cadmium, would only amount to 10% of the total sediment copper-binding capacity if the aluminosilicate was present

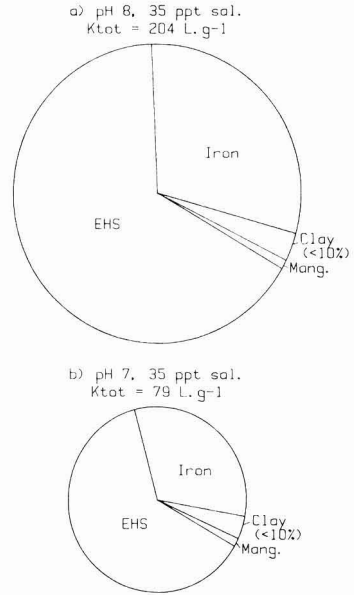


Figure 9. Copper distribution in a model estuarine sediment of average composition.

at as high a concentration as 10% by weight.

Selective extraction studies have shown that copper is mostly associated with the peroxide-extractable fraction in both anaerobic and aerobic sediments although a proportion may also be associated with the “reducible” fractions (oxides) in aerobic sediments (1-3). A significant proportion of total sediment copper may be present in the “residual” fraction extractable only by concentrated acids. This copper is probably not in equilibrium with the sediment pore water but is bound in crystalline silicate lattices. Luoma and Bryan (6) found that copper tended to correlate strongly with organic carbon and even more strongly with the humic (base-extractable) content of sediments. In sediments of low organic content the copper correlated very strongly with extractable iron. These results suggest copper is mostly associated with organics, particularly humics, and iron oxides, again providing confirmation of the predicted distributions in the study.

Cadmium Uptake on Natural Estuarine Sediments

In order to provide a direct test of the validity of the metal partitioning model, some cadmium adsorption experiments were performed with natural sediments. Table IV lists characteristics of oxidized surface sediment samples from uncontaminated estuaries on the Oregon Coast used for studies of cadmium uptake. Samples 1-4 were obtained by a diver-operated scraper which took a uniform 1 cm deep slice of surficial sediment from different locations in Yaquina Bay, OR. Samples STN 8 and STN 9 were obtained from channel stations in Coos Bay, OR, by scraping a uniform 1 cm deep slice from the top of box core samples. Cadmium adsorption studies with these natural sediment samples were performed with a methodology similar to that used for model sedimentary phases using ^{109}Cd as a tracer.

Figure 10 shows a typical plot of measured $\log K_{\text{tot}}$ values as a function of pH for the sediment samples. The data shown are for sample 4 from a tidal flat in Yaquina Bay, OR, in 32‰ natural seawater. The solid line is the $\log K_{\text{tot}}$ (pH) predicted from the distribution model with the

Table IV. Comparison of Measured and Predicted Binding Constants for Adsorption of Cadmium on Natural Estuarine Sediments^a

sample	SSC	MGS, μm	Fe_T , %	Mn_T , $\mu\text{g}\cdot\text{g}^{-1}$	VS (TOC), %	Fe:Mn:O	K_{tot} , ($\text{L}\cdot\text{g}^{-1}$, at pH 8)	
							measured	predicted
Samples from Yaquina Bay, OR (Values for 32‰ Seawater)								
1 (channel)	80:16:4	180	1.23	117	2.12	85:6:9	0.11	0.28
2 (subtidal)	44:50:16	60	1.35	95	3.14	84:4:12	0.96	0.33
3 (slough)	26:67:7	40	1.88	115	6.02	80:8:16	1.10	0.48
4 (tidal flat)	16:76:8	36	1.58	108	3.21	85:5:10	0.69	0.38
Samples from Coos Bay, OR (Values for 35‰ Seawater)								
STN8 (channel)	53:19:28	119	1.41	180	6.30 (2.84)	73:7:20	0.17	0.29
STN9 (channel)	31:39:30	61	2.42	333	10.57 (5.27)	73:7:20	0.28	0.49

^aSSC = percent sand:percent silt:percent clay ratio. MGS = Mean grain size (μm). Fe_T = total iron (%). Mn_T = total manganese ($\mu\text{g}\cdot\text{g}^{-1}$). VS = volatile solids (%) (400 °C, 6 h). TOC = total organic carbon (%). Fe:Mn:O = percent contribution to K_{tot} of iron, manganese, and organic matter.

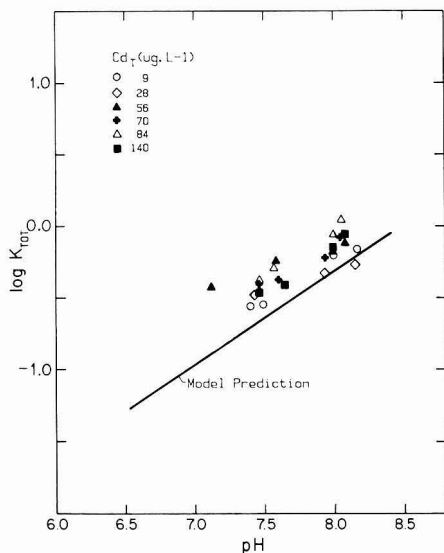


Figure 10. Cadmium uptake by sediment sample 4 from Yaquina Bay, OR, in natural seawater at 32‰ salinity. Measured data points are compared with the predicted cadmium uptake (solid line).

known sediment composition. The measured binding is somewhat higher than predicted, but the slope of the predicted line (0.67) closely matches that of the data. This confirms that iron is the dominant compartment for cadmium in this sediment since cadmium uptake on the other phases (Birnessite and organic matter) have a much lower pH dependence than ferrihydrite (Figure 4).

Plots similar to Figure 10 were obtained for the other sediments. Total sediment binding constants were calculated at pH 8 and are listed in Table IV for comparison with constants predicted by using the distribution model.

The agreement between predicted and measured cadmium uptake is encouragingly close when all the assumptions involved are considered. In three out of four of the Yaquina Bay samples the K_{tot} values are higher than predicted. Some of the discrepancy may be due to the presence of sulfides in the surficial samples (sulfide presence was confirmed in sample 1) which would tend to increase apparent cadmium uptake if cadmium sulfide precipitation occurred. Another possibility is that the affinity of the sediment-iron for cadmium may actually be higher than predicted on the basis of experiments with fresh precipitates if the adsorption of cadmium on hydrous iron oxides increases with aging.

The cadmium uptake was overestimated by the distribution model for one of the Yaquina Bay samples and for the two Coos Bay samples, all three samples being from channel areas. A possible reason for the overestimate is that a significant proportion of the iron present in these channel samples may have been crystalline detrital oxides of lower cadmium affinity than the synthetic ferrihydrite. Overall the general agreement of the measured and predicted cadmium uptake lends support to the proposed distribution model.

Significance of Model Predictions

This study has shown that the behavior in estuaries of two toxic metals, copper and cadmium, can be predicted on the basis of adsorption experiments used to calibrate a simple distribution model. Concentrations of copper and cadmium in the solution phase (water column or pore water) are dependent on the identity and concentrations of "prototype" adsorbent phases in the natural sediments.

In principle the approach of this study should apply to any adsorbate where a linear solid/solution distribution prevails for all contributing adsorbents in the sediment. Thus, it should be possible to predict the equilibrium water column concentrations in the vicinity of a dredge spoil disposal site where sediments are present as dispersed slurries. Tidally averaged metal concentrations in estuaries should express a steady state related to both the equilibrium concentration (as predicted from the distribution model) and the flushing time of the estuary. In metal-contaminated estuaries, steady-state concentrations of copper and cadmium could be significantly higher than in pristine estuaries, thus posing an environmental hazard to biota.

The values of specific phase binding constants (K_p) developed in this study have been expressed in terms of total solution metal concentration (a measured quantity) rather than free metal ion concentration (a predicted quantity). This approach obviated the uncertain calculation of metal speciation, particularly for copper where reported formation constants of important ligands vary widely. However, under similar conditions of salinity and pH, K_p values based on total solution metal concentration can be corrected to a free metal ion basis. This would permit the modeling of metal distribution in sediments to be interfaced with the modeling of solution-phase speciation.

The phase association of copper and cadmium and other toxic metals in sediments greatly affects bioavailability and thus toxicity to benthic organisms, particularly nonselective deposit feeders. This phase association can also be predicted by the distribution model which then becomes

a basis for assessing bioassay results for such organisms.

Although this study has been experimentally limited to copper and cadmium, the results have implications for the distribution of other toxic metals in estuarine environments. For example, because mercury(II) is strongly complexed by organics and by chloride, we would expect organics to dominate or at least be of great importance in mercury uptake by sediments and that this uptake would be strongly influenced by salinity. Zinc might be expected to behave somewhat similarly to cadmium because of chemical similarities although the rather different speciation of zinc in seawater (32) suggests adsorption of this metal would not be as strongly dependent on salinity as in the case with cadmium.

Conclusions

(1) Cadmium and copper distributions between estuarine sedimentary phases and water can be satisfactorily predicted with a simple model analogous to models of speciation among soluble ligands. The interaction of important constituent sedimentary phases with one another does not affect metal distributions.

(2) Cadmium binding by aerobic estuarine sediments is dominated by iron oxides which typically account for 80% of the total sediment binding capacity. Organics, primarily humic substances, and manganese oxides typically contribute 10% each of the total binding capacity. The relative importance of the sedimentary phases in cadmium partitioning depends on pH but is almost independent of salinity.

(3) Organics (humic substances) and iron oxides are the most important contributors to binding of copper by aerobic estuarine sediments. In typical estuarine sediments organics are somewhat more important than iron oxides while the contribution of manganese oxides is only about 1%. The partitioning of copper is insensitive to pH and salinity.

(4) Clay minerals are not significant trace metal sinks although they may be important in metal transport processes in that they act as substrates for the sedimentary components of higher metal affinity. Amorphous aluminosilicates are probably not significant metal sinks except in sediments containing large quantities of recently deposited volcanic ash.

Acknowledgments

R.J.D.-C. was a National Research Advisory Council Fellow sponsored by the New Zealand Ministry of Works and Development. We are indebted to Phillippe Blériot and Nicole Nivault for the generous use of some of their data obtained during their Masters Degree studies at Oregon State University.

Registry No. Cu, 7440-50-8; Cd, 7440-43-9; Fe, 7439-89-6; Mn, 7439-96-5; ferrihydrite, 39473-89-7; birnessite, 12244-32-5; montmorillonite, 1318-93-0.

Literature Cited

(1) Serne, R. J.; Mercer, B. W. Final Report U.S. Army Corps of Engineers Contract DACWO 7-73-C-0080, pp 1-215.
(2) Brannon, J. M.; Engler, R. M.; Rose, J. R.; Hunt, P. G.; Smith, I. U.S. Army Waterways experiment Station Technical Report D-76-7, 1976, pp 1-90.

(3) Engler, R. M.; Brannon, J. M.; Rose, J. A. In "Chemistry of Marine Sediments"; Yen, T. F., Ed.; Ann Arbor Science: Ann Arbor, MI, 1977; pp 163-171.
(4) Guy, R. D.; Chakrabarti, C. L.; McBain, D. C. *Water Res.* 1978, 12, 21.
(5) Rendell, P. S.; Batley, G. E. *Environ. Sci. Technol.* 1980, 14, 314.
(6) Luoma, S. N.; Bryan, G. W. *Sci. Total Environ.* 1981, 17, 165.
(7) Oakley, S. M.; Delphey, C. E.; Williamson, K. J.; Nelson, P. O. *Water Res.* 1980, 14, 1067.
(8) Luoma, S. N.; Jenne, E. A. "Estimating Bioavailability of Sediment-Bound Trace Metals with Chemical Extractants" 10th Annual Conference on Trace Substances in Environmental Health, Columbia, MO, 1976.
(9) Oakley, S. M.; Nelson, P. O.; Williamson, K. J. *Environ. Sci. Technol.* 1981, 15, 474.
(10) Jenne, E. A. In "Biological Implications of Metals in the Environment"; Drucker, H.; Wildung, R. E., Eds.; 15th Hanford Life Sciences Symposium: Richland, WA, 1977; pp 110-143.
(11) Suess, E. *Geochim. Cosmochim. Acta* 1973, 37, 2435-2447.
(12) Schwertmann, U. & Taylor, R. M. "Minerals in Soil Environments"; Soil Science Society of America: Madison, WI, 1977; pp 145-180.
(13) McKenzie, R. M. "Minerals in Soil Environments"; Soil Science Society of America: Madison, WI, 1977; pp 181-196.
(14) Van Olphen, H.; Fripiat, J. J., Eds. "Data Handbook for Clay Materials and Other Non-Metallic Minerals"; Pergamon Press: New York (1979); pp 1-346.
(15) Wada, K. "Minerals in Soil Environments"; Soil Science Society of America: Madison, WI, 1977; pp 603-638.
(16) Schnitzer, M.; and Khan, S. V. "Humic Substances in the Environment"; Marcel Dekker: New York, 1972; pp 1-327.
(17) Jackson, T. A. *Soil Sci.* 1975, 119, 56-64.
(18) Guy, R. D.; Chakrabarti, C. L.; Schramm, L. L. *Can. J. Chem.* 1975, 53, 661-669.
(19) Davies-Colley, R. J. Ph.D. Thesis, Oregon State University, 1981, pp 1-224.
(20) Greenland, D. J. *Soil Sci.* 1971, 111, 34-41.
(21) Davis, J. A.; Leckie, J. O. *Environ. Sci. Technol.* 1978, 12, 1309-1315.
(22) Murray, J. W. *J. Colloid Interface Sci.* 1973, 46, 357-371.
(23) Hem, J. D.; Roberson, C. E.; Lind, C. J.; Polzer, W. L. *Geol. Surv. Water—Supply Pap. (U.S.)* 1973, 1827-E, 1-57.
(24) Davis, J. A. In "Contaminants and Sediments"; Baker, R. A., Ed.; Ann Arbor Science: Ann Arbor, MI, 1980; Vol. 2, pp 279-304.
(25) Tullock, R. J.; Roth C. B. *Clays Clay Miner.* 1975, 23, 27-32.
(26) Carstea, D. D.; Harward, M. E.; Knox, E. G. *Soil Sci. Soc. Am. Proc.* 1970, 34, 517-521.
(27) Leckie, J. O.; James, R. O. In "Aqueous Environmental Chemistry of Metals"; Rubin, A. J., Ed.; Ann Arbor Science, Ann Arbor, MI, 1974; pp 1-76.
(28) Parks, G. A. In "Chemical Oceanography", 2nd ed.; Riley, J. P.; Skirrow, L., Eds.; Academic Press: London, 1975; pp 241-309.
(29) Sunda, W. G.; Hanson, P. J. *ACS Symp. Ser.* 1979, No. 93, 147-180.
(30) Bresnehan, W. T.; Grant, C. L.; Weber, J. H. *Anal. Chem.* 1978, 50, 1675.
(31) Van der Berg, C. M. G.; Kramer, J. R. *ACS Symp. Ser.* 1979, No. 93, 115-132.
(32) Zirino, A.; Yamamoto, S. *Limnol. Oceanogr.* 1972, 17, 661.

Received for review May 17, 1982. Revised manuscript received October 28, 1983. Accepted January 13, 1984. The research was supported by a grant from the Oregon State University Water Resources Research Institute.

On-Road Emission Rates of Carbon Monoxide, Nitrogen Oxides, and Gaseous Hydrocarbons

Robert A. Gorse, Jr.

Research Staff, Ford Motor Company, Dearborn, Michigan 48121

■ On-road emission rate measurements of carbon monoxide (CO), nitrogen oxides (NO_x), and gaseous hydrocarbons (HC) from light-duty gasoline (spark-ignition) vehicles and from heavy-duty diesel vehicles operating at constant speed highway conditions are described. The measurements were made at the Allegheny Mountain Tunnel on the Pennsylvania Turnpike during July of 1981. Over 98 000 highway vehicle km were monitored during the study. The on-road results are compared with predictions from the EPA computer model MOBILE 2 and to other vehicle emissions studies. An effective vehicle speed was determined to account for the actual power requirements of vehicles going through the tunnel. The effective speed was then used in MOBILE 2 to predict the on-road results. CO and HC emission rates calculated by MOBILE 2 for low altitude compare within the standard deviations of the on-road measurements at the Allegheny elevation of 707 m, while predicted diesel NO_x is 2.3σ above the on-road result and gasoline NO_x is 100% above the on-road upper limit. If the Allegheny elevation is sufficient to affect on-road emission rates, then MOBILE 2 also overpredicts CO emission rates by as much as 33%.

Introduction

The understanding and modeling of atmospheric air quality require the knowledge of pollutant emission rates from both stationary and mobile sources and also the relationships between emission rates and mode of operation of the source. Accurate mobile-source emission rates are necessary to assess the role of vehicle emissions in urban air pollution problems as well as in regional problems such as acidic deposition.

Motor vehicle emission rates have traditionally been measured on laboratory dynamometers by using simulated driving schedules with selected new vehicles, or engines, or with small fleets of in-use vehicles. The simulated but well-controlled conditions of the dynamometer tests have many benefits but do not necessarily represent vehicle emissions under real on-road conditions. The small number of vehicles tested in the laboratory also can never be truly representative of the distribution within the on-road vehicle fleet. The utility of the dynamometer results for assessing ambient air quality can only be evaluated by comparison of the dynamometer results with on-road emission results.

Exhaust emission rates can be measured under open-air conditions provided that exhaust plume dispersion can be thoroughly described and monitored. This process is confounded by the air turbulence generated by the motion of the traffic being monitored (1-8). The benefit of the on-road measurements is that a large number of vehicles can be monitored, over a relatively short time span, under actual vehicle-usage conditions.

Roadway tunnel emission measurements such as described in the present study have the additional advantage that exhaust plume dispersion is easily modeled and, more important, readily monitored. Previous roadway tunnel measurements have been described in reports from this laboratory (9-14) and by others (15, 16).

The results described in this report are based on the monitoring of over 53 000 vehicles traveling 98 000 km under highway driving conditions. Emission measurements were made for carbon monoxide (CO), nitrogen oxides (NO_x), and total gaseous hydrocarbons (HC). The gaseous emission results will be compared to those predicted by MOBILE 2, which is an Environmental Protection Agency (EPA) empirical model based primarily on dynamometer measurements (17), and to other recent vehicle emission studies.

Experimental Section

The experiment was performed from July 22 to July 30, 1981, at the Allegheny Mountain Tunnel in rural Pennsylvania on the Pennsylvania Turnpike (Interstate Highway 76), 21 km east of Somerset, PA, the nearest Turnpike interchange. The tunnel, shown schematically in Figure 1, has two two-lane tubes through Allegheny Mountain. All emission measurements were made in the south tube which is normally used for eastbound traffic. The tunnel is 1.85 km in length with a cross-sectional area of 48.0 m² and has an average grade of -0.5% to the east at an elevation of 707 m above sea level. The flow of air through the tunnel is promoted by three mechanisms: the flushing of ambient air through the tunnel by fans (accounting for ~60% of the total air flow); the piston action of the traffic (~30%); the prevailing westerly wind (~10%). Three fans on each side of the mountain force ambient air through regularly spaced tunnel-ceiling louvers. The piston effect and the prevailing wind force air into the entrance portal. The air entering the portal and the fan rooms is slightly contaminated by local traffic emissions so that the ambient concentrations are not quite representative of rural ambient air. All of the air that enters the eastbound tunnel leaves through the exit portal on the east side of the mountain. At the exit the tunnel air contains the integrated exhaust emissions from the vehicles as they transit the tunnel, as increments to the concentrations in the incoming ambient air. Measurements of exhaust component concentrations in the tunnel air at the exit portal (locations 1 and 2 in Figure 1) and in the intake air (location 3) allow determination of the concentrations generated by vehicles during tunnel transit. Measurements of traffic volume, vehicle types, total air flow, and tunnel length and cross section allow calculation of the vehicle emission rates. Previous reports from this laboratory have described various particulate exhaust measurements (18-21), the biological activity of the exhaust particulate extracts (22), the measurement of CO emission rates (23), and the method for derivation of emission rates from the tunnel concentration measurements (24).

A block diagram of the sample train is presented in Figure 2 for the CO, NO_x, and HC analyzers. High volume air samplers collected particulate material of <5-μm diameter at each of the three locations concurrently. The particle characterization results and other emission measurements from the 1981 experiment are described in separate reports (25-27). A continuous gas sample was drawn from each of four locations: 5.5 m inside the exit

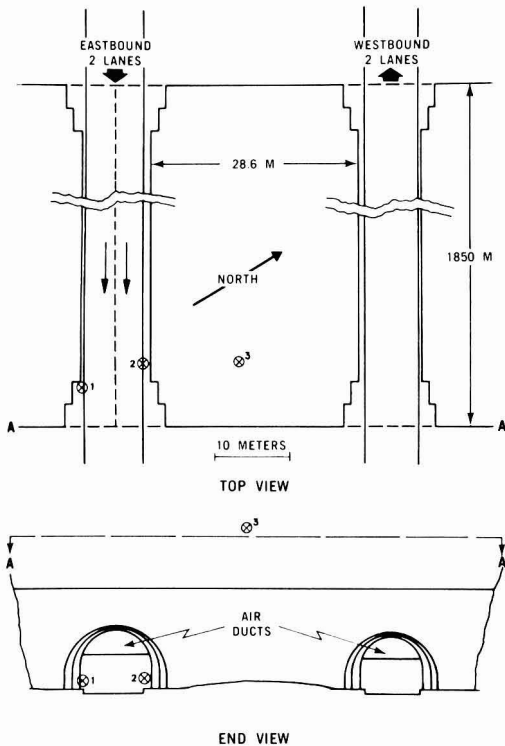


Figure 1. Allegheny Mountain Tunnel. Crosses indicate sampling locations in the exit portal: right traffic lane (1), left traffic lane (2), and on the roof of the intake fan room (3).

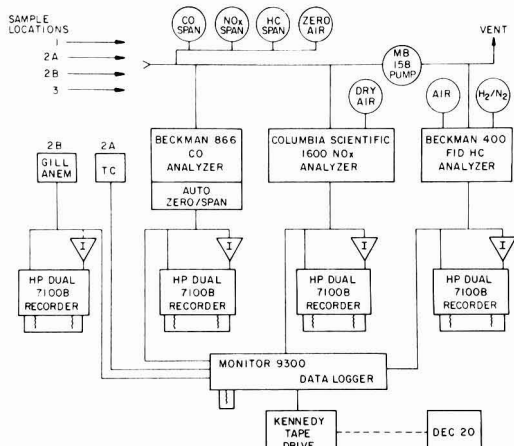


Figure 2. Block diagram of gas-analysis sample train for monitoring CO, NO_x, and HC concentrations, temperature, and air flow. Valves, flowmeters, and mixing volume omitted for clarity. (∇) Integrator.

portal adjacent to the right traffic lane 2.2 m above the roadbed (location 1); 7.3 m inside the exit portal adjacent to the left traffic lane 2.2 m above the roadbed (location 2A); 47 m inside the exit portal adjacent to the left traffic lane 2.2 m above the roadbed (location 2B); on the roof of the intake fan room on the east side of the mountain (location 3). The tunnel sample points were sufficiently in the moving air mass to avoid wall effects. The inlet of the 1 cm i.d. polyethylene sampling line to each location

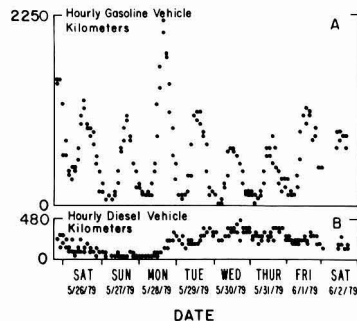


Figure 3. Typical diurnal and weekly variation in gasoline vehicle kilometers (A) and diesel vehicle kilometers (B). Monday 5/28/79 was Memorial Day.

was equipped with a 47-mm diameter glass fiber filter to remove particulate material. The tunnel inlet filters were changed daily, and the roof filter was changed every 3 days. The gas sample train could be connected to any one of the four sample lines. Intake air concentrations were determined by averaging 278 5-min measurements spaced temporally throughout the course of the experiment. The zero and span of each analyzer was checked daily with NBS-traceable gas standards.

The tunnel air speed was measured continuously with a Gill anemometer at location 2B. Hand-held anemometer measurements at three heights above the roadbed indicated uniform air velocity across the width of the tunnel. A thermocouple was used for temperature measurements at location 2A. Vehicle axles were monitored continuously with a pneumatic-tube counter outside the entrance portal and recorded as 5- or 15-min totals on paper print/punch tape. Traffic distribution by vehicle type was determined by 10-min visual counts taken during each hour. Vehicles and axles were categorized as spark ignition (cars, campers, buses and trucks, and motorcycles) or as diesel (cars, buses, and trucks). The 10-min axle totals were then normalized to the 1-h road tube axle count to get the vehicles per hour in each vehicle category. The distributions of vehicle types for 14 run periods (runs 7–20), of 305–905-min duration, corresponding to collection periods of particulate material, are listed in Table I along with the overall traffic distribution for the experiment (14 runs). As is evident from Table I, the traffic at Allegheny Tunnel is dominated by two vehicle categories—light-duty spark-ignition (gasoline) passenger cars and heavy-duty diesel trucks, which together account for 96.2% of the traffic volume.

The diurnal and weekly variations in traffic volume and distribution of vehicle types typical of Allegheny are shown in Figure 3, taken from our 1979 study (23) (weekday maintenance of the tunnels during the 1981 study resulted in shutdown of one of the tubes, preventing analyses and traffic counts between 8 a.m. and 3 p.m.). The difference between the diurnal variation of the gasoline vehicles and that of the diesel vehicles allows selection of sampling periods dominated by either gasoline or diesel vehicles. The runs listed in Table I vary between 36 and 92% gasoline vehicles, which are the practical limits for this procedure. The range and mean of the conditions and concentrations observed in these periods are listed in Table II along with a summary of the pertinent tunnel data.

The analog and integrated signals from the gas analyzers and the Gill anemometer were recorded on strip charts, and the analog signals were also fed to a data logger which calculated and recorded 5-min averages on magnetic tape from readings every 15 s. The 5-min averages were used

Table I. Allegheny Traffic Distribution

run	gasoline				diesel			total vehicles	gasoline vehicles, %
	MC, ^a %	car, %	camper, %	truck/bus, %	car, ^b %	bus, %	truck, %		
7	0	36.13	0.84	0.63	1.05	0.42	60.93	2230	37.61
8	0.59	67.80	1.92	1.18	1.96	0.74	25.81	3325	71.49
9	0	42.42	0	0.92	1.23	1.62	53.81	2018	43.34
10	0.19	79.20	1.75	0.78	2.29	0.68	15.11	5341	81.92
11	0.60	86.40	1.64	0.74	2.50	0.45	7.67	6698	89.39
12	0.19	81.94	1.13	0.76	2.37	0.57	13.04	2418	84.02
13	0.48	89.94	0.85	0.85	2.60	0.12	5.16	7612	92.12
14	0.07	67.24	0.70	0.70	1.94	0.63	28.72	7777	68.71
15	0.34	68.40	1.24	1.24	1.98	0.22	26.58	3643	71.22
16	0	45.87	0.90	0.54	1.33	0.72	50.64	2101	47.32
17	0.29	58.85	0.72	2.46	1.70	0	35.98	2863	62.31
18	0.16	37.16	0.77	1.70	1.08	0.47	58.66	2574	39.79
19	0.27	56.13	1.09	1.90	1.62	0.54	35.45	2483	59.38
20	0	36.06	0.19	0.57	1.04	0.19	61.95	2095	36.82
all	0.28	68.14	1.07	1.00	1.97	0.48	27.06	53176	70.49

^aMC = motorcycles. ^bThe fraction of light-duty diesel vehicles in over 1200 passenger cars was determined by visual count to be 0.0281. This fraction was then used throughout the experiment to calculate the number of diesel cars relative to the passenger car total.

Table II. Tunnel Data^a

parameter, units	range	mean
run dates	7/22-7/29/81	14
run time, min	305-905	511
temperature, °C	16.5-20.4	19.2
wind, m/s, exit portal	5.8-8.9	7.7
vehicle km per run	3734-14 189	6868
vehicles min ⁻¹	3.6-16.4	7.6
gasoline vehicles, %	36.8-92.1	63
ΔCO, ppm ^b	1.7-12	5.0
ΔNO, ppm	0.91-1.6	1.3
ΔNO ₂ , ppm	0.061-0.13	0.08
ΔHC, ppm	0.06-3.3	2.0

^aAdditional Data: vehicle speed = 84 ± 8 km/h; previous turnpike exit = 21 km west; heavy-duty trucks average 26 metric tons gross vehicle weight; ~74% of gasoline vehicles are catalyst equipped; road grade = -0.5%; tunnel length = 1.85 km; cross section = 48.0 m²; elevation = 707 m. Ambient levels: CO, 0.57 ppm; NO, 0.06 ppm; NO₂, 0.03 ppm; HC, 1.6 ppm. Highest 5-min average levels: (normal traffic) CO, 19 ppm; NO, 2.6 ppm; NO₂, 0.23 ppm; HC, 9.6 ppm. (Traffic stopped) CO, 82 ppm; NO, 4.9 ppm; NO₂, 0.33 ppm; HC, 13.5 ppm. ^bΔconcentrations are average observed tunnel concentrations minus the ambient levels listed above. Ambient levels were measured at sample location 3 (Figure 1) but do not represent true rural ambient levels because of recirculation of exhaust from traffic on the Turnpike.

to determine the air flow, temperature, and total mass of the emission components in the tunnel air during each of the 14 runs.

Turnpike fuel sales for July 1981 indicated that 70% of the gasoline sales were unleaded fuel for use in catalyst-equipped vehicles. We calculate, assuming that catalyst-equipped vehicles average 16.5 mpg and that noncatalyst-equipped vehicles average 13.5 mpg (28), that ~74% of the gasoline vehicles at Allegheny are catalyst equipped. This figure is appreciably above the national average of ~60%, for July 1981, reflecting the fact that the Turnpike vehicles tend to be newer vehicles used for long distance travel. Improved emission controls on newer vehicles result in lower fleet average emission factors as the fraction of newer vehicles increases. For example, the average emission rates for CO, NO_x, and HC for 1979 model year certification vehicles were 4.1, 0.91, and 0.34 g/vehicle km; in 1982 these emission rates had decreased to 1.7, 0.37, and 0.18 g/ve-

hicle km, respectively (29, 30).

Turnpike toll plaza scale records were used to determine that the average heavy-duty vehicle at Allegheny had a gross vehicle weight of 26 metric tons.

The 21 km between the tunnel and the previous exit at Somerset ensures that essentially all of the vehicles passing through the tunnel are in the hot-stabilized operation mode.

Calculation of Emission Rates. The equations describing the air quality at the Allegheny Tunnel were derived in an earlier report (24). Combining eq 3 and 6 of ref 24 gives the result

$$\begin{aligned} \Delta CWA/(v_t L) &= f e_g + (1 - f) e_d \\ &= e_g \text{ for } f = 1 \\ &= e_d \text{ for } f = 0 \end{aligned} \quad (1)$$

where $\Delta C = C_L - C_0$ is the difference in concentration of the emission species at the exit portal and in the intake air, $W = U_0 + \alpha L$ is the air speed measured at the exit portal which is the sum of the air flow at the entrance portal (U_0) and that added by the fans (αL), A is the tunnel cross-sectional area, v_t is the traffic flux, i.e., the total number of vehicles per unit time, L is the tunnel length, f is the fraction of spark-ignition (gasoline) vehicles in the total traffic, and e_g and e_d are the respective gasoline and diesel vehicle emission rates in units of mass per vehicle distance traveled.

The left side of eq 1 has a linear dependence on f with the values of e_g and e_d determined at $f = 1$ and $f = 0$, respectively, by linear least-squares regression analysis. In practice since the light-duty diesel cars were taken to be a constant fraction of the gasoline car traffic, the gasoline emission rates reported here, e_{SI} , have been calculated from the relationship

$$e_{SI} = e_g + \frac{2}{3}[x/(1 - x)]e_d \quad (2)$$

where $x = 0.0281$ is the observed fraction (see footnote to Table I) of diesel cars in the passenger car fleet. (The value of x determined similarly in the 1979 study was 0.0236.) Derivation of eq 2 assumes only that diesel cars have emission rates ~1/3 those of heavy-duty diesels, 1/3 being the approximate ratio of their fuel consumption rates.

According to eq 1 the relative uncertainty in the experimental values of e_d (or of e_g) reduces to the sum of the

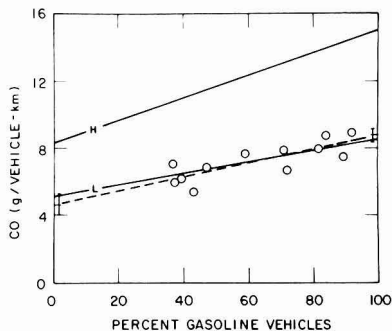


Figure 4. Regression plot of on-road grams of CO per vehicle kilometer vs. percent gasoline vehicles (—○—). MOBILE 2 61 km/h predictions for low altitude (---○---) and for high altitude (—○—). Error bars indicate $\pm 1\sigma$ values from regression analysis.

relative uncertainties in the measurement of the tunnel air pollutant concentrations, the tunnel wind speed, and the flux of diesel (or of gasoline) vehicles. Comparisons of 10-min visual vehicle counts with complete 60-min counts have shown the vehicle flux determination to be better than $\pm 5\%$. The rapid-response continuous Gill anemometer measurements are also believed to be better than $\pm 5\%$. The tunnel pollutant concentrations show a right-left asymmetry of up to 15% as the result of more traffic in the right lane. Since trucks generate more turbulence than cars, the asymmetry is at a minimum during heavy truck periods. In this study, equal-duration concentration measurements on the two sides of the tunnel were used to affect an averaging of the tunnel concentrations. We thus expect total uncertainties of $\pm 20\%$ for gasoline emission factors but closer to $\pm 10\%$ for diesel values.

Results

Tunnel Concentrations. With very low traffic intensity the analog signals from the gas analyzers responded to individual vehicles, or clusters of vehicles, during tunnel transit. Peak widths reflected the tunnel residence time of the vehicle (~ 1.4 min) and that of the trailing exhaust plume (~ 2.9 min average). With high traffic intensity, which was the norm, individual exhaust plumes were unresolvable. Minimum averaging intervals corresponded to the hourly visual traffic counts. Hourly averages were used in our 1979 CO study (23) where it was also demonstrated that the same results were obtained for much longer averaging intervals. In the present study we have used the filter collection period as the averaging interval. The average and range of concentrations observed over the 14 runs are included in Table II. Tunnel concentrations of the gas species were found to be equivalent at sample locations 2A and 2B but up to $\sim 15\%$ higher at location 1 as described previously.

Pairwise regressions were performed between the vehicle-generated mass for each gaseous emission component and the total vehicle kilometers of gasoline or diesel vehicles. The results show that the aggregate mass of CO emitted in the tunnel is predominantly from gasoline vehicles and that NO, NO₂, and NO_x are dominated by diesel vehicles whereas total hydrocarbons are contributed by both vehicle types but with nearly 3 times as much from gasoline vehicles as from diesel vehicles. Pairwise regression analyses like these are informative but are inadequate for determination of accurate emission rates.

Carbon Monoxide Emission Rates. The CO regression analysis according to eq 1 is shown in Figure 4. The

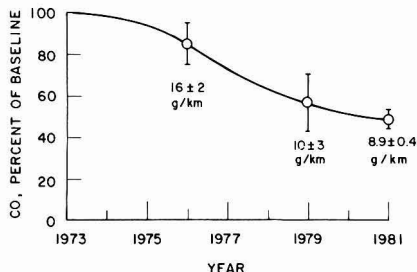


Figure 5. Plot of Allegheny Tunnel measurements of gasoline vehicle CO emission rate vs. year relative to an assumed base-line emission rate in 1973 of 18.3 g/km. Error bars indicate $\pm 1\sigma$.

MOBILE 2 predictions for low and high altitudes are included in the figure but will be discussed in the next section. The on-road CO grams per vehicle kilometer values at $f = 1$ and $f = 0$ (percentage gasoline vehicles of 100 and 0, respectively) are 8.7 ± 0.4 (e_g) and 4.6 ± 0.6 (e_d) from which $e_{SI} = 8.9 \pm 0.4$ g/vehicle km. The correlation coefficient, r , was 0.80 for 12 data points. (Two runs were discarded as outliers which changed the regression results from $e_g = 9.3 \pm 0.7$ g/vehicle km, $e_d = 4.9 \pm 1.2$ g/vehicle km, and r ($n = 14$) = 0.58). The error estimates quoted are the $\pm 1\sigma$ uncertainties from the regression analysis. The values of e_{SI} and e_d determined in the 1979 study were 10.4 ± 2.6 and 5.6 ± 2.1 g of CO/vehicle km, respectively. Figure 5 shows the e_{SI} for CO measured at Allegheny in 1976, 1979, and 1981 relative to an assumed base-line value of 18.3 g/vehicle km in 1973, indicating a continuing decrease in CO emission from gasoline vehicles as catalyst-equipped vehicles supplant older vehicles.

Nitrogen Oxide Emission Rates. Vehicle-generated NO concentrations in the tunnel averaged 1.3 ppm, significantly above the intake-air concentrations of 0.06 ppm. The calculated values of e_{SI} and e_d are 0.2 ± 0.2 and 7.9 ± 0.4 g of NO/vehicle km with an r value ($n = 14$) of 0.97. In any situation where $e_d \gg e_g$ the uncertainty in the e_g value is very large, possible even larger than indicated by σ of the regression, because it is not possible to find sampling periods sufficiently free of diesel vehicles. For example, if $e_d/e_g = 50$ for any emission component, then even with 90% gasoline traffic only 15% of the tunnel concentration is contributed by the gasoline vehicles. With the large uncertainty in e_{SI} for NO, and also for NO₂ and NO_x, they should best be considered as upper limits at $\leq (e_{SI} + 2\sigma)$.

In the tunnel, in the absence of sunlight, the tailpipe NO₂/NO ratio is preserved. Ambient O₃, typically 0.03–0.06 ppm, would be rapidly titrated by NO in the inlet air ducts during the 2.4-min average residence time, in the dark, before entering the tunnel. Actually, assuming a photostationary state (29, 30) for NO, NO₂, and O₃ ($O_3 = J(NO_2)/k(NO)$ with $J = 0.3 \text{ min}^{-1}$ and $k = 24.7 \text{ ppm}^{-1} \text{ min}^{-1}$) at the intake air sample location yields the estimate that the O₃ concentration is already below 0.006 ppm before entering the intake fan room. The average vehicle-generated NO₂ in the tunnel was 0.08 ppm (Table II), and the average intake air concentration was 0.03 ppm. Calculated e_{SI} and e_d values for NO₂ are 0.05 ± 0.02 and 0.74 ± 0.03 g of NO₂/vehicle km, respectively. Note, as with NO, the large uncertainty in the gasoline NO₂ emission rate which should be taken as ≤ 0.09 g of NO₂/vehicle km. (One data point was discarded as an outlier, changing the correlation coefficient from 0.65 ($n = 14$) to 0.97 ($n = 13$)).

NO_x emission rates are defined as the total nitrogen oxides measured as NO₂ since NO is ultimately converted

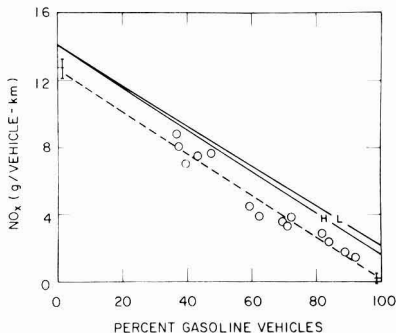


Figure 6. Regression plot of on-road grams of NO_x per vehicle kilometer vs. percent gasoline vehicles (-O-). MOBILE 2 61 km/h predictions for low altitude (-L-) and for high altitude (-H-). Error bars indicate $\pm 1\sigma$ values from regression analysis. Grams of NO_x as NO_2 .

to NO_2 in the atmosphere. The regression for total NO_x is shown in Figure 6. The e_g and e_d values calculated are 0.1 ± 0.4 and 12.7 ± 0.6 g of NO_x /vehicle km, respectively, with a correlation coefficient ($n = 14$) of $r = 0.97$. The calculated value of e_{SI} is 0.4 ± 0.4 g/vehicle km, to be quoted as ≤ 1.2 g of NO_x /vehicle km.

The NO and NO_2 emission factors indicate that at the steady-state highway conditions in the tunnel diesel NO_x is on the average only $5.8 \pm 0.5\%$ NO_2 whereas gasoline vehicle NO_x is $13 \pm 18\%$ NO_2 .

Hydrocarbon Emission Rates. Measurements of the total hydrocarbon levels in the intake air were hindered by HC contributions from the sample line. It was demonstrated in the laboratory that HC could be accurately measured through the polyethylene sample line, but during the experiment the sample line was exposed to sunlight on the roof which resulted in elevated HC levels, comparable to or greater than those in the tunnel air. We therefore have calculated the vehicle-generated HC levels with assumed intake air levels of 1.4, 1.6, and 1.9 ppm of HC. These values were chosen as approximations to the CH_4 concentration of the normal atmosphere (1.4 ppm) (31) and to determine the sensitivity of the calculated emission rates to the intake air concentration. The HC regression results shown in Figure 7 are based on the 1.6 ppm intake value. The sensitivity analysis showed that e_{SI} (1.0 ± 0.5 g/vehicle km) was essentially independent of the intake HC level but that the e_d values were 3.8 ± 0.8 , 3.2 ± 0.8 , and 2.4 ± 0.8 g/vehicle km for the assumed intake levels of 1.4, 1.6, and 1.9 ppm, respectively. In some rural areas the ambient methane level can exceed 3 ppm. We therefore conclude that whereas the gasoline HC emission rate is reliable within the stated uncertainty, the diesel value should be considered as only an upper limit (≤ 3.2 g/vehicle km). Note that the relative uncertainty in the diesel emission rate is proportional to the intake HC level and that this uncertainty is also evident in Figure 7 as an increased scatter of the data at low values of f , which correspond to low tunnel concentrations of HC. Weighting the grams of HC per vehicle kilometer data in the least-squares analysis by the variance in the tunnel concentration measurements had an insignificant effect on the calculated emission rates.

Discussion

The emission rates determined here represent an extensive data set for in-use light-duty gasoline vehicles and heavy-duty diesel vehicles under highway driving conditions. The data should be used with a full understanding

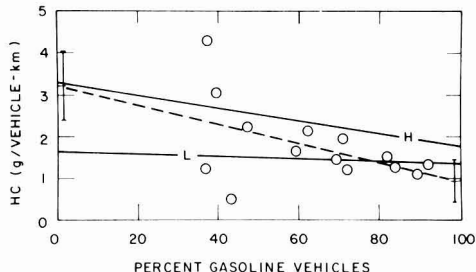


Figure 7. Regression plot of on-road grams of HC per vehicle kilometer vs. percent gasoline vehicles (-O-). MOBILE 2 61 km/h predictions for low altitude (-L-) and for high altitude (-H-). Error bars indicate $\pm 1\sigma$ values from regression analysis. Grams of HC as $\text{CH}_{1.85}$.

of the limitations discussed for the gasoline vehicle NO , NO_2 , and NO_x emission rates and for the diesel HC emission rate.

To ensure that the Allegheny emission factors are generally reflective of highway driving, it is necessary to account for the peculiar driving conditions encountered in going through the tunnel (cf. summary in Table II). Although the tunnel vehicles have an average road speed of 84 km/h, the effect of the tailwind and road grade is to reduce the required vehicle power below that needed for no-wind no-grade operation at the same speed. Thus, the vehicles operate at a power output equivalent to a no-wind no-grade condition at a significantly lower speed. With the data available it is possible to calculate the equivalent power of the tunnel vehicles in a no-wind no-grade steady-state driving condition and from this to determine an effective highway vehicle speed corresponding to this power level.

The net engine horsepower for a vehicle is the sum of the rolling resistance horsepower, the air resistance horsepower, and the grade resistance horsepower as shown in eq 3 (32-34) where C_r is the rolling coefficient (0.0136 for

$$\text{net hp} = (C_r V M R_s + C_a A_v V_w^3 + G V M) / (375 E_d) \quad (3)$$

cars, 0.0108 for trucks), V is the actual road speed in miles per hour, M is the vehicle weight in pounds (4000 for cars, 57200 for trucks), R_s is a road surface correction factor (1.2 for the tunnel asphalt), C_a is the air drag coefficient (1.06×10^{-3} for cars, 1.88×10^{-3} for trucks), G is the fractional grade (-0.005), and E_d is the drive-line efficiency (typically 0.8-0.9). V_w is the wind-adjusted speed as calculated from eq 4 (35) where W_a is the average air velocity in the tunnel

$$V_w = [V - W_a [1 - (A_v/A)]] \quad (4)$$

$(W + U_0)/2 \approx 12$ mi/h), A_v is the vehicle face area (2 m^2 for cars, 8.9 m^2 for trucks), and A is the tunnel cross section (48.0 m^2). The no-wind no-grade horsepower is calculated by eq 5 where V_e is the effective vehicle speed at the same net hp(no-wind, no-grade) =

$$(C_r V_e M R_s + C_a A_v V_e^3) / (375 E_d) \quad (5)$$

power requirement as the vehicles going through the tunnel. Setting eq 3 equal to eq 5 and solving iteratively for V_e for cars and again for trucks gave $V_e = 38.8$ and 37.4 mi/h, respectively. This result means that whereas the Allegheny vehicles travel through the tunnel at 84 km/h road speed, they operate the same as they would in an open air, no-wind, no-grade highway cruise at 61 km/h. It is this speed that should be used in describing the emission factors determined in this study. The decrease in required power in going through the tunnel should result in de-

creased fuel consumption as has been verified by fuel consumption measurements using an automobile equipped with electronic fuel injection and digital fuel economy readout (19, 27).

Comparison with MOBILE 2. MOBILE 2 is an EPA-developed computer program designed to calculate fleet average emission rates of in-use vehicles for assessments of ambient air quality in urban and rural areas in past, present, and future years. Laboratory dynamometer results from new vehicle and engine certification tests and from in-use vehicle emission evaluation programs have provided most of the input data base for calculation of emission factors. The EPA vehicle categories are motorcycles, gasoline passenger cars, light-duty gasoline trucks I and II, heavy-duty gasoline trucks, diesel passenger cars, light-duty diesel trucks, and heavy-duty diesel trucks. Basic emission rates for each vehicle category are dependent on the new-vehicle emission rate and the change in emission rate with mileage accumulation (deterioration rate). Adjustments to the basic emission rates are made to account for differences in vehicle operation mode, air temperature, vehicle age, emission control systems, altitude (152-m and 1676-m elevation), misfueling (use of leaded fuel in catalyst-equipped vehicles), vehicle speed, use of vehicle accessories, and extra vehicle loads. MOBILE 2 calculations can be performed for 49-state vehicles, California vehicles (because of the different emission standards), or high altitude vehicles.

For present purposes the best check between MOBILE 2 and the on-road results reported here is to determine how well MOBILE 2 predicts the on-road CO, NO_x, and HC emission rates. Therefore, MOBILE 2 calculations were made for vehicles in a hot-stabilized mode operating at 61 km/h at 19 °C for the national average distribution of vehicle model years in Jan 1982. Calculations were performed for low altitude and for high altitude 49-state vehicle operation. The individual vehicle category emission rates obtained were then weighted by the observed Allegheny vehicle-type distribution for each of the 14 runs to calculate a predicted low and high altitude total-fleet emission rate for each emission component for comparison with the observed on-road values. The Allegheny vehicle categories (cf. Table I) were somewhat different than the EPA categories so that some adjustments to those at Allegheny were necessary. The Allegheny camper category was assumed to represent light-duty gasoline truck II, and twice the camper category was assumed to be in the light-duty truck I category, with that percentage subtracted from the gasoline passenger car category. The light-duty diesel truck category was not detected at Allegheny. The diesel buses were included with the heavy-duty diesel trucks. A regression analysis identical with that for the on-road results was then performed to describe the regression lines shown for low and high altitude CO, NO_x, and HC in Figures 4, 6, and 7, respectively.

It is clear from Figure 4 for CO that the MOBILE 2 low-altitude 61 km/h results are very close to the on-road observations while the high altitude results are not. This is consistent with previous analyses which indicate that MOBILE 2 reasonably predicts in-use emissions for past model year vehicles but overpredicts for future model year vehicles (36). However, the Allegheny on-road results are at an elevation of 707 m, and hence, comparison should be made to a MOBILE 2 low altitude prediction adjusted to 707 m (from 152 m). EPA has not yet established a methodology for making altitude adjustments, but it is clear that the adjusted line would be between the low altitude and high altitude MOBILE 2 predictions in Figure

Table III. Comparison of On-Road Emission Rates with Selected MOBILE 2 Predictions (g/Vehicle km)

data source	CO	NO _x	HC
on-road			
<i>e_d</i>	4.6 ± 0.6	12.7 ± 0.6	≤3.2
<i>e_{SI}</i>	8.9 ± 0.4	≤1.2	1.0 ± 0.5
MOBILE 2, 61 km/h ^a			
<i>e_d</i>	5.2 (13) ^b	14.1 (11) ^b	1.6 (-50) ^b
<i>e_{SI}</i>	8.7 (<u>-2.2</u>)	2.4 (100)	1.4 (40)
MOBILE 2, 84 km/h ^a			
<i>e_d</i>	4.8 (4.3)	17.2 (35)	1.3 (-59)
<i>e_{SI}</i>	7.7 (-13)	2.6 (120)	1.2 (20)
MOBILE 2, FTP ^{a,c}			
<i>e_d</i>	9.7 (110)	16.1 (27)	2.8 (-13)
<i>e_{SI}</i>	26.1 (190)	1.5 (25)	2.6 (160)

^a MOBILE 2 results for low altitude only. 61 km/h is the horsepower-effective vehicle speed calculated for the on-road no-wind no-grade conditions. 84 km/h corresponds to the actual road speed of the tunnel vehicles. ^b Values in parentheses are the percentage difference between MOBILE 2 results and on-road results (% = ((MOBILE 2 - on-road)/on-road) × 100). Underlined values are within 1σ of the on-road measurements. ^c FTP indicates the Federal Test Procedure urban driving cycle with an average speed of 31.5 km/h which includes 20.6% cold-start, 52.1% hot-stabilized, and 27.3% hot-start vehicle operation.

4. Assuming a linear extrapolation between low and high altitude leads to CO emission rate predictions for MOBILE 2 at 707 m of 11 and 6.1 g of CO/vehicle km for gasoline and diesel vehicles, respectively, and thus 24 and 33% overpredictions of the on-road results.

The calculated gasoline and diesel emission rates from the low altitude 61 km/h MOBILE 2 predictions are compared to the on-road results in Table III. Also included for reference are the results of similar calculations from MOBILE 2 at 84 km/h (the actual Allegheny road speed) and for the urban driving cycle Federal Test Procedure (FTP). The MOBILE 2 CO predictions at the effective on-road speed of 61 km/h are within one standard deviation of both the gasoline and diesel on-road CO emission rates. The MOBILE 2 61 km/h diesel NO_x emission rate is 2.3σ above the on-road value, and the gasoline emission rate is twice the on-road upper limit. The MOBILE 2 61 km/h low altitude diesel HC prediction is half of the observed on-road limit, and the gasoline-vehicle HC emission rate is within 1σ of the on-road value.

The above-average gasoline-vehicle catalyst fraction at Allegheny cannot be taken into account in the MOBILE 2 calculations without information on the on-road vehicle model-year distribution. Rough estimates of the magnitude of the effect indicate that the impact should cause a less than 15% reduction in the MOBILE 2 HC and CO gasoline vehicle emission rates and less than a 9% reduction in the MOBILE 2 gasoline vehicle NO_x emission rate.

The on-road vs. MOBILE 2 comparisons presented here relate to hot-stabilized highway driving conditions and therefore do not address issues having to do with cold or hot-start urban driving conditions. However, on the assumption that MOBILE 2 adequately predicts relative emission rates between urban and highway driving conditions (FTP vs. 61 km/h), then these ratios can be used as multipliers to the Allegheny on-road results to estimate urban emission factors. Thus, the urban emission rates for CO, NO_x, and HC would be 27, <0.8, and 1.9 g/vehicle km for gasoline vehicles and 8.7, 14, and <6 g/vehicle km, respectively, for diesel trucks.

Comparison with Emission Studies. Bullin et al. (6) reported that MOBILE 1, the precursor to MOBILE 2, underpredicted CO emission rates by 8-400%. At four Texas

highway sites the calculated experimental CO emission rate ranged from 27 to 89 g of CO/vehicle km whereas MOBILE 1 predicted 22 g of CO/vehicle km. The data in Figure 5 indicate that MOBILE 1 was in much better agreement with the early Allegheny results for mid to late 1970 on-road vehicles than were the Texas highway values.

Emission rates determined (39) over an on-road driving course for 10 high-mileage heavy-duty diesel trucks were 14.6 (CO), 11.7 (NO_x), and 2.3 (HC) g/vehicle km. These values compare very well with the present results for diesel vehicles when one accounts for the acceleration modes in the driving course vs. the steady-state conditions at Allegheny. CO emission rates increase significantly during acceleration driving modes.

A study of 25 1970 model year high-mileage precatalyst passenger cars (40) resulted in CO, NO_x, and HC emission rates of 13, 2.3, and 1.8 g/vehicle km over the Federal Test Procedure urban driving cycle. No highway measurements were made.

An evaluation of 10 1978 and 1979 model year high-mileage catalyst-equipped passenger cars was performed by EPA (41). Emission rates for CO, NO_x, and HC were found to average 1.0, 1.2, and 0.21 g/vehicle km on the highway driving cycle and 7.9, 1.2, and 0.69 g/vehicle km on the urban cycle.

The Allegheny on-road gasoline vehicles were ~74% catalyst equipped according to the turnpike fuel sales. A linear combination of the 1970 model year noncatalyst vehicle emission rates (25%) and the 1978-1979 model year catalyst vehicle emission rates (75%) gives a combined set of emission factors for CO, NO_x, and HC of 9.1, 1.5, and 0.96 g/vehicle km, respectively. The close comparison of these figures with the on-road results must be somewhat fortuitous because it was necessary to utilize the urban driving cycle values for the two dynamometer studies.

In general, where comparisons are possible, the on-road tunnel results compare well with dynamometer measurements. The open-air on-road studies of Bullin et al. (6) appear to give anomalously high emission factors. MOBILE 2 apparently overpredicts gasoline and diesel NO_x emissions and possibly CO as well depending on the effect of intermediate elevations.

Conclusions

On-road emission rates of CO, NO_x, and HC from light-duty gasoline vehicles and from heavy-duty diesel vehicles have been measured for highway driving conditions. These measurements were the result of monitoring over 98000 vehicle km of travel through a roadway tunnel. An effective vehicle speed was calculated for the vehicles going through the tunnel by calculating the vehicle power requirements at the tunnel tailwind and road-grade conditions. The calculated no-wind no-grade vehicle speed was then used as an input parameter to EPA's MOBILE 2 for computation of predicted emission rates applicable to the tunnel conditions. Comparison of the predicted and on-road results for CO showed agreement within 1σ of the on-road measurements for both vehicle types. Consideration of the Allegheny elevation could cause the MOBILE 2 CO emission rates to be high by as much as 33%. Predicted NO_x emissions were higher than the on-road measurements. Predicted diesel NO_x was 2.3σ above the observed value. Predicted gasoline vehicle NO_x was twice the on-road upper limit. Predicted diesel HC was half of the on-road upper limit. The predicted gasoline vehicle HC value was within 1σ of the on-road result. Uncertainty in the impact of an above-average on-road gasoline-vehicle catalyst fraction would not be expected to have a large effect on the comparisons presented.

It would be desirable to find a tunnel situation where the driving conditions are more representative of urban driving in order to avoid having to make the highway-to-urban extrapolation of emission factors. The emission factors reported here are for on-road fleet averages for the 1981-1982 period and therefore should be periodically updated to account for changes in vehicle mix and emission control systems.

Acknowledgments

I wish to express my appreciation to Steve Pezda, Ford Automotive Emissions Office, for performing MOBILE 2 computations. I thank W. R. Pierson and J. M. Norbeck for many helpful discussions, Gary Duszkievicz for his efforts in assembling the sample train, A. C. Szkarlat and J. M. Norbeck for their efforts in data manipulation, and W. R. Pierson, S. M. Japar, W. W. Brachaczek, and A. C. Szkarlat for their help during the experiment. It is always a pleasure to acknowledge the assistance and cooperation of the Pennsylvania Turnpike Commission, the tunnel crew at Allegheny under the supervision of the late Robert J. Hauger, and the maintenance crew supervised by John R. Foor.

Registry No. CO, 630-08-0; NO, 10102-43-9; NO₂, 10102-44-0; NO_x, 11104-93-1.

Literature Cited

- (1) Sedefian, L.; Rao, S. T.; Petersen, W. B. *Environ. Sci. Technol.* **1981**, *15*, 364-365.
- (2) Bullin, J. A.; Polasek, J. C. *Environ. Sci. Technol.* **1981**, *15*, 365-366.
- (3) Bullin, J. A.; Moe, R. D. *Environ. Sci. Technol.* **1982**, *16*, 197-202.
- (4) Green, N. J.; Bullin, J. A. *Environ. Sci. Technol.* **1982**, *16*, 202-206.
- (5) Rao, S. T.; Sedefian, L.; Czapski, U. H. *J. Appl. Meteorol.* **1979**, *18*, 283-293.
- (6) Bullin, J. A.; Green, N. J.; Polasek, J. A. *Environ. Sci. Technol.* **1980**, *14*, 700-705.
- (7) Rodes, C. E.; Holland, D. M. *Atmos. Environ.* **1981**, *15*, 243-250.
- (8) Chock, D. P. *Atmos. Environ.* **1977**, *11*, 553-559.
- (9) Pierson, W. R.; Brachaczek, W. W. *SAE Trans.* **1976**, *85*, 209-228; *SAE Tech. Pap. Ser.* **1976**, No. 760039.
- (10) Pierson, W. R.; Brachaczek, W. W.; Hammerle, R. H.; McKee, D. E.; Butler, J. W. *J. Air Pollut. Control Assoc.* **1978**, *28*, 123-132.
- (11) Pierson, W. R.; McKee, D. E. *J. Air Pollut. Control Assoc.* **1978**, *28*, 604-607.
- (12) Pierson, W. R.; McKee, D. E.; Brachaczek, W. W.; Butler, J. W. *J. Air Pollut. Control Assoc.* **1978**, *28*, 692-693.
- (13) Pierson, W. R. "Proceedings of the Conference on Carbonaceous Particles in the Atmosphere". Berkeley, CA, 1979, Lawrence Berkeley Laboratory Report LBL-9037, pp 221-228.
- (14) Pierson, W. R.; Brachaczek, W. W.; McKee, D. E. *J. Air Pollut. Control Assoc.* **1979**, *29*, 255-257.
- (15) Ondov, J. M.; Zoller, W. H.; Gordon, G. E. *Environ. Sci. Technol.* **1982**, *16*, 318-328.
- (16) Kiyoura, R. *Proc. EPA Int. Symp. Health Eff. Diesel Engine Emiss.* **1980**, EPA-600/9-80-057a.
- (17) "Compilation of Air Pollutant Emission Factors: Highway Mobile Sources"; U.S. Environmental Protection Agency: Ann Arbor, MI, March 1981; EPA-460/3-81-005, PB81-238305.
- (18) Hampton, C. V.; Pierson, W. R.; Harvey, T. M.; Updegrave, W. S.; Marano, R. S. *Environ. Sci. Technol.* **1982**, *16*, 287-298.
- (19) Hampton, C. V.; Pierson, W. R.; Schuetzle, D.; Harvey, T. M. *Environ. Sci. Technol.* **1983**, *17*, 699-708.
- (20) Pierson, W. R.; Brachaczek, W. W. *Aerosol Sci. Technol.* **1983**, *2*, 1-40.

- (21) Japar, S. M.; Szkarlat, A. C.; Gorse, R. A., Jr. *Atmos. Environ.* 1981, 15, 2063-2070.
- (22) Pierson, W. R.; Gorse, R. A., Jr.; Szkarlat, A. C.; Brachaczek, W. W.; Japar, S. M.; Lee, F. S.-C.; Zweidinger, R. B.; Claxton, L. D. *Environ. Sci. Technol.* 1983, 17, 31-44.
- (23) Gorse, R. A., Jr.; Norbeck, J. M. *J. Air Pollut. Control Assoc.* 1981, 31, 1094-1096.
- (24) Chang, T.-Y.; Modzelewski, S. W.; Norbeck, J. M.; Pierson, W. R. *Atmos. Environ.* 1981, 15, 1011-1016.
- (25) Gorse, R. A., Jr.; Riley, T. L.; Ferris, F. C.; Pero, A. M.; Skewes, L. M. *Environ. Sci. Technol.* 1983, 17, 198-202.
- (26) Szkarlat, A. C.; Japar, S. M. *J. Air Pollut. Control Assoc.* 1983, 33, 592-597.
- (27) Pierson, W. R.; Brachaczek, W. W.; *Environ. Sci. Technol.* 1983, 17, 757-760.
- (28) "Motor Vehicle Quarterly MPG and Market Share Newsletter: MPG and Market Share Data System, 3rd Quarter-Model Year 1981"; Oak Ridge National Laboratory, Union Carbide Corp: Oak Ridge, TN, 1981; U.S. Department of Energy Contract No. W-7405-eng-26.
- (29) *Fed. Regist.* 1979, 44, 42443-42507.
- (30) *Fed. Regist.* 1982, 47, 25403-25472.
- (31) Stedman, D. H.; Jackson, J. O. *Int. J. Chem. Kinet., Symp.* 1975, No. 1, 493-501.
- (32) Harvey, R. B.; Stedman, D. H.; Chameides, W. J. *Control Assoc.* 1977, 27, 663-666.
- (33) Ehhalt, D. H.; Heidt, L. E. *Pure Appl. Geophys.* 1973, 106-108, 1352-1360.
- (34) Patterson, D. J.; Henein, N. A. "Emissions from Combustion Engines and Their Control"; Ann Arbor Science Publishers, Inc.: Ann Arbor, MI, 1972.
- (35) Barta, M. D. *SAE Tech. Pap. Ser.* 1976, No. 760831.
- (36) Meek, J. F., Ford Motor Co. Car Engineering, personal communication, 1982.
- (37) Williams, J. E.; Wallace, S. B., Ford Motor Co. Aerodynamics Department, personal communication, 1982.
- (38) "Development and Application of MVMA Passenger Car Emission Factors"; Motor Vehicle Manufacturers Association: Detroit, MI, Dec 1981.
- (39) Kennedy, G. J.; White, J. T.; Springer, K. J.; Ingalls, M. N. *SAE Tech. Pap. Ser.* 1975, No. 750901.
- (40) Edwards, J. B.; Shiller, J. W.; Fagley, W. S.; Liljedahl, D. R.; Martens, S. W.; Weaver, H. B.; Wimetete, H. J. *SAE Tech. Pap. Ser.* 1979, No. 790959.
- (41) Smith, L. R. "Characterization of Exhaust Emissions from High Mileage Catalyst-Equipped Automobiles"; Environmental Protection Agency: Ann Arbor, MI, Sept 1981; EPA-460/3-81-024, PB82-131566.

Received for review January 17, 1983. Revised manuscript received December 27, 1983. Accepted January 9, 1984.

Nonsingle-Valued Adsorption-Desorption of Bromacil and Diquat by Freshwater Sediments

Dennis L. Corwin* and Walter J. Farmer

Department of Soil and Environmental Sciences, University of California at Riverside, Riverside, California 92521

■ The adsorption and desorption of bromacil and diquat on eight freshwater sediments were studied. Nonsingle-valued adsorption-desorption isotherms of bromacil conformed to a set of Freundlich equations, while diquat nonsingular adsorption-desorption isotherms were best described by a set of Langmuir equations. A high degree of positive correlation was found to exist between the degree of bromacil adsorption and the sediment properties of organic carbon content and of charge density. Calculated Freundlich adsorption coefficients for bromacil ranged from 0.891 to 0.984 for $1/n$ and from 0.556 to 6.353 for K . The Langmuir affinity constant, k , for diquat adsorption on untreated sediments correlated well with the surface area while the adsorption maxima, b , correlated highly with the CEC for sediments treated for the removal of organic matter. For untreated sediments the Langmuir adsorption affinity constants ranged from 0.52×10^{-3} to 11.7×10^{-3} and the adsorption maxima ranged from 24331 to 69930. In general, the adsorption maxima for treated sediments decreased while the affinity constants increased when compared to the Langmuir coefficients of the untreated sediments. A surface charge density of approximately 0.2 C/m^2 ($6 \times 10^4 \text{ esu/cm}^2$) was found to result in the greatest bonding energy of the sediments for diquat. Desorption studies for both bromacil and diquat revealed that a linear relationship existed between the slope of the desorption isotherms and the initial adsorbate concentration from which desorption started.

Introduction

Recently, particular interest has been given to pesticide-sediment-water interactions (1-8) since the aquatic

environment constitutes a potential sink for many pesticides as a result of direct application, accidental spills, and/or "piggyback" transport upon eroded soil particles or in runoff waters.

Pesticides are known to be toxic to aquatic life over wide ranges of concentrations. Substantial differences in susceptibility to different compounds exist between and within species. For example, 96-h LC50 values of from 5 to 610 000 $\mu\text{g/L}$ were reported for various species of fish exposed to organophosphate pesticides (9). Since very low concentrations of certain pesticides can be potentially toxic to fish and other forms of aquatic life, it is important to have a knowledge of the chemical dynamics of pesticide-sediment-water interactions. As a result, one of the areas of prime consideration in pesticide-sediment-water interactions has been that of the adsorption and desorption of pesticides by sediments.

Adsorption-desorption pesticide studies have revealed that, in many instances, the desorption process is not completely reversible. This is not to say that there is true irreversibility of the desorption process but rather that the kinetics of desorption may be such that the desorption and adsorption paths are nonsingular. The observed hysteresis of the desorption of pesticides by soils (10-15) and sediments (16, 17) is of importance due to the fact that it results in a release of pesticide to the soil solution which is impossible to predict from adsorption isotherm data alone. Even when desorption isotherm data are available, it is difficult to predict the partitioning of the pesticide between the liquid and solid phases over long periods of time due to the continuous gradual change of pesticide concentration in the soil solution. Past models that have accounted for nonsingle-valued adsorption-desorption have been kinetic (18, 19) and empirically based models (20).

It will be the primary purpose of this paper to develop simple and multiple regression models from a compre-

* Address correspondence to this author at the U.S. Salinity Laboratory, Riverside, CA 92501.

hensive adsorption-desorption study of two chemically dissimilar herbicides on a variety of freshwater sediments. These models will make it possible to predict various pesticide sorption parameters from sediment properties. Similarly, the problem of hysteresis will be addressed by using linear regression analysis of adsorption and desorption isotherms. This approach is presented as an alternate empirical approach to account for nonsingular adsorption-desorption. An additional intention of the paper is to provide some insight into the interrelationship between some of the physical and chemical properties of sediments which in turn may influence the adsorption-desorption process.

Materials and Methods

Sediment samples were collected from eight water bodies located throughout California. These sites were selected to provide sediment samples with a wide range of physical and chemical properties. Five of the sites were from southern California and included Mockingbird Canyon Reservoir in the Riverside vicinity which receives runoff from citrus groves, San Joaquin Marsh, which is a freshwater marsh reserve located on the UC Irvine campus, and three lakes located in the San Bernardino Mountains: Baldwin Lake, Big Bear Lake, and Jenks Lake. Baldwin Lake receives secondary effluent from Big Bear City sewage treatment facility while Big Bear Lake and Jenks Lake receive water from runoff, horizontal groundwater flow, and precipitation. The three northern California water bodies included Clear Lake, which is a eutrophic lake located in Lake County, Castle Lake, which is a moderately productive cirque lake located in Siskiyou County, and the Hill Slough just outside of Fairfield in the Sacramento Delta region of Solano County.

Samples collected at each of the eight water bodies consisted of 45-cm core and 15-cm composite core sediment samples and water samples from the sediment-water interface. The samples were collected in 7.5-cm (3-in.) diameter PVC tubes at water depths ranging from 1.5 to 6 m (21). All samples were immediately sealed and frozen.

Prior to use the sediment samples were freeze-dried and passed through a 2-mm screen to remove large organic debris and gravel. Initial adsorption studies with the less than 2-mm-size fraction revealed that reproducibility problems existed due to sample heterogeneity. This problem was rectified by preparing a subsample which had been ground by using a rubber-tipped pestle to pass a 60-mesh (0.25 mm) sieve. The use of the rubber-tipped pestle reduced physical abrasion, thereby helping to prevent the reduction of particles beyond their natural particle size.

The techniques commonly used in the characterization of soils were used for the characterization of both the less than 2-mm and the less than 0.25-mm fractions of the sediments. The organic carbon content was determined by the Walkley-Black method, while organic matter was determined by treatment with H_2O_2 following the removal of salts with 1 N sodium acetate adjusted to a pH of 4.5 with acetic acid. The specific surface area was determined according to the method outlined by Mortland and Kemper (22) which provided a means of determining the external and internal surface area. Particle size analysis was carried out by means of the pipet method, and the free iron oxides (percent Fe_2O_3) were determined by the method outlined by Olson (23). Dry ash was obtained by subjecting 30-40-g subsamples to 375 °C for 16 h after pretreatment at 110 °C for 24 h to remove any adsorbed water. Cation exchange capacity (CEC) and exchange acidity (EA) were determined through the use of methods outlined by

Chapman and Pratt (24). Exchangeable bases (EB) were determined by difference.

Adsorption studies for bromacil were undertaken by using the radioassay batch technique and a 1 to 5 sediment to solution ratio. The 15-cm composite core sediment samples were used throughout the adsorption studies. Stock solutions of 1, 5, 10, 25, 50, 75, 100, and 300 $\mu\text{g}/\text{mL}$ bromacil were prepared from ^{14}C -labeled and analytical grade herbicide in 0.01 M CaCl_2 . Thin-layer chromatography performed on the radioactive-labeled samples revealed a purity of >98% for bromacil. Twenty milliliters of stock solution and 4 g of less than 0.25-mm sediment were placed in a Teflon-coated stainless steel tube and allowed to equilibrate by shaking in a constant temperature environmental chamber for 48 h. Initial kinetic studies had revealed that 48 h was sufficient time for the attainment of adsorption equilibrium. Once equilibrated, the slurry was centrifuged at 15000 rpm for 15-30 min and a $1/2$ -mL aliquot of supernatant placed into 20 mL of liquid scintillation cocktail (25) for radioassay. The pH of the supernatant was measured at this time. The amount of herbicide adsorbed was taken to be the difference between the amount added and the amount remaining in solution after equilibration. Each concentration was replicated 3-5 times.

Similarly, diquat adsorption studies were performed by using the batch technique, except that UV spectroscopy was used as the method of measurement. Stock solutions of 1000, 2500, 5000, 25000, 40000, 50000, 100000, and 125000 $\mu\text{g}/\text{mL}$ diquat dibromide monohydrate were prepared from analytical grade diquat (>99% pure). Following equilibration and centrifugation as previously described, an aliquot was taken and diluted with a buffer solution (pH 4.5) of sodium acetate and glacial acetic acid. Absorbance measurements were taken at 308 nm on a Beckman DU spectrophotometer to determine the concentration remaining in solution.

Adsorption isotherms were also determined with diquat on subsamples of the less than 0.25-mm sediment which had been repeatedly treated with H_2O_2 to remove the organic matter fraction.

Desorption studies were carried out with bromacil and diquat on selected sediments. The desorption experiments utilized the slurry from previous adsorption experiments except 10 mL of supernatant was removed from the centrifuged sample and replaced with 10 mL of 0.01 M CaCl_2 . The tube was then shaken in the environment chamber for 48 h, centrifuged, and measured as before. This stepwise desorption process was repeated for five to six successive desorptions. Desorption kinetic studies conducted over an 8-day period revealed that after 48 h over 93% of the total 8-day desorbed material had been desorbed for both bromacil and diquat; consequently, for convenience 48 h was also selected as the equilibrium time for the desorption studies.

Results and Discussion

Tables I and II summarize the physical and chemical properties of the eight freshwater sediments for both the less than 2-mm- and the less than 0.25-mm-size fractions, respectively. The tables show a wide range in properties among the selected sediments. Similarity exists amongst the sediments, however, in their high level of fine material (i.e., silt and clay). As can be seen in comparing Tables I and II, the removal of the coarse and medium sands (0.25-2 mm) had little effect on cation-exchange capacity, exchange acidity, organic carbon and organic matter content, dry ash, specific surface area, and free iron oxides. The pH of the less than 0.25-mm fraction, however, was

Table I. Chemical and Physical Characteristics of the Less Than 2-mm-Size Fraction of Freshwater Sediments^a

	Baldwin Lake	Big Bear Lake	Castle Lake	Clear Lake	Delta (Hill Slough)	Jenks Lake	Mockingbird Canyon	San Joaquin Marsh
EC _e , dS/m	1.0	1.6	0.5	1.6	6.4	0.2	3.1	9.4
EC _{1:5} , dS/m	0.6	1.0	0.2	0.8	2.1	0.2	1.2	3.0
pH _{SP} (distilled H ₂ O)	8.4	6.9	5.2	6.2	6.8	5.6	6.4	6.8
pH _{1:5} (distilled H ₂ O)	8.5	6.8	5.1	6.5	6.9	5.6	6.5	6.9
pH (in situ)	8.6	6.4	5.6	6.2	6.7	5.6	6.5	6.8
bulk density, g/cm ³	1.19	0.85	0.09	0.36	0.54	1.68	1.00	1.07
texture								
% sand	5.0	17.9	23.0	11.2	0.9	2.0	1.2	4.2
% silt	25.4	53.7	52.3	48.9	40.0	61.0	49.2	28.9
% clay	69.6	28.4	24.7	39.9	59.1	37.0	49.6	66.9
% salt (soluble + CaCO ₃)	39.4	17.1	1.1	5.0	6.1	2.6	11.5	10.7
% organic carbon (OC)	1.2	6.8	13.2	10.2	4.1	3.9	1.9	2.0
% organic matter (OM)	2.1	13.4	24.8	21.8	7.9	7.2	3.5	4.3
OM/OC	1.8	2.0	1.9	2.1	1.9	1.9	1.8	2.2
% dry ash	3.04	12.74	25.28	19.67	5.85	6.79	4.14	3.22
CEC, mequiv/100 g	37.0	55.0	40.1	50.9	31.1	21.3	29.3	37.3
EA, mequiv/100 g	0.6	7.3	23.5	21.9	8.0	9.5	9.8	2.5
EB, mequiv/100 g	36.4	47.7	16.6	29.0	23.1	11.8	19.5	34.8
% Fe ₂ O ₃	0.30	0.33	0.45	1.25	0.77	1.81	1.55	0.50
specific surface area, m ² /g								
total-untreated ^b	159.1	141.7	55.9	95.6	152.5	71.1	165.0	221.4
total-treated ^c	153.0	118.8	3.1	26.0	148.6	39.5	156.3	220.3
external-treated ^c	60.1	18.0	3.6	10.1	54.7	11.3	37.2	80.1
internal-treated ^c	9.29	100.8	0	15.9	93.9	28.2	119.1	140.2
OM basis ^d	353	177	213	320	56	440	280	61
CEC of OM, mequiv/100 g ^e	315	177	112	164	219	238	273	20
CEC of mineral fraction, mequiv/100 g	51.9	45.0	16.6	20.7	16.0	4.6	23.2	42.9

^aElectrical conductivities were determined on the saturation extract (EC_e) and for a 1 to 5 sediment to distilled water pastes (EC_{1:5}). The pH measurements were for the saturated paste (pH_{SP}) and a 1 to 5 sediment to distilled water paste (pH_{1:5}). ^bUntreated (1 N CaCl₂). ^cTreated (H₂O₂, 1 N CaCl₂). ^dArea m²/g of OM = [total^b - [total^c × (1.00 - fraction of residual OM)]]/(g of OM/g of soil). ^eCEC mequiv/100 g of OM = [total CEC - CEC of mineral fraction × [1 - (fraction of OM and salt)]]/(g of OM/100 g) × 100.

Table II. Chemical and Physical Characteristics of the Less Than 0.25-mm-Size Fraction of Freshwater Sediments^a

	Baldwin Lake	Big Bear Lake	Castle Lake	Clear Lake	Delta (Hill Slough)	Jenks Lake	Mockingbird Canyon	San Joaquin Marsh
EC _e , dS/m	1.03	2.20	0.52	1.76	7.60	0.54	2.12	9.20
EC _{1:5} , dS/m	0.54	0.50	0.21	0.72	3.20	0.14	0.60	3.11
pH _{SP} (distilled H ₂ O)	8.6	7.2	5.7	6.6	7.0	6.1	7.1	7.8
pH _{1:5} (distilled H ₂ O)	9.0	7.2	5.8	6.8	7.2	6.2	7.4	8.1
pH _{SP} (0.01 M CaCl ₂)	8.0	6.7	4.9	5.7	6.6	5.3	6.5	7.3
pH _{1:5} (0.01 M CaCl ₂)	8.0	6.7	4.8	6.0	6.6	5.4	6.7	7.1
% silt and sand	26.3	65.4	67.9	55.1	40.3	62.2	49.8	30.2
% clay	73.3	34.6	32.1	44.9	59.6	37.8	50.2	69.8
% salt (soluble + CaCO ₃)	37.3	15.6	0.6	3.6	4.5	0.8	11.3	12.3
% organic carbon (OC)	1.0	7.9	14.5	13.3	4.4	3.0	2.1	2.6
% organic matter (OM)	2.0	13.7	22.4	20.8	6.7	4.7	3.4	4.1
OM/OC	2.0	1.7	1.5	1.6	1.5	1.6	1.6	1.6
% dry ash	2.63	12.77	21.74	18.65	6.29	5.42	4.23	3.52
CEC (mequiv/100 g)	41.8	62.7	33.8	59.1	41.9	26.5	36.3	48.5
EA (mequiv/100 g)	0.2	5.5	19.0	19.1	9.4	11.1	7.1	5.8
% Fe ₂ O ₃	0.29	0.36	0.38	1.50	0.85	1.79	1.56	0.65
saturation percentage charge density, C/m ²	60.0	51.5	184.5	87.5	52.0	63.5	50.0	44.0
specific surface area, m ² /g	0.243	0.342	0.470	0.507	0.266	0.348	0.207	0.208
total-untreated ^b	165.7	177.0	69.4	112.4	151.7	73.4	168.8	225.1
total-treated ^c	158.2	168.2	27.6	63.2	148.1	58.0	150.9	217.8
external-treated ^c	60.4	27.9	27.3	22.3	54.4	18.6	36.1	78.9
internal-treated ^c	97.8	140.3	0.3	40.9	93.7	39.4	114.8	138.9
mineral fraction ^d								
total specific surface, m ² /g	196.6	100.5	27.6	63.6	130.9	50.9	87.4	251.3
CEC, mequiv/100 g	36.2	44.5	11.2	31.6	33.2	16.1	28.0	49.7
charge density, C/m ²	0.178	0.427	0.392	0.480	0.245	0.305	0.309	0.191

^aElectrical conductivities were determined on the saturation extract (EC_e) and for a 1 to 5 sediment to distilled water pastes (EC_{1:5}). The pH measurements were for the saturated paste (pH_{SP}) and a 1 to 5 sediment to distilled water paste (pH_{1:5}). ^bUntreated (1 N CaCl₂). ^cTreated (H₂O₂, 1 N CaCl₂). ^dTreated (1 N NaC₂H₃O₂·3H₂O, H₂O₂, 1 N CaCl₂).

Table III. Correlations between Sediment Properties of the Less Than 0.25-mm-Size Fraction

properties correlated	linear correlation coefficient (r)	multiple correlation coefficient (r)
pH to exchange acidity	0.865 ^e	
internal surface area to % clay	0.512	
total surface area ^a to % clay	0.622	
total surface area ^a to % silt and % clay		0.601
total surface area ^b to OM	0.393	
total surface area ^b to OM and % clay		0.502
total surface area ^b to OM, % silt, and % clay		0.503
charge density ^d to CEC ^d and total area ^d		0.954 ^e
charge density ^c to CEC ^c and total area ^c		0.907 ^e

^aTreated: sediment treated with hydrogen peroxide and 1 N CaCl₂. ^bUntreated: sediment untreated. ^cTreated: sediment treated with 1 N sodium acetate followed by hydrogen peroxide. ^dStatistically significant at the 5% level. ^eStatistically significant at the 1% level.

noticeably greater than the pH of the less than 2-mm fraction. The use of the less than 0.25-mm fraction for the adsorption-desorption studies not only would ameliorate the problem of reproducibility experienced with the less than 2-mm-size fraction but also would better accentuate the process of adsorption because of its close relation to the amount of organic matter and the amount of fine material, thus, enhancing any correlations which may be made.

Certain descriptive features were calculated for the less than 2-mm fraction of the sediments and compared with values normally reported for soils. The organic matter to organic carbon ratio (OM/OC) ranged from 1.8 to 2.2 with an average of 2.0 which is slightly higher than the 1.9 ratio for surface soils and less than 2.5 for subsoils cited in the literature (26). The area per gram of organic matter ranged from 56 to 440 m²/g which is lower than the range 558–803 m²/g cited by Bower and Gschwend (27). The cation-exchange capacity of the organic matter fraction averaged 214 mequiv/100 g when the unexplainably low organic matter cation-exchange capacity of San Joaquin Marsh (20 mequiv/100 g) was omitted. This compares favorably with soils which range from 112 to 252 mequiv/100 g of organic matter as cited by Baver (28).

Table III compares correlation coefficients of both simple and multiple correlations made between sediment properties of the less than 0.25-mm-size fraction. As can be seen, there is a high correlation between pH and exchange acidity, as would be expected, as well as a high correlation between charge density and the properties of cation-exchange capacity and total surface area. Total surface area, however, does not correlate well with organic matter and/or finer particles (i.e., silt and clay), nor does internal surface area correlate with the percent of clay material. With the possible exception of the low correlation obtained between the total surface area and the finer particle fraction, the sediment properties were generally consistent with similar properties measured on soils by other investigators.

Redox potential, pH, and organic carbon content determined at 5-cm increments for the 45-cm core samples

Table IV. Water Properties of the Eight Freshwater Sample Sites

sample site	pH	electrical conductivity, dS/m
Baldwin Lake	8.3	1.2
Big Bear Lake	7.9	0.5
Castle Lake	5.8	0.2
Clear Lake	6.9	0.3
Delta (Hill Slough)	7.4	3.4
Jenks Lake	6.9	0.2
Mockingbird Canyon	6.7	0.6
San Joaquin Marsh	8.2	6.8

revealed that, in general, the sediments varied only slightly over the depth increment selected for the composite core samples, 0–15 cm. Because of this general uniformity in properties within the top 0–15 cm, a composite of this depth increment was used for all adsorption-desorption analysis. Analysis of water samples taken from the sediment-water interface (Table IV) showed that the pH of the water in most cases tended to be higher than that of the sediment while the electrical conductivity of the water tended to be lower than the EC_e of the freeze-dried sediment, with the high electrical conductivities being high in both the water and sediment and with the low ones low.

The adsorption data for bromacil, a weakly basic herbicide, best fit a Freundlich isotherm for the range of concentrations used. That is

$$S_{ads} = K_{ads} C^{1/n} \quad (1)$$

where S_{ads} is the amount of chemical adsorbed (μg) per mass of soil or sediment (g), C is the equilibrium concentration of chemical in solution ($\mu\text{g}/\text{mL}$), and K_{ads} and $1/n$ are coefficients of adsorption. K_{ads} is a measure of the degree or strength of adsorption while $1/n$ indicates the degree of nonlinearity between solution equilibrium concentration and adsorption.

In the log form, eq 1 becomes

$$\log S_{ads} = (1/n) \log C + \log K_{ads} \quad (2)$$

Thus, K_{ads} and $1/n$ in eq 2 can be readily solved by linear regression analysis by using a log transformation or graphically by a log-log plot of the amount of herbicide adsorbed per gram of sediment (S_{ads}) and the equilibrium solution herbicide concentration (C). K_{ads} is the intercept and $1/n$ is the slope of the line. Figure 1 illustrates a typical set of bromacil adsorption-desorption isotherms for one of the sediments.

The values of K_{ads} and $1/n$ for bromacil adsorption on the untreated sediments are given in Table V. The value of $1/n$ for the eight sediments is slightly less than unity (i.e., average $1/n = 0.917$) while the adsorption partition coefficient, K_{ads} , ranges from 0.556 to 6.353. Linear regression analysis of the adsorption partition coefficient and individual sediment properties confirm previous findings with soils which show a high degree of positive correlation ($r = 0.902$) between organic carbon and the degree of adsorption represented quantitatively by K_{ads} (29–32). The following regression equation relating K_{ads} to percent organic carbon was obtained:

$$K_{ads} = 0.709 + 0.367(\% \text{ organic carbon}) \quad (3)$$

As shown by numerous previous investigators (7, 33–35, 31), when the adsorption partition coefficient is normalized to organic carbon by the following equation

$$K_{OC} = \frac{K_{ads}}{\% \text{ organic carbon}} \times 100 \quad (4)$$

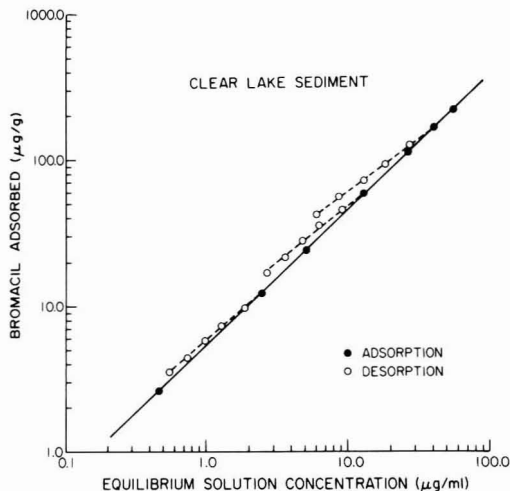


Figure 1. Representative adsorption-desorption isotherms showing the adsorption-desorption of bromacil upon Clear Lake sediment at 25 °C.

Table V. Freundlich Adsorption Partition Coefficients and K_{OC} 's for Bromacil on the Less Than 0.25-mm-Size Fraction of Untreated Sediments at 25 °C

site	Freundlich adsorption partition coefficients		
	1/n	K_{ads}	K_{OC}
Baldwin Lake	0.984	2.891	289.1
Big Bear Lake	0.860	3.926	49.7
Castle Lake	0.930	6.353	43.8
Clear Lake	0.917	5.260	39.5
Delta (Hill Slough)	0.905	2.716	61.7
Jenks Lake	0.891	1.197	39.9
Mockingbird Canyon	0.951	0.556	26.5
San Joaquin Marsh	0.900	0.684	26.3
average	0.917	2.948	41.1 ^a
standard deviation	0.038	2.134	12.5

^aThe K_{OC} value for Baldwin Lake was excluded from the calculation of the average K_{OC} .

K_{OC} is found to be generally less variable than when expressed solely on a total sediment basis (Table V). Baldwin Lake (organic carbon content = 1.0%) had higher K_{OC} than the other sediments which is commonly the case for low organic matter soils or sediments. Hamaker and Thompson (33) propose that this tendency is due to the fact that the mineral phases may be responsible for making a significant contribution to the total adsorption. Since the ratio of clay to organic carbon is very high in the case of Baldwin Lake, it is not reasonable to expect carbon to govern the sorptive response; consequently, the Baldwin Lake K_{OC} was excluded from the average K_{OC} calculation.

A positive correlation also exists between charge density and the degree of bromacil adsorption for both untreated sediments ($r = 0.846$) and sediments treated for the removal of organic matter ($r = 0.800$). Because of possible changes in the soil from such drastic treatments as wet oxidation (e.g., H_2O_2), caution should be taken in the interpretation of these data. However, the results do indicate the presence of possible adsorption sites other than those provided by organic matter.

Multiple regression analysis of the Freundlich adsorption coefficient for bromacil and sediment properties indicate

Table VI. Linear Regression Analysis of Freundlich Desorption Isotherms for Bromacil on Selected Sediments

sediment sample	S_0^a µg/g	K_{des}	1/n	regression equations	R^2
Big Bear Lake	10.02	4.773	0.712	$1/n = 0.734 + 0.0003S_0$	0.88
	43.78	5.363	0.758		
	116.25	4.851	0.797		
Castle Lake	407.09	3.931	0.860	$1/n = 0.8424 - 0.00003S_0$	0.96
	13.27	6.724	0.845		
	64.34	8.130	0.840		
Clear Lake	184.04	9.556	0.834	$1/n = 0.8158 - 0.00005S_0$	0.99
	674.71	10.556	0.820		
	12.27	5.709	0.809		
	58.37	7.709	0.791		
	161.50	11.001	0.740		

^aInitial adsorbate concentration at which desorption began.

that K_{ads} could be best predicted from the combined properties of organic matter, exchange acidity, percent Fe_2O_3 , and percent clay when used as the independent variables of a linear multiple regression equation.

$$K_{ads} = 0.800 + 0.248(\% \text{ organic matter}) - 0.007(\% \text{ exchange acidity}) + 0.011(\% \text{ clay}) - 0.810(\% Fe_2O_3) \quad (5)$$

$$R^2 = 0.986$$

The results of bromacil desorption studies performed on sediments from Big Bear Lake, Castle Lake, and Clear Lake are summarized in Table VI. The Freundlich equation is used to describe the desorption isotherm data:

$$S_{des} = K_{des} C^{1/n} \quad (6)$$

where S_{des} is the amount of chemical remaining adsorbed to the surface of the adsorbent after a desorption event per mass of the adsorbent, C is the equilibrium concentration in solution, and K_{des} and $1/n$ are constants. In this case, K_{des} reflects the degree of adsorption after desorption has occurred.

Analysis of the desorption data in Table VI for each of the three sediments using linear regression analysis on the initial surface concentration of the adsorbate and the slope ($1/n$) reveals a high correlation. The high R^2 values for the regression equations of Table VI show that it is possible to predict the desorption isotherms of bromacil for each of the three selected sediments with only the knowledge of the initial adsorbate concentration prior to any desorption. This provides a means of modeling the adsorption-desorption process as long as desorption is a continuous process uninterrupted by re-adsorption.

The adsorption isotherms for diquat showed it to be a very strongly adsorbed herbicide. Figure 2 illustrates a typical set of adsorption-desorption isotherms. The adsorption data for diquat, a strongly basic herbicide, was described by the following linear form of the Langmuir equation:

$$C/S = 1/(kb) + C/b \quad (7)$$

where S is the amount adsorbed per unit weight of adsorbent ($\mu\text{g/g}$), C is the equilibrium concentration ($\mu\text{g/mL}$), b is the adsorption maximum, and k is an affinity constant related to the bonding energy of adsorbent for adsorbate. Linear regression lines were calculated, and the Langmuir constants, b and k , were found for each of the eight sediments (see Table VII). The R^2 values for the

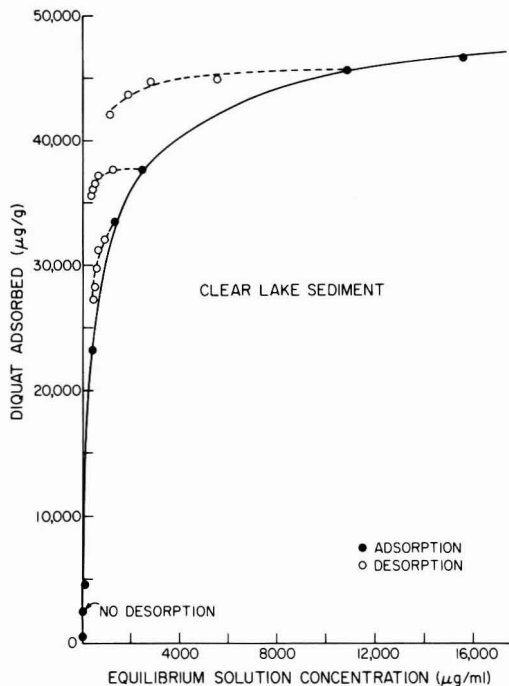


Figure 2. Representative adsorption-desorption isotherms showing the adsorption-desorption of diquat upon Clear Lake sediment at 25 °C.

Table VII. Langmuir Adsorption Maxima and Affinity Constants for Diquat on Untreated and Treated Sediments at 25 °C

site	untreated sediment		treated sediments ^a	
	adsorption maxima, <i>b</i>	affinity constants, <i>k</i> ($\times 10^{-3}$)	adsorption maxima, <i>b</i>	affinity constants, <i>k</i> ($\times 10^{-3}$)
Baldwin Lake	44 053	8.66	42 918	12.6
Big Bear Lake	52 356	8.95	40 650	10.6
Castle Lake	24 390	0.52	5 510	1.41
Clear Lake	48 309	1.51	28 736	2.01
Delta (Hill Slough)	53 191	6.19	43 668	3.34
Jenks Lake	24 331	2.54	18 727	4.25
Mockingbird Canyon	43 860	10.1	42 373	12.2
San Joaquin Marsh	69 930	11.7	68 966	21.6

^aTreated for removal of organic matter with hydrogen peroxide.

regression lines ranged from 0.997 to 1.000, indicating that the adsorption data conformed extremely well to the Langmuir linear equation over the range of selected concentrations. As expected for a cationic herbicide, the adsorption maxima for diquat were relatively high ranging from 24331 to 69930 µg/g.

Correlations between individual soil properties and the Langmuir affinity constant, *k* were performed. Surface area was the only property which was highly correlated to the affinity constant ($r = 0.937$). Of particular interest, however, was the relationship between surface charge density of the sediments and *k*. A moderate negative correlation ($r = -0.884$) between charge density and *k* was

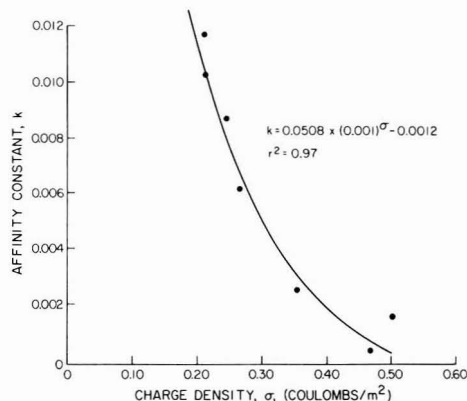


Figure 3. Langmuir affinity constant, *K*, for diquat as related to the charge density, σ , of seven freshwater sediments.

found by the linear regression analysis, but a plot of charge density and *k* revealed an interesting exponential function. Figure 3 illustrates that the affinity constants increase exponentially as a function of decreasing charge density excluding Big Bear Lake. This indicates that the charge separation of diquat is such that a charge density on the adsorbent surface of approximately 0.2 C/m² (6×10^4 esu/cm²) results in the greatest bonding energy of adsorbent for diquat over the range of observed charge densities. Furthermore, knowledge of the charge density of an adsorbent permits a means of approximating the affinity constant from the "best fit" equation

$$k = 0.0508(0.001)^\sigma - 0.0012 \quad (8)$$

where σ is the charge density.

A similar linear regression analysis between individual soil properties and the Langmuir adsorption maxima, *b*, was performed. On an individual soil property basis, *b* also correlated well with surface area ($r = 0.904$).

$$b = 8.729 + 0.254(\text{total area}) \quad (9)$$

Previous work with diquat by other investigators demonstrated that the adsorption of diquat on clays was directly related to the cation-exchange capacity and as such involved an ion-exchange mechanism of adsorption (36-40). This was also the case for the eight sediments after they were treated for the removal of organic matter. Correlations between CEC and *b* of the sediments treated for the removal of organic matter showed a high positive correlation ($r = 0.904$). Untreated sediments, however, showed little correlation between CEC and *b* ($r = 0.658$). Ostensibly, the organic matter fraction influences the process of ion exchange possibly through its varying effect upon the structure of solvating water of the macromolecular organic matter since water structure is important in determining the extent of adsorption (33).

Desorption studies were performed on each sediment at four different initial adsorbate concentrations. The desorption curves were described with the linear form of the Langmuir equation. Table VIII summarizes the adsorption maxima, *b*, and affinity constants, *k*, calculated for each desorption curve. For all eight sediments, diquat was adsorbed so tightly to the sediment surface for an initial adsorbate concentration of 2500 µg/g that no desorption occurred. As in the case of bromacil, a linear relationship was found to exist for diquat between the slope (1/*b*) of the desorption isotherm and the initial adsorbate concentration from which desorption occurred. Table VIII displays the linear regression equation for each sediment

Table VIII. Linear Regression Analysis of Langmuir Desorption Isotherms for Diquat on Eight Freshwater Sediments

sediment sample	S_0^a $\mu\text{g/g}$	b	k	regression equations	R^2
Baldwin Lake	2500				
	37240	37453	0.350	$1/b = (4.95 \times 10^{-5}) - (6.13 \times 10^{-10})S^0$	0.99
	40400	40650	0.053		
	43125	43290	0.011		
2500					
Big Bear Lake	2500				
	38600	42735	0.034	$1/b = (3.66 \times 10^{-5}) - (3.32 \times 10^{-10})S^0$	0.95
	43535	44053	0.075		
	52000	52356	0.019		
2500					
Castle Lake	2500				
	16250	16722	0.0087	$1/b = (1.009 \times 10^{-4}) - (2.57 \times 10^{-9})S^0$	0.99
	18125	18657	0.0063		
	22250	22676	0.0042		
2500					
Clear Lake	2500				
	33500	37594	0.0063	$1/b = (4.13 \times 10^{-5}) - (4.22 \times 10^{-10})S^0$	0.91
	37700	38023	0.050		
	45250	45662	0.014		
2500					
Delta (Hills Slough)	2500				
	38030	38168	0.755	$1/b = (4.48 \times 10^{-5}) - (4.94 \times 10^{-10})S^0$	0.99
	43060	43290	0.130		
	52375	52632	0.012		
2500					
Jenks Lake	2500				
	21100	21552	0.013	$1/b = (8.35 \times 10^{-5}) - (1.76 \times 10^{-9})S^0$	1.00
	22200	22472	0.015		
	24463	24691	0.007		
2500					
Mockingbird Canyon	2500				
	37500	37594	0.573	$1/b = (4.94 \times 10^{-5}) - (6.09 \times 10^{-10})S^0$	1.00
	40850	40984	0.285		
	43750	43860	0.382		
2500					
San Joaquin Marsh	2500				
	39880	40000	1.53	$1/b = (3.83 \times 10^{-5}) - (0.348 \times 10^{-9})S^0$	0.98
	49530	49505	1.35		
	69500	69444	1.22		
2500					

^a Initial adsorbate concentration at which desorption began.

as well as the corresponding R^2 values. R^2 values close to unity confirm the close relationship between the slope of the desorption isotherms for each sediment and the initial adsorbate concentration on the adsorbent surface.

Summary

Adsorption and desorption are key chemical processes in determining the amount of herbicide which is available for movement in soils and sediments. In order to attain a predictive level of knowledge of the fate of herbicides in aquatic systems, it is crucial that both the adsorption and desorption of herbicides by sediments be quantitatively characterized. The complexity of sediment as an adsorptive media makes a statistical approach to modeling adsorption and desorption a favorable one.

The calculated adsorption-desorption isotherm parameters for bromacil and diquat shown in Tables V-VIII indicate that the processes of adsorption and desorption are obviously not single valued for the predetermined equilibrium time. This hysteretic effect indicates that no single equation will describe both processes. Certain questions still remain as to whether kinetic limitations are the principal cause for the observed nonsingularity. Since desorption kinetic experiments were only carried out up to 8 days, further desorption kinetic studies on sterilized sediments for much longer periods of time (8-30 days) need to be carried out to confirm whether or not significant solute-surface interactions are still occurring.

The Freundlich equation was used to describe both the adsorption and desorption data for bromacil, while the Langmuir equation best fit the adsorption-desorption isotherms obtained for diquat. Though a single Freundlich or Langmuir equation could be used to describe the ad-

sorption isotherm for a given sediment, this was not the case for desorption which required a different set of desorption parameters for each initial adsorbate concentration at which desorption was initiated. It was found, however, that the slope of each desorption curve, whether for bromacil or diquat, was a function of the initial adsorbate concentration on the adsorbent surface. As such, linear regression equations were derived for each sediment and herbicide concentration which made it possible to predict the desorption isotherm at any point along the adsorption isotherm.

Acknowledgments

We thank E. I. du Pont de Nemours & Co. for supplying analytical grade and ^{14}C -labeled bromacil and Chevron Chemical Co. for supplying analytical grade diquat.

Registry No. Bromacil, 314-40-9; diquat, 2764-72-9.

Literature Cited

- (1) Lotse, E. C.; Graetz, D. A.; Chesters, G.; Lee, B. G.; Newland, L. W. *Environ. Sci. Technol.* **1968**, *2*, 353-357.
- (2) Nicholson, H. P.; Hill, D. W. *Relat. Agric. Soil Water Pollut., Cornell Univ. Conf.* **1970**, 178-179.
- (3) Veith, G. D.; Lee, G. F. *Environ. Sci. Technol.* **1971**, *5*, 230-234.
- (4) Weber, J. B. In "Fate of Organic Pesticides in the Aquatic Environment"; American Chemical Society: Washington, DC, 1972; Chem. Ser. pp 55-120.
- (5) Pionke, H. B.; Chesters, G. *J. Environ. Qual.* **1973**, *2* (1), 29-45.
- (6) Karickhoff, S. W.; Brown, D. S.; Scott, T. A. *Water Res.* **1979**, *13*, 241-248.
- (7) Karickhoff, S. W. *Chemosphere* **1981**, *10*, 833-846.

- (8) Goldberg, M. C. *Sci. Total Environ.* 1982, 24, 73-84.
 (9) Pickering, Q. H.; Henderson, C.; Lemke, A. E. *Trans. Am. Fish. Soc.* 1962, 91, 175-184.
 (10) Harris, C. I.; Warren, G. F. *Weeds* 1964, 12, (2), 120-126.
 (11) Yaron, B.; Swoboda, A. R. S.; Thomas, G. W. *J. Agric. Food Chem.* 1967, 15, 671-675.
 (12) Williams, J. D. H. *Weed Res.* 1968, 8, 327-335.
 (13) Huang, J. C.; Liao, C. S. *J. San. Eng. Div., Am. Soc. of Civ. Eng.* 1970, 96, 1057-1078.
 (14) Moyer, J. R.; McKercher, R. B.; Hance, R. J. *Can. J. Soil Sci.* 1972, 52, 439-447.
 (15) Mustafa, M. A.; Gamar, Y. *Soil Sci. Soc. Am. Proc.* 1972, 36, 561-565.
 (16) Huang, J. C. *J. Water Pollut. Control Fed.* 1971, 43, 1739-1748.
 (17) Peck, D. E.; Corwin, D. L.; Farmer, W. J. *J. Environ. Qual.* 1980, 9 (1), 101-106.
 (18) Lindstrom, F. T.; Boersma, L.; Stockard, D. *Soil Sci.* 1971, 112, 291-300.
 (19) Lapidus, L.; Amundson, N. R. *J. Phys. Chem.* 1952, 56, 984-988.
 (20) van Genuchten, M. Th.; Davidson, J. M.; Wierenga, P. J. *Soil Sci. Soc. Am. Proc.* 1974, 38, 29-35.
 (21) Barkley, J. H. *Bull. Environ. Contam. Toxicol.* 1971, 6, 313-315.
 (22) Mortland, M. M.; Kemper, W. D. In "Methods of Soil Analysis"; American Society of Agronomy: Madison, WI, 1965; Part I, pp 532-544.
 (23) Olson, R. V. In "Methods of Soil Analysis"; American Society of Agronomy: Madison, WI, 1965; Part I, pp 963-973.
 (24) Chapman, H. D.; Pratt, P. F. In "Methods of Analysis for Soils, Plants and Water"; University of California, Division of Agricultural Sciences: Berkeley, CA, 1961.
 (25) Lavy, T. L.; Messersmith, C. G.; Knoche, H. W. *Weed Sci.* 1972, 20 (3), 215-219.
 (26) Broadbent, F. E. *Adv. Agron.* 1953, 5, 153-183.
 (27) Bower, C. A.; Gschwend, F. B. *Soil Sci. Soc. Am. Proc.* 1952, 16, 342-345.
 (28) Bayer, L. D. *J. Am. Soc. Agron.* 1930, 22, 703-708.
 (29) Graham-Bryce, I. J. *J. Sci. Food Agric.* 1967, 18, 72.
 (30) Furnidge, C. G.; Osgerby, J. M. *J. Sci. Food Agric.* 1967, 18, 269-273.
 (31) Lambert, S. M.; Porter, P. E.; Schieferstein, R. T. H. S. *Weeds* 1965, 13, 185.
 (32) Goring, C. A. I. *Soil Sci.* 1962, 93, 211-218.
 (33) Hamaker, J. W.; Thompson, J. M. In "Organic Chemicals in the Soil Environment"; Marcel Dekker: New York, 1972; pp 49-143.
 (34) Lambert, S. M. *J. Agric. Food Chem.* 1968, 16 (2), 340-343.
 (35) Goring, C. A. I. *Ann. Rev. Phytopathol.* 1967, 5, 285-318.
 (36) Weber, J. B.; Word, T. M.; Weed, S. B. *Soil Sci. Soc. Am. Proc.* 1968, 32, 197-200.
 (37) Weber, J. B.; Weed, S. B. *Soil Sci. Soc. Am. Proc.* 1968, 32, 485-487.
 (38) Philen, O. D., Jr.; Weed, S. B.; Weber, J. B. *Soil Sci. Soc. Am. Proc.* 1970, 34, 527-531.
 (39) Dixon, J. B.; Moore, D. E.; Agnihotri, N. P.; Lewis, D. E., Jr. *Soil Sci. Soc. Am. Proc.* 1970, 34, 805-808.
 (40) Gamar, Y.; Mustafa, M. A. *Soil Sci.* 1975, 119 (4), 290-295.

Received for review April 5, 1983. Revised manuscript received January 4, 1984. Accepted January 23, 1984. The research leading to this report was supported by the University of California Water Resources Center, as part of Water Resources Center Project UCAL-WRC-W-485.

Persistence of Pesticides in Surface Soil and Relation to Sublimation

Charles A. Sleicher* and John Hopcraft

Department of Chemistry, University of Nairobi, Nairobi, Kenya

■ To help explain low concentrations of DDT found in some birds of Kenya, a field test of the rate of disappearance of DDT from soil near Lake Nakuru, Kenya, was conducted and gave a half-life of 110 days. The data suggest that the DDT sublimed directly without prior degradation to DDE. Calculated sublimation rates based on mass transfer through the boundary layer are sufficient to account for the rapid disappearance. The model gives a sublimation rate proportional to the vapor pressure of DDT, the $2/3$ power of its diffusivity in air, and the 0.60 power of the wind speed. The results show that sublimation alone can account for the disappearance of pesticides of low volatility even if they are strongly adsorbed on soils and that the uncontrolled use of DDT in Kenya may affect wildlife to a lesser extent than had been feared.

A field test of the rate of disappearance of DDT from a tropical soil is reported. Kenya was chosen for the test because it places no restrictions on the use of DDT and other insecticides, and so these chemicals form a potential threat to both the human population and the spectacular wildlife for which Kenya is renowned. Because DDT is cheap and useful for control of malaria and agricultural pests, reduction of its use might cause significant economic and health problems.

* Address correspondence to this author at the Department of Chemical Engineering, University of Washington, Seattle, WA 98195.

The threat posed to wildlife by uncontrolled use of DDT is particularly severe at Lake Nakuru, a small lake (42 km²) at an elevation of 1758 m in the Great Rift Valley 35 km south of the equator. Over 400 species of birds have been identified there, and the lake is a principal feeding ground of the lesser flamingo (*Phoeniconotais minor*), more than a million of which can sometimes be seen. The lake was declared a National Park in 1968—the first national park in Africa to be set aside on account of its bird life, though it is also a refuge for over 50 species of mammals.

Lake Nakuru is unusually vulnerable to pollution. Its average depth is about 2 m, it has no outlet, and it is the low point in a basin of about 1940 km² largely devoted to agriculture. The lake also receives storm sewers and sewage outfall from the city of Nakuru, which is adjacent to the Park boundary, has a population of 100 000, and is the fastest growing major city in Kenya.

Ecologically Lake Nakuru is simple and, therefore, probably vulnerable to perturbations. The lake is so alkaline (pH 10.5) that few forms of life can survive there. The abundant blue-green alga (*Spirulina platensis*) is the basis of its food chain. The principal herbivores are the lesser flamingo, a single species of fish (*Tilapia grahami*), and a small copepod (*Lovelulu sp.*), all of which feed on algae. The fish and copepods in turn are the principal foods of an estimated 27 000 other aquatic birds. Rainfall averages 8 cm/month from March through November and about 3 cm/month from December through February. The daily average maximum, mean, and minimum tempera-

tures are relatively constant throughout the year and are 27 ± 3 , 18 ± 2 , and 10 ± 2 °C. Midday relative humidity averages about 50%. Wind speeds range from dead calm to strong, but on a typical day there is a breeze in the range 1–5 m/s.

A study of chlorinated hydrocarbon residues at Lake Nakuru was made by Koeman et al. in 1970 (1). Samples from several species of piscivorous birds and fish were collected and analyzed for DDT, DDE, DDD, and dieldrin, and endrin. The results, gratifyingly low, ranged from <0.001 to 0.064 $\mu\text{g/g}$. Frank et al. (2), on the other hand, found much higher values in birds of prey taken from Nakuru; the median concentration of 15 samples was 1.2 $\mu\text{g/g}$, which is low compared to birds of prey in temperate latitudes. A 4.7-g sample of copepods from the lake analyzed by us in 1972 contained 0.003 $\mu\text{g/g}$ DDT and 0.007 $\mu\text{g/g}$ DDE. We also analyzed algae and mud samples from the lake but found no DDT or DDE (limit of detectability approximately 0.001 $\mu\text{g/g}$).

The low level of pesticide residues found in these studies suggests that these insecticides disappear more rapidly at Lake Nakuru than in temperate climates, where the rate of disappearance of pesticides from soil has been the subject of numerous studies, excellent reviews of which are available (3–5). The disappearance is caused by sublimation, chemical degradation, bacterial degradation, and transportation by wind erosion of surface dust. The rates of these processes depend upon many variables (5–7) and are often characterized by a half-life, which implies an exponential decay law, $C = C_0 \exp(-0.693/t) t$ where C_0 is the initial concentration and t' is the half-life. This law follows from the condition that the rate is proportional to the amount present.

The exponential law is an inaccurate description of DDT disappearance in many cases (4, 6–9). For example, the idealized case of sublimation from a single smooth, flat area with a uniform deposit of DDT would give a constant mass-transfer rate and a linear decay of concentration as long as the area of the deposit remained constant. If, however, the surface were rough or of complex geometry or the thickness of the insecticide layer nonuniform, the area of the deposit and hence mass-transfer rate would decrease with the time. If the area were proportional to the amount of pesticide present, the decay would be exponential. The process is further complicated by adsorption of DDT on soil surfaces and by diffusion of insecticide into the soil followed by diffusion back to the surface as surface layers become depleted. Lichtenstein et al. (6) give a particularly compelling discussion of the limitations of the half-life concept.

Though the exponential law is not a good model of DDT disappearance under all circumstances, it often provides a useful measure of disappearance rate provided that the time span is not too large and that it is understood that the half-life is a function of many other variables. In this spirit, measurements of the half-life of DDT in soil have been reported and range from 16 weeks for surface application in England (10) to 30 years for forest soils of Canada (11). Edwards (3) reports a mean value of 10 years. The data from the Sudan of El Zorgani (12) give a half-life of 18 days.

Field Tests

To test the rate of disappearance of DDT from soil in Kenya, a field test was begun in 1972 on the Baharini Wildlife Sanctuary, now part of Lake Nakuru National Park. Two small plots (2.5 m by 2.5 m) were sprayed with a water emulsion of commercial DDT (about 80% of the *p, p'* isomer) at the rate of 2 lb of DDT/acre or 1.3 g/plot.

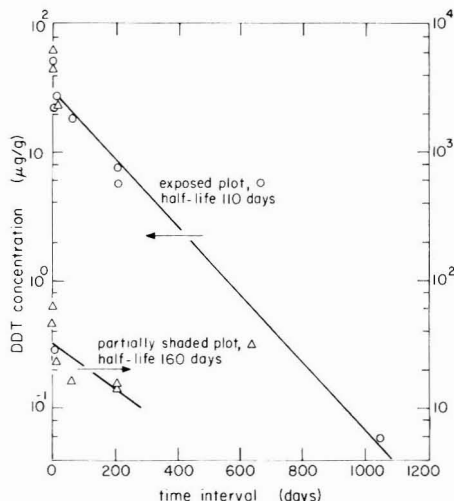


Figure 1. Rate of disappearance of DDT from Nakuru soil.

One plot was level, open grassland exposed to solar radiation, and the other was under the partial shade of yellow thorn trees (*Acacia xanthophloe*). At the time of spraying both plots had short grass (<20 cm) and were wired to prevent access by cattle. No other vegetation existed near the sites.

Soil analysis of the fully exposed plot gave the following composition: organic matter, 16%; clay, 23%; silt, 11%; sand, 50%. Corresponding figures for the partially shaded plot were 54, 11, 4, and 31%.

Spraying took place under conditions of no wind with a pressurized hand sprayer held about 30 cm above the ground. Samples of surface soil and grass were collected consecutively from each of nine 45 cm × 45 cm squares located symmetrically within but away from the edges of the plots. Grass samples weighed about 1 g; soil samples weighed 7–10 g and were collected from the upper 4–5 mm of soil. The samples were extracted with an equivolume mixture of benzene and 2-propanol, which was concentrated and then analyzed by gas chromatography (2-m silanized glass column filled with an equal mixture of 10% DC-200 and 15% QF on Gas-Chrom Q, electron capture detection). Blanks and spiked samples were frequently processed. A variety of extraction times and conditions were tried, and on spiked samples the best procedure gave recoveries that usually exceeded 90% and always exceeded 70%. Except for the 1975 sample no cleanup was necessary because of the high concentrations of DDT. The 1975 sample weighed 37 g, and a 17-cm long Florisil column was used for cleanup.

Results and Discussion

The results are shown in Table I and Figure 1. In the figure the lines are least-squares fits to the data; for each plot, data for 1, 2, and 7 days were used in both calculations since the plots were sprayed in a similar manner and little DDT loss was experienced in that time.

No DDE or DDD, the principal metabolites of DDT, were detected. Since the grass tissue continually grew and died, the DDT concentrations in the grass have little meaning other than to show that the grass collected large amounts of DDT. Rainfall occurred periodically during the sampling but had no apparent effect on DDT levels. (At Nakuru the surface soil usually dries rapidly following rain.) The heaviest rainfall prior to the Dec 13 sample was

Table I. DDT Concentration in Soil

time, days	p,p'-DDT concentration				
	exposed plot		shaded plot		
	grass	soil	grass	soil	
Oct 13, 1972	4	210	22	190	46
Oct 15, 1972	2	230	52	410	63
Oct 21, 1972	7	230	27	370	23
Dec 13, 1972	61	24	18	105	16
May 12, 1973	206		5.5		16
May 12, 1973			7.5		14
Aug 30, 1975	1046		0.06		

1.5 cm, which occurred on Oct 14-15, 1972, before the second sample was collected.

The importance of the single point at 1046 days for the exposed plot is evident, though it is consistent with other points. The half-life of DDT on the exposed plot is but 110 days, or 0.3 year, with correlation given by $r^2 = 0.96$. This half-life is much lower than values usually found in temperate climates. Unfortunately, a late sample for the shaded plot could not be obtained, and the estimate of 160 days for the partially shaded plot is rough, $r^2 = 0.48$.

Loss of DDT from the soil can occur by direct sublimation or degradation to DDE (and possibly other products) followed by sublimation of the DDE, which has a vapor pressure about 8 times higher than that of DDT. Spencer and Cliath (13) advance the latter mechanism, but the prevailing mechanism probably depends on local conditions.

In our case no DDE was found in any soil sample, and a quantity of 1% of the DDT level would have been easily detected in all samples except the one at 1046 days. This finding is compelling evidence that the dominant mechanism in our studies was the direct sublimation of DDT; for if DDE had formed, it would have been found in the samples even though it sublimates more rapidly than DDT. To make this clear, consider the following analysis: Let M_0 = mass of DDT initially present, M_1 = mass of DDT at any time, M_2 = mass of DDE at any time, k_1M_1 = sublimation rate of DDT, k_1 constant, k_2M_1 = degradation rate of DDT in DDE, k_2 constant, and k_3M_2 = sublimation rate of DDE, k_3 constant.

This model assumes that the degradation and sublimation rates are proportional to the amount present. Now put $k_3 = 8k_1$, since the sublimation rate is proportional to the vapor pressure, the vapor pressure of DDE is about 8 times that of DDT, and other factors affect k_1 and k_3 equally. This yields the following differential equations:

$$\begin{aligned} \frac{dM_1}{dt} + (k_1 + k_2)M_1 &= 0 \\ \frac{dM_2}{dt} + 8k_1M_2 - 0.9k_2M_1 &= 0 \end{aligned} \quad (1)$$

where the 0.9 is the ratio the molecular weight of DDE to DDT. The solutions are

$$\frac{M_1}{M_0} = e^{-(k_1+k_2)t} \quad \frac{M_2}{M_0} = \frac{0.9k_2}{7k_1 - k_2} [e^{-(k_1+k_2)t} - e^{-8k_1t}] \quad (2)$$

The solutions are functions of the dimensionless time k_1t and the ratio k_1/k_2 . While M_1/M_0 decreases exponentially from 1, M_2/M_0 rises from 0 to a maximum before falling exponentially. The ratio of M_2/M_1 is shown vs. M_1/M_0 in Figure 2. For all values of $k_1/k_2 > 1/7$, the ratio rises and approaches its asymptotic value of $0.9k_2/k_1(7 - k_2/k_1)$, which decreases with increasing k_1/k_2 . The model provides a method of estimating the relative importance

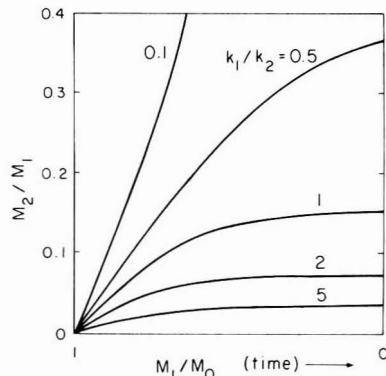


Figure 2. Ratio of DDE to DDT in sublimation model.

of sublimation and degradation from measurements of DDT and DDE in a soil sample. At $k_1/k_2 = 10$, the maximum value of M_2/M_1 is 0.0130. Since this value would have been detected in all soil samples except the 1046-day sample but was not detected in any, the analysis suggests that k_1/k_2 must have been greater than 10; i.e., the rate of loss by direct sublimation must have been at least 10 times more rapid than the loss by degradation to DDE.

Other models are, of course, possible. Another reasonable one would be to assume that the mass-transfer areas are proportional to the $2/3$ power of the masses, which would occur if geometric similarity were preserved during sublimation. This model gives nonlinear differential equations which must be solved numerically. We have made these calculations for $k_1/k_2 = 1$ and $k_1/k_2 = 2$, and the results are that the peak values of M_2/M_1 are a factor of about 4 smaller than those of the linear model. Hence, this model also supports the direct sublimation mechanism.

Another model is that a thin layer of DDE forms on the DDT surfaces and prevents its direct sublimation. If the dehydrochlorination (degradation) step were rapid and the sublimation step relatively slow, then all of the DDT would appear as DDE in the atmosphere. This does not appear to be a major component of the transfer mechanism since DDT has been found to be widespread in the environment, even under conditions that would promote photolysis to DDE. Moreover, we think it likely that we would have detected a trace of DDE in some of our samples unless the postulated surface layer were very thin indeed.

Supporting Evidence from a Mathematical Model

The loss of volatilization of pesticides applied to fields has been an active area of research in the past decades and has recently been reviewed by Taylor (14). The method is to measure the concentration profile above a sprayed plot and to calculate the vertical flux, j , from

$$j = K_y \frac{\partial c}{\partial y} \quad (3)$$

where c is the pesticide concentration at the distance y above the surface and K_y is an eddy diffusion coefficient, which can be estimated or measured independently. In the present case measurement of c was not possible, and so we cannot use this technique to show that sublimation of DDT (or DDE) was responsible for the loss rate found. However, the following mathematical model of the sublimation process shows that sublimation of DDT is a feasible mechanism of the DDT loss.

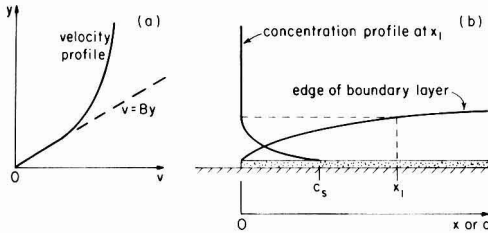


Figure 3. Boundary layer formation.

The mass flux of a material from a surface over which a fluid is flowing is described for the present problem by

$$j = k \frac{M_{r,DDT} P_{DDT}}{RT} \quad (4)$$

where $M_{r,DDT}$ is the molecular weight of DDT, R is the gas constant, T is absolute temperature, and k is the mass-transfer coefficient (15). Thus, the sublimation rate is proportional to P_{DDT} , the vapor pressure of DDT at soil conditions.

To determine if a theoretical value of sublimation rate is high enough to account for the observed loss rate, we compare the experimental mass flux to one calculated from a conservative estimate of the mass-transfer coefficient. To calculate a mass-transfer coefficient, we use the analysis of a concentration boundary layer on a smooth wall over which fluid flows at a steady rate. For thermally neutral buoyancy conditions the local time-averaged velocity is linear, $v = By$, in a very thin region near the surface and logarithmic well outside of the thin layer. From the theory of these flows (16) B can be found, if the wind speed at a specified height is given, from eq 5 where ν is kinematic viscosity.

$$\frac{v}{\sqrt{\nu B}} = 5.1 + 2.5 \ln \sqrt{\frac{B}{\nu} y} \quad (5)$$

Figure 3a shows the linear velocity in an enlarged region near the surface. The air flows over a surface upon which is deposited a thin patch of chemical having a finite vapor pressure, as shown in Figure 3b. As the chemical sublimates, it forms concentration profiles, $c(x,y)$, one of which is illustrated. Also shown is the concentration boundary layer, formed by the locus of $c = 0.01c_s$ where c_s is the equilibrium concentration at the surface. The equations describing this system are:

$$v \frac{\partial c}{\partial x} = (D + K_y) \frac{\partial^2 c}{\partial y^2} \quad (6)$$

$c(0, y > 0) = 0$ $c(x > 0, \infty) = 0$ $c(x > 0, 0) = c_s$
 where x is the distance downstream from the edge of the patch and D is the mass diffusivity. K_y is proportional to y^3 in the limit as $y \rightarrow 0$ (17) and is linear in y in the region not too close to the surface where velocity is logarithmic in y . In this region, $K_y \gg D$. For the general case in which v is a fully developed turbulent velocity profile, the solution to this equation has not to our knowledge been reported. However, the solution is known when $v = By$ and $K_y \ll D$ throughout the concentration boundary layer. This condition occurs only near the upstream edge of the patch where the concentration boundary layer is still very thin. For larger x , the boundary layer will extend into the nonlinear region of the velocity profile, and more important, it will extend to the region where eddy diffusion becomes important. The neglect of eddy diffusivity will give conservatively low values of the mass-transfer rate, which is all that is required for our purposes. With $v =$

Table II

wind speed at 2 m above ground, m/s	B, s^{-1}	$k, m/s$	$j, g/(m^2 s)$
1	140	0.00078	1.3×10^{-8}
2	490	0.0012	2×10^{-8}
10	9100	0.0031	5×10^{-8}

By and $D \gg K_y$ eq 6 is a well-known problem, and its solution is the Lévêque solution (15, 18) which gives for the mass-transfer coefficient:

$$k = 0.539 \left(\frac{BD^2}{x} \right)^{1/3} \quad (7)$$

For DDT in air $D = 0.052 \text{ cm}^2/\text{s}$, and at 30°C (a reasonable average daytime temperature for exposed soil at Nakuru) the vapor pressure of p,p' -DDT is $8.8 \times 10^{-7} \text{ mmHg}$ (19). Then applying Equations 4 and 7 to the center of the plot ($x = 1.25 \text{ m}$) gives the results shown in Table II for three wind speeds at thermally neutral buoyancy conditions.

Over dry soils Spencer and Cliath (13) have shown that adsorption of DDT onto soil can cause its vapor pressure to be depressed by a factor as small as 0.04, which would yield $j = 5 \times 10^{-10} \text{ g}/(\text{m}^2 \text{ s})$ at the low wind speed of 1 m/s . This estimate is presumably very conservative because the wind speed is usually higher, the mass-transfer area is much greater than that of a flat plate, and eddy diffusion was neglected. Moreover, unstable conditions caused by sun-heated ground would greatly increase the rate. Even this conservative rate, however, is 5 times higher than needed to account for the maximum DDT loss rate found, $10^{-10} \text{ g}/(\text{m}^2 \text{ s})$, which occurred at the beginning of the field tests. Two possible reasons for the lower loss rates found in the field tests are that the surface was not uniformly and completely covered during application and that the lowering of vapor pressure by adsorption of DDT in the soil was even greater than that found by Spencer and Cliath. We conclude that sublimation of DDT is sufficient to account for the rapid loss of DDT from Nakuru soil even if it is strongly adsorbed to the soil and that this can occur without degradation of DDT to DDE or other products.

Equations 4 and 7 and the behavior of B with wind speed show that the sublimation rate is proportional to the vapor pressure, the $2/3$ power of the diffusivity, and the 0.60 power of the wind speed. It is also, of course, a function of the geometry of the exposed surfaces, as described clearly by Taylor (14). It must be emphasized that this solution is valid only for small patches of pesticide such as on a single leaf or a small patch of ground but not for a large patch or even a large leaf, though it is possible that the functional behavior of the flux with diffusivity and wind speed is approximated well.

Conclusion

The relatively rapid disappearance of DDT from soil in Kenya helps to account for the low residue concentrations found there. This encouraging view is tempered by the possibility that DDT and other pesticides may be more strongly adsorbed in soils elsewhere in Kenya and Africa. If so, they would persist longer than in the environment of Lake Nakuru.

Acknowledgments

We thank the Government of Kenya for its cooperation and the Perkin-Elmer Corp. for the loan of an amplifier and detector.

Literature Cited

- (1) Koeman, J. H.; Pennings, J. H.; de Goeij, J. J. M.; Tjioe, P. S.; Olindo, P. M.; Hopcraft, J. *J. Appl. Ecol.* 1972, 9, 411.
- (2) Frank, L. G.; Jackson, R. M.; Cooper, J. E.; French, M. C. *East Afr. Wildl. J.* 1977, 15, 295.
- (3) Edwards, C. A. *Residue Rev.* 1966, 13, 83.
- (4) Edwards, C. A. "Persistent Pesticides in the Environment", 2nd ed.; CRC Press: Cleveland, OH, 1973; pp 6-20.
- (5) Glotfelty, D. E.; Caro, J. H. In "Removal of Trace Contaminants from the Air"; Deitz, V. R., Ed.; American Chemical Society: Washington, DC, 1975; ACS Symp. Ser. No. 17.
- (6) Lichtenstein, E. P.; Fuhremann, T. W.; Schulz, K. R. *J. Agric. Food Chem.* 1971, 19, 718.
- (7) Lichtenstein, E. P. "Degradation of Synthetic Organic Molecules in the Biosphere"; National Academy of Sciences: Washington, DC, 1972; pp 190-205.
- (8) Guenzi, W. D.; Beard, W. E. *Soil Sci. Soc. Am. Proc.* 1970, 34, 443.
- (9) Farmer, W. J.; Igue, K.; Spencer, W. F.; Martin, J. P. *Soil Sci. Soc. Am. Proc.* 1972, 36, 443.
- (10) Wheatley, G. A. *Ann. Appl. Biol.* 1965, 55, 325.
- (11) Dimond, J. B.; Belyea, G. Y.; Kadunce, R. E.; Getchell, A. S.; Blease, J. A. *Can. Entomol.* 1970, 102, 1122.
- (12) El Zoragani, G. A. *Bull. Environ. Contam. Toxicol.* 1976, 15, 378.
- (13) Spencer, W. F.; Cliath, M. D. *J. Agric. Food Chem.* 1972, 20, 645.
- (14) Taylor, A. W. *J. Air Pollut. Control Assoc.* 1978, 28, 922.
- (15) Bird, R. R.; Stewart, W. E.; Lightfoot, E. N. "Transport Phenomena"; Wiley: New York, 1960; pp 636-652, 363-364.
- (16) Tennekes, H.; Lumley, J. L. "A First Course in Turbulence"; MIT Press: Cambridge, MA, 1972; pp 153-158, 169-170.
- (17) Notter, R. H.; Sleicher, C. A. *Chem. Eng. Sci.* 1971, 26, 161.
- (18) Lévêque, M. A. *Ann. Mines* 1928, 13, 201.
- (19) Dickinson, W. *Trans. Faraday Soc.* 1956, 52, 31.

Received for review April 8, 1983. Accepted March 13, 1984. This work was part of a project supported by the SEED Program of the National Science Foundation. The paper was presented in the symposium Biologically Active Chemicals in Air at the joint American Chemical Society-Chemical Society of Japan Meeting, Honolulu, HI, April 1-6, 1979.

Henry's Law Constants for the Trihalomethanes: Effects of Water Composition and Temperature

Brenton C. Nicholson,* Brian P. Maguire, and Donald B. Bursill

State Water Laboratories, Engineering and Water Supply Department, Salisbury, South Australia, Australia 5108

■ Henry's law constant for each of the trihalomethanes (THMs) was determined in various waters which included distilled water, natural potable water samples of relatively high dissolved salts and organic matter, and water to which humic acid had been added. The values obtained were not affected by the presence of other THMs or by water composition and were in good agreement with published and predicted values. In the range 10-1000 µg/L they were independent of concentration. The values obtained in distilled water can thus be used in the design of aeration facilities for THM removal. The temperature dependence of Henry's law constants was also established.

Introduction

The trihalomethanes chloroform (CHCl₃), bromodichloromethane (CHCl₂Br), dibromochloromethane (CHClBr₂), and bromoform (CHBr₃) are formed through reactions involving the chlorine used for disinfection of water, the naturally occurring organic material (fulvic and humic acids), and bromide (1, 2). The possibility of these compounds causing adverse health effects when present in drinking water has been one of the major water quality issues of recent years with U.S. authorities having set a standard of 100 µg/L for THMs (3). THM levels in South Australian waters are consistently above 100 µg/L(4), and control measures are indicated if standards of this nature are to be met.

There are a number of approaches that can be considered for the control or removal of trihalomethanes. The use of aeration techniques, either diffused air or packed tower aeration, can be employed in existing distribution systems where alternative methods of control may be impractical or uneconomical.

The design of air-stripping facilities requires a knowledge of Henry's law constants for the compounds to be

removed. Some values are available in the literature, but effects of water composition and temperature have not been reported.

Mackay et al. (5) showed that Henry's law constant, *H*, for a compound could be related to its change in concentration when stripped from solution by a stream of gas. Gossett (6) derived the following relationship between *H* and concentration when samples of the solution being stripped are taken for analysis during the experiment:

$$\ln \left(\frac{C_t}{C_0} \right) = - \frac{HG}{RT} \sum_{j=1}^i \frac{\Delta t_j}{V_j} \quad (1)$$

where *C_t* = concentration in liquid at time *t*, *C₀* = initial concentration in liquid, *H* = Henry's law constant, *G* = gas flow, *R* = gas constant, *T* = temperature, Δt_j = duration of the *j*th interval, and *V_j* = volume during the *j*th interval. Thus, a plot of $\ln(C_t/C_0)$ vs. $\sum_{j=1}^i(\Delta t_j/V_j)$ is a straight line of slope $-HG/(RT)$ from which *H* can be readily calculated. This relationship was used as a basis for determining *H* for the THMs.

Experimental Section

Apparatus. A stripping vessel similar to that shown by Mackay et al. (5) was used except that air entered through the top of the vessel by means of a Dreschel head, the diffuser being as close to the bottom of the vessel as possible. Air was supplied by a cylinder through a rotameter (to set the approximate flow) and a Dreschel bottle containing water (to saturate the air with water vapor and prevent evaporation). Connections were made with Swagelok fittings and Teflon tubing. The exit gas flow rate was determined accurately by using a bubble flowmeter. The system was maintained at the desired temperature by circulating water from a thermostatically controlled water bath. The temperature of the solution being stripped was

Table I. Henry's Law Constants for THMs at 20 °C

compound	$H, \text{m}^3 \text{atm mol}^{-1}$					predicted
	distilled water	Milang water	Myponga water	Myponga water + 20 mg/L humic acid	literature	
CHCl ₃	$(3.0 \pm 0.1) \times 10^3$ ^a	3.3×10^{-3}	2.9×10^{-3}	3.1×10^{-3}	3.6×10^{-3} ^{e,f} (7) 3.1×10^{-3} ^{e,g} (8) 4.8×10^{-3} ^h (9)	3.1×10^{-3} ⁱ
CHCl ₂ Br	$(1.6 \pm 0.2) \times 10^{-3}$ ^b	1.6×10^{-3}	1.5×10^{-3}	1.5×10^{-3}	2.3×10^{-3} ^{e,f} (7) 2.1×10^{-3} ^h (9)	
CHClBr ₂	$(8.7 \pm 0.2) \times 10^{-4}$ ^c	8.5×10^{-4}	8.0×10^{-4}	7.7×10^{-4}	8.4×10^{-4} ^{e,f} (7) 8.7×10^{-4} ^h (9)	
CHBr ₃	$(4.3 \pm 0.3) \times 10^{-4}$ ^d	4.6×10^{-4}	4.1×10^{-4}	4.3×10^{-4}	5.8×10^{-4} ^{e,f} (7)	4.3×10^{-4} ^j

^a Error is standard deviation of four results. ^b Error is standard deviation of three results. ^c Error is standard deviation of two results. ^d Error is standard deviation of three results. ^e Calculated from dimensionless values. ^f Temperature not given. ^g 25 °C. ^h Calculated from dimensionless values which were in turn calculated from the temperature dependence relationships given. ⁱ Vapor pressure and solubility data from ref 10. ^j Vapor pressure at 20 °C (4 mmHg) estimated from a graph of vapor pressure vs. temperature; data from ref 10 and 11. Solubility at 20 °C (3.1 g/L) estimated from data for 15 and 30 °C (11), assuming a linear relationship.

Table II. Characteristics of Waters Used in Determinations of Henry's Law Constants

water	pH	total dissolved salts mg/L	alkalinity, mg/L as CaCO ₃	color, hazen units	turbidity, NTU ^a	total organic carbon, mg/L	suspended solids, mg/L
Milang	8.4	700	140	9	51	13	110
Myponga	7.6	370	60	25	1.4	10	
Myponga + 20 mg/L humic acid	7.9	370	68	100	3.4	17	

^a NTU, nephelometric turbidity units.

measured and was within ±0.1 °C of the recirculated water.

Procedure. The circulation of water for temperature control was commenced and the solution to be stripped (1 L) added to the stripping vessel. After 15 min was allowed for equilibration, the air flow was started and adjusted to the desired flow (300–350 mL/min) with the rotameter. The air flow was measured accurately by using the bubble flowmeter at the beginning and end of each run. These flow measurements were averaged for subsequent calculations. The flow tended to increase by 2–3% during a run due to the decrease in head pressure within the stripping vessel.

Sampling. At the beginning of each run (approximately 1 min after the air was adjusted to the required flow) a 6-mL sample of the solution being stripped was taken for analysis (C_0) in a stoppered graduated centrifuge tube and the stopwatch started at this time. Further 6-mL aliquots were taken for analysis at required intervals.

Analysis. A 5.0-mL aliquot of sample taken for analysis was withdrawn as soon as possible and extracted immediately with 1.0 mL of methylcyclohexane containing 1 mg/L tetrachloroethane as an internal standard. The extracts were analyzed on a Varian 2700 gas chromatograph equipped with a short vitreous silica SE-30 capillary column at 60 °C. Quantification of peaks was achieved with a Hewlett Packard 3390A integrator. Concentrations were determined from the appropriate calibration curves.

Solutions. Stock solutions of the individual THMs were prepared by dissolving 100 mg of each THM in water (50 mL). Stirring for approximately 24 h was required. Dilutions of the stock solutions were carried out to prepare the standards and the solutions to be stripped by using the water of interest; i.e., standards and the solution to be stripped were of identical water composition. Distilled rainwater was used for preparing the distilled water solutions; distilled deionized water contained unacceptably high levels of THMs.

Results and Discussion

The accurate determination of H requires that the gas exiting from the liquid is in equilibrium with the liquid with respect to the compound of interest. This was assumed since the apparatus and flow conditions used in this work were very similar to those of Mackay et al. (6) for which equilibrium had been demonstrated. Henry's law constants were determined by stripping various waters containing a mixture of all four THMs each at 200 µg/L. The values obtained with distilled water were in excellent agreement with those obtained for each THM individually in distilled water, indicating that the constant obtained is independent of the presence of other THMs; i.e., ideal solution behavior applies at these low concentrations. Similarly, there was no significant difference between the values of H determined with initial concentration at 1000 µg/L.

The relationship between $\ln(C_t/C_0)$ and $\sum_{j=1}^i(\Delta t_j/V_j)$ for CHCl₃ for distilled water from which the Henry's law constants were calculated at various temperatures is shown in Figure 1. The very high correlation coefficients obtained in all experiments is good evidence of the validity of the approach used; i.e., Henry's law constant is indeed constant over the concentration ranges produced in each experiment (10–200 µg/L), and the exiting gas is in equilibrium with the solution with respect to the THMs.

The values of H obtained with the various waters at 20 °C and the literature and predicted values are shown in Table I. The characteristics of the waters used are shown in Table II. The composition of water, i.e., dissolved salts and humic material, has little, if any, effect on the values of H obtained, the slight differences being within experimental error. Thus, the values obtained in distilled water could be used in treatment plant design. The excellent agreement between the experimental Henry's law constants and those predicted from vapor pressure and solu-

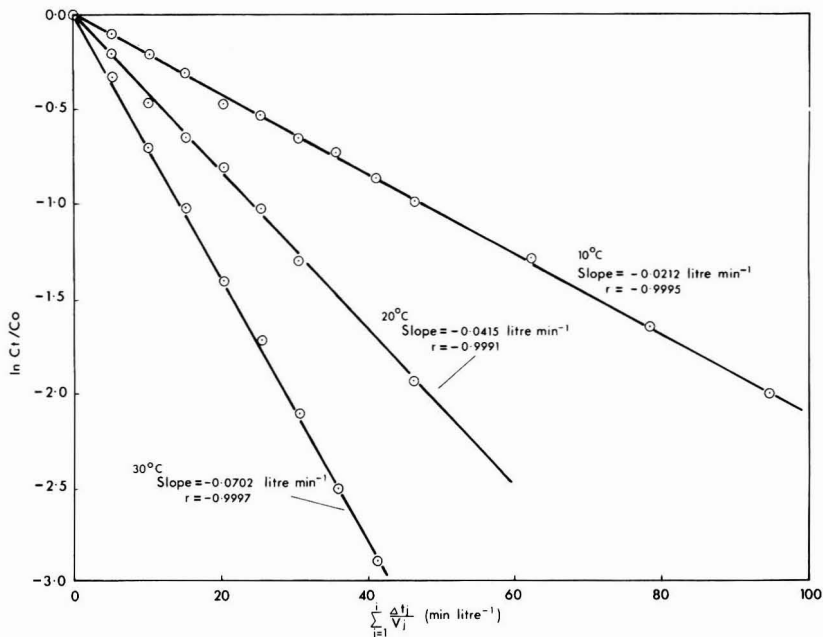


Figure 1. Plot of $\ln C_1/C_0$ vs. $\sum_{j=1}^n (\Delta t_j/V_j)$ for CHCl_3 at various temperatures.

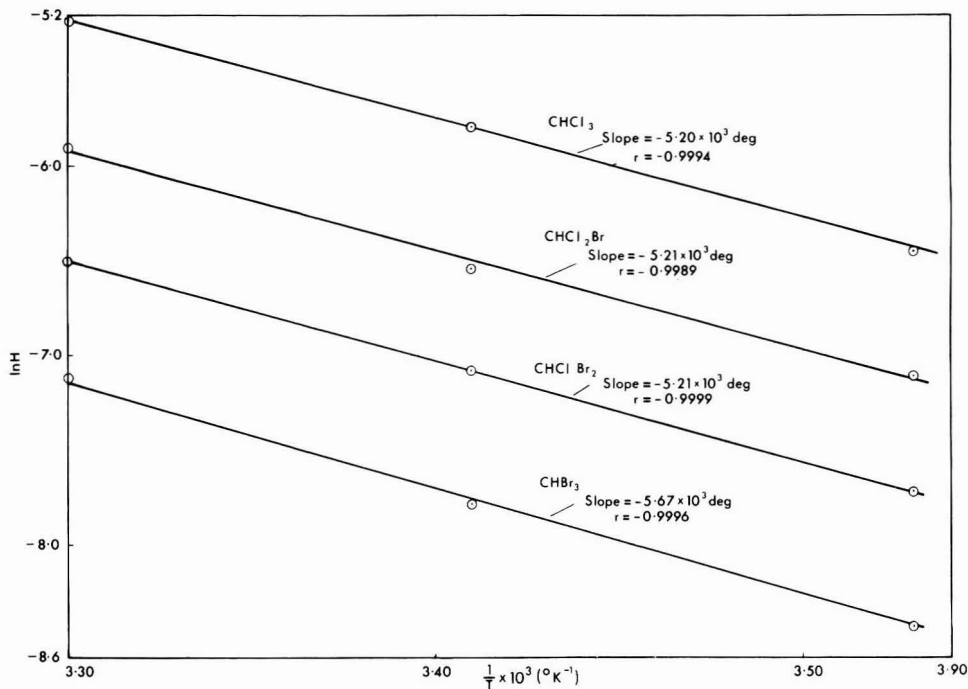


Figure 2. Plot of $\ln H$ vs. $1/T$ for the trihalomethanes.

bility data, where available, indicates that values predicted from these data may be very good approximations of the true constants for volatile halogenated compounds.

Henry's law constants were determined in distilled water at various temperatures with solutions containing a mixture of all four THMs, each at an initial level of $200 \mu\text{g/L}$. The value of H was found to double approximately for each 10°C rise in temperature.

The following relationship between H and temperature should apply:

$$\ln H = \frac{-\Delta H^\circ}{RT} + K \quad (2)$$

The relationship between $\ln H$ and $1/T$ for the THMs is shown in Figure 2. The very high correlation coefficients support the appropriateness of the relationship. The

Table III. Equations Describing Dependence of *H* on Temperature for THMs

compound	<i>H</i> , m ³ atm mol ⁻¹
CHCl ₃	exp(11.9 - 5200/ <i>T</i>)
CHCl ₂ Br	exp(11.3 - 5210/ <i>T</i>)
CHClBr ₂	exp(10.7 - 5210/ <i>T</i>)
CHBr ₃	exp(11.6 - 5670/ <i>T</i>)

equations describing the temperature dependence of *H* for the THMs obtained from these data are shown in Table III.

From the vapor pressure and solubility data for chloroform (11), Henry's law constant can be predicted at a number of temperatures and a relationship between *H* and temperature established. The relationship using these data is

$$H \text{ (m}^3 \text{ atm mol}^{-1}\text{)} = \exp(10.3 - 4720/T) \quad (3)$$

the linear correlation coefficient for the relationship between ln *H* and 1/*T* being -0.9996. This relationship is similar to that determined experimentally in this study, indicating once again that for volatile chlorinated hydrocarbons Henry's law constants predicted from vapor pressure and solubility data are good approximations of the true values.

Registry No. CHCl₃, 67-66-3; CHCl₂Br, 75-27-4; CHClBr₂, 124-48-1; CHBr₃, 75-25-2.

Optimal Sampling Geometry for Hazardous Waste Sites

David F. Parkhurst

School of Public and Environmental Affairs and Biology Department, Indiana University, Bloomington, Indiana 47405

■ Regularly spaced sampling grids are often used to search for toxic materials buried in abandoned dumps and landfills. This paper demonstrates that triangular grids are preferable to square grids for this purpose because triangles give better coverage. In particular, if the maximum distance from any point on an area to the nearest sampling well is held fixed, then 23% fewer wells are required with a triangular layout than with squares. Cost savings should be comparable. The paper also considers whether sampling wells should be distributed regularly or randomly. When the toxic materials are not randomly distributed, then the sampling wells should be. These analyses are applicable to many other area-based sampling problems as well.

It is now a platitude that our country has a plethora of uncontrolled hazardous waste sites. Over the next decade, some billions of dollars are likely to be spent by industries, states, and the federal government to investigate, control, and remove toxic materials from orphan dumps. The purpose of this paper is to suggest optimal sampling schemes for studying these dumps and the related problems of waste spills.

Consider an abandoned landfill suspected of having clusters of buried toxic waste containers, some of which may be leaking. The clusters might be uniformly distributed, if placed by bulldozers when the landfill was active. At other sites, the clusters might be more or less randomly distributed, if they had been dumped in place from trucks which arrived sporadically during landfill

Literature Cited

- (1) Rook, J. J. *J.—Am. Water Works Assoc.* 1976, 68, 168-172.
- (2) Oliver, B. G.; Lawrence, J. *J.—Am. Water Works Assoc.* 1979, 71, 161-163.
- (3) *Fed. Regist.* 1979, 44 (231), 68624-68707.
- (4) Bursill, D. B. paper presented at the 10th Federal Convention, AWWA, Sydney, Australia, April 11-15, 1983.
- (5) Mackay, D.; Shiu, W. Y.; Australand, R. P. *Environ. Sci. Technol.* 1979, 13, 333-337.
- (6) Gossett, J. M. "Packed Tower Air Stripping of Trichloroethylene from Dilute Aqueous Solution", final report of Contract F49620-79-C-0038, 1980.
- (7) Symons, J. M.; Stevens, A. A.; Clark, R. M.; Geldreich, E. E.; Love, O. T., Jr.; DeMarco, J. "Treatment Techniques for Controlling Trihalomethanes in Drinking Water". U.S. EPA, Drinking Water Research Division, Municipal Environmental Research Laboratory, Sept 1981, EPA-600/2-81-156.
- (8) Dilling, W. L., Tefertiller, N. B.; Kallos, C. J. *Environ. Sci. Technol.* 1975, 9, 833-838.
- (9) "Trace Organics Removal by Air Stripping", prepared by Environmental Science and Engineering, Inc., for American Water Works Association Research Foundation, May 1980, ESE No. 79-337-001.
- (10) Verschuereen, K. "Handbook of Environmental Data on Organic Chemicals"; Van Nostrand Reinhold: New York, 1977.
- (11) "Chloroform, Carbon Tetrachloride and Other Halomethanes—An Environmental Assessment", National Research Council (U.S.), 1978.

Received for review June 1, 1983. Revised manuscript received December 21, 1983. Accepted January 19, 1984.

operation. The latter condition could easily occur in a landfill which took small amounts of industrial wastes amid large amounts of general municipal wastes. A third possibility would be that a given hauler might consistently have unloaded in the same section of a dump.

In studying sites where toxic wastes are buried, it is common practice to lay out a square grid of points and to drill at these points to (a) search for waste drums and (b) take soil samples to be analyzed for toxic chemicals. Two questions arise about this practice: (1) Is a square grid system the most efficient layout and (2) should drill sites be uniformly spaced or randomly located in some fashion? Consider these questions in turn.

Triangular vs. Square Grids. First, suppose for now that we choose to sample in a regular pattern. I show here that a triangular grid is likely to yield more information per well drilled (and hence per dollar spent) than will a square grid.

Consider first the square sampling grid shown in Figure 1. It is clear that, in order not to miss concentrated wastes, we would like to minimize *D*_{max}, the maximum distance between any point in the overall area and its closest sampling point. Elementary trigonometry tells us that *D*_{max} = *R* = 0.7070*S*. It also seems desirable to minimize *D*, the average distance from any point on the area to the nearest sampling point. Because of symmetry, *D* for the whole area is the same as *D* for the shaded triangle, i.e.

$$\bar{D} = \frac{1}{(S^2/8)} \int_0^{S/2} \int_0^x (x^2 + y^2)^{1/2} dy dx = \alpha S \quad (1)$$

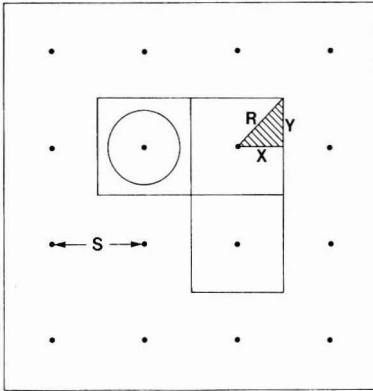


Figure 1. Regular square grid of sampling points. The points are S units apart, and each samples a square area like the three shown. The shaded triangle allows calculation of D_{\max} ($=R$) and of \bar{D} . Note that $X = Y = S/2$ and $R = S/2^{1/2}$. The circle has a radius of \bar{D} .

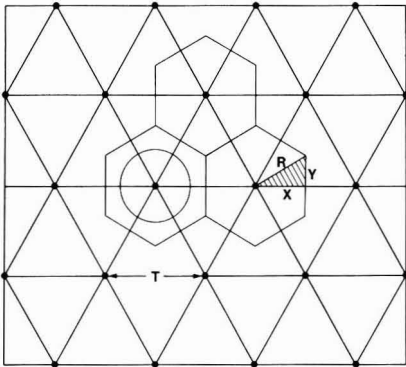


Figure 2. Regular triangular grid of sampling points. The triangles are equilateral, with sides of length T . Each grid point samples a hexagonal area like the three shown; each such area is equal to the area of one of the squares in Figure 1. The shaded triangle allows calculation of D_{\max} ($=R$) and of \bar{D} . Note that $X = T/2$, $Y = T/[(2)(3^{1/2})]$, and $R = 3^{1/2}T$. The circle has a radius of \bar{D} .

where $\alpha = [2^{1/2} + \ln(1 + 2^{1/2})]/6 = 0.383$. The circle in Figure 1 has a radius equal to \bar{D} calculated from eq 1.

Next consider the triangular sampling grid shown in Figure 2. For this grid, $D_{\max} = R = 0.5774T$, and \bar{D} (using the shaded triangle) is

$$\bar{D} = \frac{1}{(A_H/12)} \int_0^{T/2} \int_0^{x/3^{1/2}} (x^2 + y^2)^{1/2} dy dx = \beta T \quad (2)$$

where A_H is the hexagonal area ($0.866T^2$) and $\beta = 0.351$. The circle in Figure 2 has a radius of \bar{D} calculated from eq 2. The grid sizes in the two figures have been adjusted so both sample the same area per well.

To compare the effectiveness of the square and triangular grids, consider a hectare (2.5 acres) of land with a 10-m (30-ft) square grid. A square 100 m on a side is 1 ha, so we have $A = 10^4 \text{ m}^2$, $S = 10 \text{ m}$, and $N = 100$ wells. For this square grid, the resulting distances to a well are $D_{\max} = 7.07 \text{ m}$ and $\bar{D} = 3.83 \text{ m}$.

With a triangular grid, each well in Figure 2 would represent, or sample, one of the hexagonal areas shown, with $A = 3^{1/2}T^2/2$. When $T = 10.746 \text{ m}$, then $A = 100 \text{ m}^2$, and a grid of 100 such wells would cover 1 ha. Thus, on this grid $D_{\max} = 6.204 \text{ m}$ and $\bar{D} = 3.772 \text{ m}$; for a given drilling cost, we will have sampled more thoroughly.

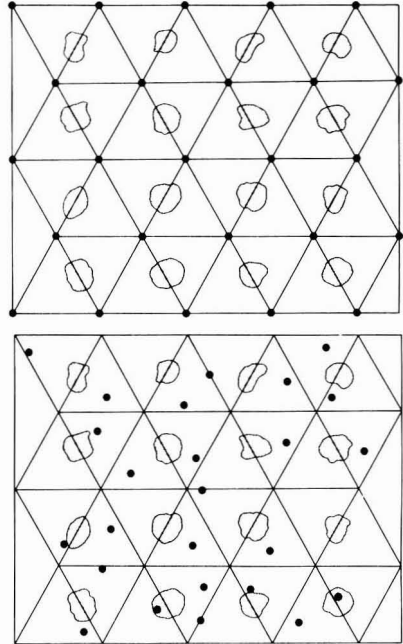


Figure 3. (Top) Grid of 25 regularly spaced wells (on a triangular grid) used to sample a regular distribution of toxic wastes. (Bottom) Stratified random sample using 25 wells on the same dump.

An alternative comparison involves adjusting T on the triangular grid until $D_{\max} = 7.07 \text{ m}$ (the value for the square grid). This would require only 77 wells, for a 23% cost savings. Or, if T is adjusted to make $\bar{D} = 3.83 \text{ m}$ (the mean distance for the square grid), then 97 wells are required. The cost saving is 3%.

The mathematical results above can also be understood geometrically. The hexagonal area sampled by each well in the triangular grid is more like a circle than is the square sampled by each well in the square grid. With the hexagons, there is less chance that the wastes sought can "hide out" in the corners because there is less corner to hide out in. Put another way, the distance from a well to the boundary of the area it samples varies less with compass direction for the hexagonal areas than for the square ones. These effects make the triangular grid more effective than the squares. Although it might be slightly more difficult to lay out a triangular grid rather than a square one, the cost saving (or gain in coverage) is substantial when maximum distance from an arbitrary point to a sampling well is considered.

These results have been derived for a rectangular area, but they will also apply to areas with irregular boundaries.

Random vs. Regular Sampling. The second major question involves the possible need for randomly placed sample wells. If the wastes either are distributed at random or at least are thoroughly dispersed (at scales much smaller than the sampling grid), then a regular grid of samples will work well and will be simplest to lay out and to keep track of.

On the other hand, if the wastes themselves are laid out in a more or less regular grid, then severe sampling problems could result from a regular sampling grid with a spacing which was some multiple of the waste spacing. On the average over many such dumps, there would be no bias. That is, the expected value of the number of wells detecting wastes would be the correct mean number. How-

ever, the *variance* from one site to another could be very high compared with that for a random sampling scheme, because any particular set of samples is likely to detect too few or too many pockets of waste (Figure 3, top). Such waste distribution may at first seem unlikely, but at least two mechanisms might produce it. The first could occur if one load a day (or week etc.) of the toxic wastes were dumped at a municipal landfill with a fairly uniform filling rate. Or, a trash hauler might set a pattern of dumping a more or less fixed distance from his previous load (to protect his tires, or to stay away from smelly materials, or whatever).

It would probably be rare for a regularly spaced sample grid to "just miss" a regular spacing of wastes, but it would also be quite undesirable. (This problem of regular sampling of regular grids is similar to the "aliasing" problem in periodic sampling of periodic phenomena (1) and to problems in stereological morphometry (2).)

A randomized sampling scheme, for example, one based on a random number table as in Figure 3 (bottom), would be a better choice for regularly spaced wastes. Figure 3 (bottom) shows a stratified random sampling using 25 wells (the same number as in Figure 3 (top)) on 32 triangles. First, 25 of the 32 triangles were selected at random to be sampled. For each of those, three uniformly distributed random numbers (x_1, x_2, x_3) were selected from a table. Then $y_i = x_i / (x_1 + x_2 + x_3)$ was calculated for $i = 1, 2, 3$; then two of these are independent because their sum is unity. Finally, the three y 's form the coordinates of the sampling point in a triangular coordinate system similar to that used for describing soil texture as percentages of clay, silt, and sand (3).

The randomizing scheme just described was stratified across triangles. However, with random location of samples, there is no longer any advantage to triangles, and the samples could more easily be stratified on a square or rectangular grid. A randomized grid would be harder to lay out, but its advantages ought at least to be considered for some applications. It is worth reiterating that if the wastes themselves are located at random in the dump, then a regularly spaced grid will work as well as random samples.

A further consideration is that the goal in sampling a dump containing toxic wastes may not be to obtain an unbiased estimate of the density of waste clusters but rather to find *all* such clusters. In this case, the sampling network will need to be very dense, and a regular triangular grid will then be best.

Finally, the ideas above are very general, and should apply to many other area-based sampling problems. Indeed, one anonymous reviewer stated that triangular grids are commonly used in mineral exploration, but I have not been able to corroborate that statement.

Literature Cited

- (1) Panofsky, H. A.; Brier, G. W. "Some Applications of Statistics to Meteorology"; Pennsylvania State University: University Park, PA, 1968.
- (2) Parkhurst, D. F. *Am. J. Bot.* 1982, 69, 31.
- (3) Brady, N. C. "The Nature and Properties of Soils", 8th ed.; Macmillan: New York, 1974.

Received for review June 15, 1983. Accepted December 14, 1983.

Mutagenic Changes in Dilute Wood Smoke as It Ages and Reacts with Ozone and Nitrogen Dioxide: An Outdoor Chamber Study

Richard M. Kamens,*† Glenn D. Rives,† Jean M. Perry,† Douglas A. Bell,† R. Flynn Paylor, Jr.,† Randall G. Goodman,† and Larry D. Claxton†

Department of Environmental Sciences and Engineering, School of Public Health, University of North Carolina, Chapel Hill, North Carolina 27514 and U.S. Environmental Protection Agency, Research Triangle Park, North Carolina 27711

■ Dilute wood smoke from a residential wood stove was added to two 25-m³ outdoor Teflon film chambers. The smoke was permitted to age by itself or react with sub-ppm levels of NO₂, NO₂ + O₃, or O₃ in the presence and absence of natural sunlight. Most wood smoke particles fell into the 0.07–0.23 μm size range. The shape of the particle size distributions did not subsequently change during a 4-h reaction period. After reaction with O₃ + NO₂, the direct-acting bacterial mutagenicity (TA98–S9) of wood smoke extracts increased 2–10-fold. These changes occurred very rapidly. Increases were also observed when wood smoke was exposed to NO₂ alone, but these increases were not as great as those resulting from combined effects of O₃ + NO₂. Preliminary experiments with wood smoke aged in the dark or in the light in the presence of low levels of NO₂ and O₃ (i.e., <0.06 ppm) did not show increases in bacterial mutagenicity.

Introduction

Over the past decade many researchers have attempted to document the impact that the increased use of resi-

dential wood combustion could have on both the indoor and outdoor environment. Various investigators have found that during the winter months, emissions from wood combustion can contribute between 60 and 80% of the ambient fine particle loading observed over some communities (1, 2). Since the organic extractable mass of wood smoke particles is very high, it is not surprising that other estimates (3) have shown that residential wood combustion accounts for more of the annual emission of polycyclic organic compounds (POC) than any other source. This is further supported by Lewtas (4), whose calculations show that, in the U.S. on an annual basis, more than 30% of the mutagenic material emitted into the atmosphere comes from wood combustion.

Little is known about the extent to which these POC react once they are emitted into the atmosphere. There is some preliminary and indirect evidence to indicate that changes do occur. In 1978, Pitts and co-workers (5) reported that the bacterial mutagenicity of selected polycyclic aromatic hydrocarbons (PAH) adsorbed on filters was strongly enhanced by drawing sub-ppm concentrations of nitrogen dioxide (NO₂) across the filters. Trace levels of nitric acid (HONO₂) in the NO₂ gas stream were thought to be primarily responsible for promoting the observed

*Department of Environmental Sciences and Engineering.

†U.S. Environmental Protection Agency.

blower. This provided impetus for the smoke to move from the chimney to the chambers. With an average flow through the pipe of ~50 L/min, smoke particles spent 6–8 s in the transfer manifold.

Seasoned red oak was used as the combustion wood. It was split into two sizes which were approximately 6 cm or 12 cm in diameter and 0.5 m in length. Fires were usually started with 0.25 kg of oak kindling, with the split logs being added soon thereafter. This fire was permitted to burn with the stove vents open for 15 min. If a low burn rate was desired (i.e., <2 kg/h), the stove was loaded with ~8 kg of the 12-cm wood. After the initial 15-min burn period, the air intakes to the stove were completely closed, and another 15–20 min of burn was permitted. In the high burn rate case (4–8 kg/h), 6-cm split wood was used to load the firebox with 8–16 kg of wood, and the air intakes were opened. Crude estimates of the burn rate were made by removing and reweighing the wood from the stove after the chamber injection process was completed. In a few experiments dried North Carolina peat was burned in the stove and peat smoke injected into the chambers.

During injection of smoke into one or both chambers, the total aerosol concentration was monitored with either an Environment/One condensation nuclei (CN) counter or a Thermo Systems, Inc., Model 3030 electrical aerosol analyzer (EAA). This facilitated the injection of desired soot concentrations into both chambers at the same time. At the start of an experiment, background conditions were determined. A high concentration of wood smoke was then injected into both chambers. After the smoke was permitted to equilibrate in the chambers for 15–30 min, wood smoke particles were collected on T60A20 Pallflex 13.34-cm Teflon-impregnated glass fiber filters. Approximately 5–40 mg of wood soot was collected over a 10-min period at a flow rate of 0.9 m³/min. These initial samples were used to establish the base-line bacterial mutagenicity of the unreacted chamber wood smoke. After this sample was taken, O₃, NO₂, or both were added from an electrical discharge ozone generator or high concentration NO₂ (in nitrogen) tank. At the conclusion of the experiment, another 13.34-cm filter sample was taken. Since aerosol mass was lost from the chambers over the course of an experiment, these final or reacted filter samples were taken for 30–40 min.

Instrumentation. During most wood soot experiments, chamber gas-phase concentrations of NO, NO₂, and O₃ were monitored with Bendix Model 8101-B and 8002 analyzers. Vapor-phase C₂–C₁₀ individual hydrocarbons were monitored with an automated Carle 211 gas chromatograph; a Beckman Model 6800 gas chromatograph was used to monitor CO and CH₄. In selected experiments, C₁–C₈ aldehydes were traced with a modified 2,4-dinitrophenylhydrazine–HPLC technique (12).

Aerosol characterization data were derived from three different aerosol instruments. A condensation nuclei counter, which is not size discriminatory, measured particles in the 0.01–0.3- μ m range. Particles in the 0.013–0.750- μ m range were counted and sized by an electrical aerosol analyzer (EAA) while a Climet Model CI-208 optical particle counter (OPC) was used for particles in the optical range (0.3–5 μ m). Teflon-impregnated 47-mm filter samples (Pallflex) were also taken to monitor the particle mass concentration. A flow rate of 0.07 m³/min and a sample time of 10 min were used.

Sample Workup and Mutagenicity Testing. The 13.34-cm filter samples for bioassay analysis were immediately Soxhlet extracted in the dark for 16 h with 100 mL of methylene chloride (MeCl₂). The soot extract was then

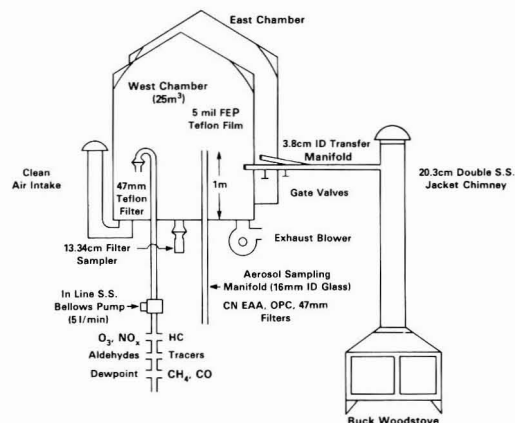


Figure 1. Illustration of UNC 25-m³ outdoor Teflon film chambers, sampling manifolds, and associated wood stove (not to scale).

increase in nitroaromatic product formation (6, 7) and corresponding increases in mutagenicity. This underscores the potential importance of nitric acid–organic reactions because nitric acid (HONO₂) can be formed in the atmosphere from the reaction of NO₂ and O₃. In this reaction sequence, O₃ and NO₂ react to produce NO₃ which can further react with NO₂ to give N₂O₅. The significance of this reaction is apparent when one considers that the reaction of N₂O₅ and water to yield HONO₂ could take place on soot particle surfaces. This would provide ample opportunity for the reaction of HONO₂ with surface-adsorbed or condensed POC.

It could be also speculated (8) that NO₃ from the reaction of O₃ and NO₂ may react with the phenolic group of hydroxy-PAH and form hydroxynitro-PAH. This mechanism was originally proposed by others (9) for the smog formation of hydroxynitrotoluenes from cresols and NO₃ and could possibly be extended to higher molecular weight aromatic species. In addition to nitrogen species–POC reactions, reactions of PAH with light, O₃, and O₂ could potentially lead to the production of mutagenic compounds. A review of these and other related atmospheric reactions has been presented by Pitts (8).

To provide more direct evidence on possible atmospheric mutagenic and chemical transformations of particle-bound POC, an outdoor chamber study was undertaken. This paper describes some of the mutagenic changes that dilute wood smoke can undergo as it ages in the dark or the light and/or reacts with sub-ppm levels of O₃ and NO₂.

Experimental Approach and Procedures

Chambers and Injection of Wood Smoke. The two 25-m³ outdoor Teflon film chambers (referred to as the east chamber and west chamber) in this study were constructed at the University of North Carolina Ambient Air Research Facility (10) and have been described in detail elsewhere (11). A two-chamber system was used so that the effect of two different species on the same wood smoke could be observed under the same outdoor conditions. The chamber system, wood stove injection manifold, and sampling apparatus are illustrated in Figure 1.

Combustion aerosol was added to the chambers from a free-standing, medium size Buck wood stove (Smoky Mt. Enterprises, Asheville, NC). A 4.5 m × 3.81 cm i.d. iron pipe connected the chamber with the stove chimney. During injection, a slight vacuum (~0.7 cm of H₂O) was applied to the chambers with the main chamber exhaust

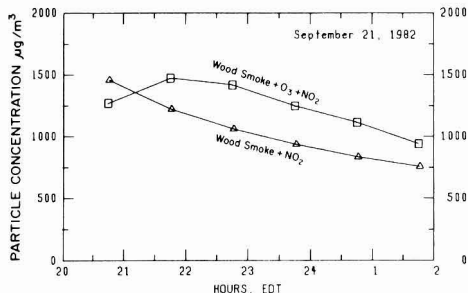


Figure 2. Wood smoke particle concentrations vs. time as determined with 47-mm Teflon-impregnated glass fiber filters (T60A20, Pallflex).

concentrated by rotary evaporation to 5 mL. Extraction of the 47-mm filter samples was performed in 25-mL micro Soxhlets for 16 h, followed by concentration to 2 mL with micro Snyder columns (Supelco). Mass determination of the extracts was made by adding small aliquots of the extract onto 47-mm Teflon-impregnated glass fiber filters, evaporating the solvent, and determining the gain in mass. In general 65–80% of the unreacted particle mass was observed in the solvent extract. After reaction the wood soot particle extracts declined to 50–65%. Extract samples were prepared for bioassay by solvent exchange with dimethyl sulfoxide.

The *Salmonella typhimurium* plate incorporation assay was performed as described by Ames et al. (13) with minor modifications (14). All assays were conducted at the Environmental Protection Agency laboratories, Research Triangle Park, NC. The bioassays were performed by using TA98 with triplicate plates at five to six doses with and without metabolic activation (\pm S9). When sample extracts were low in mass (<1.0 mg), only duplicate plates were run. Overall quality control of the tester strains was monitored and maintained on a weekly basis, and TA98 was evaluated during each experiment for response to 2-anthramine (+S9) and 2-nitrofluorene (-S9).

Results and Discussion

Wood Smoke Particle Behavior in the Chambers.

Filter mass data from over 20 experiments have shown that approximately 40–50% of the chamber particle mass disappeared in 3.5–5 h. An illustration of this loss is plotted in Figure 2. Chamber leaks together with gas and aerosol sampling accounted for approximately 10–15% of this loss. Particle losses were presumed to be a function of agglomeration, settling, and electrostatic processes (15). On a number of occasions, a slight initial increase in particle mass concentration was observed after the addition of NO₂ and O₃ (Figure 2). A possible explanation is that O₃ and NO₂ immediately reacted with vapor-phase species forming polar compounds which had lower vapor pressures than the original reactants. These products then condensed on existing particle surfaces giving rise to an increased initial aerosol mass.

Typical EAA number and volume vs. particle diameter distributions for wood smoke immediately after injection into the chambers and after 4 h of aging are shown in Figure 3. These distributions are similar in shape to those reported by Dasch (16) for fireplace emissions. A decline in the number of particles in the 0.076- and 0.133- μ m range occurred over the 4-h period. During this period a slight shift to larger particle sizes was observed for both the number and volume distributions. Nevertheless, number and volume distributions did not significantly change. Generally, particles in the 0.1–0.3- μ m range made the

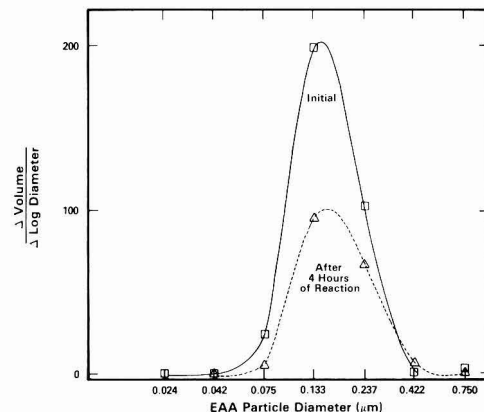
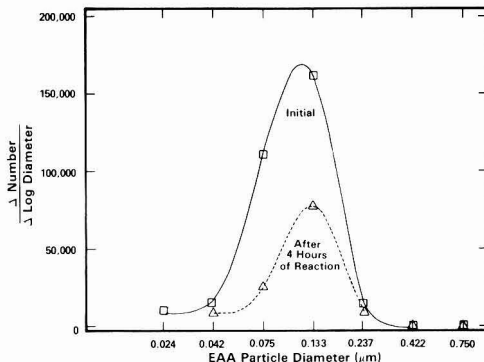


Figure 3. EAA number and volume particle size distributions for wood smoke in UNC 25-m³ chambers.

largest contribution to the volume and, hence, the mass in the EAA size range. Optical particle counter measurements showed that most of the particles in the optical range were below 0.5 μ m in diameter while almost no particles were larger than 1 μ m in optical diameter (11). In addition, no shift in particle size distribution in this range was observed over time. It is important to note that the OPC and EAA were used primarily for qualitative size distribution analysis. Previously stated limitations on the use of these instruments apply here (15). Nevertheless, it was felt that the observed trends in both the EAA and OPC data do approximate the overall particle behavior in the system.

Mutagenic Behavior of Dilute Wood Smoke Systems without Metabolic Activation. As mentioned previously, there is evidence that NO₂ or HONO₂ can react with polycyclic organic compounds on airborne soot and increase the mutagenicity of the soot particle extracts. Since nitric acid can be formed in the atmosphere from the reaction of O₃ with NO₂, O₃ + NO₂ systems were among the first tested. Data characterizing the conditions for all of the experiments presented are given in Table I. Representative vapor-phase concentrations that appeared with dilute wood smoke in the chamber are shown in Table II.

An example of the NO₂, NO, and O₃ concentration vs. time plots for a typical dual chamber wood smoke run is shown in Figure 4. The purpose of this experiment was to compare the effects of NO₂ alone to those of O₃ + NO₂ on dilute wood smoke. Note the presence of combustion NO and NO₂ as wood smoke was simultaneously added to

Table I. Summary Data from Dilute Wood Smoke Experiments

run date	Rate chamber	burn rate, kg/h	reaction time, h	particle concn, $\mu\text{g}/\text{m}^3$	initial concn, ppm			final concn, ppm			slope ^b from dose-response curves			
					NO ^a			NO ₂ ^a			TA98-S9, rev/ μg		TA98+S9, rev/ μg	
					NO	NO ₂	O ₃	NO	NO ₂	O ₃	initial	final	initial	final
09-07-82	east	ND ^f	dark/3.5	1286	0.00	0.86	0.53	0.00	0.23	0.05	0.11	1.36	0.51	0.79
	west	ND	dark/3.5	1436	0.11	0.05	0.00	0.14	0.00	0.00	0.07	0.11	0.23	0.18
09-21-82	east	ND	dark/4.0	1271	0.00	0.32	0.22	0.01	0.12	0.00	0.24	0.83	0.27	0.34
	west	ND	dark/4.0	1457	0.02	0.31	0.00	0.10	0.22	0.00	0.09	0.21		
12-02-82	east		dark/0.8	16	0.00	0.39	0.27	0.00	0.23	0.17		0.18		
	west	4.2	dark/0.8	2549	0.00	0.27	0.27	0.00	0.16	0.15	0.18	0.41		
12-07-82	east	6.2	dark/3.0	1535	0.00	0.55	0.37	0.00	0.15	0.06	0.12	2.32		
	west	6.2	dark/3.0	1402	0.00	0.54	0.00	0.01	0.46	0.00	0.17	0.69	0.73	1.10
12-14-82	east	1.8	dark/4.0	3850	0.00	0.62	0.42	0.00	0.11	0.05	0.17	1.7		
	west	1.8	dark/3.0	1509	0.00	0.05	0.57	0.00	0.02	0.42	0.14	0.62		
02-15-83	east ^d	0.6	dark to midday/19.0	2597	0.00	0.48	0.32	0.00	0.06	0.23	0.06	0.61	0.24	0.45 ^f
	west	4.8	dark to midday/19.0	7717	0.00	0.47	0.26	0.00	0.12	0.09	0.34	1.04	0.98	0.83
03-16-83	west	3.1	morning to next afternoon/27.0	2345	0.02	0.03	0.00	0.00	0.01	0.00	0.03	0.02	0.12	ND
04-12-83	east	3.3	night/3.0	4813	0.00	0.54	0.24	0.00	0.17	0.06	0.08	~0.8		
05-25-83	west	>4	days/5.0	1998	0.01	0.05	0.00	0.00	0.03	0.01 ^e	0.18	0.23	0.87	0.43

^a Chemiluminescent NO and NO₂. ^b Estimated linear slope from dose-response curves. Points up to the 300- μg dose range were used unless toxicity resulted, and then doses up to 200 μg were used. ^c Not determined. ^d Peat smoke. ^e Photochemically generated O₃. ^f Mutagenicity after 4 h.

Table II. Initial Conditions after Initial Bioassay Sample in Both Chambers for Sept 21, 1982, Dilute Wood Soot Run

	east chamber	west chamber
particle concn, $\mu\text{g}/\text{m}^3$	1270	1456
NMHC, ppm of C	3.1	3.3
CO, ppm	11.5	11.5
CH ₄ , ppm	3.24	3.53
ethane, ppm of C	0.04	0.05
ethylene, ppm of C	0.10	0.14
propane, ppm of C	0.04	0.05
propylene, ppm of C	0.07	0.08
C ₆ -C ₈ , ppm of C	1.48	1.62
formaldehyde, ppm	0.12	0.18
acetaldehyde, ppm (volume)	0.08	0.11
propionaldehyde, ppm (volume)	0.10	0.13
acetone, ppm (volume)	0.05	0.06
C ₄ carbonyls, ppm (volume)	~0.06	~0.06
dew point, °F	60	62
temperature, °F	65	65

both chambers and the decline in NO and NO₂ concentrations when the initial unreacted wood smoke filter samples were taken. As O₃ from the high concentration O₃ generator was added to the east chamber, an immediate titration of combustion NO to NO₂ occurred. Continued O₃ injection resulted in a concentration of 0.37 ppm of O₃. NO₂ was then added from a cylinder to a concentration of 0.55 ppm. In the west chamber a small injection of O₃ was made to titrate existing combustion NO to NO₂. This was followed by a 0.54-ppm injection of NO₂. Note that after 40 min, only a slight loss in NO₂ concentration was observed in the west chamber (wood smoke + NO₂). However, in the east chamber (wood smoke + NO₂ + O₃), both O₃ and NO₂ disappeared rapidly. These two observations suggest that in the east chamber much of the NO₂ loss was due to reaction with O₃ to form NO₃. This was followed by the subsequent production of N₂O₅, and ultimately nitric acid.

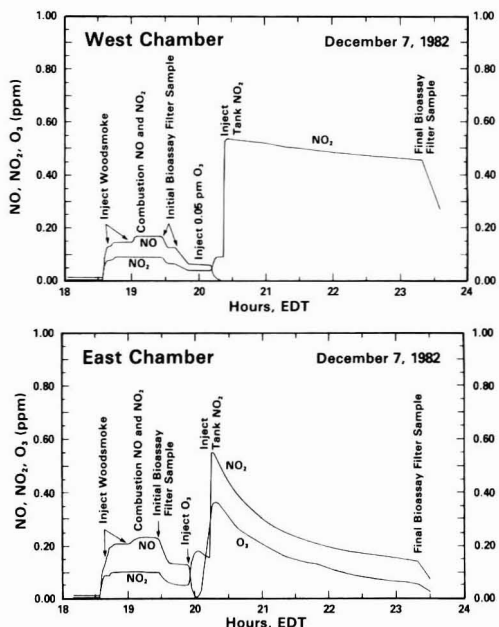


Figure 4. Comparison of the dark behavior of NO₂ + O₃ vs. NO₂ alone in dilute wood smoke.

The relative mutagenic dose-response (TA98-S9) curves for the wood smoke systems described in Figure 4 are shown in Figure 5. The initial wood soot samples from both chambers had very similar dose-response curves. We have found this to be generally true if wood smoke injections were made into both chambers simultaneously and if the bioassay analysis of the wood soot extracts were conducted on the same day. Both NO₂ and NO₂ + O₃ greatly increased the mutagenicity of dilute wood soot. However, the enhancement due to O₃ + NO₂ was much

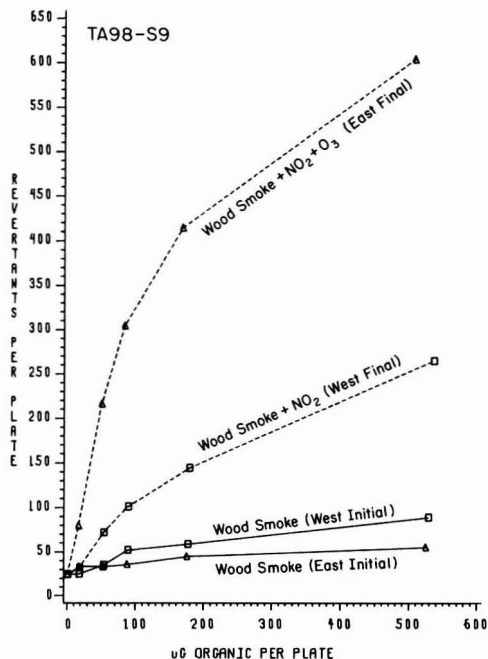


Figure 5. TA98-S9 mutagenic dose-response curves for the Dec 7, 1982, dilute wood smoke experiment.

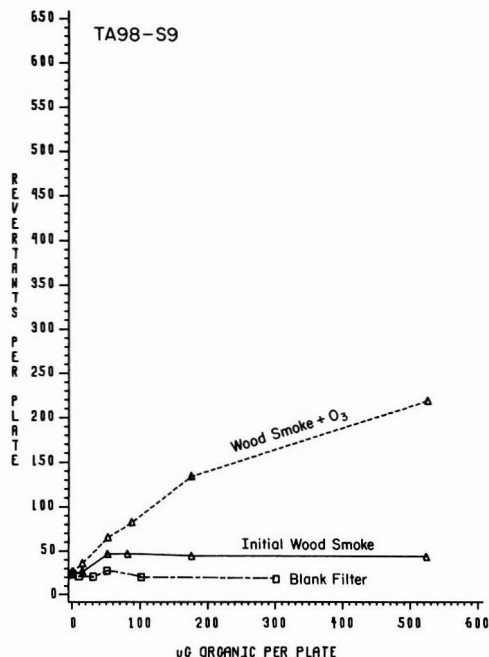


Figure 7. TA98-S9 mutagenic dose-response curve from a dilute wood smoke + O_3 experiment on Dec 14, 1982.

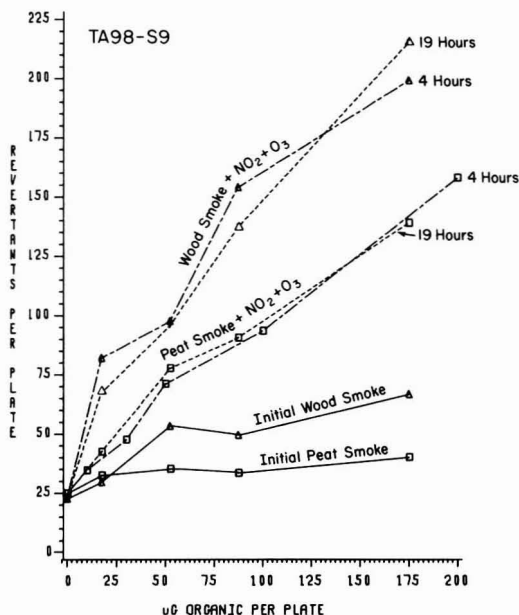


Figure 6. TA98-S9 mutagenic dose-response curves from a dual experiment on Feb 15, 1983, with O_3 + NO_2 + dilute peat smoke in one chamber and O_3 + NO_2 + wood smoke in the other chamber.

larger than that of NO_2 alone. Other experiments illustrating this effect are shown in Table I.

We have also observed that the above-mentioned NO_2 and O_3 effect is not unique to wood soot emissions. This is illustrated in Figure 6 in which both dilute wood smoke and dilute peat emissions were reacted in the dark with O_3 + NO_2 . After 4 h of dark reaction both wood and peat soot showed an increase in -S9 mutagenicity. After 19 h

of reaction, most of which occurred during the daylight hours, the original 4-h (TA98-S9) mutagenic enhancements were unchanged. An increase in indirect-acting mutagenicity occurred, however, between the 4-h and 19-h exposure period.

It is important to mention that contaminating, low ppb levels of nitric acid (as in the Pitts et al. (5) PAH-filter experiments) were possibly added to the chambers during the NO_2 (cylinder) injections. The extent to which this promoted some of the observed mutagenic increase in NO_2 -wood smoke systems is unknown. To determine the effects of O_3 alone on dilute wood smoke was also a difficult task. Ideally, these experiments should have been conducted so that wood soot particles appeared in the chambers in the complete absence of combustion NO_x . This would preclude the production of nitric acid when O_3 was added. Although this was not possible, attempts were made to minimize the amount of combustion NO_x injected by using low wood burn rates. In one such experiment, which occurred on Dec 14, 1982, 0.05 ppm of NO_x ($\sim 92 \mu g/m^3$ as NO_2) and $1523 \mu g/m^3$ wood soot particles were present in the chamber after the initial bioassay filter sample was taken. Ozone was then injected to a level of 0.57 ppm. As shown in Figure 7, an increase in direct-acting mutagenicity resulted. Given, however, that more than half of the $92 \mu g/m^3$ NO_2 disappeared in the O_3 + wood smoke experiment, it is probable that nitric acid formed. Thus, as in the NO_2 -wood smoke experiments, the $HONO_2$ contribution to the observed mutagenic increases in the O_3 -wood smoke experiment could not be estimated.

Concurrent with the previously described experiments, an evaluation of wood smoke aged in the dark was undertaken. Dilute wood smoke was injected into one chamber and compared to the second chamber containing wood smoke reacted with O_3 + NO_2 . The dose-response curves for both chambers from this experiment are shown in Figure 8. Note that, as before, the chamber (east) which

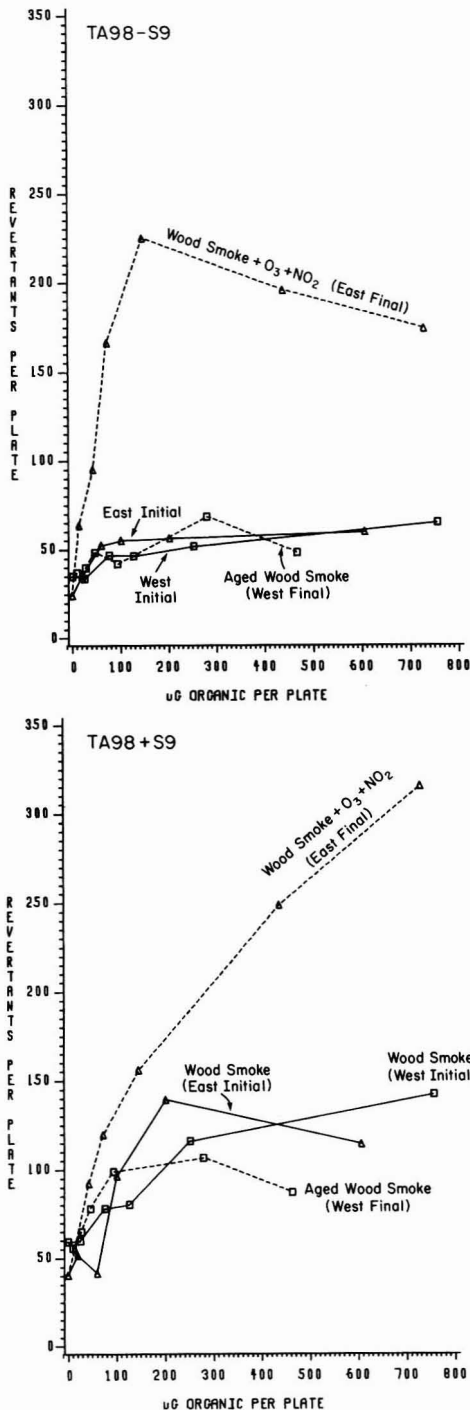


Figure 8. TA98±S9 mutagenic dose-response curves for a dark dual-chamber experiment on Sept 7, 1982, which compared the effects of aging dilute wood smoke without additional O₃ or NO₂ vs. the effects of adding O₃ + NO₂.

received both O₃ and NO₂ showed a sharp increase in direct (-S9) mutagenic activity. The west chamber, containing only dilute wood smoke, did not show any mutagenic

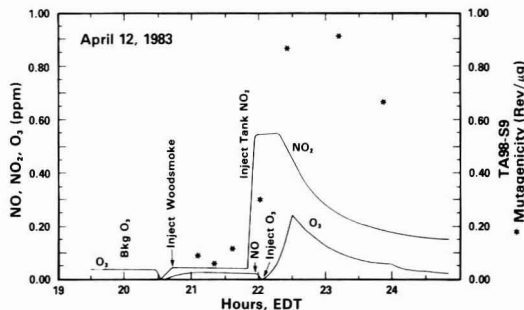


Figure 9. Rate of TA98-S9 mutagenic increase of dilute wood smoke after exposure to O₃ + NO₂.

difference between initial and final samples.

Preliminary wood soot experiments were also conducted in the sunlight (Table I, March 16 and May 25, 1983, experiments). Low burn rate conditions were used to limit the amount of combustion NO_x injected into the chambers to less than 0.06 ppm. This created a NO_x-limited photochemical mixture (HC/NO_x = ~50/1 ppm of C/ppm) due to the high gas-phase volatile hydrocarbon concentrations which were similar to those shown in Table II. The high HC/NO_x ratio and possible O₃ losses to the wood soot particle surfaces tended to limit the levels of photochemically generated O₃ which appeared in these systems. Hence, it was not surprising that less than 0.01 ppm of O₃ was measured in these daytime experiments. Under these conditions, no increase in either direct-acting or indirect-acting mutagenicity was observed.

Mutagenicity of Wood Smoke Systems with Metabolic Activation. Bioassays of the particle extracts from more than 20 initial dilute wood smoke chamber samples (17) showed that the mutagenicity with S9 activation was always higher than without S9 activation. Lewtas (18) reported mutagenic activity of wood stove emissions using a nonlinear model (19) to determine the slope of the dose-response curve. When oak was burned, a slope of 0.9 revertant/µg (rev/µg) of organic extract was observed with the addition of S9 and 0.15 revertant/µg without metabolic activation. To provide a comparison, the slope values in this study were also calculated by using the same nonlinear model (19). This gave dilute wood smoke slope values similar to those reported by Lewtas (18). The average nonlinear model slope was 0.83 revertant/µg in an activated system and 0.28 revertant/µg without S9 activation.

For wood smoke exposed to O₃ + NO₂, indirect-acting (+S9) mutagenicity showed a less dramatic increase than direct-acting (-S9) mutagenicity (Figure 8). This suggests a greater production of direct-acting mutagens than of indirect-acting mutagens from NO₂ + O₃ systems.

Rate of Mutagenic Increase and Sampling Artifacts. In order to assess the rate at which the mutagenic nature of wood smoke was increased by O₃ + NO₂, a separate experiment was conducted. The 47-mm filter samples, which were typically used to monitor particle concentrations, were extracted and bioassayed with TA98-S9. This permitted much better time resolution of the mutagenic changes. The mutagenic results of this experiment are plotted in Figure 9 along with the NO₂ and O₃ behavior of the system. The mutagenicity of each filter sample reported in Figure 9 was calculated from the linear portion of the dose-response curve. Note that three filter samples were taken soon after wood smoke was injected into the chambers. This established the base-line mutagenicity of the dilute wood smoke soon after it was injected and before NO₂ and O₃ were added. Ten minutes after NO₂ was

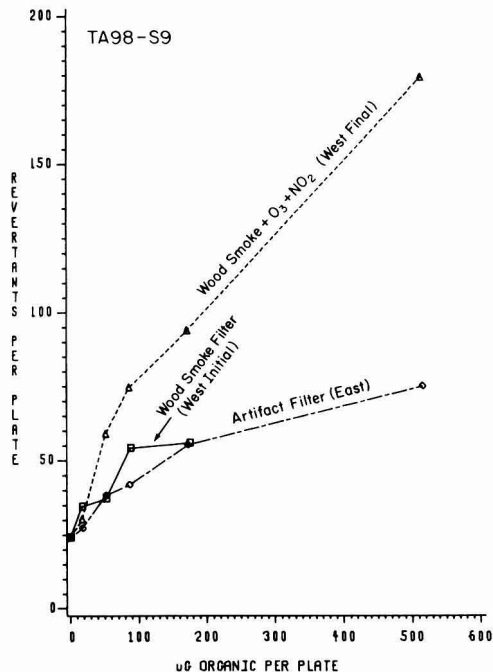


Figure 10. Wood smoke mutagenicity filter artifact experiment with $O_3 + NO_2$.

injected another filter sample was taken and the -S9 mutagenicity of the particle extract had increased from approximately 0.1 to 0.3 rev/ μg . After O_3 was added, the mutagenicity increase was even more striking. These results suggest that mutagenic increases from wood soot exposure to O_3 and NO_2 occur very rapidly.

There has been much concern about the potential for confounding mutagenic artifact formation during the filter sampling process (6, 7, 20, 21). For this reason, experiments were designed to distinguish between mutagenic changes which occur while particles were in the airborne state and possible mutagenic artifact processes which occur during sampling.

These experiments differed from others in that wood smoke was injected into only one of the chambers. The other chamber was closed to the surrounding atmosphere and the wood stove injection manifold. Hence, it contained only rural background air. Two filter samples were taken from the chamber that had just received the wood smoke injection. One of these wood soot filter samples was placed in the sampling apparatus of the background air chamber. This sample was designated as the artifact filter. The other wood soot sample was used to establish the initial base-line wood soot mutagenicity of the unreacted chamber wood smoke. Ozone and NO_2 were then added to both chambers. After ~ 1 h, air from the background air chamber (with $O_3 + NO_2$) was drawn across the artifact filter. Simultaneously, a final sample was collected from the chamber which contained dilute wood smoke, O_3 , NO_2 , and other reaction products.

The results for an experiment conducted on Dec 2, 1982, are illustrated by the dose-response curves shown in Figure 10. The NO_2 and O_3 concentrations in the chambers both before and after reaction are reported in Table I. Note that higher concentrations of O_3 and NO_2 were drawn over the wood smoke artifact filter than those which were present in the wood smoke + $O_3 + NO_2$ chamber (when

the final bioassay filter sample was taken). As expected, the $O_3 + NO_2$ reacted wood smoke sample was more mutagenic (TA98-S9) than the initial unreacted sample. Most important, however, was that little difference could be discerned between the initial, unreacted, and artifact filter samples. These types of experiments suggest that, at the sampling rates and times used and at the O_3 and NO_2 concentrations typically present in the chambers when final filter samples were taken, significant artifact effects on direct-acting TA98 mutagenicity did not result.

Summary

In this study dilute wood smoke at particle concentrations of 1300-8000 $\mu g/m^3$ was aged in the dark or in sunlight for several hours in outdoor Teflon film environmental exposure chambers. The shapes of the particle size distributions of wood soot in the chambers did not appreciably change over a period of 4 h. Aging dilute wood smoke in the presence of low levels of combustion-generated NO_2 , either in the sunlight or in the dark, did not increase the TA98 bacterial mutagenicity of dilute wood smoke. The addition of sub-ppm mixtures of $O_3 + NO_2$ (in the 0.3-0.9 ppm range) to dilute wood smoke substantially increased the direct-acting mutagenicity of the particle extracts. This enhancement in direct mutagenic activity occurred within a period of minutes. The indirect-acting or promutagenic activity of wood smoke particle extract was also increased by $NO_2 + O_3$ mixtures, but to a lesser extent. When NO_2 alone was reacted with wood smoke, the increase in direct mutagenic activity was not as great as from combined $NO_2 + O_3$ systems. Systems containing $NO_2 + O_3$ most probably have a high potential for heterogeneous nitric acid formation on the surface of soot particles. The observed increased bacterial mutagenicity of the wood soot extracts in such systems, therefore, may be caused by the direct reaction of this surface-generated nitric acid with particle-bound organics.

Preliminary results also indicate that emissions from peat combustion react with O_3 and NO_2 in a manner similar to wood combustion products. This result suggests that particulate emissions from other combustion fuels such as coal, oil, diesel, or gasoline may also be subject to atmospheric transformation. It is our contention that as air pollution research advances and research findings are translated into regulatory policy, there will be a need to go beyond the characterization of stack or tailpipe emissions, to an approach which factors in the potential "atmospheric mutagenicity" resulting from atmospheric processes. However, a realistic assessment of these atmospheric changes, and their possible health implications, will require a substantial increase in the study of both real and simulated atmospheres.

Acknowledgments

We acknowledge the help of Joellen Lewtas for the useful discussions in the initial phase of this program, Ronald Bradow, who designed the bioassay sampling apparatus, and Michael Osborne for making available the stove used in this study. The data processing efforts of Jeff Hoffner, the laboratory assistance of Maurice Jackson and Ed Edmondson, and the document preparation of Donna Simmons, Bobette Eckland, and Marybeth Hollenman were appreciated.

Registry No. Ozone, 10028-15-6; nitrogen dioxide, 10102-44-0; ethane, 74-84-0; ethylene, 74-85-1; propane, 74-98-6; propylene, 115-07-1; formaldehyde, 50-00-0; acetaldehyde, 75-07-0; propionaldehyde, 123-38-6; acetone, 67-64-1; carbon monoxide, 630-08-0; methane, 74-82-8.

Literature Cited

(1) Imhoff, R. E.; Manning, J. A.; Cooke, W. M.; Hayes, T. L. Proceedings of APCA Specialty Conference on Residential Wood and Coal Combustion, Louisville, KY, March 1982.

(2) DeCesar, R. T.; Cooper, J. A. *Proc.—Int. Conf. Resid. Solid Fuels: Environ. Impact Solutions* 1981, 349.

(3) Peters, J. A. *Proc.—Int. Conf. Resid. Solid Fuels: Environ. Impacts Solutions* 1981, 267.

(4) Lewtas, J. Symposium on the Application of the Short-Term Bioassays of Complex Environmental Mixtures, U.S. Environmental Protection Agency, 1981.

(5) Pitts, J. N., Jr.; Van Cauwenberghe, K. A.; Grosjean, D.; Schemid, J.; Fitz, D.; Beiser, W.; Knudson, G.; Hynds, P. *Science (Washington, D.C.)* 1978, 202, 515-519.

(6) Van Cauwenberghe, K. A.; Van Vaecck, L. *Mutat. Res.* 1983, 116, 1-20.

(7) Grosjean, D.; Fung, K.; Harrison, J. *Environ. Sci. Technol.* 1983, 17, 679-685.

(8) Pitts, J. N., Jr. *EHP, Environ. Health Perspect.* 1983, 47, 115-140.

(9) Atkinson, R.; Carter, W. P. L.; Darnall, K. R.; Winer, A. M.; Pitts, J. N., Jr. *Int. J. Chem. Kinet.* 1980, 12, 780-836.

(10) Jeffries, H. E.; Fox, D. L.; Kamens, R. M. *Environ. Sci. Technol.* 1975, 10, 1006-1010.

(11) Kamens, R. M.; Rives, G. D.; Perry, J. M.; Goodman, R. G.; Bell, D. A.; Saucy, D. A. APCA Proceedings, 1983, Atlanta, GA, 1983, Paper 83-54.12.

(12) Kuntz, P.; Lonneman, W.; Namie, G.; Hull, L. A. *Anal. Lett.* 1980, 13, 1409-1415.

(13) Ames, B. N.; McCann, J.; Yamasaki, E. *Mutat. Res.* 1975, 31, 347-364.

(14) Claxton, L. D.; Kohan, M.; Austin, A.; Evans, C. *U.S. Environ. Prot. Agency* 1982, EPA-HERL-0323.

(15) Saucy, D. A.; Kamens, R. M.; Linton, R. W. *Atmos. Environ.* 1983, 17 (12), 2617.

(16) Dasch, J. M. *Environ. Sci. Technol.* 1982, 16, 639-645.

(17) Rives, G. D. Masters Thesis, University of North Carolina, Chapel Hill, 1983.

(18) Lewtas, J. *Proc.—Int. Conf. Resid. Solid Fuels: Environ. Impacts Solutions* 1981, 606-619.

(19) Stead, A.; Hasselblad, V.; Creason, J.; Claxton, L. *Mutat. Res.* 1981, 85, 13-27.

(20) Schuetzle, D.; Perez, J. M. *J. Air Pollut. Control Assoc.* 1983, 33, 751-755.

(21) Risby, T. H.; Lextz, S. S. *Environ. Sci. Technol.* 1983, 17, 621-624.

Received for review July 21, 1983. Revised manuscript received December 19, 1983. Accepted January 17, 1984. This work was supported by Grant R808112 from the U.S. Environmental Protection Agency and Contract 57 from the North Carolina Energy Institute.

Effect of Censoring Trace-Level Water-Quality Data on Trend-Detection Capability

Robert J. Gilliom,* Robert M. Hirsch, and Edward J. Gilroy

U.S. Geological Survey, Reston, Virginia 22092

■ Monte Carlo experiments were used to evaluate whether trace-level water-quality data that are routinely censored (not reported) contain valuable information for trend detection. Measurements are commonly censored if they fall below a level associated with some minimum acceptable level of reliability (detection limit). Trace-level organic data were simulated with best- and worst-case estimates of measurement uncertainty, various concentrations and degrees of linear trend, and different censoring rules. The resulting classes of data were subjected to a nonparametric statistical test for trend. For all classes of data evaluated, trends were most effectively detected in uncensored data as compared to censored data even when the data censored were highly unreliable. Thus, censoring data at any concentration level may eliminate valuable information. Whether or not valuable information for trend analysis is, in fact, eliminated by censoring of actual rather than simulated data depends on whether the analytical process is in statistical control and bias is predictable for a particular type of chemical analyses.

Introduction

Certain key types of water pollutants, principally synthetic organic compounds and some metals, often occur only in trace-level concentrations and yet are environmentally important at trace levels. Trace-level concentrations are herein defined as being so low that their detection and identification based on a single analytical determination is reasonably in doubt—the probability of incorrectly deciding that the compound is present is greater than about 5%. Both imprecision and the potential for systematic error in quantitative measurements of trace levels are generally high and poorly understood. The

combination of uncertain detection and poor reliability of trace-level measurements has led laboratories to adopt rules that specify concentration levels, usually referred to as detection limits but called data-reporting limits in this report, below which measurements are not reported to data users. From the standpoint of statistical data analysis, this practice results in "censored" data sets. The term censored is used strictly in the statistical sense and is not intended to imply that laboratories are intentionally withholding valuable information or have anything but the data users' best interest in mind. Measurements that are censored are usually reported as "not detected" or as "less than" the reporting limit.

Many typical statistical analyses such as comparisons of means or variances and regression analyses are difficult or impossible to apply to censored data sets (1). The reliability of statistical analyses that can be applied to censored data generally decreases as the degree of censoring increases. The adverse effects of censoring are particularly acute for data on trace-level contaminants of surface waters because dilution is commonly great, resulting in low concentrations and high degrees of censoring. For example, quarterly data collected for 5 years at more than 150 stations as part of the National Pesticide Monitoring Network for Rivers indicate that more than 95% of measured concentrations for 25 pesticides were censored. Such degrees of censoring and resulting difficulties with statistical analysis may not be important for chemicals that have environmental effects only at high concentrations. But, for many of the 25 pesticides, for example, data-reporting limits were near or above water-quality criteria.

Censoring according to data reporting limits that are above concentrations that may have adverse effects on

water quality or give early indication of a trend toward such concentrations is not desirable. There are two possible approaches to alleviating this situation. First, better analytical methods may be available or might be developed that would allow lowering data reporting limits even though the limits would still be determined by the same reliability criteria. Second, the same analytical methods can be used but with lower or no reporting limits so that less reliable measurements are reported. Or, both the method could be improved and the reliability limit could be relaxed. The present study was aimed at investigating the potential benefits of lowering or eliminating data reporting limits applied to data with different degrees of measurement uncertainty.

The purpose of this report is to demonstrate that trace-level data that are routinely censored may contain valuable information despite their greater uncertainty, and that, given certain conditions, adopting a "no censoring" rule increases the data analyst's ability to detect actual trend in data. This conclusion was reached by the Monte Carlo experiment described in this report. Trace-level organic data were simulated with best- and worst-case estimates of measurement uncertainty, various degrees of linear trend, and different censoring rules. The resulting classes of data were subjected to a nonparametric statistical test for trend. The effect of different degrees of censoring is shown by comparing the power (effectiveness) of trend detection, as determined from Monte Carlo experiments, for the different classes of data with different censoring rules.

Background on Study Approach and Trend-Detection Method

While a strong argument can be made for not censoring data simply because they are the best concentration estimates available, direct demonstration of the information lost due to censoring is difficult. Systematic error may be great and is highly uncertain, and the effectiveness of parametric (distribution-dependent) analyses is difficult to ascertain. Questionable or unsupportable distributional assumptions are required to apply parametric analyses to censored data. Some nonparametric (distribution-free) statistical analyses, however, can be legitimately applied to both censored and uncensored data. A key example is a nonparametric test for trend over time, originally described by Mann (2) as a particular application of Kendall's τ (3), and which was described for application to water-quality data by Hirsch and others (4). Trend is here defined as a monotonic change in magnitude with time. Analysis for trend is one of the most basic and important types of water-quality assessment. Kendall's τ trend test is valid even for data that are biased, as long as the relationship between bias and concentration is constant over time. The test is not valid if changes occur over time in the relationship between concentration and bias that are not corrected for before applying the test. In general, if a change occurs in the relationship between variance and concentration, changes in the relation between bias and concentration should also be suspected.

Kendall's τ trend test provides a tool for evaluating the loss of information incurred by censoring. This evaluation is accomplished in this study by application of the trend test to both censored and uncensored versions of a large number of data sets. The trend test can be applied to censored data with no difficulty, by considering all of the censored values to be tied with each other and to be less than all uncensored values. The correction for ties (3) is then used in computing the variance of the test statistic.

Simulation of Data

Simulated data were used in our experiments because no trace-constituent data were available for concentrations below present-day data reporting limits and no data for higher concentrations of trace constituents or for macro-constituents had comparable degrees of measurement uncertainty. Simulated data were designed to be representative in terms of concentration levels, measurement uncertainty, and censoring levels, of data that might be observed for such trace-organic constituents as the chlorinated hydrocarbon and organophosphorus groups of pesticides. Analytical laboratories have a long history of experience with these chemicals compared to other trace-organic compounds and, thus, chemists are able to provide useful estimates of measurement uncertainty even at the very low concentrations below present data-reporting limits. The general approach taken for generating synthetic data sets was to (1) specify a probability distribution that would typically describe the population of concentration values at a river water-quality station, (2) estimate the probable worst-case and best-case estimates of measurement uncertainty, and (3) add various amounts of linear trend to the data. Representative classes of data sets were simulated by varying the underlying population parameters and the measurement uncertainty. Different censoring rules were then applied to the resulting data sets.

Population of Concentrations. Populations of concentrations occurring in samples of water taken at a river station, under the condition of no trend, were simulated to follow log-normal distributions, which describe the distribution of many water-quality data. If $y = \ln x$, where x is the actual concentration of a chemical, then the probability distribution of y is normal with a mean, μ_y , and variance, σ_y . The mean and variance of y are readily computed from the mean and variance of x (5):

$$\mu_y = \ln(\mu_x) - 0.5[\ln[(\sigma_x/\mu_x)^2 + 1]] \quad (1)$$

$$\sigma_y = [\ln[(\sigma_x/\mu_x)^2 + 1]]^{1/2} \quad (2)$$

For generating data sets for the Monte Carlo experiments, the population mean, μ_x , and coefficient of variation, σ_x/μ_x , were specified at desired levels and used to calculate μ_y and σ_y . Then a data set of true concentrations, x_i , of any number of values, n , could be generated by

$$x_i = \exp(\mu_y + \sigma_y \epsilon_i) \quad (3)$$

where ϵ_i is a randomly chosen value from a normal distribution with a mean of zero and variance of one.

Measurement Uncertainty. The true concentration of a trace constituent in the i th sample is x_i , but the attempt to measure x_i is imperfect and results in a measurement u_i . The value u_i is an uncertain estimate of x_i . To simulate the uncertainty associated with u_i , the probability distribution of measurements about x_i was estimated. Estimation of this distribution is difficult because, in the range of interest (at or below present detection limits), there are no actual data documenting analytical capabilities. Therefore, best-case and worst-case total-error limits estimated by two experienced chemists were used as the basis for approximating best- and worst-case error distributions.

The chemists estimated total-error limits by considering the potential for both systematic and random error (6). As applied in this study, the limits describe the range about a true concentration in which there is a "very high" probability that the measurement lies. For trace analyses the lower bound is always zero if negative measurements are not reported and the upper bound, or very high

Table I. Estimated Total-Error Bounds for Typical Pesticide Analyses at Various Concentration Levels (8)

concn, $\mu\text{g/L}$	best-case uncertainty estimate (measurement as percentage of true concentration)	worst-case uncertainty estimate (measurement as percentage of true concentration)
0.02	0-150 (160) ^a	0-200 (250) ^a
0.005	0-200 (190)	0-500 (400)
0.001	0-400 (350)	0-1000 (1200)
0.0005	0-500 (550)	0-2000 (2200)

^a Values in parentheses are those computed from eq 4 and 5, which approximate the chemists' estimates.

probability level, is arbitrarily taken to represent the 98th percentile of the measurement distribution. The issue of whether or not negative values should be reported is not important to this study, but the reader is referred to ASTM (7) on this topic.

Estimated total-error bounds are shown in Table I for representative trace-level concentrations. For example, the best-case 98th percentile for 0.02 $\mu\text{g/L}$ is 150%, or 0.03 $\mu\text{g/L}$, so that about 98% of the measurements of a true concentration of 0.02 $\mu\text{g/L}$ would be expected to be between 0 and 0.03 $\mu\text{g/L}$. For estimation of the 98th percentile, $u_{i,98}$, of measurements of any true concentration, x_i , simple linear equations were used to approximate the best- and worst-case error bounds estimated by the chemists. Least-squares regressions were evaluated for the pairs of x_i and $u_{i,98}$ estimated by the chemists for both best- and worst-case scenarios. Slopes of the least-squares equations were adjusted within their standard error bounds to improve the fit in the low concentration range, for which most of our analysis was conducted. The equations allow rapid estimation of percentiles in the simulations. The best-case (lowest uncertainty) equation is

$$u_{i,98} = 0.002 + 1.5x_i \quad (4)$$

The slope was changed to 1.5 from the least-squares value of 1.4 ± 0.1 . The worst-case (greatest uncertainty) is

$$u_{i,98} = 0.010 + 2x_i \quad (5)$$

where $u_{i,98}$ is in micrograms per liter. The slope for eq 5 was changed to 2.0 from the least-squares value of 1.5 ± 0.6 . Estimates of $u_{i,98}$ from eq 4 and 5 are given in percent $[(u_{i,98} \times 100)/x_i]$ in Table I for the concentrations shown and are shown as a function of concentration in Figure 1.

Given a generated true concentration, x_i , we derived the measurement error distribution from the estimate of the 98th percentile. The error bounds in Table I suggest a measurement error distribution with positive skew. The distribution of measurements, u_i , was therefore assumed to be log normal, such that w_i is normal where $w_i = \ln u_i$, because there is greater room for error in the positive direction from the actual value. Note that the choice of a log normal distribution means that no simulated measurements will be equal to zero, when in reality some measurements may be zero or even negative. Further, the median of the distribution of measurements was assumed to equal the true concentration because the chemists felt that, even given the lopsided potential magnitude of errors in the positive and negative directions, overestimates and underestimates would occur at about the same frequency. Therefore, by the properties of the logarithmic transform

$$\mu_{w_i} = \ln(x_i) \quad (6)$$

$$w_i = \ln(u_{i,98}) \quad (7)$$

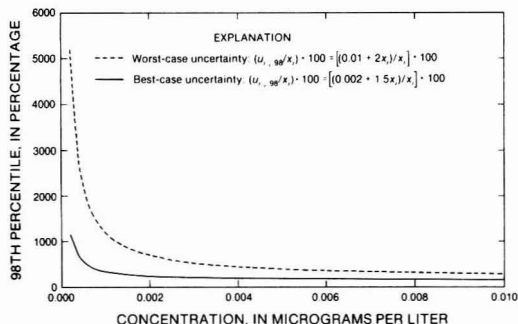


Figure 1. Ninety-eighth percentile of measurement distribution, $u_{i,98}$, as a function of the true concentration, x_i .

By the properties of the normal distribution, the standard deviation of measurements in log space can be computed:

$$\sigma_{w_i} = (w_{i,98} - \mu_{w_i})/2.055 \quad (8)$$

Values of the transformed variable, w , can then be generated by

$$w_i = \ln(x_i) + \sigma_{w_i}\epsilon_i \quad (9)$$

where ϵ_i is normally distributed with a mean of zero and variance of one. Finally, the simulated data in actual concentration units, with measurement uncertainty incorporated, are

$$u_i = \exp(w_i) \quad (10)$$

Addition of Trend. The foregoing relationships allow the generation of realistic trend-free sets of trace-constituent data. Linear trend is simple to add by causing the specified population mean, μ_x , to increase at a constant rate, m , with time, t . The coefficient of variation was left constant at the original value, σ_x/μ_x , implying that the standard deviation, σ_x , increases with μ_x . Thus, the data-generating procedure is altered at eq 1 as follows:

$$\mu_y = \ln(\mu_x + mt) - 0.5[\ln[(\sigma_x/\mu_x)^2 + 1]] \quad (11)$$

The standard deviation in log space, σ_y , is constant over time (eq 2). For the Monte Carlo experiments, 10 different positive trends (m) were added to each data set generated. The amount of trend added increased from the no-trend case to the maximum trend in equal increments. The maximum trend was determined by trial and error to best facilitate comparison of Monte Carlo results.

Summary of Data-Generating Algorithm. Data sets of any length are generated by the following steps: (1) A log normally distributed set of true water-sample concentrations, x_i , with any specified initial mean, μ_x , coefficient of variation, σ_x/μ_x , and trend slope, m , is generated by eq 11 and 3. (2) Given x_i from step 1, best- and worst-case estimates of log measurement standard deviation, σ_{w_i} , are computed by eq 4-8. (3) Given x_i and σ_{w_i} , individual measurements, u_i , are generated by eq 9 and 10.

Characteristics of Simulated Data. Simulated data sets and censoring rules were designed to be as realistic as possible. All uncensored data sets contain 40 simulated measurements. This represents, for example, 10 years of data from the National Pesticide Monitoring Network for Rivers, operated by the U.S. Environmental Protection Agency and the U.S. Geological Survey, for which sampling was quarterly. Four classes of data, where data in a class are from the same population at time zero and have the same measurement uncertainty, were evaluated in the Monte Carlo experiment.

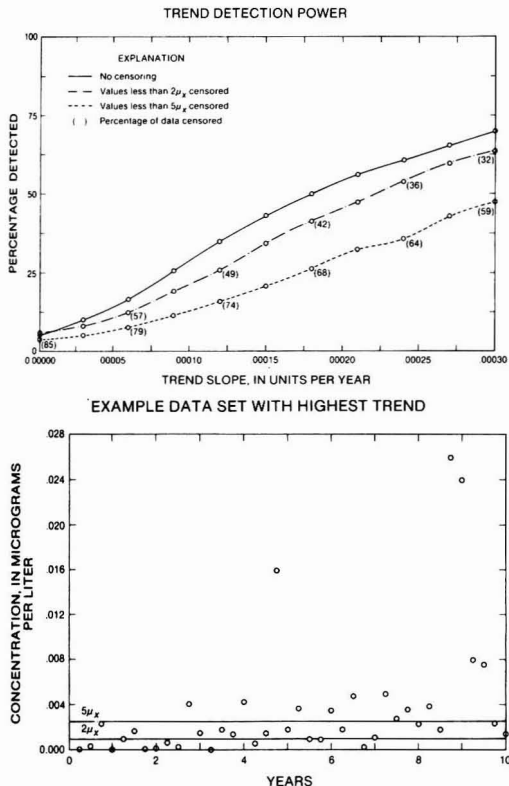


Figure 2. (Case 1) Effect of censoring on trend-detection power for data with lowest population mean, $\mu_x = 0.0005 \mu\text{g/L}$, and highest measurement uncertainty, eq 5.

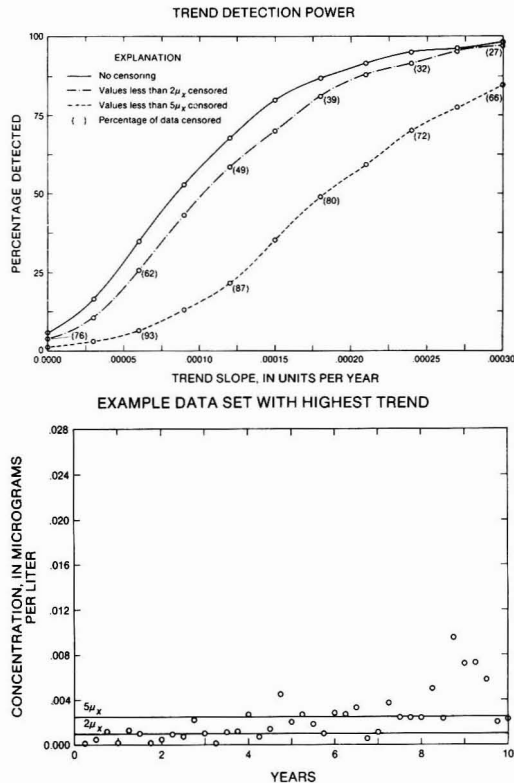


Figure 3. (Case 2) Effect of censoring on trend-detection power for data with lowest population mean, $\mu_x = 0.0005 \mu\text{g/L}$, and lowest measurement uncertainty, eq 4.

Class 1: Low Population Mean and High Measurement Uncertainty. The trend-free population mean of $0.0005 \mu\text{g/L}$ was chosen to be well below routinely applied censoring levels applied to most trace-organic data, which typically range from 0.001 to $0.05 \mu\text{g/L}$. As for all classes of data, the coefficient of variation of the population was specified to be 0.5 . The measurement uncertainty specified was the worst-case relationship shown in Figure 1 and described in concentration terms by eq 5. In the absence of trend, most data in this class are censored by most laboratories, and the uncertainty in an individual measurement is extremely high.

Class 2: Low Population Mean and Low Measurement Uncertainty. This class is identical with the first except that best-case estimates of measurement uncertainty were used. These uncertainty estimates are shown in Table I and are expressed by eq 4. In the absence of trend, most data in this class would normally be censored, but the simulated measurement uncertainty is not as great as in class 1.

Class 3: High Population Mean and High Measurement Uncertainty. The trend-free population mean of $0.005 \mu\text{g/L}$ was chosen to be at a level where, given the population variability (coefficient of variation = 0.5) and measurement error, a substantial number of measurements would be above the censoring level of some laboratories (in the absence of trend). The measurement uncertainty was determined from the worst-case relationship, eq 5. Data in class 3 have smaller percent standard errors than data in either class 1 or class 2.

Class 4: High Population Mean and Low Measurement Uncertainty. Class 4 data are identical in character to class 3 data except that measurement uncertainty is lower as described by eq 4. As shown in Figure 1, however, the difference in measurement reliability between the best and worst cases is not as large at this concentration level compared to the lower levels.

Censoring Rules. Three censoring rules were applied to each generated data set, regardless of the class, resulting in three sets of data for trend analysis from each iteration of the data-generation procedure. The three censoring rules were (1) no censoring, (2) all values less than $2\mu_x$ were censored, and (3) all values less than $5\mu_x$ were censored. Recall that μ_x is the initial mean concentration. These rules were chosen to yield a representative range of presently used censoring rules. The application of the second and third censoring rules to the four classes of data yields a representative range of data that would be available to data users under present-day censoring practices and the expected range of measurement errors. A common condition not considered, but easily inferred from the tests conducted, is even more severe censoring.

Monte Carlo Experiments

The Monte Carlo experiments consisted of generating 500 data sets of a particular class and applying the non-parametric test for trend, Kendall's τ at $\alpha = 0.05$, to each data set at a range of trends (10 values of m starting with

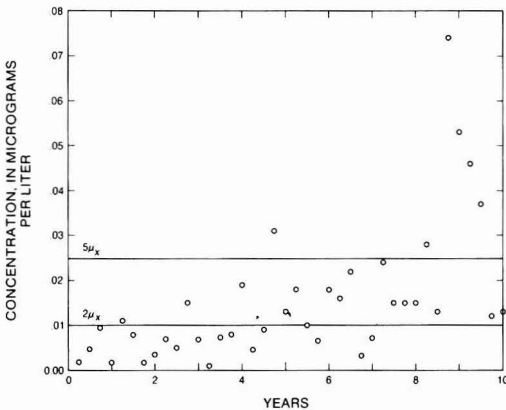
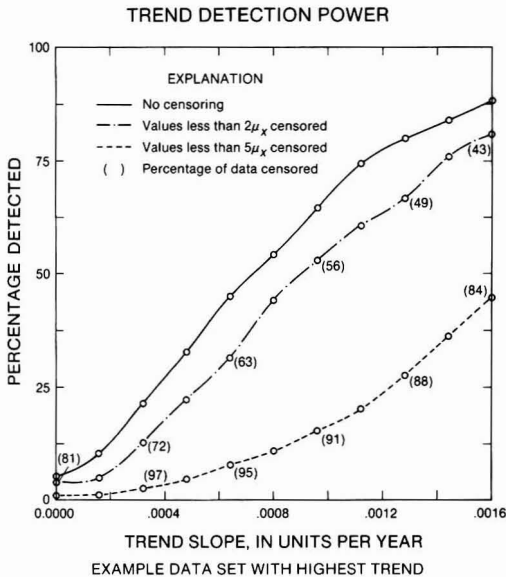


Figure 4. (Case 3) Effect of censoring on trend-detection power for data with highest population mean, $\mu_x = 0.005 \mu\text{g/L}$, and highest measurement uncertainty, eq 5.

$m = 0$) for each of the three censoring levels. The results of these experiments can be expressed by showing the frequency that trend was detected in the 500 iterations as a function of degree of trend for each censoring rule. This amounts to expressing the relationship between power (effectiveness) of trend detection and degree of censoring.

Results of the Monte Carlo experiments are shown in Figures 2-5. Each figure shows trend-detection power related to trend slope for each of the censoring levels. Also shown in each figure is an example data set from simulations for that data class at the maximum trend level. The actual trend units are not important because they are difficult to interpret and the reader is referred to the graphs of the data for a visual indication of the degrees of trends added. A progressively increasing level of data reliability occurs from Figure 2 to Figure 5. However, there is a much greater difference between best-case (Figure 2) and worst-case (Figure 3) estimates of uncertainty for the low concentration data classes than for the highest concentration classes (Figures 4 and 5). This reflects the greater uncertainty about the reliability of data at very low concentrations.

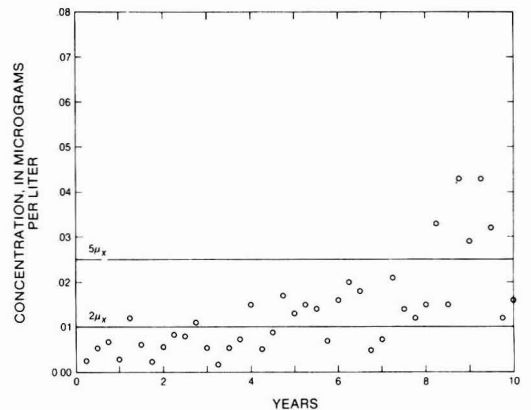
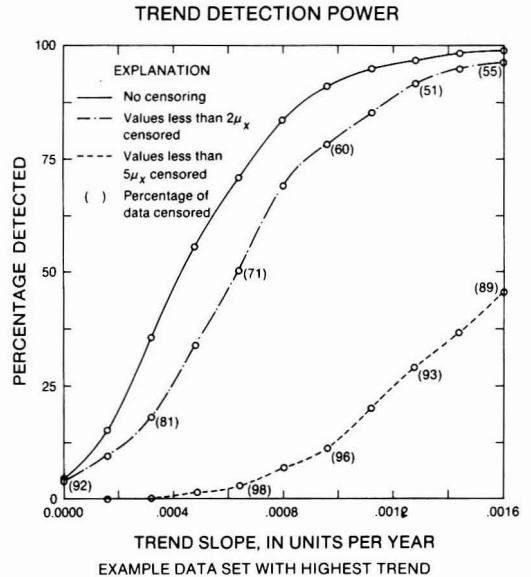


Figure 5. (Case 4) Effect of censoring on trend-detection power for data with highest population mean, $\mu_x = 0.005 \mu\text{g/L}$, and lowest measurement uncertainty, eq 4.

Results in Figures 2-5 show that, for all conditions evaluated, (1) detection of actual trend was more reliable for uncensored data compared to censored data and (2) the detrimental effects of censoring increase with increasing reliability of data. That detection of actual trend is more reliable for uncensored data is demonstrated by the solid curves representing trend detection for uncensored data in Figures 2-5, which are always above the trend-detection effectiveness for censored data. The increasing detrimental effects of censoring as data reliability increases is shown by comparison of results for class 1 data in Figure 2 and class 2 data in Figure 3, between which the only difference is measurement uncertainty. Comparison of results for class 3 data in Figure 4 and class 4 data in Figure 5 shows the same phenomenon. For both sets of comparisons the difference between trend-detection efficiency for uncensored data compared to that for the most censored data is greater for the lowest measurement uncertainty. Adverse effects of censoring increase with increasing data reliability because more reliable data contain more information than less reliable data and, thus, more information is lost when data are censored.

Discussion and Conclusions

For all classes of data evaluated, trends were most effectively detected in uncensored data as compared to censored data even when the data censored were highly unreliable. Censoring data at any concentration level, especially given our lack of knowledge about prevailing concentrations, may eliminate valuable information. The more reliable the data censored, the greater the information lost and the more detrimental the effects of censoring.

Whether or not valuable information for trend analysis is in fact eliminated by censoring of actual rather than simulated data depends mainly on whether bias is predictable for a particular type of chemical analyses and the measurement process is in statistical control. To be in statistical control, the location and shape of the measurement error distribution must be reasonably constant at each concentration. If there are changes in bias over time that are unknown and cannot be compensated for, then valid trend tests are not possible.

The use of simulated data in this study assured statistical control and a constant and predictable relation between bias and concentration. How well and how commonly this condition would be met for actual trace-level measurements is presently difficult to assess except on a case-by-case basis. In general, the condition probably holds true for measurements made by one laboratory by a constant measurement process. If the measurement process changes over time, or if measurements from more than one laboratory are to be used, then the required condition of a constant relation between bias and concentration may well not be met. In either of these cases, only careful evaluation of and correction for differences in bias would allow valid use of the data for trend analysis. Note that the need for such evaluations applies equally to data that

are above present data reporting limits—these reporting limits are not magic boundaries for the absence or presence of statistical control.

The results of the present study lend strong support to the argument, earlier advanced by Rhodes (1) and generally followed in new ASTM standards (7), that data should not be routinely censored by laboratories. Uncensored data should always be retained in permanent records available to data users even if policy makers of a laboratory decide that some censoring or other form of qualification is necessary before general public release of data. Measurement data should not be discarded unless the lack of statistical control in the measurement process is clearly demonstrated.

Registry No. Water, 7732-18-5.

Literature Cited

- (1) Rhodes, R. C. In "Environmetrics 81: Selected Papers"; SIAM Institute for Mathematics and Society: Philadelphia, 1981; pp 157-162.
- (2) Mann, H. B. *Econometrica* 1945, 13, 245-249.
- (3) Kendall, M. G. "Rank Correlation Methods"; Charles Griffin: London, 1975.
- (4) Hirsch, R. M.; Slack, J. R.; Smith, R. A. *Water Resour. Res.* 1982, 18, 107-121.
- (5) Aitchison, J.; Brown, J. A. C. "The Log Normal Distribution"; University Press: Cambridge, 1957.
- (6) Eisenhart, C. *Science (Washington, D.C.)* 1968, 160, 1201-1204.
- (7) ASTM, Subcommittee 019.02. *Annu. Book ASTM Stand.* 1983, 11.01, Chapter D, 4210-4283.
- (8) Gilliom, R. J. U.S. Geological Survey, Reston, VA, unpublished data, 1983.

Received for review July 27, 1983. Accepted January 27, 1984.

Determination of Subnanogram per Liter Levels of Earthy-Musty Odorants in Water by the Salted Closed-Loop Stripping Method

Cordella J. Hwang,* Stuart W. Krasner, Michael J. McGuire, Margaret S. Moylan, and Melissa S. Dale

The Metropolitan Water District of Southern California, Water Quality Branch, La Verne, California 91750

■ Grob closed-loop stripping analysis (CLSA), coupled with gas chromatography/mass spectrometry (GC/MS), has been used to analyze for low levels of earthy-musty odorants in potable water supply systems. An increase in both sensitivity and stripping rate has been achieved by raising the ionic strength of the water samples with sodium sulfate (Na_2SO_4) before stripping. Concentrations from 0 to 300 g/L Na_2SO_4 were studied. A practical condition of 80 g/L Na_2SO_4 was combined with a shorter 1.5-h stripping time to double the sensitivity of the unsalted 2-h CLSA. A detection limit of 0.8 ng/L was achieved for each of the following earthy-musty compounds: 2-isopropyl-3-methoxypyrazine, 2-isobutyl-3-methoxypyrazine, 2-methylisoborneol, geosmin, and 2,3,6-trichloroanisole. The method was validated by comparison, precision, and accuracy studies using natural source-water samples. Recoveries of dosed geosmin and 2-methylisoborneol were $105 \pm 15\%$ and $106 \pm 15\%$, respectively. This salted procedure is a valuable modification of the CLSA when higher sensitivity or reduced stripping time is required.

Introduction

Water utilities have long been plagued by recurring earthy-musty taste and odor problems. Two such odor-

ants, geosmin and 2-methylisoborneol (MIB), have been implicated in incidents throughout the world (1-3). They are secondary metabolites of certain blue-green algae and actinomycetes (4). These odorants, which have been found periodically in source-water reservoirs of The Metropolitan Water District of Southern California (Metropolitan) during the past 4 years, were the primary target of this study. Detection of concentrations below the odor threshold can act as an early warning procedure, permitting utilities to take action to avoid or mitigate an odor problem. Three other earthy-musty compounds, 2-isopropyl-3-methoxypyrazine (IPMP), 2-isobutyl-3-methoxypyrazine (IBMP), and 2,3,6-trichloroanisole (TCA), were also studied.

These five earthy-musty odorants have odor thresholds at low nanogram per liter levels (8-12) which are well below the detection limits of classical analytical techniques. Two methods developed for concentrating trace organics in water are the purge-and-trap technique (13) and closed-loop stripping analysis (CLSA) (14, 15). The purge-and-trap technique has been used to detect relatively insoluble, volatile organic compounds at low microgram per liter levels. In 1980, the Master Analytical Scheme (16) presented a "salted-out" modification of the purge-and-trap

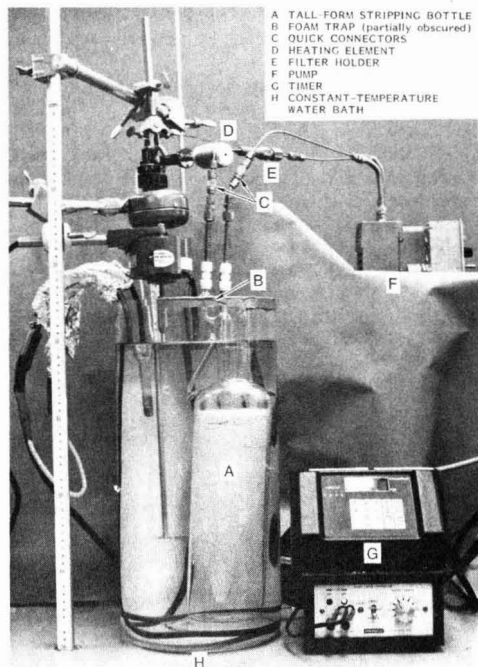


Figure 1. Closed-loop stripping apparatus.

method, using 60 g of anhydrous Na_2SO_4 /200 mL of sample, to lower detection limits to 0.1 $\mu\text{g/L}$ levels. Trussell and co-workers (17) developed a purge-and-trap gas chromatography/mass fragmentography (GC/MF) method using 10 g of Na_2SO_4 /25 mL of sample for determining the levels of geosmin and MIB. Independently, Yagi and co-workers (18) reported the use of a purge-and-trap GC/MF technique with the addition of 10 g of sodium chloride/100 mL of sample. Concentration of the odorants by a purge-and-trap method is less sensitive than CLSA, thus requiring MF (also called selected ion monitoring) to achieve low nanogram per liter detection levels. This limitation precludes full-scan mass spectral identification of the odorants and other compounds present in a sample. In 1980, Krasner and co-workers (19) adapted the Grob CLSA with GC/MS (full scan) for the determination of low nanogram per liter levels of geosmin, MIB, IPMP, IBMP, and TCA in water, sediments, and cultures.

The purpose of this study was to investigate the impact of ionic strength adjustment on the CLSA of earthy-musty odorants in water and to define and evaluate practical modifications to improve recoveries, lower detection limits, and shorten analysis time.

Experimental Section

Apparatus. Analyses were performed on a modified Grob CLSA apparatus (see Figure 1) in which semivolatile organic compounds were air stripped from a water sample and trapped on a 1.5-mg activated carbon (AC) filter (20). The system was used with the 1-L, "tall-form" stripping bottle (76 mm o.d. \times 318 mm height below ground-glass joint), which was essential to obtain the efficient stripping observed in this work. The carbon disulfide filter extracts were analyzed on a Finnigan Model 4023 GC/MS.

It is critical that the rate of gas (air) flow in the stripping system be consistent from run to run. Increased resistance due to a clogged filter or frit can alter recoveries significantly. Stripping-bottle frits were cleaned every 2 weeks

(about 40 runs) with chrome-sulfuric cleaning solutions, rinsed thoroughly with demineralized water, organic-free water, acetone, and methanol, and baked at 180 $^\circ\text{C}$ for 4 h. The pump and filter-holder assembly were cleaned whenever sample carry-over was observed. The system, with the quick-connects open and the pump on, was flushed with approximately 100 mL each of organic-free water, acetone, and methanol. After the last rinse, a heat gun was used to dry the system until there was no trace of residual methanol.

To clean the AC filters, the longer glass tube above the charcoal was filled with reagent-grade solvents, which were allowed to gravity-flow through the filter disk. The solvents were added as follows: (1) acetone, (2) organic-free water, (3) acetone, (4) carbon disulfide, (5) acetone 3 times, and (6) methylene chloride 3 times. The filter was then vacuum dried for approximately 5 min to remove residual solvent. The water rinse removed any deposited salts. The cleaning procedure, beginning with step 4, was repeated just prior to filter use. The time necessary to empty the last methylene chloride rinse (0.3-mL volume) from the top of the filter tube to the surface of the carbon was measured. This filter free-flow rate was checked before each use. Filters with flow rates lower than 0.6 mL/min were not used.

Reagents. Organic-free water was made by irradiating Millipore Super-Q water with ultraviolet light for 1 h in a Sybron/Barnstead ORGANICpure unit. Baker reagent-grade, granular, anhydrous sodium sulfate was baked at 625 $^\circ\text{C}$ for 2 h before use. Each sodium sulfate lot was checked with a blank CLSA and pH measurement (acceptable range of water and salt pH = 6–8). For sources of other reagents, see ref 20.

Procedure. Samples were collected, without headspace, in "1-L" glass bottles, with Teflon-lined caps, and stored at 5 $^\circ\text{C}$. Each sample was brought to room temperature just prior to analysis by immersing the sample bottle in a 25 $^\circ\text{C}$ water bath for approximately 15 min. No pH adjustment was made, since preliminary data showed no significant differences between standards stripped at pH 6 and pH 8, the typical range of water samples containing 80 g/L Na_2SO_4 . An 800-mL fraction of the sample was transferred to the stripping bottle and stirred on a magnetic stirrer while baked sodium sulfate was quickly added. The bottle was covered, and mixing continued until all salt dissolved (less than 1 min). After the stirring bar was removed, the remaining 200 mL of sample was added, rinsing and wetting the inside neck of the bottle. Then the fritted stopper was loosely inserted. The stopper was raised momentarily while the internal-standard spiking solution was injected below the liquid level to give a concentration of 100 ng/L each of 1-chlorooctane (Cl-C₈), 1-chlorodecane (Cl-C₁₀), and 1-chlorododecane (Cl-C₁₂). The bottle was tightly stoppered, placed in the 25 $^\circ\text{C}$ CLSA water bath, and connected to the recirculating system. The air in the headspace was flushed through an auxiliary AC filter for 10 s to remove contaminants. The sample-collection 1.5-mg AC filter was then placed in the filter holder, and the sample was stripped for the set time. The filter was removed and extracted with two 10- μL aliquots and one 5- μL aliquot of carbon disulfide. The extracts were analyzed by electron-impact GC/MS according to the conditions given in Table I. The closed-loop stripping procedure, including filter extraction and GC/MS analysis, is described in detail by Krasner et al. (20). Stripping times were varied from 1 to 4 h. Samples were checked, especially at the start of stripping, for excessive foaming. If necessary, 900-mL samples were stripped to

Table I. GC/MS Parameters

sample size	1.6 μ L
injector	200 $^{\circ}$ C; split closed 1.5 min
GC column	DB-5 fused silica capillary column; 30 m long \times 0.25 mm i.d.
column temperature program	ambient 1 min; 57–130 $^{\circ}$ C at 4 $^{\circ}$ C/min; 130–255 $^{\circ}$ C at 7 $^{\circ}$ C/min
carrier gas	helium at 29 cm/s linear velocity
interface oven temperature	200 $^{\circ}$ C
electron energy	70 eV
ionizer temperature	270 $^{\circ}$ C
source pressure	$\sim 5 \times 10^{-7}$ torr
mass scanning program	41–75 and 77–400 amu ^a in 0.6 s

^aBase peak of carbon disulfide, 76 amu, omitted.

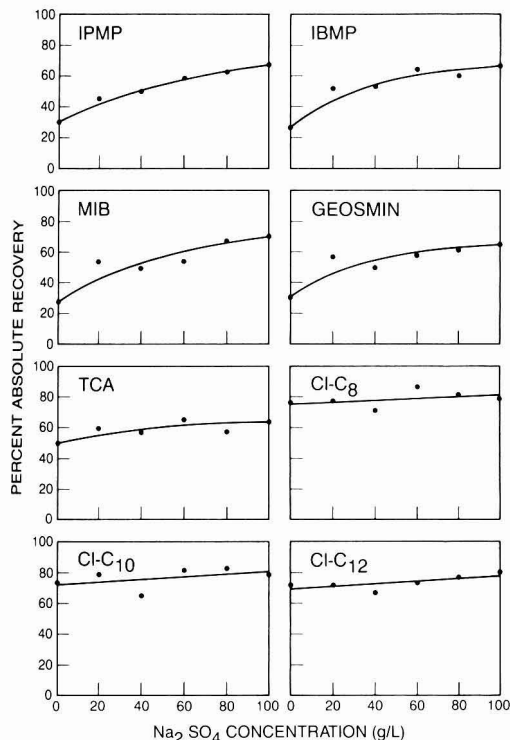


Figure 2. Recoveries of earthy-musty odorants and internal standards with respect to sodium sulfate concentration from 4-h stripping of standards.

prevent foam or liquid carry-over into the system.

Results and Discussion

Development of the Method. Because sodium sulfate has been successfully used as the ionic strength adjuster for the purge-and-trap technique (16, 17) and is readily available and purifiable in most laboratories, its effects on CLSA, in concentrations from zero to almost saturation, were investigated. Large sodium sulfate additions of 300 and 100 g/L were unmanageable and marginally acceptable, respectively, because of poor rates of dissolution and an excessive tendency to contaminate and clog the stripping system. Therefore, detailed studies of the effects of ionic strength on recoveries and stripping efficiencies were confined to the range 0–100 g/L Na₂SO₄.

Standards (20 ng/L each of the five odorants and 100 ng/L each of the three internal standards) were analyzed, with a 4-h stripping time to maximize recoveries and minimize the effect of incomplete stripping. This series

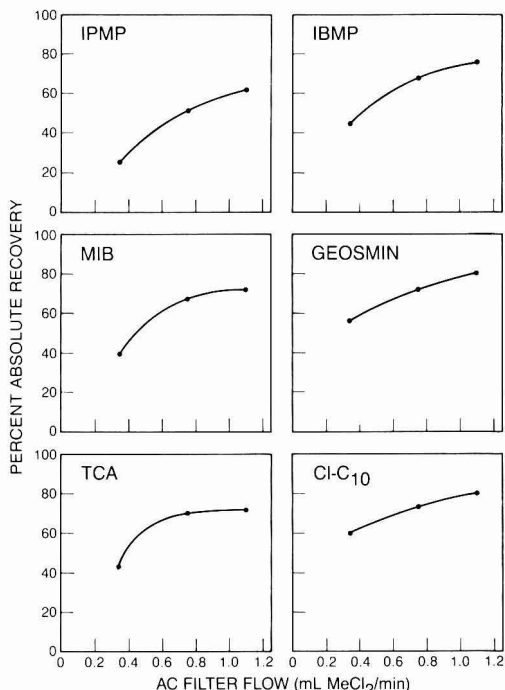


Figure 3. Effect of filter resistance, measured as flow, upon recovery of earthy-musty odorants and Cl-C₁₀ internal standard.

of results was then compared with direct GC/MS injections of standards of the spiking solutions in acetone, diluted with carbon disulfide to the same volume as the extracts. These standards gave values comparable to analogous standards of carbon disulfide only.

Percent absolute recoveries of the five odorants and internal standards are shown in Figure 2. For IPMP, IBMP, MIB, and geosmin, approximately 30% recoveries were observed for the CLSA of unsalted samples. With the addition of 20 g/L Na₂SO₄, the recoveries increased to approximately 50%. With higher salt concentrations, recoveries approached plateaus of 60–70%. TCA, the most easily stripped of the five compounds (21), had a 50% recovery in the unsalted CLSA, which increased to 65% with the use of salt. The internal standards were relatively unaffected by the salting out; absolute recoveries were around 80%.

As shown in Figure 2, all five odorous compounds plateaued at the same percentage recovery range, regardless of solubilities, suggesting that other parameters may be limiting. One factor which influenced absolute recoveries was AC filter resistance. Figure 3 shows the variation in

Table II. Relative Percent Recovery^a as a Function of Incremental Stripping Time and Sodium Sulfate Concentration

compound	incremental stripping time, h	relative recovery, %				
		20 g/L Na ₂ SO ₄	30 g/L Na ₂ SO ₄	60 g/L Na ₂ SO ₄	80 g/L Na ₂ SO ₄	100 g/L Na ₂ SO ₄
2-isopropyl-3-methoxypyrazine	1st	24	56	53	70	86
	2nd	34	24	28	20	10
	3rd	36	9	10	7	4
	4th	5	11	9	3	<1
2-isobutyl-3-methoxypyrazine	1st	29	76	85	99	100
	2nd	40	18	14	1	<1
	3rd	28	3	1	<1	<1
	4th	3	3	<1	<1	<1
2-methylisoborneol	1st	29	74	80	96	99
	2nd	39	16	18	4	1
	3rd	28	6	2	<1	<1
	4th	4	4	<1	<1	<1
2,3,6-trichloroanisole	1st	50	85	92	97	100
	2nd	39	15	8	3	<1
	3rd	11	<1	<1	<1	<1
	4th	<1	<1	<1	<1	<1
geosmin	1st	39	91	97	100	100
	2nd	40	9	3	<1	<1
	3rd	20	<1	<1	<1	<1
	4th	1	<1	<1	<1	<1

^a 100% corresponds to the total amount of material recoverable in 4 h of stripping.

percent absolute recoveries resulting from the use of three filters, each with different resistances or free-flow rates. In this experiment, CLSAs were performed with 80 g/L Na₂SO₄ and 1.5-h stripping times. IPMP, IBMP, and MIB showed the greatest reductions in recovery with decreased filter flow rates. Rates for new, commercially prepared filters ranged from 0.3 to 1.1 mL/min methylene chloride. Filter flow rates also decreased with use. It was therefore decided that in all future work, a set of filters matched to within 0.1 mL/min should be used for each group of standards and samples.

At higher ionic strengths, the stripping air bubbles decreased in size and increased in number, suggesting more rapid establishment of the gas-phase equilibrium and therefore faster stripping rates. To determine the rates of recovery, 20 ng/L mixed standards at each of the sodium sulfate concentrations were stripped for four consecutive 1-h intervals (using a different AC filter for each hour). The results given in Table II show that the stripping time required for maximum recovery decreased as sodium sulfate concentrations increased. With 80 or 100 g/L Na₂SO₄, relative recoveries for all the odorants except IPMP reached 96% or better in the first hour of stripping, with no improvement in the third and fourth hours. IPMP has never been found in Metropolitan's source waters, and a small reduction in sensitivity (and also in precision and accuracy) for this compound could be tolerated. Recovery of the internal standards, the 1-chloroalkanes, was almost complete after the first hour of stripping at all levels of sodium sulfate studied. Their stripping rates more closely paralleled those of the five odor-causing compounds at the higher ionic strengths of 80–100 g/L Na₂SO₄, making them more valid internal standards for the salted than for the unsalted CLSA. As a compromise among ease of handling, speed, and recovery, and to provide leeway for any retardation in stripping efficiency, standardized conditions were set at a 1.5-h stripping time and 80 g/L Na₂SO₄.

With these conditions, detection limits of 0.8 ng/L were reached for all five compounds, with identification based on a spectrum of at least the three major mass fragments.

Table III. Mean Percent Recoveries of Spiked Samples

compound	% recovery ± standard deviation	no. of spiked samples
2-isopropyl-3-methoxy-pyrazine	120 ± 24	44
2-isobutyl-3-methoxy-pyrazine	106 ± 18	48
2-methylisoborneol	106 ± 15	48
2,3,6-trichloroanisole	99 ± 22	45
geosmin	105 ± 15	48

By use of retention time alone for identification, the base peaks were quantitated for 0.5 ng/L IBMP, MIB, and geosmin.

Natural Water Supplies. This salted CLSA method was applied to over 500 source-water samples from the California and Colorado River aqueducts and their five terminal reservoirs. These were untreated surface waters, with the two sources containing approximately 300 and 700 mg/L total dissolved solids, respectively. Forty-eight samples were spiked with 4–20 ng/L each of two or more of the earthy-musty odorants. Salted CLSA using both internal and external calibration gave average, standard-adjusted recoveries of 99–120%, as shown in Table III. These results were within acceptable experimental limits.

Replicate samples were collected in the field and carried independently through salted CLSA. Of the five compounds, only MIB and geosmin occurred naturally in Metropolitan's source waters. Analysis of 14 pairs of samples containing 2–28 ng/L geosmin showed a mean difference of 1.0 ± 1.3 ng/L. The mean difference for 23 pairs with MIB ranging from 3 to 36 ng/L was 0.8 ± 1.1 ng/L.

Parallel analyses of typical source-water samples by this salted method and by unsalted CLSA were performed. Comparison of 11 pairs of geosmin and MIB results at 2–28 ng/L levels showed the mean difference to be 1.3 ± 1.3 ng/L (see Table IV). This was approximately the same precision obtainable with the individual procedures. An

Table IV. Comparison of Salted and Unsalted CLSA

sample location	MIB, ng/L		geosmin, ng/L	
	salted	unsalted	salted	unsalted
Castaic Lake ^a	5	5	6	6
	9	10	28	24
	1	<2	1	<2
Lake Mathews ^b	4	3	2	<2
	6	9	1	<2
	6	6	2	<2
Devil Canyon	<1	<2	7	8
	<1	<2	6	5
Lake Perris ^a	7	8	<1	<2
	5	7	<1	<2

^aWater from the California Aqueduct. ^bWater from the Colorado River Aqueduct.

advantage of the salted technique was shown by the detection of geosmin and MIB in four samples at the 1 and 2 ng/L levels which were not found by the unsalted CLSA.

Reduction of the stripping time from 2 to 1.5 h made it possible to obtain results more rapidly and increased the number of samples that could be analyzed per day by 30%. This benefit was especially important during the peak odor-production months, when Metropolitan's analytical systems were used to capacity.

Summary and Conclusions

The addition of sodium sulfate in the CLSA improved the rates and amounts of recovery for five earthy-musty compounds: IPMP, IBMP, MIB, TCA, and geosmin. The increases in ionic strength apparently shifted the solubility of the odorants and resulted in higher recoveries and hence greater sensitivity. AC filter and frit resistances were found to affect stripping efficiency and reproducibility. Filters with free flows matched to ±0.1 mL/min should be used. The use of 80 g/L Na₂SO₄ made it possible to shorten the stripping time to 1.5 h while still maintaining high recoveries. Detection limits for the salted (compared to unsalted) CLSA method were lowered by a factor of 2 or more to 0.8 ng/L for each compound. Geosmin and MIB were found in samples at levels at or below the unsalted detection limits. This salted method was applied to untreated surface waters over a 1-year period, with good spike recoveries averaging 107% and replicates with average differences of about 1 ng/L. Precision and accuracy were comparable to those of the unsalted method. This sodium sulfate salted CLSA method is a viable alternative

to be used when higher sensitivity or reduced stripping time is required.

Registry No. IPMP, 25773-40-4; IBMP, 24683-00-9; MIB, 2371-42-8; TCA, 50375-10-5; Na₂SO₄, 7757-82-6; water, 7732-18-5; geosmin, 19700-21-1.

Literature Cited

- (1) Rosen, A. A.; Mashni, C. I.; Safferman, R. S. *Water Treat. Exam.* **1970**, *19*, 106-119.
- (2) Piet, G. J.; Zoeteman, B. C. J.; Kraayeveld, A. J. A. *Water Treat. Exam.* **1972**, *21*, 281-286.
- (3) Tsuchiya, Y.; Shudo, K.; Okamoto, T. *Eisei Kagaku* **1979**, *25*, 216-220.
- (4) Safferman, R. S.; Rosen, A. A.; Mashni, C. I.; Morris, M. E. *Environ. Sci. Technol.* **1967**, *1*, 429-430.
- (5) Medsker, L. L.; Jenkins, D.; Thomas, J. F. *Environ. Sci. Technol.* **1968**, *2*, 461-464.
- (6) Medsker, L. L.; Jenkins, D.; Thomas, J. F.; Koch, C. *Environ. Sci. Technol.* **1969**, *3*, 476-477.
- (7) Tabachek, J. L.; Yurkowski, M. J. *Fish. Res. Board Can.* **1976**, *33*, 25-35.
- (8) Buttery, R. G.; Seifert, R. M.; Guadagni, D. G.; Ling, L. C. *J. Agric. Food Chem.* **1969**, *17*, 1322.
- (9) Seifert, R. M.; Buttery, R. G.; Guadagni, D. G.; Black, D. R.; Harris, J. G. *J. Agric. Food Chem.* **1970**, *18*, 246.
- (10) Tuorila, H.; Pyysalo, T.; Hirvi, T.; Vehviläinen, A. K. *Vatten* **1980**, *3*, 191-199.
- (11) Guadagni, D. G.; Buttery, R. G. *J. Food Sci.* **1978**, *43*, 1346-1347.
- (12) Persson, P.-E. *Water Sci. Technol.* **1983**, *15* (6/7), 1-11.
- (13) Bellar, T. A.; Lichtenberg, J. J. *J. Am. Water Works Assoc.* **1974**, *66*, 739-744.
- (14) Grob, K. *J. Chromatogr.* **1973**, *84*, 255-273.
- (15) Grob, K.; Zürcher, F. *J. Chromatogr.* **1976**, *117*, 285-294.
- (16) Gebhart, J. E.; Ryan, J. F.; Cox, R. D.; Pellizzari, E. D.; Michael, L. C.; Sheldon, L. S. In "Advances in the Identification and Analysis of Organic Pollutants in Water"; Keith, L. H., Ed.; Ann Arbor Science: Ann Arbor, MI, 1981; Vol. 1, pp 31-48.
- (17) Trussell, A. R.; Moncur, J. G.; Lieu, F. Y.; Leong, L. Y. C., presented at the 1981 AWWA Water Quality Technology Conference, Seattle, WA, Dec 7, 1981.
- (18) Yagi, M.; Kajino, M.; Matsuo, U.; Ashitani, K.; Kita, T.; Nakamura, T. *Water Sci. Technol.* **1983**, *15* (6/7), 311-321.
- (19) Krasner, S. W.; Hwang, C. J.; McGuire, M. J. In "Advances in the Identification and Analysis of Organic Pollutants in Water"; Keith, L. H., Ed.; Ann Arbor Science: Ann Arbor, MI, 1981; Vol. 2, pp 689-710.
- (20) Krasner, S. W.; Hwang, C. J.; McGuire, M. J. *Water Sci. Technol.* **1983**, *15* (6/7), 127-138.
- (21) Lalezary, S.; Pirbazari, M.; McGuire, M. J.; Krasner, S. W. *J.-Am. Water Works Assoc.* **1984**, *76*, 83-87.

Received for review August 8, 1983. Accepted January 12, 1984.

Organic Photochemistry. 19. Quantum Yields for *O,O*-Diethyl *O*-(3,5,6-Trichloro-2-pyridinyl) Phosphorothioate (Chlorpyrifos) and 3,5,6-Trichloro-2-pyridinol in Dilute Aqueous Solutions and Their Environmental Phototransformation Rates[†]

Wendell L. Dilling,* Lori C. Lickly, Tim D. Lickly, and Patrick G. Murphy

Environmental Sciences Research Laboratory, The Dow Chemical Company, Midland, Michigan 48640

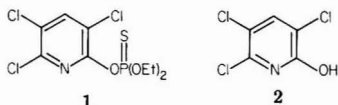
Richard L. McKellar

Agricultural Products Research and Development, The Dow Chemical Company, Midland, Michigan 48640

■ The quantum yields, measured at 313 nm for chlorpyrifos (1) and 3,5,6-trichloro-2-pyridinol (2) at $\sim 1 \text{ mg L}^{-1}$ in aqueous solutions at pH 7.0 and 25 °C, were 0.0048 ± 0.0004 and 0.16 ± 0.01 , respectively. A significant correction for a small amount of light at 302 nm was required in the calculation of the quantum yield for 1. These quantum yields and the measured absorption spectra were used to estimate the environmental photochemical half-lives of 1 and 2 in water under conditions of variable light intensity using the computer program (SOLAR) developed by Zepp and Cline. Typical half-lives for phototransformation of 1 and 2, respectively, at 40° north latitude were as follows: midsummer at a depth of 0.001 cm, 31 days (all times in terms of diurnal days), 4.4 min; midwinter at a depth of 0.001 cm, 345 days, 15 min; midsummer at a depth of 1 m in pure water, 43 days, 5.4 min; midsummer at a depth of 1 m in river water, 2.7 years, 2.0 h.

Introduction

Chlorpyrifos [*O,O*-diethyl *O*-(3,5,6-trichloro-2-pyridinyl) phosphorothioate] (1), the active ingredient in several in-



secticides, has been introduced into the environment during its normal use. It hydrolyzed to 3,5,6-trichloro-2-pyridinol (2) (2, 3) at rates that were dependent on temperature, pH, and the presence of Cu^{2+} or other materials (2-7). At $\sim 25 \text{ °C}$ the half-life of thiophosphate 1 varied from ~ 1 to 120 days in water that ranged from different natural waters to that which had been purified (2, 3, 5, 7-9). The half-life was shorter at high Cu^{2+} concentrations (4, 6).

Photolysis of chlorpyrifos (1) in water also produced the pyridinol 2 (10, 11), which photolyzed faster than 1 to give Cl^- , CO_2 , NH_3 , and other products, some of which were suggested to be polyhydroxychloropyridines and their oxidation products (10). Previous workers reported that ester 1 photolyzed with half-lives of <1 -108 days under typical sunlight conditions; the rate depended on pH and probably other parameters (8, 10, 11). The photolysis rate of 1 was not accelerated appreciably by the green alga *Chlorogonium* sp. (12). The half-life for photolysis of pyridinol 2 at pH 8 was ~ 1.2 h when the irradiation was performed with a 275-W sunlamp at a distance of a few inches (10).

The vapor pressures (13, 14) and solubilities in water (3, 15) of chlorpyrifos (1) and pyridinol 2 allow calculation

(16) of air-water partition coefficients of 2.5×10^{-4} and 1.2×10^{-6} , respectively. These data indicate that both compounds will reside in the hydrosphere to a much greater extent than in the atmosphere.

The purpose of the present work was to more accurately define the photolysis rates of compounds 1 and 2 under a variety of illumination conditions in the aquatic environment by measuring their quantum yields and UV absorption spectra and applying Zepp and Cline's SOLAR computer program (17).

Experimental Section

Equipment. UV spectra were recorded on a calibrated Cary 118C spectrophotometer using 10-cm quartz cells.

Photolyses were performed on solutions contained in screw-capped 1.61 cm (o.d.) \times 12.5 cm Kimax glass culture tubes placed in an unslotted turntable apparatus. Each tube was rotated about its own axis in addition to being rotated about the lamp. The light from a 450-W Hanovia medium-pressure mercury arc lamp, type 679A, was filtered through Corning 7-54 glass filters and 0.41 cm of 0.8 g of $\text{K}_2\text{CrO}_4 \text{ L}^{-1}$ of 0.2% aqueous Na_2CO_3 , which was circulated through the quartz immersion well around the lamp and through a heat exchanger (18). The tubes and lamp were suspended in a refrigerated constant temperature water bath at $25 \pm 1 \text{ °C}$.

The effective path length (19) of the sample tubes (1.45 cm) was determined by multiplying the measured inside diameter (1.41 cm) by the ratio of effective pathlength to the inside diameter for cylindrical tubes (1.03) determined by Mabey (20) under conditions similar to ours.

The emission spectrum of the lamp with its filter system, except for the Kimax glass (sample tubes), was measured with an International Light IL783 spectroradiometer system.

Materials. Technical grade chlorpyrifos (1) was recrystallized from CH_2Cl_2 -hexane. The purity was 99.8% as determined by differential scanning calorimetry (21). The absence of significant quantities of impurities ($>0.1\%$) was confirmed by gas chromatography with flame ionization detection and by liquid chromatography.

Technical-grade pyridinol 2 was recrystallized from 2-propanol and from toluene. The purity was 99.8% as determined by differential scanning calorimetry and an extraction-solubility (in hexane) method (22).

Photolyses. Solutions of ester 1 or pyridinol 2 were prepared by diluting 1-mL acetonitrile solutions containing $\sim 1 \text{ mg}$ of 1 or 2 to 1 L with pH 7.0 buffer solution. The buffer solution consisted of 5 mM KH_2PO_4 - K_2HPO_4 (23) in water purified via a Milli-Q system and filtered through a 0.45- μm filter. Air was bubbled through the solutions for 5 min prior to irradiation. Ten-milliliter solutions in the culture tubes were irradiated for 70-72.5 h (1) or 2.5

[†]For parts 17 and 18 of the series, see ref 1.

Table I. Photolyses of Chlorpyrifos (1) and Pyridinol 2

compd	C_0 , mg L ⁻¹	k_i , h ^{-1a}	k_d , h ^{-1a}	k_p , h ^{-1a}	$\sum I_{0\lambda}$, mEinstein ^b L ⁻¹ h ^{-1a}	Φ , mol einstein ^{-1c}
1	0.82 ^d	$(2.30 \pm 0.15) \times 10^{-2d}$	$(1.08 \pm 0.71) \times 10^{-3d}$	$(2.19 \pm 0.17) \times 10^{-2}$	12.93 ± 0.22	$(4.90 \pm 0.44) \times 10^{-3e}$
1	0.62	$(2.29 \pm 0.21) \times 10^{-2}$	$(2.0 \pm 1.7) \times 10^{-3}$	$(2.09 \pm 0.27) \times 10^{-2}$	12.75 ± 0.20	$(4.75 \pm 0.65) \times 10^{-3e}$
2	0.99 ^f	$44.18 \pm 0.99f$	0	44.18 ± 0.99	12.37 ± 0.92	0.160 ± 0.014

^aStandard deviation of the mean given. ^bmEinstein = milliEinstein = 10⁻³ einstein. ^cEstimate of error derived from standard deviations and other errors estimated for parameters involved in eq 2 or 3 (see text). ^dShown in Figure 1. ^eMean value = $(4.83 \pm 0.39) \times 10^{-3}$. ^fShown in Figure 2.

min (2). The solutions were analyzed for 1 or 2 prior to and periodically during the irradiations. Similarly prepared reaction solutions were maintained in the dark as controls.

Analyses. Analyses for chlorpyrifos (1) were performed by extracting a 2-mL aliquot of the photolysis solution with hexane (2 × 2 mL), diluting the combined extracts to 10 mL, and injecting a 10-μL aliquot into a gas chromatograph equipped with a 1.8 m × 3 mm column packed with 3% OV-17 and 8% QF-1 on 80/100 mesh Gas Chrom Q at 205 °C (200 cm³ of N₂ min⁻¹, *t_R* = 1.4 min, phosphorus flame photometric detection). Recovery of 1 from standard solutions was 98 ± 2% (mean and 95% confidence limits of the mean).

Analyses for pyridinol 2 were performed by acidifying a 2-mL aliquot of the photolysis solution with 1-mL of concentrated HCl and extracting it with 10 mL of benzene. One milliliter of this extract was treated with 10 μL of *N,O*-bis(trimethylsilyl)acetamide reagent, diluted to 10 mL with benzene, and injected (4 μL) into a gas chromatograph equipped with a 6 ft × 3 mm column packed with 3% OV-1 on 100/120 mesh Gas Chrom Q at 139 °C [60 cm³ of Ar-CH₄ (95:5) min⁻¹, *t_R* = 3.5 min, ⁶³Ni electron capture detector]. Recovery of 2 from standard solutions was 100 ± 8%.

Concentrations of 1 and 2 were determined by comparing the peak heights with standard curves prepared by analyzing standard solutions in the manner described above.

Actinometry. Potassium ferrioxalate (0.02 M) (24–26) solutions (10 mL) were irradiated at the same time as the solutions of 1 or 2 for 4–7.5 min in the same type of tubes used for the solutions of 1 and 2. Several such actinometer irradiations were performed during the course of the photolysis of 1. The standard colorimetric method (26) of Fe²⁺ analysis was used. The refractive indexes at 589 nm (sodium D line) and 25 °C of the actinometer solution and the solutions of 1 or 2 were 1.335 and 1.333, respectively. The refractive indexes at 313 nm, estimated from dispersion measurements with a Bausch & Lomb Abbe-3L refractometer, were 1.359 and 1.354, respectively. Thus, no significant errors caused by the cylindrical sample tubes are expected.

Results

The first-order kinetic curves for the photolysis of chlorpyrifos (1) and pyridinol 2 are shown in Figures 1 and 2, respectively. The rate constants for these reactions in the light, *k_i*, and dark, *k_d*, as well as those for a second run with ester 1 are given in Table I. Pyridinol 2 in the buffer solution was stable in the dark during the time required for the photolysis. The photolysis rate constant, *k_p*, for thiophosphate 1 was taken as the difference between *k_i* and *k_d*. The precision of *k_d* for 1, which corresponds to half-lives for hydrolysis of 27 ± 18 and 15 ± 13 days for the two runs, is low because of the low conversion but agrees ap-

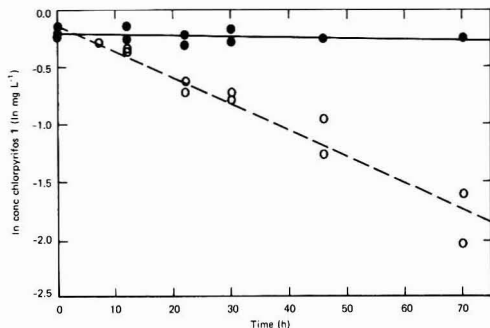


Figure 1. Photolysis (O) of 0.82 mg L⁻¹ (2.3 μM) chlorpyrifos 1 in pH 7.0 aqueous phosphate buffer solution with 0.1% MeCN. Dark control (●).

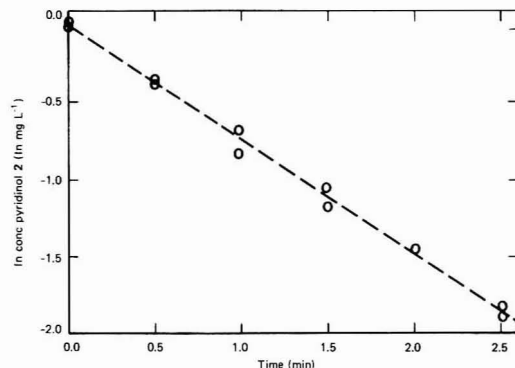


Figure 2. Photolysis of 0.99 mg L⁻¹ (5.0 μM) pyridinol 2 in pH 7.0 aqueous phosphate buffer solution with 0.1% MeCN.

proximately with values reported previously (2). The low precision for *k_d* is of little consequence here because the value of *k_d* is relatively low compared with that of *k_i*.

Equation 1 given by Zepp (19) for the quantum yield,

$$\Phi = \frac{-\text{slope}}{2.303I_{0\lambda}(A/V)\epsilon_{\lambda}l} \quad (1)$$

when monochromatic radiation is used, was modified to give eq 2 because our lamp with its filter system emitted

$$\Phi = \frac{k_p}{2.303I_{0\lambda}(\sum I_{0\lambda}'\epsilon_{\lambda})} \quad (2)$$

a small amount of light centered at 302 nm in addition to the strong band at 313 nm (Figure 3). In eq 2, *k_p* is the -slope in eq 1, *l* is the effective path length of light, *I_{0λ}'* is the light intensity at wavelength λ and is equivalent to *I_{0λ}*(*A/V*) in eq 1 [*A* = exposed area, and *V* = cell volume (19)], and *ε_λ* is the molar absorptivity of the absorbing

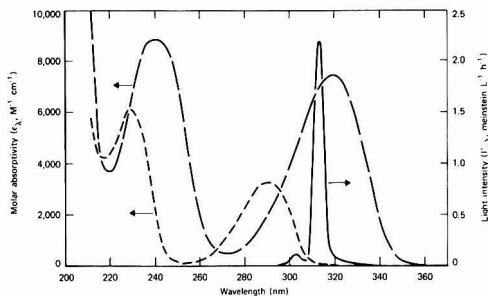


Figure 3. UV absorption spectra of 2.9 μM chlorpyrifos 1 (---) and 7.6 μM pyridinol 2 (—) in pH 7.0 aqueous phosphate buffer solutions with 0.01% and 0.02% MeCN, respectively (left scale). Light intensity ($I_{0\lambda}'$) from lamp with its filter system used for quantum yield measurements (—) (right scale).

compound at λ (Figure 3). The values of $I_{0\lambda}'\epsilon_{\lambda}$ for 1-nm bandwidths were summed over the wavelength range where the emission spectrum from the lamp with its filter system overlapped the absorption spectrum of the compound.

The ferrioxalate actinometer measures $\sum_{\lambda} I_{0\lambda}'$ (Figure 3) and is usable in these experiments because its quantum yield, 1.24 (25), is essentially constant over the wavelength range used (295–337 nm). These calculations assume that the Φ values for 1 and 2, given in Table I, are constant over this same wavelength range. This assumption should be valid because these solution-phase photolyses were conducted within single absorption bands (Figure 3).

The error estimates for the Φ values given in Table I were derived either from the standard deviations of mean parameters in eq 2, where standard errors could be calculated, or from maximum errors estimated for the other parameters in eq 2 on the basis of their probable uncertainties. Equation 2 was expanded to eq 3 to show

$$\Phi = \frac{k_p C l_c}{2.303 I_{0\lambda}' (\sum_{\lambda} I_{0\lambda}') \left[\sum_{\lambda} \left[\left(\frac{t_{\lambda} i_{\lambda} \lambda A_{\lambda}}{f_{\lambda}} \right) / \left(\sum_{\lambda} \frac{t_{\lambda} i_{\lambda} \lambda}{f_{\lambda}} \right) \right] \right]} \quad (3)$$

the individually measured quantities or other values that make up the terms in eq 2. In eq 3, C is the concentration (g L^{-1}) of the solution whose UV absorption spectrum is measured to obtain ϵ_{λ} , l_c is the path length (cm) of the spectrophotometer cell, M_r is the molecular weight of the solute, t_{λ} is the fractional transmittance of the Kimax glass tube wall at λ , i_{λ} is the spectroradiometer current (A) at λ , A_{λ} is the absorbance at λ of the solution whose UV absorption spectrum is measured, and f_{λ} is the calibration factor ($\text{A nm cm}^2 \text{W}^{-1}$) at λ for the spectroradiometer. The standard deviations for the mean values of k_p and $\sum_{\lambda} I_{0\lambda}'$ are given in Table I. The estimated maximum errors for the other terms in eq 3 were as follows: C (1%), l_c (0.01%), l (3.2%), M (0.0014% for 1; 0.0025% for 2), λ (1.5 nm at all λ), and A_{λ} (3%). Constant percentage changes in t_{λ} , i_{λ} , and f_{λ} at different λ have no effect on the value of the double summation term that contains them. Maximum and minimum values of this summation term were calculated (3% variation). All of these estimated errors, treated as standard deviations, were combined by standard statistical methods (27–29) to give the estimate of error shown in Table I. This procedure slightly overestimates the standard deviation for Φ if one assumes that the estimated maximum errors are all slightly larger than the standard deviations for these terms.

Table II. Calculated Environmental Half-Lives for Photolyses of Chlorpyrifos (1) and Pyridinol 2 at pH 7.0 and 40° North Latitude

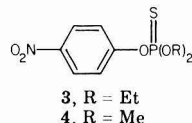
season	depth, m	type of water	half-life	
			1, day	2, min
summer	10^{-5}	"pure"	31	4.4
winter	10^{-5}	"pure"	345	15
summer	1	"pure"	43	5.4
summer	1	river ^a	980	120

^a Average light attenuation coefficients for 10 river water samples from southeastern U.S. used (17).

The computer program SOLAR (17, 30) was used to calculate environmental half-lives for photolyses of chlorpyrifos (1) and pyridinol 2 under various conditions. Representative values are shown in Table II. Application of this type of calculation to a specific water body would require a knowledge of the light attenuation coefficients for that water body. For a detailed discussion of the calculation of aquatic environmental photolysis rates, see ref 31.

Discussion

The pyridinate anion is the major species absorbing light in solutions of the pyridinol 2 at pH 7.0. At this pH, 97.3% of 2 is present as the anion, calculated on the basis of its pK_a of 5.45 (32). The ionic or ionizable character of 2 may be partially responsible for the fact that Φ for 2 is much higher than Φ for chlorpyrifos (1). Conceptually the anion of 2 on excitation could easily eliminate chloride ion (10). The initial photochemical reaction of un-ionized 1 involves cleavage of the thiophosphate ester moiety (10, 11). The quantum yields of two other thiophosphate esters, parathion (3) and methyl parathion (4), 2×10^{-4} and 1.7×10^{-4} , respectively, at 313 nm in aqueous solutions, were also low (33).



Using eq 2, instead of eq 1 and assuming that all the light is emitted at 313 nm, is especially important in calculating Φ for chlorpyrifos (1). If one assumes that the entire $I_{0\lambda}'$ were at 313 nm, the calculated Φ would be 0.016, a 230% error. The reason for this large error is the very low ϵ_{λ} at 313 nm, $32 \text{ M}^{-1} \text{ cm}^{-1}$, and the much higher ϵ_{λ} at 302 nm, $1540 \text{ M}^{-1} \text{ cm}^{-1}$. The value of $I_{0\lambda}'\epsilon_{\lambda}$ is larger at 302 nm than at 313 nm, implying that more photolysis occurred at 302 nm than at 313 nm. Calculating Φ for pyridinol 2 using eq 1 and assuming all the light absorbed is at 313 nm is much less critical (2% error) than for ester 1 because ϵ_{λ} is larger at 313 nm, $6840 \text{ M}^{-1} \text{ cm}^{-1}$, than at 302 nm, $4330 \text{ M}^{-1} \text{ cm}^{-1}$.

The calculated photolysis half-life of chlorpyrifos (1) of 31 days (Table II) agrees reasonably well with the value of 22 days determined experimentally by Meikle and co-workers for photolysis at pH 6.9 under conditions simulating midday sunlight at Walnut Creek, CA, in August (11).

The combination of a significantly higher quantum yield and much stronger absorption of trophospheric solar radiation for pyridinol 2 than for chlorpyrifos (1) implies that phototransformation is a much more significant environmental process for 2 than for 1. The results in Table II

suggest that phototransformation of pyridinol 2 is an important environmental process when the compound is in water that sunlight can penetrate. In contrast, phototransformation of chlorpyrifos (1) is probably significant only under conditions of high sunlight intensity, i.e., in the summer in clear shallow water bodies. Under these favorable conditions, phototransformation may compete with hydrolysis in the absence of significant concentrations of species that catalyze hydrolysis. Under conditions unfavorable for photolysis, other environmental transformation processes, including hydrolysis, occur. We have not explored the possibility that the photolyses may be catalyzed or sensitized by other materials.

Acknowledgments

We thank R. Hummel, D. Kaufman, D. A. Laskowski, W. R. Mabey, R. Matalon, W. B. Neely, D. W. Osborne, H. O. Senkbeil, and R. G. Zepp for helpful discussions and experimental assistance.

Registry No. 1, 2921-88-2; 2, 6515-38-4.

Literature Cited

- (1) (a) Dilling, W. L.; Miracle, G. E.; Boggs, G. U. *Prepr. Pap. Natl. Meet., Div. Environ. Chem., Am. Chem. Soc.* **1983**, *23*, No. 2, 343-346; (b) Dilling, W. L. *Chem. Rev.* **1983**, *83*, 1-47.
- (2) Meikle, R. W.; Youngson, C. R. *Arch. Environ. Contam. Toxicol.* **1978**, *7*, 13-22.
- (3) Macalady, D. L.; Wolfe, N. L. *J. Agric. Food Chem.* **1983**, *31*, 1139-1147.
- (4) Mortland, M. M.; Raman, K. V. *J. Agric. Food Chem.* **1967**, *15*, 163-167.
- (5) Freed, V. H.; Chiou, C. T.; Schmedding, D. W. *J. Agric. Food Chem.* **1979**, *27*, 706-708.
- (6) Blanchet, P.-F.; St-George, A. *Pestic. Sci.* **1982**, *13*, 85-91.
- (7) Macalady, D. L.; Wolfe, N. L. *Prepr. Pap. Natl. Meet., Div. Environ. Chem., Am. Chem. Soc.* **1982**, *22*, No. 1, 229-301.
- (8) Schaefer, C. H.; Dupras, E., Jr. *Proc. Calif. Mosq. Control Assoc.* **1969**, *37*, 67-75.
- (9) Schaefer, C. H.; Dupras, E. F., Jr. *J. Econ. Entomol.* **1970**, *63*, 701-705.
- (10) Smith, G. N. *J. Econ. Entomol.* **1968**, *61*, 793-799.
- (11) Meikle, R. W.; Kurihara, N. H.; DeVries, D. H. *Arch. Environ. Contam. Toxicol.* **1983**, *12*, 189-193.
- (12) Zepp, R. G.; Schlotzhauer, P. F. *Environ. Sci. Technol.* **1983**, *17*, 462-468.
- (13) "DURSBAN Insecticides, Technical Data Sheet"; Dow Chemical U.S.A.: Midland, MI.
- (14) Laskowski, D. A.; The Dow Chemical Company, Midland, MI, personal communication, 1982.
- (15) Hummel, R.; The Dow Chemical Company, Midland, MI, personal communication, 1982.
- (16) Dilling, W. L. In "Environmental Risk Analysis for Chemicals"; Conway, R. A., Ed.; Van Nostrand Reinhold: New York, 1982, pp 154-197.
- (17) Zepp R. G.; Cline, D. M. *Environ. Sci. Technol.* **1977**, *11*, 359-366.
- (18) Moses, F. G.; Liu, R. S. H.; Monroe, B. M. *Mol. Photochem.* **1969**, *1*, 245-249.
- (19) Zepp, R. G. *Environ. Sci. Technol.* **1978**, *12*, 327-329.
- (20) Mabey, W. R.; SRI International, Menlo Park, CA, personal communication, 1981.
- (21) Plato, C.; Glasgow, A. R., Jr. *Anal. Chem.* **1969**, *41*, 330-336.
- (22) Stenger, V. A.; Crummett, W. B.; Kramer, W. R. *Anal. Chem.* **1953**, *25*, 974-977.
- (23) Christian, G. D.; Purdy, W. C. *J. Electroanal. Chem.* **1962**, *3*, 363-367.
- (24) Parker, C. A. *Proc. R. Soc. London, Ser. A* **1953**, *A220*, 104-116.
- (25) Hatchard, C. G.; Parker, C. A. *Proc. R. Soc. London, Ser. A* **1956**, *A235*, 518-536.
- (26) Murov, S. L. "Handbook of Photochemistry"; Marcel Dekker: New York, 1973; pp 119-123.
- (27) Wang, C. H.; Willis, D. L.; Loveland, W. D. "Radiotracer Methodology in the Biological, Environmental, and Physical Sciences"; Prentice-Hall: Englewood Cliffs, NJ, 1975; p 301.
- (28) National Council on Radiation Protection and Measurements, Washington, DC, 1978, NCRP Report No. 58, p 291.
- (29) Wold, S. *Anal. Chem.* **1974**, *46*, 1614.
- (30) Zepp, R. G.; U.S. Environmental Protection Agency, Athens, GA, personal communication, 1981.
- (31) Wolfe, N. L.; Zepp, R. G.; Schlotzhauer, P.; Sink, M. *Chemosphere* **1982**, *11*, 91-101.
- (32) Norton, F. H.; The Dow Chemical Company, Walnut Creek, CA, personal communication, 1981.
- (33) Harris, J. C.; In "Handbook of Chemical Property Estimation Methods"; Lyman, W. J.; Reehl, W. F.; Rosenblatt, D. H., Eds.; McGraw-Hill: New York, 1982; pp 8-1-8-43.

Received for review August 1, 1983. Accepted January 19, 1984. Presented at the 14th Central Regional Meeting, American Chemical Society, Midland, MI, June 16-18, 1982 (Abstract 111), and the XIth International Conference on Photochemistry, College Park, MD, August 21-26, 1983 (Abstract R13).

Comparison of Micron and Submicron Fly Ash Particles Using Scanning Electron Microscopy and X-ray Elemental Analysis

N. Kaufherr[†] and David Lichtman*

Department of Physics and Laboratory for Surface Studies, University of Wisconsin—Milwaukee, Milwaukee, Wisconsin 53201

■ Fly ash particles from the Bull Run Power Station of TVA were studied in the submicron range (average size 0.6 μm) and in the micron range (2–7 μm) by means of a scanning electron microscope (SEM) equipped with an energy-dispersive spectrometer for X-ray elemental analysis (EDX). It was found, for the fly ash studied, that the submicron particles were very similar to the particles in the micron range. Both types of particles were spherical and contained Si, Al, K, Fe, Ti, and S as the main components. The submicron particles were distinguished only in some enrichment in sulfur content.

Introduction

The particulate residue from coal-burning power stations, its nature, and its impact on environment and health have been of particular interest in recent years due to the increased significance of coal as a power source and short-term solution for the energy crisis. Presently, the general and broader earlier studies are giving place to a more subtle approach. At this stage, the aim is to obtain a better understanding of the particles in view of burning conditions, type of coal, and other characteristics of the power station on one hand and the relations between inherent properties of the particles and their chemistry on the other. Methods of particle collection and the means by which they are studied are becoming more and more sophisticated.

In this study we concentrate on the question as to the similarities or differences between micron and submicron particles in view of the belief that submicron particles are major contributors to the hazards of fly ash (1). The following results are a summary of the SEM-EDX studies on micron and submicron particles. It should be remembered that EDX of particles in this size range provides essentially semiquantitative bulk composition analysis. An attempt was made to understand the uniqueness of submicron particles compared to larger particles, as well as their common features. Data were critically evaluated in view of the capabilities of EDX analysis.

Experimental Section

The fly ash particles studied were collected at the Bull Run Steam Plant of TVA, Oak Ridge, TN. The coal used in the plant contained 7.1% moisture, 15.0% ash, and 0.9% sulfur. Particles were collected on stainless steel substrates in the stack at 138 °C by means of impact collectors, according to their aerodynamic size.

Particles studied were from stages 2, 5, and 8 with a calculated aerodynamic diameter of 4.8, 1.4, and 0.2 μm , respectively (assumed density 2.5; see also section 1 under Results). Particles were assigned as FA-C-8, FA-C-5, or FA-C-2 if originating from stage 8, 5, or 2, respectively, and FA-C-2,5 if originating from both stages 2 and 5. The

diameter of each particle analyzed was measured prior to analysis. The total number of particles that was studied in detail was 66. In an attempt to randomize data, a number of samples were analyzed from each stage.

The particles were studied by means of SEM-EDX, carried out in a JEOL Model JSM U3 scanning electron microscope (SEM), and energy dispersive X-ray analysis data were obtained from single particles by means of a Kevex 7000 unit. For analysis, particles were transferred from the stainless steel support by means of a graphite tip to a highly polished carbon stub. This method of transfer was found to be especially convenient for submicron particles. The soft graphite also assured no transfer of support material.

Particles were slightly carbon coated prior to analysis. X-ray analysis was performed in spot mode with a current of 150–300 pA at 25 kV. Data were accumulated for 200–300 s. X-ray analysis data were processed by a standardless semiquantitative routine supplied by Kevex, and results were normalized to 100% on the basis of oxide composition.

Carbon content was analyzed in a JEOL 35C SEM with a 35FCS four crystal wavelength dispersive spectrometer. Analysis was done at a 15-kV accelerating voltage and a current of 0.14 μA . Sodium carbonate was used for a standard, and zero corrections were made for stainless steel substrate carbon content.

Results

(1) **Particle Size and Morphology.** In addition to the size measurement of the particles analyzed and the calculated aerodynamic size, a particle size distribution was carried out for stages 2 and 4 to verify the degree of accuracy of the calculated diameter and efficiency of collections. It was found that the major part of the particles were 5 and 2 μm , respectively, in agreement with calculations, although some larger and smaller particles were observed as well. The submicron particles which were examined were 0.6 μm , on the average (Table I). Examination of the morphology of particles of stages 2, 4, and 8 showed the major part of be spherical (see Figures 1 and 2) with only a small fraction of the particles of different shape. For the submicron particles in stage 8, it was found that, from time to time, two particles were connected by what was believed to be a partial fusion. Irregular shapes were observed for particles in the micron range. Some of them were reminiscent of a crystal; others were perforated. The particles of irregular shape were analyzed, and their composition was given separately as certain shapes seemed to be connected with a high SiO_2 content (Table II).

(2) **Chemical Analysis.** (a) **Main Group of Particles.** Si, Al, K, Fe, Ti, Mg, and S were the most common elements analyzed both in the micron and submicron particles (Tables I and III) (in the latter are also given, for comparison, the composition of fly ash from the literature as cited in ref 2, 3, and 4). Ca, P, Na, Cl, and Ni were detected in a small number of particles while Cr, Mn, V, and Cu could be identified from time to time, but the

[†] Permanent address: I.M.I. Institute for Research and Development, Haifa 31002, Israel.

Table I. Average Composition of Main Group of Particles from EDX Analysis on Individual Particles (Weight Percent Oxide)

type of particle ^a	particle size, μm	SiO ₂	Al ₂ O ₃	Si/Al ^b	K ₂ O	FeO	TiO ₂	MgO	SO ₃
FA-C-8									
\bar{x}	0.6	53.0	31.3	1.4	4.3	4.3	1.3	0.9	7.2
σ	0.2	2.8	2.4	0.1	1.5	0.9	0.7	0.9	3.0
<i>N</i>	19	19	19	19	19	19	10	5	15
FA-C-2,5									
\bar{x}	2	54.7	34.3	1.4	4.2	2.9	1.2	1.5	1.6
σ	0	2.7	2.5	0.1	0.6	0.6	0.6	0.3	0.9
<i>N</i>	18	18	18	18	18	17	15	13	10
FA-C-2									
\bar{x}	5	53.8	35.0	1.3	4.7	2.3	0.9	1.7	1.2
σ	0	2.2	1.9	0.1	0.5	0.6	0.5	0.4	0.8
<i>N</i>	10	10	10	10	10	10	10	8	8
FA-C-2									
\bar{x}	6.6	53.1	34.5	1.3	4.9	2.6	1.7	1.9	0.9
σ	0.7	0.4	1.2	0.1	0.7	0.4	0.7	0.3	0.5
<i>N</i>	6	6	6	6	6	6	6	6	4

^a \bar{x} , average value; σ , standard deviation; *N*, number of particles. ^b Atomic ratio.

Table II. Composition of Nonspherical Particles from Stage 2 (FA-C-2) (Weight Percent Oxide)

SiO ₂	Al ₂ O ₃	Si/Al	K ₂ O	FeO	TiO ₂	MgO	SO ₃	remarks
51.5	33.4	1.3	5.5	2.8	2.7	1.5	2.5	two fused particles
53.8	34.5	1.3	4.9	3.3	0.4		1.4	center of one particle
47.1	32.9	1.2	6.0	4.7	2.7		5.6	center of other particle
60.1	34.2	1.5	3.6	0.9	0.4		0.9	junction of the two particles
88.4	7.2	10.4	1.3	0.6	0.6	0.7	1.1	perforated particle
80.9	10.8	6.4	5.1	1.8	0.5		0.9	crystalline-like particle
87.7	7.2	10.3	1.8	0.7	0.5		2.1	crystalline-like particle

Table III. Comparison of the Concentration of Main Constituents of Different Fly Ashes in Weight Percent of Elements

type of fly ash and size	Si	Al	K	Fe	Ti	Mg	S	O
FA-C-8, <1 μm^a	24.8	16.6	3.6	3.3	0.8	0.5	2.9	47.4
FA-C-2,5, 2 μm^a	25.6	18.2	3.6	2.3	0.7	0.9	0.6	48.2
FA-C-2, 5 μm^a	25.2	18.5	3.9	1.8	0.5	1.0	0.5	48.5
FA-C-2, >5 μm^a	24.8	18.3	4.1	2.0	1.0	1.1	0.4	48.5
average fly ash constituents of American power plants ^b	21.4	13.8	1.2	12.0	0.7	0.7	1.5	50.3
fly ash from Illinois Basin coal, 5-15 μm^c	8.7	7.5	0	30.3	0	0.2	2.2	33.2
fly ash from western coal ^d	24.6	17.3	0.9	2.5	1.0	1.0	0.9	48.3

^aPresent work. Data from Table I. ^bNBS data as quoted in ref 2. ^cData from ref 3, EDX analysis. ^dData from ref 4, EDX analysis.

concentration was too low for quantitative analysis. Si, Al, K, and Fe were found in all particles. The Si content ranged between 24.8 and 25.6%, and Al concentration was 18.3% for particles in the micron range and 16.6% for submicron particles. This corresponds to an atomic ratio for Si/Al of 1.3-1.4. The concentration of K ranged between 3.6 and 4.1%. Fe content was 3.3% in submicron particles and 1.8-2.3% for particles in the micron range.

Ti was found in all the particles of $\geq 5 \mu\text{m}$, in 80% of the particles of 2 μm , but only in about 50% of the submicron particles. The concentration of Ti was 0.5-1.0% for the different groups but did not change regularly with particle size.

Mg was found in 25% of the submicron particles and more than 70% of the particles in the micron range. Its concentration varied between 0.5 and 1.1%, but again, as with Ti, it could not be correlated to particle size.

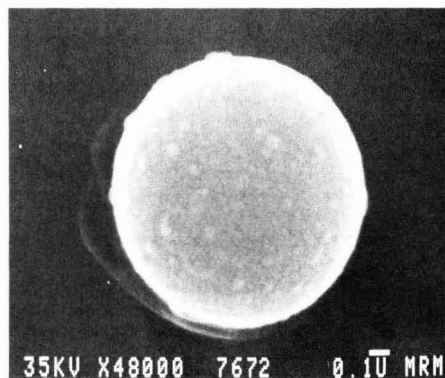


Figure 1. Typical spherically shaped fly ash particle.

Table IV. Composition of Particles of Those Deviating Considerably from Average Particle Values (Weight Percent Oxide)

notation	particle size, μm	SiO ₂	Al ₂ O ₃	Si/Al	K ₂ O	FeO	TiO ₂	CaO	MgO	SO ₃
FA-C-8	0.66	50.2	28.8	1.5	3.0	3.9	12.1	0.9	1.2	
FA-C-8	0.4	8.5	12.8			13.4	65.3			
FA-C-8	0.85	10.4	8.6				79.0			0.9
FA-C-8	0.4	50.2	24.7	1.7	1.6	16.9	2.5	1.6	2.5	
FA-C-8	0.6	33.8	16.7	1.7	1.0	6.3	39.4			2.8
FA-C-5	2	72.4	16.7	3.7	6.7	1.5			1.8	0.8
FA-C-2	5	65.9	25.2	2.2	5.7	1.6	0.9		0.6	
FA-C-2	7.5	71.7	17.1	3.6	5.8	1.5	1.7	0.5	1.0	0.7

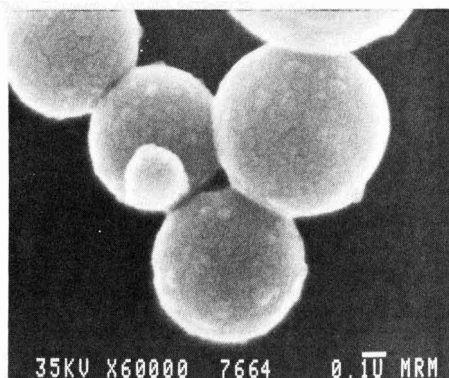


Figure 2. Submicron fly ash particles.

S was present in 50–80% of the particles and at a concentration of 2.9, 0.6, 0.5, and 0.4% for particles with a diameter of <1, 2, 5, and <5, μm , respectively.

The concentrations of a number of elements were not given in Table I due to either high uncertainty in determination of the concentration as in the case of Ca and P, limited occurrence as in the case of Ni, Na, and Cl, or ambiguity in their determination as in the case of V, Mn, and Cr (see also Discussion). Ca was identified in about 50% of the micron particles while in the submicron particles it was only occasionally determined. Concentrations ranged between 0.1 and 1.4% Ca. P was found in a few particles in concentrations as high as 1.2%.

C, as determined for particles in the micron range (1–8 μm), was less than 2.2%.

(b) Particles with Chemical Composition Deviating from Average Values. About 20% of the submicron particles studied deviated markedly from the average chemical composition given in Table I, featuring either a very high iron or a very high titanium content (Table IV). The number of particles was too small to try to elaborate on the influence of either a high iron or a high titanium content on the rest of the elements present.

About 8% of the particles in the micron range showed deviation from the average value and were marked by a high silicon content, increasing the atomic ratio of Si/Al beyond 2 as described in section 2c under Results.

(c) Particles with Irregular Shape. The particles of irregular shape which were examined were all from stage 2 (Table II). Some of the particles observed exhibited crystalline features and had an extremely high silica content of over 80%, with a corresponding Si/Al atomic ratio of 6.5–10.0. The “perforated” particle examined had a nearly average composition. Two spherical particles joined together had an average value, but the merging point ex-

hibited a definite increase in sulfur content.

Discussion

We observed a remarkable consistency in the composition of the major part of the particles, both in the submicron and in the micron size, which allowed very reasonable statistics for the major part of the particles studied. All of the particles in the statistics contained Si, Al, K, and Fe. Si, Al, and K were fairly constant for both the micron and submicron particles. The concentration of the aluminosilicate material amounts to over 80% of the fly ash, with an atomic ratio for Si/Al of 1.3–1.4. Concentrations of Si, Al, and K are, on the average, 25.1%, 17.9%, and 3.8%, respectively. Fe is somewhat enriched in the submicron particles, with a value of 3.3% compared to an average value of 2.0% for the rest of the particles. Ti is the next common element. Ti is found in most of the particles in the micron range but only in about 50% of the submicron particles. Though it is less common in submicron particles, particles with exceptionally high Ti concentration (Table IV) were sometimes observed. Mg is also less common in submicron particles. The concentration of Ti and Mg is, however, independent of particle size. There is an obvious enrichment of S concentrations in the submicron particles. The accuracy of S determination is certainly limited by the EDX method of determination. However, the high value of 2.9% S in submicron particles compared to 0.5% for the micron range is significant. Sulfur occurs in only some of the particles, but no correlation between particle size and frequency of occurrence can be pointed out. The high S content in submicron particles is in agreement with results indicating a surface enrichment with respect to sulfur (3, 5). However, preferential absorption should not be ruled out.

The EDX method, though quick and thus very convenient for the present type of work of analysis of a larger number of particles, has a limited energy resolution (6). This will cause, in the study of systems which contain both K and Ca, with K being the major constituent, an ambiguity in the determination of Ca. Hence, though we believe that the fly ash studied has low Ca content, its identification and concentration are greatly hampered. V and Cr were believed to be present in a minority of the particles, but here again no assertion could be made because of limited resolution.

The EDS routine employing the ZAF correction scheme as supplied by the KeveX Co. seems a reasonable approach to studying particles with diameters larger than a few tenths of a micrometer (7). Work, with available oxide standards, is in progress to determine allowed deviations for the semiquantitative routine used. At this stage, we would like to point out the low deviations observed for Si and Al. Higher deviations of 20–30%, as found for K, Fe, and Mg, are very common for this type of material.

Table V. Average Concentration of Silica, Al, K, Fe, Mg, Ca, Na, and Cl in Various Types of U.S. Coals^a

type of coal	SiO ₂	Al	K	Fe	Mg	Ca	Na	Cl
Western U.S.	1.3	0.86	0.03	0.49	0.12	1.5	0.06	0.02
Eastern U.S.	2.6	1.6	0.21	1.3	0.05	0.34	0.03	0.10
Illinois Basin	2.3	1.2	0.16	1.9	0.05	0.51	0.03	0.08

^aSee ref 8.

Fly ash composition may vary with source of coal and type of combustor. In Table V are given the main mineral constituents of three different types of coal (8). We would like to relate our results to the average values for the American power station fly ash composition worked out by the American Bureau of Standards (NBS) (Table III). We find that the fly ash in our collection, in the size range studied, tends to be low in Ca and Fe and high in K concentration. The aluminosilicate ratio is somewhat lower, with an Si/Al atomic ratio of 1.3–1.4 compared to that of 1.5 in the NBS data. Also given in Table III are previous results carried out in our group on fly ash from the Kincaid power station using Illinois Basin coal (3) as well as results of analysis of Rothenberg et al. on western coal in a conventional burner (4). Unfortunately, the work carried out by Hullet et al. (9), who studied Bull Run fly ash, differed so much in analysis techniques that it does not allow any valid comparison. However, it might be worth noting that the atomic ratio of Si/Al of the mullite–quartz fraction in that work was 1.35.

Though the issue of the composition of minority populations (Tables II and IV) was not pursued deeply, there might be a basic difference in composition of those populations in the submicron and micron range, with particles of high metal content, Ti and Fe, in the former and Si in the latter. It was also observed that particles with nonspherical shape were essentially crystalline-like and exhibited an exceptionally high Si content. Similar observations for particles of nonspherical shape were made for particles in the 100–200- μ m range by Hullet et al. (9).

Though the main group of particles studied indicated a spherical shape, recent data at higher magnifications (150 000 \times) of submicron particles revealed a fine structure of the surface. These features are still under investigation.

At this point we would like to refer to the rather small (in the statistical sense) number of particles in our population. Although few in number, this sample seems to be representative for the properties reported in this paper, namely, the chemical composition of the main constituents of the major part of the population and their spherical shape. Also, additional studies of particles of this fly ash fit into the above results, indicating that little further understanding would be gained by studies of a larger population of particles.

Conclusions

Our studies showed that the submicron particles and

particles in the micron range were essentially of the same nature, with regard to both morphology and chemical composition. The major part of both types of particles studied was spherical. Submicron particles consisted of an aluminosilicate skeleton, and the main components were Si, Al, K, Fe, Ti, and S which were similar to those of the micron particles. Little variation in concentration of these elements was observed aside from an enrichment of sulfur in the submicron particles.

Acknowledgments

We thank M. MacLaurin for much of the SEM data and Susan Mroczkowski of Midwest Research Microscopy, Milwaukee, WI, for the carbon analysis work.

Registry No. Ca, 7440-70-2; P, 7723-14-0; C, 7440-44-0; Si, 7440-21-3; Al, 7429-90-5; K, 7440-09-7; Fe, 7439-89-6; Ti, 7440-32-6; Mg, 7439-95-4; S, 7704-34-9.

Literature Cited

- (1) "Planning Studies for Measurements of Chemical Emissions in Stack Gases of Coal-Fired Power Plants" report prepared for EPRI, Palo Alto, CA, by Southern Research Institute, Birmingham, AL, Battelle Columbus Laboratory, Columbus, OH, and Roth Associates, Inc., Rockville, MD (EA-2892, Research Project 1776-1), March 1983.
- (2) Torrey, S., Ed. Noyes Data Corp., Park Ridge, NJ, 1978, Pollution Technology Revue No. 48.
- (3) Hock, J. L.; Lichtman, D. *Environ. Sci. Technol.* **1982**, *16*, 423.
- (4) Rothenberg, S. R.; Denee, P.; Holloway, P. *Appl. Spectrosc.* **1980**, *34* (5), 549.
- (5) Linton, R. W. Department of Chemistry, The University of North Carolina, Chapel Hill, NC, personal communication, 1983.
- (6) Goldstein, J. I., et al. "Scanning Electron Microscopy and X-ray Microanalysis"; Plenum Press: New York, 1981.
- (7) Small, J. A. In "Scanning Electron Microscopy"; SEM Inc.: Chicago, IL, 1981; Vol. I, pp 447–461.
- (8) Valkovič, V. "Trace Elements in Coal: Vol. I"; CRC Press: Boca Raton, FL, 1983.
- (9) Hullett, L. D., et al. *Science (Washington, D.C.)* **1980**, *210*, 1356.

Received for review August 8, 1983. Revised manuscript received December 19, 1983. Accepted January 20, 1984. This work was supported by EPRI, Project RP 1625-1.

Analysis of Coal Fly Ash Properties of Importance to Sulfur Dioxide Reactivity Potential

Gregory D. Reed,* Wayne T. Davis, and Randal E. Pudelek

Department of Civil Engineering, The University of Tennessee, Knoxville, Tennessee 37996-2010

■ Twenty-two fly ashes selected to provide a representative cross section of coal classification and combustion techniques were analyzed for physical and chemical characteristics that might indicate a potential for reaction with SO_2 in a flue gas desulfurization process. Each ash was tested for its SO_2 removal potential as a slurry injected into a 1000 CFM spray dryer/fabric filter pilot plant. The reactivity of the fly ashes correlated with a combined effect of total slurry alkalinity in conjunction with the available surface area which suggested a surface-controlled reaction. The results further suggested the utilization of slower reacting alkaline species such as carbonate could be enhanced by a longer contact time with the flue gas such as is provided in a bag house filter operation.

There has been an increasing interest in spray dryer technology as a technically and economically viable solution to flue gas desulfurization (FGD). In the spray-drying process, a liquid containing an alkali sorbent is atomized in a drying chamber and reacted with sulfur dioxide (SO_2). The hot flue gas is used as the drying agent. The FGD reactions proceed as a function of the drying time, eventually yielding a dried suspended particulate in the gas stream. A fraction of the particles falls in to a hopper in the bottom of the drying chamber while the remaining reacted product plus fly ash proceeds to a fabric filter collector where further FGD reactions occur with unreacted alkali or to an electrostatic precipitator for particulate removal only.

One common method used in the design of spray dryers incorporates the use of slaked lime as the alkali sorbent. However, the alkaline content of many fly ashes has been suggested for use as a possible supplement or replacement for lime-based slurries. Further, the application of spray dryers with a continuous partial recycle of the collected spray-dried product, and fly ash provides additional access to the alkaline content of the fly ash which has been slurried. The successful utilization of the fly ash could produce a potential cost reduction in the control of SO_2 for many industries.

One of the best examples of the significance of fly ash in FGD was presented by Hurst and Bielawski (1). They reported SO_2 removal efficiencies of up to 65% with a slurry containing only a highly alkaline fly ash. Ness and Selle (2) have utilized highly alkaline western coal fly ashes at their wet scrubber pilot plant. Davis and Fiedler (3) demonstrated that the amount of sulfur retained by fly ash was highly correlated with the levels of alkaline metal oxides (CaO , Na_2O , MgO , and K_2O) contained within the ash. Hulett and Weinberger (4), Ensor et al. (5), and Ray and Parker (6) also found that decreasing particle sizes exhibited an increase in sulfur content of the ash product, suggesting a specific surface area related phenomenon. Davis and Reed (7) examined these effects further and found very good correlations of the combination of fly ash slurry available alkaline content and surface area vs. SO_2 removal.

The introduction of the physical parameter, surface area, raises the question of whether there might be a surface chemical reaction that would be enhanced by a concen-

trating effect of chemicals on the fly ash surface. Davidson et al. (8) found that chemicals such as Ca and K showed no concentration trends relative to the surface. Therefore, the amount of chemical available for reaction on the surface would be a linear function of the total surface area, and the fraction of chemical available would be a function of the specific surface area. This lack of surface concentration effect was also reported by Hock and Lichtman (9) while examining the conductivity of fly ashes. This would indicate that a physical property such as surface area would be predictive of the reactivity of a fly ash with SO_2 .

The work reported here was designed to examine the physical and chemical characteristics of a broad range of fly ashes and the relative potential for reactivity with SO_2 in various kinds of air pollution control reactors. The success of this approach would reduce the amount of virgin alkaline reactant required to achieve SO_2 removal from flue gas.

Physical Description of Fly Ashes

In an effort to obtain samples for study, approximately 22 different electric utilities and/or power plants were contacted with a request to provide a 200-lb. sample of the ash collected from their plants. Table I includes (1) a summary of the power plants/utilities that responded with samples of ash, (2) the rank of the coal used to produce the ash, and (3) the source of the coal. There were five lignite, eight subbituminous, and nine bituminous ashes. All but one of the ashes (identification no. 37) were collected from the hoppers of an electrostatic precipitator.

Table II provides a summary of the physical properties of each of the fly ashes including the mass mean diameter (MMD), the geometric standard deviation, the particle density, and the specific surface area. The MMD ranged from 7.4 to 18.0 μm with an average of 11.8 μm . The geometric standard deviations ranged from 1.7 to 2.8 with an average of 2.1. The particle density ranged from 1.5 to 3.2 g/cm^3 (1500–3200 kg/m^3) with an average value of 2.5 g/cm^3 . The surface area of the fly ashes ranged from 0.21 to 3.39 m^2/g of ash with an average of 1.59 m^2/g . One exception to the above was fly ash 49 (obtained from a stoker-fired boiler) which had a surface area of 12.5 m^2/g . This was attributed to the high carbon content of the ash which was typically 30–40%. The above surface areas were measured with a Micromeritics surface area analyzer which utilized the BET low-temperature nitrogen adsorption technique. The average surface area was 1.59 m^2/g when the BET procedure was used. This surface area is greater than the value determined by assuming perfect spheres and determining the surface of the spheres (0.98 m^2/g), suggesting that the fly ashes had some interstitial surface area. The BET-measured values of surface area reported in Table II were used in all statistical evaluations in the paper.

Chemical Description of Fly Ashes As Received

Table III is a summary of the chemical characteristics of each fly ash determined by conducting an ASTM mineral analysis of the ashes. The ASTM mineral analysis is an acid digestion method which measures the total mineral

Table I. Origin of the Fly Ashes

fly ash identification no.	company: plant	source
Lignite		
27	Texas Utility Generating Co.: Big Brown	Freestone County
38C	Basin Electric Power: Coop Unit 1	Consolidated Coal Co., Stanton, ND
41	Milton R. Young Station: Center Unit 1	Bankol-Noonan Mine, Center, ND
42	United Power Association/Coop Power Association	Falkirk Mine, Underwood, ND
44	Otter Tail Power: Hoot Lake Unit 2	Knife River Coal Mining Co., Beula, ND
Subbituminous		
13 ^a	Minnesota Power and Light: Clay Boswell Station	Big Sky Mine, Colstrip, MT
14	Nebraska Public Power: Gerald Gentleman Station	Black Thunder Mine, Campbell Co., WY
18A	Pacific Power and Light: Wyodak	Wyodak Resources, Wyodak Mine
37	SWPS: Harrington Station	Black Thunder Mine, Gillette, WY
38B	Laramie River Station	Cordero Mine, WY
43	Black Hills Power and Light Company	Wyodak Mine, WY
45 ^a	Minnesota Power and Light: Clay Boswell Station	Big Sky Mine, Colstrip, MT
46	San Antonio Public Service: Monifer Resources	Cordero Mine, WY
Bituminous		
6	Belews Creek Steam Station	Low sulfur eastern coal
10	Bowen Steam Plant	eastern Kentucky
18B	Hunter Steam Plant	Wilberg Mine, Emery County, UT
23B	Cherokee 4	Colorado western slope
24	Public Service of Indiana: Gallagher Station II	Amax Aryshire
34	New Madrid Power Plant 2	southern Illinois
36	Ohio Edison Gorge	Ohio strip mine
49	University of Tennessee Steam Plant	eastern Kentucky
50	Duke Power: Marshall Steam Plant	low-sulfur eastern coal

^aThese fly ashes were obtained from the same source; however, their production resulted from different combustion conditions.

Table II. Summary of Fly Ash Physical Characteristics

fly ash identification no.	MMD, μm	geometric deviation	particle density, g/cm ³	specific surface ^a , area, m ² /g
Lignite				
27	9.5	2.5	2.4	0.74
38C	15.6	2.6	3.2	0.76
41	12.0	1.8	2.7	3.27
42	9.4	1.9	2.6	0.29
44	11.0	1.9	2.7	2.37
Subbituminous				
13	9.4	1.9	1.5	0.21
14	9.5	1.8	2.7	2.09
18A	15.0	1.9	2.5	0.73
37	7.4	2.5	2.7	1.15
38B	11.5	2.2	2.6	1.66
43	18.0	2.4	2.5	1.03
45	10.0	2.0	2.5	3.39
46	8.5	1.8	2.5	1.48
Bituminous				
6	12.0	2.3	2.7	1.31
10	14.8	2.2	2.1	2.14
18B	7.8	1.9	2.3	2.14
23B	14.9	2.8	2.2	2.85
24	12.3	2.2	2.7	2.88
34	9.2	1.7	2.5	1.23
36	15.3	2.0	2.6	0.22
49	12.9	1.9	2.1	12.52
50	14.0	2.1	2.2	1.47

^aBET adsorption techniques.

content and is reported as an oxide. The test does not provide information on the true alkaline content nor does it distinguish between chemicals on the surface and those located deeper into the particle. The test does provide a relative indicator of chemical content and the maximum potential for each compound.

The total alkaline metal oxide content (TAMO) was also reported for each ash. This value was determined by weighting each constituent by its molecular weight according to the following equation

$$TAMO = \left[\frac{\text{g of CaO}/100 \text{ g}}{56.1 \text{ g}/(\text{g}\cdot\text{mol})} + \frac{\text{g of Na}_2\text{O}/100 \text{ g}}{62.0 \text{ g}/(\text{g}\cdot\text{mol})} + \frac{\text{g of MgO}/100 \text{ g}}{40.3 \text{ g}/(\text{g}\cdot\text{mol})} + \frac{\text{g of K}_2\text{O}/100 \text{ g}}{94.2 \text{ g}/(\text{g}\cdot\text{mol})} \right] \left(\frac{56.1 \text{ g of CaO}}{\text{g}\cdot\text{mol}} \right)$$

The TAMO had values of 8.9–45.6% by weight. The lowest value was associated with the stoker-fired ash which had a very high surface area due to its high unburned carbon content.

On the basis of the prior data which suggested that reactions on the surface of the fly ash might also be important relative to the retention of sulfur, a series of analyses were conducted which consisted of determining the available alkalinity of the fly ash slurry and that of the filtrate. While the digestion method used in the ASTM analysis measures the total alkaline metal content of the sample, the quick liquid titration used here measures the soluble alkalinity plus the "surface" alkalinity which is readily available for reaction. A summary of both the slurry and filtrate titrations is shown in Table IV for the 15% fly ash slurries at 60 °C. The results of these analyses revealed that some ashes had considerably more alkalinity available on the surface than in solution.

Results of Fly Ash Slurry Testing at the FGD Facility

Each of the above 22 fly ashes were tested in a 1000 CFM spray dryer/fabric filter pilot plant. The results of the tests in which each fly ash was slurried at 174 g/L of water and atomized into the flue gas in the spray dryer are summarized in Table V. The concentration was chosen since it was equivalent to the fly ash present in flue gas with a nominal grain loading of 3 grains/ft³ (0.69 g/m³).

Table III. Summary of Fly Ash Chemical Characteristics

fly ash identification no.	% S	% CaO	% Na ₂ O	% MgO	% K ₂ O	TAMO ^a
Lignite						
27	0.66	14.99	11.19	2.40	1.70	28.33
38C	0.00	13.95	35.88	5.58	3.69	56.47
41	4.06	18.01	16.68	3.98	1.52	32.47
42	1.02	18.96	10.97	3.79	1.90	33.57
44	0.75	23.80	17.71	4.57	1.14	45.56
Subbituminous						
13	0.49	13.96	10.96	2.79	1.79	28.06
14	0.73	22.91	10.96	3.49	1.29	38.22
18A	0.70	18.96	10.78	3.79	1.50	33.73
37	0.78	24.95	10.98	3.59	1.00	39.19
38B	0.72	21.81	13.48	2.97	1.29	37.70
43	0.66	6.97	10.76	1.00	2.49	18.50
45	0.68	11.63	10.66	2.71	1.45	24.68
46	0.75	28.90	14.94	3.98	1.39	47.47
Bituminous						
6	0.43	7.79	10.71	0.97	2.53	19.61
10	0.32	5.44	9.42	0.91	2.36	16.03
18B	0.45	9.72	10.89	2.14	1.94	22.83
23B	1.87	7.88	10.25	1.18	1.68	16.54
24	1.22	8.60	9.94	1.91	0.76	17.67
34	1.04	6.76	11.79	0.97	2.90	18.78
36	0.36	0.98	12.69	0.39	5.56	15.75
49	2.19	4.02	6.97	0.94	1.94	8.89
50	0.41	5.75	12.47	1.44	2.78	20.01

^aTotal alkaline metal oxides reported in g/100 g as CaO.

Table IV. Summary of Slurry and Filtrate Alkalinity Species^a

ID no.	slurry			total	filtrate total
	OH	CO ₃	HCO ₃		
Lignite					
27	0	2141	428	2569	1700
38C	1713	3854	0	5567	1600
41	0	8135	7065	15200	1100
42	0	8564	1285	9849	3700
44	0	16701	8350	25051	1300
Subbituminous					
13	4496	3425	0	7921	3800
14	6637	3854	0	10491	2500
18A	3426	0	0	3426	1200
37	5352	13702	0	19054	1800
38B	642	5139	0	5781	1500
43	3426	8564	0	11990	2100
45	0	3854	1070	4924	1600
46	0	5566	2569	8135	1600
Bituminous					
6	0	0	0	0	200
10	0	0	8564	8564	500
18B	1285	5995	0	7280	3400
23B	2783	0	0	2783	1800
24	1285	3426	0	4711	2900
34	0	0	0	0	0
36	2141	0	0	2141	1400
49	0	0	0	0	0
50	0	0	0	0	0
30A	0	0	0	0	0

^aAll values are mg/L as CaCO₃.

Table V. Sulfur Retention by Fly Ash

fly ash identification no.	SO ₂ removal, %	
	spray dryer	total (system)
Lignite		
27	1	5
38C	11	15
41	17	21
42	8	9
44	15	16
Subbituminous		
13	5	17
14	33	30
18A	20	21
37	25	26
38B	17	26
43	21	26
45	11	24
46	12	13
Bituminous		
6	0	1
10	10	7
18B	24	23
23B	2	2
24	5	6
34	5	6
36	0	0
49	11	29
50	0	1

ash present in the test facility flue gas.

A comparison of Tables IV and V reveals that there was a general relationship between SO₂ removal efficiency and total slurry alkalinity. A slurry with a higher total alkalinity tended to have a higher removal efficiency (see Figure 1). It was further hypothesized that the relatively fast-reacting species of OH and HCO₃ along with the soluble CO₃ would react in the short detention time of the spray

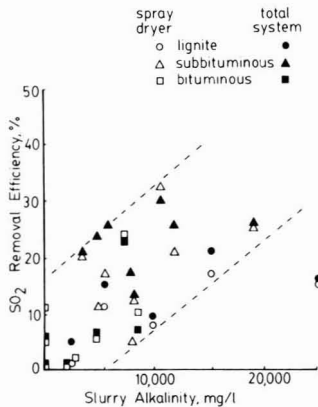


Figure 1. Relationship of SO₂ removal efficiency and the slurry total alkalinity.

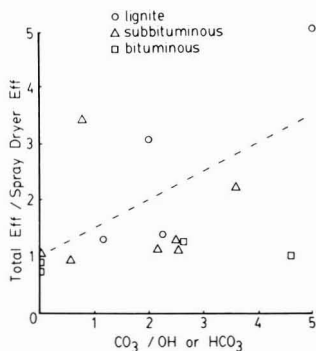


Figure 2. Effect of carbonate content on bag house SO₂ removal. The dashed line is a linear least-squares fit through the data ($R^2 = 0.55$).

dryer (10 s) and that the relatively slower reacting insoluble CO₃ would also react in the longer detent in time of the bag house (several hours); therefore, a fly ash that produced a slurry with a predominant CO₃ content could produce an increase in total system SO₂ removal (spray dryer plus bag house) as compared to the spray dryer only. This hypothesis was tested by comparing the ratio of the efficiencies (total system removal divided by spray dryer removal) to the ratio of carbonate to hydroxide or bicarbonate. In this manner an efficiency ratio of 1 would imply that the system achieved no increased removal compared to the spray dryer which would correspond to a carbonate ratio of zero and should increase with increasing carbonate content. The scatter in the data is partially a result of the indistinct end point during the alkalinity titration. Additionally, soluble carbonate would have reacted quickly while the insoluble carbonate on the surfaces would have reacted more slowly. A least-squares fit was conducted on the data in Figure 2. While the intercept did approach 1.0 at the low carbonate content, the correlation was found to be low ($R^2 = 0.55$), indicating that there was no conclusive trend. While not conclusive, some of the data in Figure 2 suggested that increases in the ratio of the carbonate compared to the hydroxide or bicarbonate content tend to increase the system SO₂ removal compared to the spray dryer efficiency, indicating that the above hypothesis should be studied further.

A comparison of the specific surface area data with SO₂ removal efficiency was less clear. While high efficiencies were achieved at high surface areas, low efficiencies were

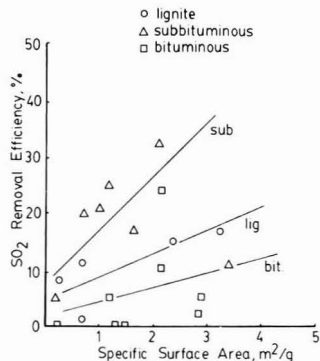


Figure 3. Relationship of SO₂ removal efficiency and the fly ash specific surface area. The lines are a least-squares best fit for each overall classification.

also achieved at high surface areas (see Figure 3), although weak trends did exist within the three coal classification categories. If the reaction is a surface phenomenon, then some relationship between efficiency and alkalinity and surface area should prevail. A close examination of the individual data triplets reveals that low alkalinity fly ashes do not produce high efficiencies even with high surface areas. However, high alkalinity fly ashes produce good efficiencies with improvement at higher surface areas. The higher the specific surface area the more relative mass of alkalinity will reside on or near the surface for direct reaction rather than relying on diffusion to produce reactions at greater depths in the particles. One test was conducted in which fly ash 44 was ball milled, resulting in an increase in filtrate alkalinity of 62% and an increase in surface area of 17% compared to the values in Tables III and IV. The system SO₂ removal efficiency increased from 16% to 46%, which further supports the coupling of alkalinity and surface area as the primary components.

The scatter in the data can be at least partially attributed to changes in drying conditions in the spray dryer, inaccuracies in coal classification, nonuniformity in fly ash composition within the collection hopper, and difficulties with end points in slurries. But the data do provide insight into the general trends and an indication of the factors that influence SO₂ removal.

Conclusions

The ability of a fly ash slurry to achieve removal of SO₂ in a spray dryer/bag house system was a function of the amount of alkaline content exposed at a surface for reaction. This was measured as a coupling of the fly ash slurry alkalinity and the fly ash specific surface area. A combined increase in each parameter produced SO₂ removal efficiencies of up to 46%. The form of the alkaline content appeared to play a role in where the SO₂ reaction took place—in the spray dryer vs. in the bag house. Fly ashes that were predominately hydroxide or bicarbonate tended to produce SO₂ removal only in the spray dryer while fly ashes with a high carbonate content produced a proportionately higher removal in the bag house where the ash is held in contact with the flue gas at a high solids level and for a longer residence time. While the fly ashes tested in this study did not provide sufficient SO₂ removal efficiencies to be used as a total substitute for alkaline-based slurries, the data suggest that high slurry concentrations of some fly ashes could be used as a partial lime substitute in a spray dryer/bag house flue gas desulfurization system. Further, it has been demonstrated that specific laboratory

analyses can be of value in determining the potential usefulness of a given fly ash.

Registry No. SO₂, 7446-09-5; S, 7704-34-9; CaO, 1305-78-8; Na₂O, 1313-59-3; MgO, 1309-48-4; K₂O, 12136-45-7.

Literature Cited

- (1) Hurst, T. B.; Bielawski, G. T. EPA Symposium on Flue Gas Desulfurization, Houston, TX, 1980.
- (2) Ness, H. M.; Selle, S. J. DOE Symposium on Environmental Control Activities, Washington, DC, 1978.
- (3) Davis, W. T.; Fiedler, M. A. *Air Pollut. Control Assoc.* 1982, 32, 395.
- (4) Hulett, L. D.; Weinberger, A. J. "Some Etching Studies of the Microstructure and Composition of Large Aluminosilicate Particles in Fly Ash From Coal Burning Power

- Plants". Oak Ridge National Laboratory, Oak Ridge, TN, 1979.
- (5) Ensor, D. S.; Cahill, T. A.; Sparks, L. E. 68th Annual Meeting of APCA, Boston, MA, June 1975.
- (6) Ray, S. S.; Parker, F. G. U.S. EPA Contract 600/7-77-010, January 1977.
- (7) Davis, W. T.; Reed, G. D. Grand Forks, ND, May 1983, DOE Report GFETC DE-AC18-81FC10492 (available from NTIS).
- (8) Davidson, R. L.; Natusch, D. F.; Evans, C. A.; Wallace, J. R. *Environ. Sci. Technol.* 1974, 8, 1107-1112.
- (9) Hock, J. L.; Lichtman, D. *Environ. Sci. Technol.* 1982, 16, 423-427.

Received for review August 26, 1983. Accepted January 16, 1984.

Mercury in Recent and Century-Old Deep-Sea Fish

Richard T. Barber* and Patrick J. Whaling

Marine Laboratory, Duke University, Beaufort, North Carolina 28516

Daniel M. Cohen

Los Angeles County Natural History Museum, Los Angeles, California 90007

■ To determine if mercury discharges to the environment in the last century have increased the mercury content of marine fish, a sample of 21 specimens of one deep-sea fish species collected in the 1880s was compared with a sample of 66 specimens of the same species collected in the 1970s. The specimens of *Antimora rostrata* were collected from between 2000 and 3000 m in the western North Atlantic Ocean. In both recent and old fish mercury increased as a function of length, but comparison of the two concentration vs. length relationships shows that there has not been an increase in mercury concentration in deep-sea fish in the last century. This result supports the idea that the relatively high concentrations of mercury found in marine fish that inhabit the surface and deep waters of the open ocean result from natural processes, not 20th century industrial pollution.

The observed increase of mercury in freshwater fish and sediments (1, 2) in conjunction with the increase of industrial mercury discharges in the middle of the 20th century suggests that a time series comparison of marine fish could be used to determine if recent activities have increased the mercury content in ocean-dwelling fish. A finding that mercury concentrations are lower in marine fish caught a century ago would be clear evidence that significant changes have taken place in the 20th century. When the first mercury analyses of museum specimens of ocean fish were made a decade ago (3), results were interpreted to indicate that mercury concentrations have not changed throughout the 20th century, but the National Academy of Science report on mercury published in 1978 (4) stated that time series comparisons on museum specimens "lack enough statistical confidence to draw comparisons that indicate the degree and extent of mercury pollution in the present marine ecosystem." The Academy report (4) argues that since the extent of mercury contamination during preservation is not well-known, comparisons of museum and contemporary specimens must be viewed as inconclusive. In this report we present evidence indicating that mercury contamination did not occur

in the century-old museum specimens used in our comparison and that, therefore, a valid test for contamination by 20th century activities can be carried out.

Earlier work on mercury in marine fish (5-7) established that concentration comparisons must be made within one species since different species-specific mercury accumulation patterns and rates are found among species that share common habitats and food habits. Because mercury concentration increases with size in a well-defined relationship within a species (8, 9), it is necessary to compare concentration normalized to size rather than the mean concentration of mercury in a particular sample of fish. To test for a change in mercury content in the last century, two samples of the benthopelagic deep-sea fish named blue hake (*Antimora rostrata*) were analyzed. Specimens over a large size range were available for each sample, so it was possible to determine a well-defined concentration vs. length relationship for both. *Antimora rostrata* is resident throughout the world's oceans at depths of 1000-3000 m (10, 11) but does not venture into depths shallower than 800 m; therefore, this deep-sea species is not exposed to local estuarine, coastal, or atmospheric inputs of mercury. There is no doubt that local inputs such as those at Minimata Bay (12) greatly increase the mercury content of fish in that locality; the question addressed in this study is whether 20th century industrial activity has increased mercury in a fish that occupies the deep-sea habitat below the permanent thermocline of the ocean. The significance of this question is that if deep-sea fish have been affected, then industrial mercury pollution has reached the habitat most remote from coastal and atmospheric inputs of anthropogenic mercury.

Experimental Procedures

The obligate deep-sea species *Antimora rostrata* has been used in earlier mercury (5, 6) and organochlorine (13) studies as well as in numerous physiological and biochemical studies (14), and the biology and physiology of this abundant deep-sea fish are relatively well-known. Therefore, the species is useful for studies of contamination

of the deep ocean habitat in a manner analogous to the use of mussels in worldwide monitoring of pollution in the coastal ocean (12).

The recent fish analyzed in this study were collected in 1972, 1973, and 1974 from between 2000 and 3000 m off the east coast of the United States. The collection site was beneath the mean axis of the Gulf Stream and on the upper continental rise about 50 km southeast of Cape Hatteras. The fish were collected by a standard otter trawl net; the net tows lasted 2 h and covered a distance over the bottom of 4–10 km. As the trawl was brought on board, the cod end of the net was prevented from touching the vessel's side or deck, and the contents were dumped directly into enamel pans. The fish were sorted and frozen separately at -20°C for 1–3 months before analysis. The old fish were selected from specimens in the U.S. National Museum of Natural History in Washington, DC, which were collected on ALBATROSS cruises in the early 1880s in the same region off the east coast of the United States where the recent fish were collected.

Axial muscle was taken from deep within the muscle mass of the middorsal region. Total mercury was determined by the cold vapor atomic adsorption method of Hatch and Ott as modified by the U.S. Environmental Protection Agency (15). Bias or systematic error in the determination of mercury would seriously flaw this time series comparison, so our analytical procedure was intercalibrated with (1) the National Bureau of Standards, Washington, DC, (2) International Atomic Energy Agency, Monaco, (3) Fish and Wildlife Service, Ann Arbor, MI, and (4) National Marine Fisheries Service, Beaufort, NC, by running blind analyses of material that was also analyzed by the four laboratories.

Preservation of fish causes a decrease in length and a decrease in weight due to the loss of water from tissues (16, 17). To determine shrinkage, freshly caught *Antimora rostrata* were fixed in formalin and stored in 70% ethyl alcohol for several years with repeated measurements throughout the period. A 4.25% decrease in standard length was found during the first year, with no detectable shrinkage after the first year, so a correction of standard length was found during the first year, with no detectable shrinkage after the first year, so a correction of standard length was therefore applied to the old fish. To determine the weight loss in the old fish, a comparison of wet weight normalized to dry weight was carried out on recent and old fish axial muscle. A decrease of 16% was found in the museum fish, a value similar to the weight loss found by other workers (16, 17), so a correction was applied to the museum fish. Although expression of the mercury on a dry weight basis would be a simpler solution to the problem of weight decrease, this solution was not used because the wet weight basis is used in virtually all scientific (4) and legal (18) work on mercury in fish.

Results

A type II regression analysis (19) of the results of the intercalibration comparison (Table I and Figure 1) shows that the slope is not significantly different from 1.0 ($p = 0.01$), confirming that there is no bias or systematic error in the concentration of mercury determined at Duke relative to the concentration reported by the four other laboratories. The correlation coefficient, $r^2 = 0.99$, indicates that the variance of the reported values was well reflected in the Duke analyses. The intercalibration results as well as the length and mercury concentration data for the recent and century-old fish are available as supplementary material (see paragraph at end of paper regarding supplementary material).

The next issue to evaluate is the possibility of contamination of the century-old museum fish during storage.

Table I. Intercalibration Comparisons of Mercury Concentrations Determined at Duke University and the Reported Values Provided to Duke by the Laboratories Listed

material	mercury concentration, $\mu\text{g}\cdot\text{g}^{-1}$ wet weight	
	reported value	this work
U.S. National Bureau of Standards (Washington, DC)		
bovine liver	0.02 ± 0.005	0.02 ± 0.005
coal	0.12 ± 0.02	0.07 ± 0.005
orchard leaves	0.16 ± 0.02	0.12 ± 0.01
International Atomic Energy Agency (Monaco)		
fish	0.07 ± 0.02	0.07 ± 0.005
oyster	0.21 ± 0.02	0.16 ± 0.01
Fish and Wildlife Service (Ann Arbor, MI)		
fish	0.09 ± 0.01	0.12 ± 0.05
fish	0.40 ± 0.05	0.36 ± 0.06
fish	0.77 ± 0.07	0.74 ± 0.10
National Marine Fisheries Service (Beaufort, NC)		
fish	0.65 ± 0.13	0.61 ± 0.16

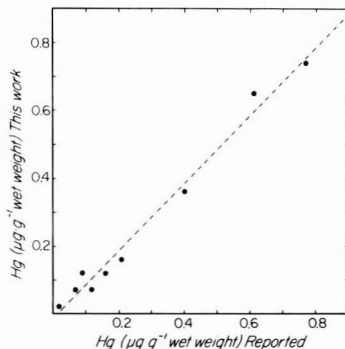


Figure 1. Relationship between reported mercury concentrations provided by four laboratories and concentration determined at Duke University on the same material. The slope of the relationship is not significantly different from 1.0 which indicates that there is no bias or systematic error in the Duke analysis relative to those of the four laboratories.

Evans et al. (1) used freshwater museum fish to demonstrate the increase in mercury that took place in fish from Lake St. Clair and western Lake Erie after 1945 when chloralkali plants started operation, but Gibbs et al. (20) pointed out the possibility of trace metal contamination of museum specimens using fish from the U.S. National Museum of Natural History. Although this museum is the source we used for our museum fish, there is an important difference between our study and that of Gibbs et al. (20). They used myctophids, small ocean fish that were 10 times smaller in weight than the smallest *Antimora rostrata* we analyzed and about 100 times smaller than the largest *Antimora rostrata*. The much greater surface to mass ratio of the small fish increases the possibility of external contamination of the axial muscle. A second point to note is that Gibbs et al. (20) found relatively large changes in lead, copper, and zinc, with lead being elevated 100-fold in the 1880s myctophids, but they found little change in mercury.

The first step in our investigation of contamination consisted of determining if the mercury concentration in old fish varied in a systematic manner with length, weight, or age as it does in recent fish that have not been stored

in a preservative (1, 5-9, 21); we found that mercury did vary systematically in the old fish, and the nature of the relationship was that longer fish had higher mercury concentrations. Mercury concentration in the old fish has a higher correlation with increasing length than it does with age or weight; Olsson (21) also found this in the fish he studied, and he provides a physiological explanation for this condition. Linear, quadratic, and exponential regression equations were tested for fit to the mercury concentration vs. length data from the old fish. An exponential relationship of the form

$$y = ae^{bx} \quad (1)$$

where y = mercury concentration in micrograms per gram (wet weight) and x = standard length of the fish in centimeters gave the best fit with a correlation coefficient of $r^2 = 0.56$ for the old fish and $r^2 = 0.81$ for the recent fish. The equations for the two samples were for 1880s fish

$$\text{Hg} = 0.07e^{0.06(\text{length})} \quad (2)$$

and for 1970s fish

$$\text{Hg} = 0.04e^{0.06(\text{length})} \quad (3)$$

The mercury vs. length correlation was highly significant ($p < 0.001$) in both samples. Contamination from containers, labels, or preserving fluids would enter fish by diffusion through the skin and gut, a process regulated by a surface to mass relationship. Small specimens with a greater surface to mass ratio would acquire more mercury per unit weight than larger fish. The positive values for the regression slopes in eq 2 and 3 show that the highest concentrations of mercury are in the largest fish, those with the smallest surface to mass ratio; this pattern is the opposite of the pattern that would result if mercury concentrations were determined by contamination.

Further evidence for absence of contamination of the museum fish is provided by the similarity of mercury vs. length slopes, 0.06 in eq 1 and 2, in the recent and old fish despite the difference in how the two samples of fish were handled between capture and analysis. Contamination by diffusion would not reproduce in museum fish a mercury vs. length slope that is quantitatively the same as that in recent fish that have never been exposed to containers, labels, or preserving fluids. These results together with the results of Gibbs et al. (20) show that the time series comparisons of museum fish are valid when the species of fish is relatively large and the trace metal or interest is mercury rather than lead, copper, or zinc.

The initial question this analysis addressed is whether recent fish have elevated mercury concentrations relative to the century-old fish. If industrial activity has increased mercury levels in deep-sea fish during the last century, the mercury vs. length regression line for the 1970s fish will lie above values for the 1880s fish; that is, recently collected fish of a given length should have a higher concentration than a fish of the same length collected in the 1880s. This comparison is made by examining the relative position of regression lines that characterize the two samples. A linear transform of the mercury vs. length relationship as shown in Figure 2 makes this comparison straightforward; Figure 2 shows that the line for the recent fish does not lie above the line for the old fish. Recent fish of a given length do not contain more mercury than fish of the same length collected in the 1880s.

A more formal test of the hypothesis that there has been an increase in mercury in the last century can be carried out by analysis of covariance (ANCOVA) on the combined data of the two samples of fish (19). The results of the analysis of covariance are given in Table II, and they are

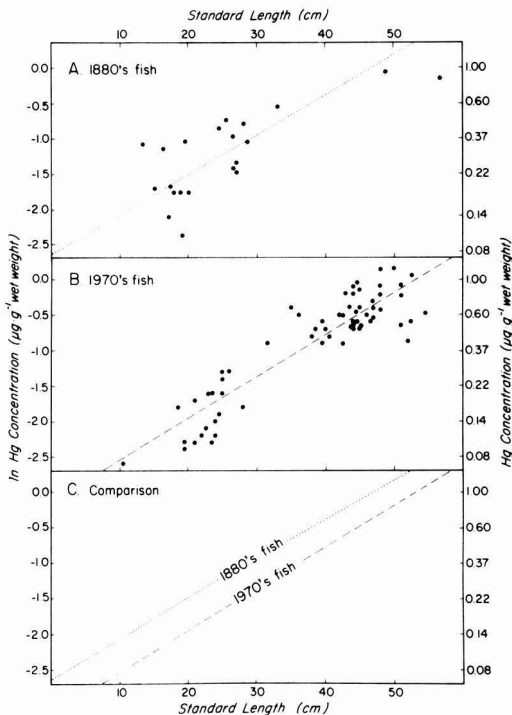


Figure 2. Linear regression analysis of the natural logarithm of mercury concentration vs. length in the deep-sea fish *Antimora rostrata*. (A) Fish collected in the 1880s; (B) fish collected in the 1970s; (C) comparison of regression lines for the 1880s fish and 1970s fish.

Table II. Analysis of Covariance of Mercury Concentration and Length in Century-Old and Recent Deep-Sea Fish

source of variation	degrees of freedom	sum of squares	mean square	F value
model	2	33.42	16.71	139.37
error	84	10.07	0.12	
corrected total	86	43.49		

significant at $\alpha = 0.0001$ ($r^2 = 0.77$). The length-adjusted mean mercury concentration for the recent fish was lower ($0.34 \mu\text{g}\cdot\text{g}^{-1}$ wet weight) than that in century-old fish ($0.51 \mu\text{g}\cdot\text{g}^{-1}$ wet weight). Thus, the hypothesis that there has been an increase must be rejected; that is, mercury in these deep-sea fish as not increased in the last century.

Discussion

A corollary of the finding that mercury has not increased in the 20th century is that contemporary concentrations higher than the U.S. Food and Drug Administration action level of $1.0 \mu\text{g}\cdot\text{g}^{-1}$ wet weight (19) can be natural occurrences in ocean fish. Mercury concentrations exceeding the U.S. Food and Drug Administration action level are common in marine fishes and mammals (4), and these elevated concentrations have been interpreted as evidence that the entire ocean food chain is polluted with mercury from industrial sources (22). Our results indicate that this interpretation of elevated mercury concentration is probably incorrect.

In freshwater and estuarine environments where point source industrial contamination has occurred, the elimi-

nation of mercury discharges to the environment has been successful in improving environmental quality. The worse situations, such as Minamata Bay, have improved dramatically (12), and time series comparisons from freshwater environments (2, 21, 23) have shown significant improvements whenever discharges from chloralkali plants or pulp mills were controlled. Sediment cores from Saguenay Fjord in Quebec show an increase in mercury in strata deposited annually after the startup of a chloralkali plant in 1948 and a subsequent decrease in sediment mercury after the plant complied with mercury-limiting regulations imposed in 1971 (2). Similarly, nine species of the most common fish in Canada's Lake St. Clair have shown a highly significant decrease in mercury concentration during the period between 1970 and 1980 after two chloralkali plants on Lake St. Clair were shut down (23). Time series studies from Europe (21) as well as those from North America (2, 23) show repeatedly that the elimination of industrial discharges of mercury is a cost-effective regulation that improves environmental quality of rivers, lakes, and estuaries that had been receiving mercury discharges. However, the results described here for deep-sea fish and those of Miller et al. (3) with surface-dwelling species indicate that in the ocean, elevated mercury concentrations in fish are natural phenomena that have persisted without change from the late 19th century. The conclusion we reach is that potentially harmful concentrations (24) of mercury in marine fish can occur naturally and are not the result of anthropogenic contamination.

Acknowledgments

We thank Sheryan Epperly of the North Carolina Division of Marine Fisheries, Morehead City, NC, for performing the statistical analyses and for help in interpreting the results of the analyses. D.M.C. selected appropriate specimens of *Antimora rostrata* from museum collections while he was a member of the National Marine Fisheries Service stationed in the U.S. National Museum of Natural History. We acknowledge the cooperation and assistance of both organizations.

Supplementary Material Available

Length and mercury concentration data for the recent and century-old fish as well as the mercury concentration intercalibration data (3 pages) will appear following these pages in the microfilm edition of this volume of the journal. Photocopies of the supplementary material from this paper or microfiche (105 × 148 mm, 24× reduction, negatives) may be obtained from Microforms Office, American Chemical Society, 1155 16th St., N.W., Washington, DC 20036. Full bibliographic citation (journal, title of article, author, page number) and prepayment, check or money order for \$6.00 for photocopy (\$8.00 foreign) or \$6.00 for microfiche (\$7.00 foreign), are required.

Registry No. Hg, 7439-97-6.

Literature Cited

- (1) Evans, R. J.; Bails, J. D.; D'Itri, F. M. *Environ. Sci. Technol.* **1972**, *6*, 901-905.
- (2) Smith, J. H.; Loring, D. H. *Environ. Sci. Technol.* **1981**, *15*, 944-951.
- (3) Miller, G. E.; Grant, P. M.; Kishore, R.; Steinkruger, F. J.; Rowland, F. S.; Guinn, V. P. *Science (Washington, D.C.)* **1972**, *175*, 1121-1122.
- (4) National Research Council "An Assessment of Mercury in the Environment"; National Academy of Sciences: Washington, DC, 1978.
- (5) Barber, R. T.; Vijayakumar, A.; Cross, F. A. *Science (Washington, D.C.)* **1972**, *178*, 636-639.
- (6) Cross, F. A.; Hardy, L. H.; Jones, N. Y.; Barber, R. T. *J. Fish. Res. Board Can.* **1973**, *30* (9), 1287-1291.
- (7) Cutshall, N. H.; Naidu, J. R.; Pearcy, W. G. *Science (Washington, D.C.)* **1978**, *209*, 1489-1491.
- (8) Johnels, A. G.; Westermark, T. "Chemical Fallout"; Miller, M. W.; Berg, G. G., Eds.; Charles C. Thomas Publisher: Springfield, IL, 1969.
- (9) Bache, C. A.; Gutenmann, L. J.; Lisk, L. J. *Science (Washington, D.C.)* **1971**, *172*, 951.
- (10) Wenner, C. A.; Musick, J. A. *J. Fish. Res. Board Can.* **1977**, *34*, 2362-2368.
- (11) Small, G. J. *Proc. Calif. Acad. Sci.* **1981**, *42*, 341-348.
- (12) Goldberg, E. D. In "Impact of Man on the Coastal Environment"; Duke, T. W., Ed.; U.S. Environmental Protection Agency: Washington, DC, 1982.
- (13) Barber, R. T.; Warlen, S. M. *Environ. Sci. Technol.* **1979**, *13*, 1146-1148.
- (14) Iwamoto, T. *Comp. Biochem. Physiol. B* **1975**, *52B*, 7-11.
- (15) U.S. Environmental Protection Agency "Manual of Methods for Chemical Analysis of Water and Wastes"; National Environmental Research Center: Cincinnati, OH, 1974; EPA-625/6-74-003.
- (16) Parker, R. R. *J. Fish. Res. Board Can.* **1963**, *20* (6), 1441-1445.
- (17) Hile, R. *Bull. U.S. Bur. Fish.* **1936**, *48*, 211-317.
- (18) Kennedy, D. *Fed. Regist.* **1979**, *44* (14), 3990-3993.
- (19) SAS Institute, Inc. "Statistical Analysis Systems (SAS) Users Guide"; SAS Institute, Inc.: Cary, NC, 1982.
- (20) Gibbs, R. H., Jr.; Jarosewich, R. E.; Windom, H. L. *Science (Washington, D.C.)* **1974**, *184*, 475-477.
- (21) Olsson, M. *Ambio* **1976**, *5*, 73-76.
- (22) Beary, J. F. *Science (Washington, D.C.)* **1979**, *206*, 1260.
- (23) Ogilvie, D. M. *Ambio* **1981**, *10*, 350-351.
- (24) Turner, M. D.; Marsh, D. O.; Smith, J. C.; Inglis, J. B.; Clarkson, T. W.; Rubio, C. E.; Chiriboga, J.; Chiriboga, C. *Arch. Environ. Health* **1980**, *35*, 367-378.

Received for review September 22, 1983. Accepted January 4, 1984. Shiptime on R/V EASTWARD for the collection of recent deep-sea fish was supported by the National Science Foundation; research support was by NSF Grant OCE 75-23722 to R.T.B. and NIEHS Center Grant ESO-1908 to J. Bonaventura.

Effects of Temperature and Pressure on the Photochemical Reactivity of a Representative Aviation Fuel

William P. L. Carter,* Roger Atkinson, and Arthur M. Winer

Statewide Air Pollution Research Center, University of California, Riverside, California 92521

■ A series of NO_x /air irradiations of the widely used military jet fuel JP-4 have been carried out in the SAPRC 5800-L evacuable, thermostated chamber in order to evaluate the effects of temperature and pressure on the potential for photochemical oxidant formation from in-flight dumping of this fuel. Irradiations were carried out under simulated atmospheric conditions at ground level and 10000- and 20000-ft altitude, and additional irradiations were carried out in which temperature (272-303 K) and pressure (350-735 torr) were varied separately. The maximum O_3 yields were found to decrease with increasing simulated altitude or with decreasing temperature while the NO oxidation rates decreased with increasing pressure and with decreasing temperature. However, after correction for the effect of temperature on the chamber radical source, the NO oxidation rates were found to be relatively insensitive to temperature, implying that if this chamber radical source is absent in the open atmosphere (which is not known), then the NO oxidation rate caused by JP-4 will increase with altitude.

Introduction

Military jet aircraft flight procedures make it necessary to jettison excess fuel at various altitudes, and these fuel expulsions can be sizable (on the order of 5000 lb min^{-1}) (1). Along with the oxides of nitrogen ($\text{NO} + \text{NO}_2 = \text{NO}_x$) formed in the exhaust, such fuel dumping can represent a significant perturbation of atmospheric concentrations of hydrocarbons and NO_x , relative to their low background levels (2-8). Moreover, in the presence of sunlight the jettisoned fuel is expected to react with the NO_x emitted from the exhaust, causing the formation of ozone and other constituents of photochemical smog.

However, at the elevated altitudes for these fuel dumping procedures [generally between 5000 and 30000 ft (1)], both the temperature and the pressure are considerably lower than at ground level. Thus, for example, at 10000-ft altitude the temperature and pressure are (9, 10) ~ 245 -285 K and ~ 500 -535 torr, respectively, while at 20000-ft altitude the temperature and pressure are ~ 230 -265 K and ~ 330 -365 torr, respectively. Furthermore, with increasing altitude the solar flux increases in intensity, with a corresponding shift toward a shorter wavelength cutoff (11, 12), leading to enhanced photochemical activities (13, 14).

Although a large amount of experimental and computer modeling work has been carried out on various aspects of photochemical air pollution at ground level, including studies of representatives of the various classes of organic compounds present in the jet fuels (15-22) and of the jet fuels themselves (23), there is no information available concerning the chemical transformations of these fuels in the presence of NO_x under atmospheric conditions representative of those at elevated altitudes.

In order to evaluate the combined effects of temperature and pressure on the potential of such fuels to cause photochemical oxidant formation, a series of NO_x /air irradiations of JP-4, a widely used military jet fuel (1), were carried out in the SAPRC 5800-L evacuable, thermostated environmental chamber with temperatures, total pressure,

and light intensity varied between values appropriate for ground level and those for 20000-ft altitude.

Experimental Section

The experimental techniques and procedures employed are described in detail elsewhere (24). Irradiations of JP-4/ NO_x /air and NO_x /air mixtures were carried out in a 5800-L Teflon-coated evacuable, thermostated environmental chamber with a 25-kW solar simulator (25). For the irradiations simulating 0° zenith angle (see below), a 0.64 mm thick Pyrex pane was used to match the solar simulator spectral distribution to that of sunlight in the lower troposphere. For the irradiation simulating a 70° zenith angle, a further 0.32 mm thick Pyrex pane was also inserted (24).

Prior to each run the chamber was evacuated to $\leq 2 \times 10^{-5}$ torr. For the majority of the experiments the chamber was initially filled to ~ 10 torr total pressure with dry N_2 , and then NO and NO_2 were flushed into the chamber from a ~ 5 -L Pyrex bulb attached to a vacuum gas handling system by a stream of ultrahigh purity nitrogen. For the experiments for which this injection procedure was not used, the NO and NO_2 were flushed into the chamber from the ~ 5 -L Pyrex bulb by a stream of ultrahigh purity N_2 either during or after filling the chamber with pure air. The NO was purified by passage through a trap containing activated Linde Molecular Sieve 13X, while NO_2 was prepared by reaction of this purified NO with O_2 which had also been passed through activated Molecular Sieve 13X.

The jet fuel JP-4 (petroleum derived; supplied by the Fuels Branch, Fuels and Lubrication Division, Aero-Propulsion Laboratory, Wright-Patterson Air Force Base, OH) was injected by using procedures previously developed for this purpose (23). The desired quantity of the liquid fuel (ranging from 21 μL for 5 ppm of C to 430 μL for 100 ppm of C in the chamber) was placed in an ~ 1 -L Pyrex bulb, fitted with high-vacuum greaseless stopcocks. The bulb was then flushed with N_2 at a flow rate of 5 L min^{-1} for ~ 15 min, while being heated with a heat gun. After this time all of the liquid fuel had disappeared, and tests showed that reasonably complete and reproducible injections were obtained by using this technique (24).

The chamber was filled with purified matrix air (26) to the desired pressure. For two runs the diluent gas was a synthetic N_2/O_2 mixture where the requisite pressures of ultrahigh purity N_2 and O_2 were introduced into the chamber from cylinders. Mixing of the reactants was assured by means of two mixing fans, which were turned off during the irradiations. During the irradiations the temperature of the irradiated mixture was maintained as the desired value by means of the chamber's heating/cooling system (25).

Control experiments (27, 28), consisting of NO_x /air irradiations with ~ 10 ppb each of propane and propene tracers, were interdispersed among the fuel/ NO_x /air runs. The NO and NO_2 were injected as described above, while the desired amounts of the tracers were introduced into the chamber from the vacuum gas handling system or by injection using all-glass, gas-tight syringes.

The parameters monitored and the methods employed were the following: O₃ by chemiluminescence (Monitor Labs Model 8410) and, for runs at 740 torr total pressure, ultraviolet absorption (Dasibi Model 1003AH); NO and NO_x by chemiluminescence (Thermo Electron Model 14B); light intensity and spectral distribution by an absolute radiometer (EG&G Model 550) and by a double monochromator-photomultiplier combination, respectively (24); HCHO using an improved chromatographic acid technique (16). The absolute light intensity was determined periodically by using the rate of photolysis of NO₂ in N₂ to determine *k*₁, the NO₂ photodissociation rate constant (16, 24). The chemiluminescent monitoring instruments for NO, NO_x, and O₃ were calibrated for operation at reduced pressure by introducing known pressures of these gases into the evacuable chamber at the desired total pressures (24).

The ≥C₅ fuel components were monitored by capillary column gas chromatography employing a 30-m SE-52 coated fused silica capillary column. The procedure for injecting the gas sample onto the capillary column was similar to that described previously (23). A 100-mL gas sample was flushed through an ~10-cm³ silylated Pyrex loop, and the contents of this loop were then transferred over a 12-min time span to the head of column, which was held at 183 K. The GC oven temperature was raised to 223 K over a 1.5-min time period and then temperature programmed from 223 to 473 K at 8 K min⁻¹. This system was capable of monitoring most of the individual C₅-C₁₃ components of the JP-4 fuel.

Peroxyacetyl nitrate (PAN) was monitored during the irradiations by gas chromatography with electron capture detection using an 18 in. × 0.125 in. Teflon column of 5% Carbowax 400 on Chromasorb G (80/100 mesh), operated at ambient temperature (16).

For the NO_x/air irradiations, the propane and propene tracers were monitored by using a 34 ft × 0.125 in. stainless steel column of 10% 2,4-dimethylsulfolane on C-22 Firebrick held at 273 K (16). Background concentrations of ≥C₂ oxygenates and C₁ and C₂ hydrocarbons in the matrix air were monitored by gas chromatography (16) prior to fuel injection. However, the long retention times of the fuel components precluded the use of these columns during the fuel/NO_x/air irradiations.

In order to investigate the photochemical reactivity of JP-4 under conditions pertaining to elevated altitudes, the following sets of experiments were carried out: (a) irradiations of JP-4/NO_x/air mixtures under temperature and pressure conditions designed to simulate ground level and 10 000- and 20 000-ft altitude, with the relative light intensities and spectral distributions (see above) being adjusted to correspond to these altitudes at a zenith angle of 0°; (b) an additional irradiation of a JP-4/NO_x/air mixture (100 ppm of C for JP-4, 0.5 ppm of NO_x) at simulated 20 000-ft altitude with the light intensity and spectral distribution adjusted to correspond, on a relative basis, to a zenith angle of 70°; (c) a set of JP-4/NO_x/air irradiations at constant light intensity as a function of total pressure at 303 K and as a function of temperature at 740 torr total pressure. The temperatures and pressures chosen were those used in the various simulated altitude experiments (i.e., ~265, 284, and 303 K and 350, 500, and 740 torr total pressure). These latter runs were designed to determine the effect of independently varying the total pressure and temperature on the photochemical reactivity of JP-4.

For the fuel/NO_x/air irradiations simulating ground level, the pure matrix air (26) was humidified to ~50%

relative humidity in order to approximate ambient atmospheric conditions. For the irradiations simulating 10 000- and 20 000-ft altitudes, and for the set of irradiations in which temperature and pressure were varied independently, dry (≤5% relative humidity based on 300 K) matrix air or cylinder O₂ and N₂ were used as the diluent gases.

We have previously shown that chamber radical sources are significant in this and other environmental chambers (27, 28). Hence, in order to interpret the results of the fuel/NO_x/air irradiations (see Discussion), it was necessary to measure the chamber radical source strengths during this work. Therefore, a series of organic tracer/NO_x/air irradiations were interdispersed among the fuel/NO_x/air runs, with the NO_x levels and reaction conditions (temperature, pressure, humidity, and lighting conditions) chosen to be the same as those in the corresponding fuel runs. As discussed in detail elsewhere (28), the OH radical levels can be calculated from the rate of change of the organic tracers, and the radical input rate, *R*_{in}, can be calculated on the basis of the fact that the rate of initiation and termination must balance.

Since in NO_x/air irradiations, after HONO reaches steady state, essentially all the net radical termination is due to the reaction



[the reactions of the low levels of organic tracer have a negligible perturbation on radical initiation and termination in this system (27, 28)], then

$$R_{\text{in}} \approx k_1[\text{OH}][\text{NO}_2] \quad (1)$$

Known radical sources in NO_x/air irradiations, other than HONO photolysis, are negligible (22, 28), and thus, values of *R*_{in} measured after 1 h of irradiation, when any initially present HONO will have achieved steady state, yield the chamber radical source (which is presumed also to be present in the corresponding fuel/NO_x/air irradiations). The radical input rates observed in these experiments were within the range previously observed for the SAPRC evacuable chamber (28).

It should be noted that in addition to measuring the radical source, NO_x/air irradiations are also useful for determining whether there is any significant contamination by reactive organics, since such contamination causes excess rates of NO oxidation over those expected from the known species present. In all cases, the NO oxidation rates observed were also within the range previously observed in the SAPRC evacuable chamber (28), indicating that offgassing of reactive organics or contamination by the fuel from previous runs was not significant in these experiments.

Results

Detailed data tabulations for all of the fuel/NO_x/air and the NO_x/air runs performed in this study are given in ref 24. Selected relevant results of the simulated ground level and 10 000- and 20 000-ft JP-4/NO_x/air runs are summarized in Table I, and selected results of those experiments where the temperature and pressure were varied separately are given in Table II. The specific results summarized include the maximum ozone concentration and the time at which the maximum occurred (for those runs where a maximum ozone level was reached), the NO oxidation rate (-d[NO]/dt) observed in the first hour of the irradiation, and the average OH radical concentration observed in these runs, estimated from the relative rates of decay of *o*-xylene and *n*-hexane. For comparison purposes, the OH

Table I. Photochemical Reactivity of JP-4/NO_x/Air Irradiations at Simulated Ground Level and 10000- and 20000-ft Altitude and Selected Results of Associated NO_x/Air Irradiations

EC run no.	nominal initial concn		O ₃ maximum ^a		approx estimated ^b [OH], ×10 ⁻⁶ cm ⁻³	-d[NO]/dt (0-60 min), ppb min ⁻¹	(-d[NO]/dt)/R _u ^c (0-60 min)	associated NO _x /air ^d		
	fuel, ppm of C	NO _x , ppm	concn, ppm	time, h				EC run no.	[OH], ×10 ⁻⁶ cm ⁻³	R _u , ppb min ⁻¹
(A) Simulated Ground Level (740 torr, 303 K, 50% RH, k _{NO₂} = 0.33 min ⁻¹) ^e										
489	50	0.5	0.47	5.25	0.4	4.7	21	488	2.5	0.23
492	50	0.5	0.52	5.0		4.5	21	493	1.9	0.17
515	100	0.5	0.61	3.0	~0.0	6.4	28	514	2.7	0.24
491	5	1.0	-	>6.0	1.0	1.8	8			
490	50	1.0	-	>6.0	0.6	5.2	20			
(B) Simulated 10000 ft (500 torr, 284 K, ≤5% RH, k _{NO₂} ≈ 0.44 min ⁻¹) ^e										
506	50	0.5	-	>6.0	0.3	3.4	43	505	1.4	0.09
509	100	0.5	0.42	6.0	0.1	4.2	54	511	1.1	0.07
510	100	0.5	0.45	≥6.0	0.5	4.5	56			
508	50	1.0	-	>6.0	0.8	2.9	29	507	0.6	0.10
(C) Simulated 20000 ft (350 torr, 265 K, ≤5% RH, k _{NO₂} ≈ 0.47 min ⁻¹) ^e										
498	50	0.5	-	>6.0	0.3	1.8	36	496	1.0	0.05
502	50	0.5	-	>6.0	0.1	1.8	36	503	1.2	0.05
500	100	0.5	-	>6.0	0.2	3.8	76			
517	50	1.0	-	>6.0	~0.0	2.6	52	499	0.5	0.05
(D) Simulated 20000 ft, 70° Zenith Angle (350 torr, 265 K, ≤5% RH, k _{NO₂} ≈ 0.35 min ⁻¹) ^e										
517	50	0.5	-	>6.0	~0.0	1.3	43	518	0.6	0.03

^a Time given is to the nearest 0.25 h. (-) indicates no maximum O₃ yield attained during the irradiation. ^b Estimated from slope of plot of d(ln [o-xylene]/[n-hexane])/dt using k(OH + o-xylene) = 1.5 × 10⁻¹¹ cm³ molecule⁻¹ s⁻¹ and k(OH + n-hexane) = 1.7 × 10⁻¹¹ exp [-650/(RT)] cm³ molecule⁻¹ s⁻¹ (29). The uncertainty in absolute concentrations is approximately ±0.5 × 10⁶ cm⁻³. ^c R_u = radical input rate, taken from the results of the associated NO_x/air irradiations, except for the simulated ground level runs, where R_u was taken from regressions of plots of R_u vs. [NO₂]_{avg} using a much larger set of NO_x/air irradiations (28). ^d For a more complete summary of the results of these runs, see ref 24. ^e Nominal pressure, temperature, humidity, and NO₂ photolysis rate, respectively.

Table II. Photochemical Reactivity of JP-4 (100 ppm of C)/NO_x (0.5 ppm)/Air (≤5% RH) Mixtures as a Function of Temperature and Pressure and Selected Results of Associated NO_x/Air Irradiations

EC run no.	temp, K	pressure, torr	O ₃ maximum ^a		approx estimated ^b [OH], ×10 ⁻⁶ cm ⁻³	-d[NO]/dt (0-60 min), ppb min ⁻¹	(-d[NO]/dt)/R _u ^c (0-60 min)	associated NO _x /air ^d		
			concn, ppm	time, h				EC run no.	[OH], ×10 ⁻⁶ cm ⁻³	R _u , ppb min ⁻¹
587	272	740	-	>6.0	0.7	1.0	33	586	0.4	0.03
588	285	740	-	>6.0	0.7	4.7	59	584	0.8	0.08
575	303	740	0.72	2.5	~0.0	6.4	40	574	1.9	0.16
578	303	500	0.58	2.5	0.3	11 ^e	105	577	1.8	0.10
580	303	350	0.51	2.25	0.4	15 ^f	132	579	1.8	0.11
581	303	350 ^g	0.42	2.5	0.2	13 ^f	139	582 ^g	1.7	0.07

^a Time given is to the nearest 0.25 h. (-) indicates no maximum O₃ yield attained during the irradiation. ^b Estimated from slope of plot of d(ln [o-xylene]/[n-hexane])/dt using k(OH + o-xylene) = 1.5 × 10⁻¹¹ cm³ molecule⁻¹ s⁻¹ and k(OH + n-hexane) = 1.7 × 10⁻¹¹ exp [-650/(RT)] cm³ molecule⁻¹ s⁻¹ (29). The uncertainty in absolute concentrations is approximately ±0.5 × 10⁶ cm⁻³. ^c R_u = radical input rate, taken from the results of the associated NO_x/air irradiations except for the simulated ground level runs, where R_u was taken from regressions of plots of R_u vs. [NO₂]_{avg} using a much larger set of NO_x/air irradiations (28). ^d For a more complete summary of the results of these runs, see ref 24. ^e For t = 0-45 min only; significant O₃ formation occurred after 45 min. ^f For t = 0-35 min only; significant O₃ formation occurred after 30 min. ^g 200 torr of N₂ + 150 torr of O₂ used instead of air.

radical levels and the radical input rates for the corresponding NO_x/air control irradiations are also given in these tables.

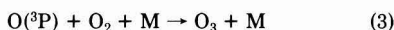
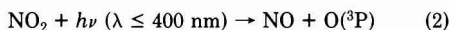
The experimental data shown in Table I indicate that the observed reactivities of the fuel/NO_x/air mixtures in the SAPRC 5800-L environmental chamber, whether measured by the ultimate ozone yields or by the initial rate of oxidation of NO, decreased significantly with increasing simulated altitude, despite the fact that the overall light intensity increased. The results shown in Table II indicate that temperature was the dominant effect causing this result, since all aspects of reactivity decreased significantly when the temperature was decreased at constant pressure. On the other hand, when the pressure was decreased at a constant temperature, the NO oxidation rate actually increased, although the maximum ozone yield decreased

slightly. However, it should be noted that chamber effects, particularly the chamber radical source, must be taken into account in interpreting these results. This is discussed in the following section.

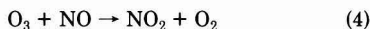
Discussion

The release and dispersion characteristics of aircraft fuels at high altitudes or near ground level has been discussed in detail by Clewell (1). These fuel releases may have a number of potentially significant atmospheric impacts in addition to ozone formation, such as the formation of toxic organic oxidation products and/or aerosol production (23). However, in this discussion we shall only consider reactivity relative to ozone formation and NO oxidation rates, since these are the only aspects of reactivity which our present data address.

The direct cause of the formation of ozone in atmospheric systems is the photolysis of NO₂

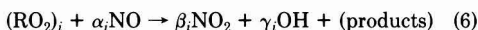
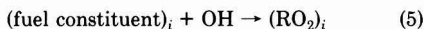


and there are no other significant primary sources of O₃. Since O₃ reacts rapidly with NO

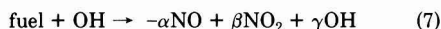


then at the photostationary state the O₃ yield is determined by the [NO₂]/[NO] ratio. Hence, processes which consume NO or convert NO to NO₂ are responsible for O₃ formation in these systems.

The major constituents of the fuel studied here are the higher alkanes and aromatics (23), with (23) ~19% aromatic hydrocarbons, the remainder being straight chain, branched, and cyclic alkanes. These alkanes and aromatic hydrocarbons are consumed in the atmosphere almost exclusively by reaction with hydroxyl radicals (29). The mechanisms for the atmospheric reactions of alkanes (18, 22) and aromatics (21, 22) are rather complex and, particularly for the aromatics, somewhat uncertain. However, the major overall processes for both types of fuel constituents can be represented as indicated below:



where α_i , β_i , and γ_i are stoichiometric coefficients for the *i*th fuel component. Therefore, to a reasonably good approximation, the overall process for the whole fuel can be represented as follows:



where α is the efficiency of the fuel in oxidizing NO, thus causing O₃ formation, $\alpha - \beta$ is its efficiency in removing active NO_x from the system, which has the effect of decreasing the maximum amount of O₃ which will be formed, and $1 - \gamma$ is the efficiency of the fuel in removing radicals from the system, which, if significant, will tend to decrease the overall rates of fuel consumption, NO oxidation, and O₃ formation.

One important aspect of reactivity concerns the tendency of the reactions of the fuel to either inhibit or enhance radical levels. In particular, if the fuel components are oxidized to a significant extent to form species that undergo rapid photodissociation to form radicals, or that react with ozone to form radicals, then γ may be greater than unity. Thus, in principle it is possible for a fuel to enhance radical levels, and for example, toluene and other aromatics present in these fuels are known to form products that rapidly photolyze to produce radicals (21, 22, 30); this obviously tends to lead to higher radical levels. On the other hand, alkyl nitrate formation via the radical-terminating reaction



is known to be important in the NO_x/air photooxidations of the heavier alkanes present in these fuels (31, 32), and this tends to lead to reduced radical levels. Since JP-4 contains both aromatics and heavier alkanes (1, 23), it is difficult to predict, a priori, which of the above effects will be more important.

The estimated average OH radical levels observed in the JP-4/NO_x/air irradiations (Tables I and II) are highly scattered but can be seen in most cases to be ~2-10 times lower than those observed in the corresponding NO_x/air

irradiations carried out with the same initial NO_x levels and reaction conditions (temperature, pressure, etc.). It can therefore be concluded that the presence of JP-4 in NO_x/air mixtures leads to values of γ significantly less than unity. The data in Table II also suggest that this suppression of radical levels becomes less important at lower temperatures and more important at higher pressures. However, the OH radical levels in the fuel runs are suppressed to such low values that their concentrations are uncertain by at least a factor of 2, and any conclusions concerning the precise values of γ , or the effect of temperature and pressure on this parameter, must be considered to be highly uncertain.

A more precise indication of the effect of temperature and pressure on the reactivity of the fuels can be obtained by examining their effects on the initial rates of NO oxidation, $-d[\text{NO}]/dt$, which are also summarized in Tables I and II. It can be seen from Table I that these NO oxidation rates depend on the initial reactant concentrations but in general decrease with increasing simulated altitude. Table II shows that these rates decrease significantly as the temperature is reduced but increase with decreasing pressure. Since the NO oxidation rates decrease slightly with increasing simulated altitude, it is obvious that the effect of decreasing temperature dominates those due to pressure and increased light intensity, at least for the SAPRC evacuable chamber.

However, this observed effect of temperature on the NO oxidation rate may be primarily due to the effect of temperature on the chamber-dependent radical input rate (28), and this effect must be considered when analyzing the results of these experiments concerning the reactivity of these fuel/NO_x mixtures in the ambient atmosphere, where such chamber radical sources are presumably absent.

An approximate correction for the effect of the chamber radical source on the NO oxidation rates can be made as described below. If (a) the fuel is considered to consist of a single compound which reacts with OH radicals with a rate constant of k_f according to reaction 7, (b) reaction of the fuel is assumed to be the major cause of NO oxidation, and (c) only the initial period of the irradiation when $[\text{NO}] \gg [\text{O}_3]$ (and thus NO oxidation is manifested primarily by NO consumption rather than O₃ buildup) is considered, then

$$-d[\text{NO}]/dt \approx \alpha k_f [\text{fuel}][\text{OH}] \quad (\text{II})$$

If it is further assumed that the major radical source in these fuel/NO_x/air irradiations is the chamber radical source, which has been shown to be linearly dependent on light intensity (27, 28) and is represented by



(which occurs with a rate of R_u), and that the major radical sink, other than reactions of the fuel components (reaction 7), is via the reaction of OH radicals with NO₂ (reaction 1), then a steady-state analysis yields

$$[\text{OH}] \approx \frac{R_u}{k_1[\text{NO}_2] + (1 - \gamma)k_f[\text{fuel}]} \quad (\text{III})$$

Hence

$$\frac{-d[\text{NO}]/dt}{R_u} \approx \frac{\alpha k_f [\text{fuel}]}{k_1 [\text{NO}_2] + (1 - \gamma)k_f [\text{fuel}]} \quad (\text{IV})$$

$$\frac{-d[\text{NO}]/dt}{R_u} \approx \left[\frac{1 - \gamma}{\alpha} + \frac{k_1 [\text{NO}_2]}{\alpha k_f [\text{fuel}]} \right]^{-1} \quad (\text{V})$$

Equation V shows that the initial NO oxidation rate can

be normalized by dividing by the chamber-dependent radical input rate (obtained from the corresponding NO_x/air irradiations) to obtain a quantity that does not depend on chamber effects but rather depends only on the fuel reactivity parameters α , γ , and k_t and the $[\text{NO}_2]/[\text{fuel}]$ ratio. Unfortunately, our data are insufficient to derive $(1 - \gamma)/\alpha$ and $k_1/(\alpha k_t)$ from eq V by plotting $[(-d[\text{NO}]/dt)/R_u]^{-1}$ vs. $[\text{NO}_2]/[\text{fuel}]$. However, the use of eq IV and V allows the effect of the chamber radical source to be factored out, at least approximately, as discussed below.

Since it is observed that the fuel significantly suppresses OH radical levels below those in NO_x/air irradiations, eq IV and V can be further simplified. Since $\gamma < 1$, when the fuel concentration is sufficiently high, the majority of the OH radical termination in the fuel/ NO_x/air runs occurs via OH radical reaction with the fuel components. Thus, $(1 - \gamma)k_t[\text{fuel}] \gg k_1[\text{NO}_2]$ and

$$\frac{-d[\text{NO}]/dt}{R_u} \approx \frac{\alpha}{1 - \gamma} \quad (\text{VI})$$

Hence, at sufficiently high fuel concentrations the normalized NO oxidation rate, $(-d[\text{NO}]/dt)/R_u$, depends only on the efficiency of the fuel in oxidizing NO and removing radicals.

The normalized NO oxidation rates derived from the fuel/ NO_x/air irradiations carried out in this study are summarized in Tables I and II. Since the radical input rates generally exhibit a $\pm 50\%$ scatter, these quantities must be considered to be uncertain by at least that amount. Despite these uncertainties, Table I indicates that the efficiency of JP-4 in oxidizing NO increases with the $[\text{fuel}]/[\text{NO}_x]$ ratio, as predicted by eq V. Table I also indicates a progressive increase in the efficiency of JP-4 in oxidizing NO upon going from simulated ground level to simulated altitudes of 10 000 and 20 000 ft.

The effects of total pressure and of temperature, when varied independently of each other, on the NO oxidation rate can be obtained from the data given in Table II. The results of EC runs 575, 588, and 587 reveal that the normalized NO oxidation efficiency does not depend strongly on temperature and that the strong temperature dependence of the overall reactivity observed in our chamber experiments must be due almost entirely to the temperature dependence of the chamber radical source. This suggests that in the atmosphere, in the absence of chamber effects, the rate of ozone formation from fuel/ NO_x/air mixtures may be relatively insensitive to temperature, contrary to conclusions derived from our data without due consideration of the role of chamber effects.

The data in Table II further show that the NO oxidation efficiency of JP-4 increases significantly with a decrease in pressure. This can be attributed in part to the fact that radical termination from the reaction



which is important in the oxidation of heavier alkane fuel constituents (31), becomes less important as the total pressure decreases (32). The increased efficiency of NO oxidation at lower pressures may also be due in part to decreased radical termination due to the reaction of OH radicals with NO_2 (reaction 1) at lower pressures. However, this cannot be the only factor since k_1 decreases only by a factor of ~ 1.4 in going from 735 to 350 torr (22), while the normalized NO oxidation rate increases by a factor of > 2 under those conditions, and in any case eq VI predicts that the normalized NO oxidation rate should not be significantly affected by k_1 for these high $[\text{fuel}]/[\text{NO}_x]$ ratio

runs. This suggests that in the troposphere, in the (presumed) absence of the overwhelming effect of chamber radical sources, the rate of NO oxidation and ozone formation in fuel/ NO_x/air mixtures will increase with altitude, primarily as a result of the pressure (as opposed to temperature) effect.

The above discussion has been concerned primarily with factors influencing the rate of ozone formation in fuel/ NO_x/air irradiations, rather than the ultimate maximum O_3 yields which would occur if the irradiations were allowed to proceed for a sufficiently long time. Although the conditions in a majority of our experiments were such that the rate of NO oxidation and O_3 formation were too slow for the maximum ozone yield to be obtained in 1 day of simulated irradiation, several runs were sufficiently reactive for ozone maxima to be observed. The results of these runs indicate that there may be a slight decrease in the maximum O_3 yield from JP-4/ NO_x/air irradiations with increased simulated altitude (Table I) and with decreasing pressure at constant temperature (Table II). However, the effect is relatively small, especially when compared to the effects of varying temperature and pressure on the rates of NO oxidation and O_3 formation.

The implications of these data concerning the impact on tropospheric ozone caused by fuel dumping at various altitudes will of course depend on other factors besides the temperature, pressure, and light intensity. For example, differential evaporation of the fuel components following their release (1) may lead to stratification of their concentrations which would complicate the chemistry involved. In addition, the NO_x levels present at the time of the fuel release are of particular importance. If the fuel is dumped under extremely NO_x -poor conditions, as is the case for the unpolluted troposphere regardless of altitude (7), relatively little O_3 will be formed. The O_3 yields will then reflect (on a relative basis) the maximum O_3 yields observed in those of our experiments which were sufficiently reactive for all the NO_x to be consumed, and on the basis of these experiments, they will be relatively insensitive to temperature and pressure.

However, if there is sufficient NO_x present from the exhaust of the aircraft at the time the fuel is dumped such that the $[\text{NO}_x]/[\text{fuel}]$ ratio is similar to or exceeds those employed in most of our experiments, then the amount of O_3 formed will be determined by the rate at which the fuel oxidizes NO. We observed this to increase with decreasing pressure and, when normalized for the chamber radical source, to be relatively insensitive to temperature. Thus, the amount of O_3 formed in the atmosphere should increase with altitude provided there is no "chamber" radical source in the troposphere, which has not been established. Furthermore, if there are indeed no unknown radical sources in the atmosphere, then the radical levels would be much lower than in our chamber experiments, and the O_3 yields would be limited by its formation rates under a much wider range of conditions (i.e., lower $[\text{NO}_x]/[\text{fuel}]$ levels) than those observed in our environmental chamber. However, the $[\text{NO}_x]/[\text{fuel}]$ ratios characteristic of typical fuel dumps are presently not known, and until more information concerning this is available, the atmospheric implications of fuel dumps at high altitudes will remain uncertain.

Acknowledgments

We thank William D. Long, Sara M. Aschmann, and Frank R. Bursell for valuable assistance in conducting the chamber experiments and James N. Pitts, Jr., for encouraging this work. The support and contribution to the

conduct of this research by Daniel A. Stone, Project Officer, and Ron Channell are gratefully acknowledged.

Registry No. NO_x, 11104-93-1; O₃, 10028-15-6.

Literature Cited

(1) Clewell, H. J., III March 1980, USAF Final Report ESL-TR-80-17; *J. Aircr.* 1983, 20, 382.
 (2) Cronn, D.; Robinson, E. *Geophys. Res. Lett.* 1979, 6, 641.
 (3) Fabian, P.; Borchers, R.; Flentje, G.; Matthews, W. A.; Seiler, W.; Giehl, H.; Bunse, K.; Muller, F.; Schmidt, U.; Volz, A.; Khedim, A.; Johnen, F. *J. Geophys. Res.* 1981, 86, 5179.
 (4) Rudolph, J.; Ehhalt, D. H.; Tonnissen, A. *J. Geophys. Res.* 1981, 86, 7267.
 (5) McFarland, M.; Kley, D.; Drummond, J. W.; Schmeltekopf, A. L.; Winkler, R. H. *Geophys. Res. Lett.* 1979, 6, 605.
 (6) Schiff, H. I.; Pepper, D.; Ridley, B. A. *J. Geophys. Res.* 1979, 84, 7895.
 (7) Kley, D.; Drummond, J. W.; McFarland, M.; Liu, S. C. *J. Geophys. Res.* 1981, 86, 3153.
 (8) Noxon, J. F. *Geophys. Res. Lett.* 1981, 8, 1223.
 (9) U. S. Standard Atmosphere. Committee on Extension to the Standard Atmosphere, NASA, U.S. Government Printing Office, Dec 1962.
 (10) U. S. Standard Atmosphere Supplements. Environmental Science Services Administration, NASA, U.S. Government Printing Office, 1966.
 (11) Peterson, J. T. June 1976, EPA 600/4-76-025.
 (12) Peterson, J. T. *Atmos. Environ.* 1977, 11, 689.
 (13) Akimoto, H.; Sakamaki, F.; Hoshino, M.; Inoue, G.; Okuda, M. *Environ. Sci. Technol.* 1979, 13, 53.
 (14) Winer, A. M.; Breuer, G. M.; Carter, W. P. L.; Darnall, K. R.; Pitts, J. N., Jr. *Atmos. Environ.* 1979, 13, 989.
 (15) Pitts, J. N., Jr.; Darnall, K. R.; Winer, A. M.; McAfee, J. M. Feb 1977, EPA 600/3-77-014b.
 (16) Pitts, J. N., Jr.; Darnall, K.; Carter, W. P. L.; Winer, A. M.; Arkinson, R. Nov 1979, EPA 600/3-79-110.

(17) Hendry, D. G.; Baldwin, A. C.; Barker, J. R.; Golden, D. M. June 1978, EPA 600/3-78-059.
 (18) Carter, W. P. L.; Lloyd, A. C.; Sprung, J. L.; Pitts, J. N., Jr. *Int. J. Chem. Kinet.* 1979, 11, 45.
 (19) Whitten, G. Z.; Hogo, H.; Meldgin, M. J.; Killus, J. P.; Bekowies, P. J. Jan 1979, Interim Report, Vol. 1, EPA 600/3-79-001a.
 (20) Whitten, G. Z.; Killus, J. P.; Hogo, H. Feb 1980, Final Report, Vol. 1, EPA 600/3-80-028a.
 (21) Atkinson, R.; Carter, W. P. L.; Darnall, K. R.; Winer, A. M.; Pitts, J. N., Jr. *Int. J. Chem. Kinet.* 1980, 12, 779.
 (22) Atkinson, R.; Lloyd, A. C. *J. Phys. Chem. Ref. Data*, in press.
 (23) Carter, W. P. L.; Ripley, P. S.; Smith, C. G.; Pitts, J. N., Jr. Nov 1981, USAF Final Report ESL-TSR-81-53, Vol. 1.
 (24) Winer, A. M.; Atkinson, R.; Carter, W. P. L.; Long, W. D.; Aschmann, S. M.; Pitts, J. N., Jr. Oct 1982, USAF Final Report ESL-TR-82-38.
 (25) Winer, A. M.; Graham, R. A.; Doyle, G. J.; Bekowies, P. J.; McAfee, J. M.; Pitts, J. N., Jr. *Adv. Environ. Sci. Technol.* 1980, 10, 461.
 (26) Doyle, G. J.; Bekowies, P. J.; Winer, A. M.; Pitts, J. N., Jr. *Environ. Sci. Technol.* 1977, 11, 45.
 (27) Carter, W. P. L.; Atkinson, R.; Winer, A. M.; Pitts, J. N., Jr. *Int. J. Chem. Kinet.* 1981, 13, 735.
 (28) Carter, W. P. L.; Atkinson, R.; Winer, A. M.; Pitts, J. N., Jr. *Int. J. Chem. Kinet.* 1982, 14, 1071.
 (29) Atkinson, R.; Darnall, K. R.; Lloyd, A. C.; Winer, A. M.; Pitts, J. N., Jr. *Adv. Photochem.* 1979, 11, 375.
 (30) Plum, C. N.; Sanhueza, E.; Atkinson, R.; Carter, W. P. L.; Pitts, J. N., Jr. *Environ. Sci. Technol.* 1983, 17, 479.
 (31) Atkinson, R.; Aschmann, S. M.; Carter, W. P. L.; Winer, A. M.; Pitts, J. N., Jr. *J. Phys. Chem.* 1982, 86, 4563.
 (32) Atkinson, R.; Carter, W. P. L.; Winer, A. M. *J. Phys. Chem.* 1983, 87, 2012.

Received October 6, 1983. Accepted January 26, 1984. This research was funded by USAF Contract F08635-80-C-0359.

Avoidance Responses of Estuarine Fish Exposed to Heated-Dechlorinated Power Plant Effluents

Lenwood W. Hall, Jr.,* Dennis T. Burton, William C. Graves, and Stuart L. Margrey

The Johns Hopkins University, Applied Physics Laboratory, Aquatic Ecology Section, Shady Side, Maryland 20764

■ Avoidance responses of striped bass (*Morone saxatilis*) and Atlantic menhaden (*Brevoortia tyrannus*) exposed to simultaneous dechlorinated waters (using SO₂ to dechlorinate total residual chlorine (TRC) concentrations of 0.00, 0.05, 0.10, and 0.15 mg/L TRC) and elevated temperatures (0, 2, 4 and 6 °C) were evaluated at acclimation temperatures of 15, 20, 25, and 30 °C. Both species showed minimal avoidance to dechlorinated estuarine water (no ΔT) at all acclimation temperatures. Elevated temperature (ΔT) or a combination of ΔT and dechlorination were the most important factors influencing avoidance of the test species. Acclimation temperature was an important factor influencing the avoidance behavior of both species exposed to heated-dechlorinated power plant conditions. Greatest avoidance of all test conditions generally occurred at an acclimation temperature of 30 °C. Both species avoided 34 °C when acclimated to 30 °C regardless of the dechlorinated condition.

Introduction

The use of chlorine for biofouling control in power plant cooling water systems has been subjected to stringent

regulation due to possible ecological effects related to the discharge of chlorine and chlorine-produced residuals in power plant effluents (1). Presently, chlorine is the dominant biocide used in the United States for biofouling control in power plant condensers (2). Burton (3) has proposed several alternatives that could be used for preventing biofouling in both once-through and recirculating cooling systems of power plants. Detoxification of chemical antifouling agents is one such alternative. Several methods of chemical dechlorination have been used: (1) sodium bisulfite (4), (2) sulfur dioxide (5-8), (3) sodium sulfite (9), and (4) sodium thiosulfate (10, 11). Sulfur dioxide (SO₂) is considered one of the most feasible methods to use for large volumes of water (3). Sulfur dioxide provides an excellent means of dechlorination due to ease of handling and metering, availability, and rapid reaction with chlorine residual fractions. Sulfur dioxide reacts rapidly with free and combined chlorine and immediately forms sulfurous acid. The sulfite radical formed reacts with chlorine compounds to form mainly sulfuric and hydrochloric acids in small quantities. Chlorides and sulfites are the by-products of sulfonation.

Table I. Water Quality Data during Acclimation and Testing

acclimation temp, °C	salinity, ‰	pH ^a	dissolved oxygen, ^a mg/L	ammonia N, mg/L
15	9-11	7.2-7.8	5.5-6.2	≤0.20
20	9-11.5	7.1-7.6	5.5-6.5	≤0.20
25	9-10	7.1-7.5	5.0-6.2	≤0.20
30	11-11.5	7.2-7.4	5.0-6.0	≤0.20

^apH and dissolved oxygen did not change during testing.

Acute toxicity of SO₂ dechlorinated water to aquatic biota in both fresh (5-7) and estuarine water (8) has been investigated. Generally, dechlorinated water was found to be nontoxic to most aquatic biota during acute exposures. Hamel and Garey (11) have shown that dechlorination with sodium thiosulfate rapidly reduced both free and combined chlorine residuals in seawater; however, this chemical agent did not reduce halogenated organics that might be responsible for sublethal effects on aquatic organisms. Scott (12) also reported that exposure of marine invertebrates to dechlorinated effluents produced significant physiological effects.

The avoidance responses of fish which may simultaneously encounter dechlorinated water and elevated temperature near power plant facilities are not known. The objectives of this study were (1) to determine the avoidance response of juvenile striped bass (*Morone saxatilis*) and Atlantic menhaden (*Brevoortia tyrannus*) simultaneously exposed to dechlorinated waters (using SO₂ to dechlorinate total residual chlorine (TRC) concentrations of 0.00, 0.05, 0.10, and 0.15 mg/L) and elevated temperatures (0, 2, 4 and 6 °C) at acclimation temperatures of 15, 20, 25, and 30 °C and (2) to establish and compare regression models at the above acclimation temperatures useful for assessing avoidance responses of these species to heated-dechlorinated power plant effluents. Striped bass and Atlantic menhaden were selected for this study due to their recreational and/or commercial importance on the east coast and due to their presence in the vicinity of many east coast power plants. The various dechlorination-ΔT conditions were used to simulate power plant effluent conditions at temperatures (15-30 °C) when estuarine plants normally chlorinate.

Materials and Methods

General. Juvenile striped bass were obtained from the following hatcheries: Orangeburg National Fish Hatchery, Orangeburg, SC; Front Royal Fish Culture Station, Front Royal, VA; Delmarva Ecological Laboratory, Middletown, DE. Juvenile Atlantic menhaden were collected from the Parish Creek area of Chesapeake Bay near Shady Side, MD, by using a 3.7-m cast net. Striped bass (mean total length = 9.3 cm) and Atlantic menhaden (mean total length = 7.0 cm) were acclimated under continuous flow conditions in the laboratory for a minimum of 2 weeks at each respective test temperature (15, 20, 25, and 30 °C) before testing. If acclimation to test temperatures was required, a rate of 1 °C/day change was used until the desired acclimation temperature was obtained followed by 2 weeks at the acclimation temperature. All fish were fed finely ground trout chow daily and supplemented by plankton present in the incoming Chesapeake Bay water. The basic water quality during acclimation and testing is presented in Table I. A photoperiod simulating natural conditions was used during the acclimation period. A light intensity of approximately 215 lx at the water surface was used during the avoidance tests.

Table II. Unbalanced 3-Factor Factorial Design Used in the Avoidance Tests at Acclimation Temperatures of 15, 20, 25, and 30 °C^a

TRC, mg/L, before dechlorination	ΔT, °C			
	0	2	4	6
0.00	XX	XX	XX	XXXX
0.05	XX	XXXX	XXXX	XX
0.10	XX	XXXX	XXXX	XX
0.15	XXXX	XX	XX	XX

^aTRC concentrations were dechlorinated at approximately a 1:1 ratio of SO₂ to TRC during the dechlorination tests. An X denotes an individual (striped bass) or a group (10 Atlantic menhaden) tested at a designated condition.

Experimental Procedures. All tests were conducted during daylight hours in a modified dual subtrough (2.44 × 0.23 × 0.31 m) avoidance unit located in an isolation room (13, 14). Separate 378-L mixing head tanks were used for control (ambient water), chlorinated water, SO₂-treated water, and TRC-SO₂ conditions. TRC and SO₂ entered a mixing head tank equipped with heaters used to obtain the desired ΔT condition. A ratio of 0.9 SO₂:1.0 HOCl is recommended for complete neutralization of residual chlorine (15). Maintaining this extract ratio was difficult due to equipment limitations; therefore, slight overdosing of SO₂ (<0.05 mg/L) was used to ensure complete dechlorination.

Water from the TRC-SO₂ mixing head tank and control head tank then entered opposite ends of each subtrough and drained at the center, thus providing test specimens with a choice of a control or a dechlorinated-ΔT test condition. The influence of position was corrected by having water from the head tanks supply opposite ends of the subtroughs. Flow rates of approximately 3.0 L/min (1.5 L/min from each end) were used in each subtrough.

Preliminary tests were conducted to determine if experiments with individuals or a group of individuals should be conducted with each test species. Initial trials involved testing groups of 6-10 individuals of each species during separate experiments. Group testing was used if groups of fish moved together as a group after orientation to the test unit. Atlantic menhaden formed tight schools and moved together as a unit during these initial experiments; therefore, group testing (10 individuals per group) was used in later experiments (16). Group testing with striped bass was not satisfactory as this species would not move together as a school in the test unit. Thus, the species was tested individually.

Test species were introduced in the control area of each subtrough and allowed a 20-30-min orientation period followed by a 20-min observation. The amount of time spent in the control area, test area, or mixing area (≈7-cm area near center drain) was remotely monitored by the use of a closed circuit television system. Stopwatches were used to record the time spent in each respective area.

During the dechlorination-ΔT avoidance studies, TRC concentrations were measured amperometrically (17) in the TRC and mixing head tanks. Sulfite concentrations were measured amperometrically in the SO₂ head tank and mixing head tank and at 0.24-m intervals in the unit by using a Princeton applied research polarographic analyzer (Model 174A) (6). A series of 22 thermistors was located peripherally around each subtrough at distances ranging from 8 to 30 cm. These thermistors were used to monitor temperature throughout the tests.

All simultaneous dechlorinated-ΔT conditions were tested by using the unbalanced 3-factor factorial design

Table III. Mean Percent Time in Control for Striped Bass Exposed to Various Dechlorinated- ΔT Conditions at 15, 20, 25, and 30 °C^a

ΔT , °C	TRC before dechlorination, mg/L	mean % time in control at each acclimation temp., °C			
		15	20	25	30
0	0	49	47	49	50
	0.05	51	51	57	53
	0.10	49	41	79	48
	0.15	44	75	77	60
2	0	51	51	57	67
	0.05	58	50	65	80
	0.10	67	58	64	65
	0.15	41	56	71	77
4	0	37	57	68	78
	0.05	66	50	64	82
	0.10	51	68	61	97
	0.15	43	87	69	58
6	0	47	54	68	90
	0.05	52	67	57	94
	0.10	55	68	55	99
	0.15	39	88	58	97

^aThis was a percentage of the total experimental time (20 min).

shown in Table II. The range of TRC concentrations (0.00, 0.05, 0.10, and 0.15 mg/L) and subsequent concentrations of SO₂ needed to dechlorinate along with ΔT conditions (0, 2, 4, and 6 °C) were selected to simulate a range of effluent discharge conditions that may occur at various once-through power plant facilities. The control condition (0 mg/L TRC-0 °C ΔT) was used to test for position effects in the test unit.

Statistical Procedures. Regression techniques were used for data analysis. The logistic transformation was used to transform the binomially distributed proportions to normally distributed logits. The response variable for these regression analyses was a logit transformation of the proportion of time fish were present in the control area. The specific transformation was

$$z = \ln \left[\frac{p + 0.005}{1 - (p - 0.005)} \right] \quad (1)$$

where z = response variable and $1 - p$ = proportion of time in the control area. The constant 0.005 was used in the numerator and denominator to ensure that z would have a bounded and reasonable value if p were equal to 1 or 0.

A fully quadratic regression model (all squares and cross products) was fitted to the avoidance responses at each

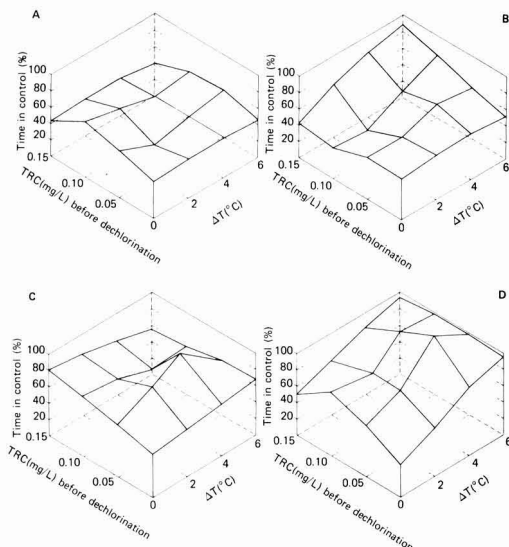


Figure 1. Three-dimensional response surface of percent avoidance (time in control) for striped bass subjected to simultaneous dechlorinated- ΔT conditions at 15 (panel A), 20 (panel B), 25 (panel C), and 30 °C (panel D).

acclimation temperature by using the regression program BMD-PIR (18). The models were used to derive equations to plot response surfaces and also used in the covariance analysis testing for different response patterns at designated acclimation temperatures.

All possible regressions were examined by using BMD-P9R (18) to assess the relative importance of the independent variables. Independent variables yielding the “best” predictive model were determined by partial F statistics and Mallows’ Cp statistic (19).

Results

Striped Bass. The mean percent time in the control area (avoidance time) for striped bass exposed to dechlorinated- ΔT conditions at acclimation temperatures of 15, 20, 25, and 30 °C is presented in Table III. Regression models for striped bass are shown in Table IV. These equations were used to derive Figure 1 (panels A, B, C, and D) for this species at acclimation temperatures of 15, 20, 25, and 30 °C, respectively. No significant avoidance to any of the test conditions occurred at 15 °C (Figure 1, panel A). The regression model (Table IV) and response

Table IV. Regression Models for Striped Bass and Atlantic Menhaden Subjected to Simultaneous Dechlorinated- ΔT Conditions at Various Acclimation Temperatures^a

acclimation temp., °C	regression model	F statistic	probability level
Striped Bass			
15	$p = 1 - [1 + \exp(0.1933 - 0.103t - 14.152c + 0.109tc + 0.017t^2 + 99.100c^2)]^{-1}$	2.676	0.036
20	$p = 1 - [1 + \exp(-0.034 - 0.082t + 10.357c - 2.569tc + 0.012t^2 - 53.260c^2)]^{-1}$	3.031	0.021
25	$p = 1 - [1 + \exp(-1.106 - 0.122t - 9.257c + 2.191tc + 0.003t^2 + 1.980c^2)]^{-1}$	2.329	0.061
30	$p = 1 - [1 + \exp(0.578 - 0.448t - 30.218c + 1.099tc - 0.023t^2 + 174.738c^2)]^{-1}$	8.653	0.001
Atlantic Menhaden			
15	$p = 1 - [1 + \exp(0.182 + 0.155t - 3.520c - 0.004tc - 0.170t^2 + 13.634c^2)]^{-1}$	2.230	0.071
20	$p = 1 - [1 + \exp(0.178 + 0.190t + 3.765c - 0.106tc - 0.032t^2 - 37.353c^2)]^{-1}$	1.505	0.211
25	$p = 1 - [1 + \exp(-0.027 + 0.138t + 1.241c + 0.231tc - 0.049t^2 - 15.693c^2)]^{-1}$	6.525	0.001
30	$p = 1 - [1 + \exp(0.239 - 0.235t + 5.592c + 0.091tc - 0.103t^2 - 36.745c^2)]^{-1}$	51.676	0.001

^aThe following abbreviations are used: p = percent time in control area, t = elevated temperature (ΔT) (°C), and c = total residual chlorine concentration (mg/L) that was dechlorinated with SO₂ at approximately 1 to 1 ratio.

Table V. Mean Percent Time in Control for Atlantic Menhaden Exposed to Various Dechlorinated- ΔT Conditions at 15, 20, 25, and 30 °C^a

ΔT , °C	TRC before dechlorination, mg/L	mean % time in control at each acclimation temp, °C			
		15	20	25	30
0	0	47	44	53	46
	0.05	50	47	55	46
	0.10	50	48	55	31
	0.15	52	52	53	47
2	0	37	55	48	74
	0.05	39	23	38	51
	0.10	43	46	45	51
	0.15	44	44	53	83
4	0	38	45	48	86
	0.05	48	31	66	93
	0.10	41	53	57	86
	0.15	43	47	62	87
6	0	38	45	72	99
	0.05	33	42	72	100
	0.10	49	59	54	100
	0.15	41	44	73	99

^aThis was a percentage of the total experimental time (20 min).

surface (Figure 1, panel B) at 20 °C show (1) avoidance increased at the 0.15 mg/L TRC-dechlorination condition as ΔT increased from 0 to 6 °C, (2) avoidance increased at 6 °C as TRC-dechlorination increased from 0 to 0.15 mg/L, and (3) the interaction term (dechlorinated- ΔT condition) was the most important factor influencing avoidance. The model and response surface for striped bass at 25 °C (Table IV and Figure 1, panel C) show (1) a decrease in avoidance at 0.15 mg/L TRC dechlorinated as ΔT increased from 0 to 6 °C ΔT , (2) an increase in avoidance as dechlorinated concentrations increased from 0 to 0.15 mg/L at 0 °C ΔT , (3) an increase in avoidance at 0.05 mg/L dechlorination as ΔT increased from 0 to 4 °C ΔT followed by a sharp decrease at 6 °C ΔT , and (4) the interaction term (ΔT -dechlorination) as the most important term influencing avoidance. The response surface at 30 °C (Figure 1, panel D) show (1) a strong avoidance was exhibited at 4 and 6 °C ΔT regardless of the dechlorination condition, (2) avoidance increased at 0.15 mg/L TRC-dechlorination as ΔT increased from 0 to 6 °C ΔT , and (3) dechlorination was the most important factor influencing avoidance.

There was a significant difference among avoidance models for the four acclimation temperatures. Greatest avoidance of all test conditions generally occurred at 30 °C.

Atlantic Menhaden. The percent time in the control area (avoidance time) for Atlantic menhaden exposed to dechlorinated- ΔT conditions at acclimation temperatures of 15, 20, 25, and 30 °C is presented in Table V. Regression models for Atlantic menhaden are presented in Table IV. Figure 2 (panels A, B, C, and D) was derived from these equations at acclimation temperatures of 15, 20, 25, and 30 °C, respectively. The regression model and response surface at 15 °C (Table IV and Figure 1, panel A) show (1) increases in avoidance at all dechlorination conditions as ΔT 's increased from 0 to 6 °C, (2) strong avoidance responses at 4 and 6 °C ΔT conditions regardless of the dechlorination conditions, and (3) ΔT as the most important term influencing avoidance. The regression model at 20 °C (Table IV) shows no significant avoidance to any of the test conditions (Figure 2, panel B). At 25 °C the response surface (Figure 2, panel C) shows (1) a

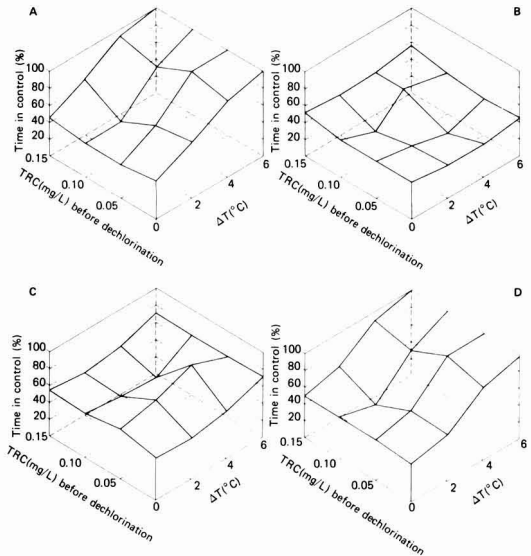


Figure 2. Three-dimensional response surface of percent avoidance (time in control) for Atlantic menhaden subjected to simultaneous dechlorinated- ΔT conditions at 15 (panel A), 20 (panel B), 25 (panel C), and 30 °C (panel D).

slight increase in avoidance at the 0.15 mg/L TRC-dechlorination as ΔT increased from 0 to 6 °C and (2) ΔT as the most important term influencing avoidance. The regression model and response surface at 30 °C (Table IV and Figure 2, panel D) show (1) a strong avoidance at 4 and 6 °C ΔT at all dechlorination conditions, (2) an increase in avoidance at all dechlorination conditions as ΔT 's increased from 0 to 6 °C, and (3) ΔT as the most important term influencing avoidance.

Regression models at 20, 25, and 30 °C were found to be significantly different. Models at 15 and 20 °C were not significantly different. Generally, the greatest avoidance of all test conditions occurred at 30 °C.

Discussion

Striped Bass. Presently there are no available data on the avoidance responses of striped bass or other fish species exposed to dechlorinated waters. Results from our study show that this species exhibited little reaction to SO_2 -dechlorinated water without ΔT . It can be seen from Figure 1 that avoidance of these dechlorinated conditions usually occurred at the higher levels of dechlorination with ΔT as a major contributing factor. The avoidance response of striped bass to dechlorination without ΔT was minimal at all acclimation temperatures except 25 °C.

Previous investigators have evaluated the toxicity of dechlorinated effluent to various fish species (6-8, 11). These studies have generally shown that dechlorination reduces the toxicity of residual chlorine to fish. Hammel and Garey (11) have suggested that although dechlorination can reduce chlorine residuals in seawater, this process does not reduce halogenated organics that could cause sublethal effects on aquatic biota. For example, these investigators reported that the three-spine stickleback, *Gasterosteus aculeatus*, exhibited repressed sexual activity when exposed to dechlorinated waters for a 3-week period. This sublethal effect could have been eliminated in the natural environment if the species could detect and avoid dechlorinated waters. Our results suggest that avoidance

of SO₂-dechlorinated conditions by striped bass is possible under certain conditions.

In a previous 96-h toxicity study in our laboratory, we reported that striped bass larvae exposed to SO₂-dechlorinated waters which initially contained 0.06 and 0.13 mg/L TRC experienced slightly higher mortality (\approx 14%) than the controls (8). These data suggested that possible bromo organics remaining after dechlorination may have had a slight effect. In the present study, a strong avoidance was not generally exhibited by this species exposed to the various dechlorinated test conditions at any acclimation temperature. However, there is evidence to indicate that this species can detect and avoid dechlorinated water at 25 °C (Figure 1, panel C; 0.15 mg/L TRC before dechlorination, 0 °C ΔT).

Our temperature avoidance data (Figure 1, panel D, no dechlorination) with striped bass confirms data collected in other studies (14, 20). Striped bass will avoid temperatures of 34 °C or greater when acclimated to temperatures of 27–30 °C.

Atlantic Menhaden. Atlantic menhaden did not demonstrate a strong avoidance response to dechlorination when ΔT was absent. ΔT was found to be the most important factor influencing the avoidance response of this species at all acclimation temperatures. Previous investigators have reported that Atlantic menhaden avoid 33.7–34.9 °C when acclimated to 25 °C (21). Meldrim et al. (22) reported that this species avoided 32 °C when acclimated to 27 °C. Other data collected in our laboratory show that this species avoids 31 and >32 °C when acclimated to 25 and 30 °C, respectively (23). The results presented in Figure 2 (panel D) show that Atlantic menhaden avoid 34 °C when acclimated to 30 °C. Our data and the results of other investigators demonstrate that this species will avoid a temperature of approximately 34 °C regardless of the dechlorination condition present.

The present study suggests that Atlantic menhaden do not detect and/or avoid possible bromo organics that may be present after dechlorination. Bromoform was likely the most dominant bromo organic (24). In a previous study, Gibson et al. (25) reported a 96-h LC50 of 12 mg/L bromoform for Atlantic menhaden, thus indicating that bromoform is not highly toxic. Concentrations of bromoform that may have been present in the present study were probably much lower than this lethal concentration; therefore, lack of avoidance to this nontoxic condition is not surprising.

Previous investigators have reported that dechlorinated waters can cause sublethal effects to fish (11). If fish species such as Atlantic menhaden cannot detect and subsequently avoid a dechlorinated effluent, there could be problems if these conditions are harmful after long exposures. This is probably not the case in this study, however, due to the short exposure time in dechlorinated water.

Summary

Direct verification of the avoidance responses of the test species subjected to dechlorinated- ΔT conditions in the field is not available. However, other investigators using similar methods have determined that avoidance of toxicant concentrations in the laboratory accurately predicted avoidance that occurred in the field (26–29). Therefore, it is likely that the methods used to evaluate laboratory avoidance behavior of these test species exposed to dechlorinated- ΔT conditions provide data that apply to field conditions. The general conclusion from this study is that dechlorinated conditions up to 0.15 mg/L TRC-dechlorination (no ΔT) do not generally cause avoidance by the

two test species. On the basis of avoidance behavior, it appears that the use of short-term intermittent chlorination schedules by power plants would minimize effects on these fish species if dechlorination practices were used.

The most important factors influencing avoidance by these test species were ΔT or a combination of ΔT and dechlorination. Striped bass avoidance behavior was influenced by a combination of both dechlorination and ΔT in most cases. Avoidance behavior of Atlantic menhaden was greatly influenced by ΔT at all acclimation temperatures; dechlorination was relatively unimportant. The attraction of fish to warm water effluents can cause problems if temperature preference overrides the avoidance response of fish subjected to a toxic condition (30). In this study, there is no evidence to indicate that such a sequence of events would occur. In fact, neither species demonstrated a strong preference for a warm temperature when tested at acclimation temperatures ranging from 15 to 30 °C. In some cases, avoidance of higher temperatures may prevent possible effects that could occur due to extended exposures to dechlorinated waters.

Acknowledgments

Thanks are extended to the following individuals for their assistance in supplying striped bass: T. Dingley of the Orangeburg National Fish Hatchery, Orangeburg, SC; R. Harrell and J. Bayless of the Dennis Wildlife Center, Bonneau, SC; K. Mitchell of the Front Royal Fish Culture Station, Front Royal, VA; W. Basin of Delmarva Ecological Laboratory, Middletown, DE. We also acknowledge E. Perry for performing the statistical analyses and B. Knee for typing the report. Special consideration is extended to P. Miller and M. J. Garris for technical review of the manuscript.

Literature Cited

- (1) Costle, D. M.; Schaffer, R. B.; Lum, J.; Wright, T. *U.S. Environ. Prot. Agency* 1980, EPA 440/1-80-029-B.
- (2) Zeitoun, I. H.; Reynolds, J. Z. *Environ. Sci. Technol.* 1978, 12, 780.
- (3) Burton, D. T. *Condens. Biofouling Control Symp. Proc.* 1980, 251–266.
- (4) Esvelt, L. A.; Kaufman, W. J.; Selleck, R. E. *J. Water Pollut. Control Fed.* 1973, 45, 1558.
- (5) Collins, H. F.; Deane, D. G. *Proc. Am. Soc. Civ. Eng.* 1973, 99, 761.
- (6) Arthur, J. W.; Andrew, R. W.; Mattson, V. R.; Olson, D. T.; Glass, G. E.; Halligan, B. J.; Walbridge, C. T. *U.S. Environ. Prot. Agency* 1975, EPA-600/3-75-012.
- (7) Ward, R. W.; DeGraeve, G. M. *Water Resour. Bull.* 1978, 14, 696.
- (8) Hall, L. W., Jr.; Burton, D. T.; Graves, W. C.; Margrey, S. L. *Environ. Sci. Technol.* 1981, 15, 573.
- (9) Grossnickel, N. E. M.S. Thesis, University of Wisconsin, Milwaukee, WI, 1974.
- (10) Zillich, J. A. *J. Water Pollut. Control Fed.* 1972, 44, 212.
- (11) Hamel, A. R.; Garey, J. F. *Condens. Biofouling Control Symp. Proc.* 1980, 419–428.
- (12) Scott, G. I. In "Water Chlorination: Environmental Impact and Health Effects"; Jolley, R. L.; Brungs, W. A.; Contruvo, J. A.; Cumming, R. B.; Mattice, J. S.; Jacobs, V. A., Eds.; Ann Arbor Science Publishers: Ann Arbor, MI, 1983; pp 827–841.
- (13) Shelford, V. E.; Allee, W. C. *J. Exp. Zool.* 1913, 14, 207.
- (14) Meldrim, J. W.; Gift, J. J. Ichthyological Associates Inc., 1971, Bulletin No. 11.
- (15) White, G. C. "Handbook of Chlorination"; Van Nostrand Reinhold: New York, 1972.
- (16) Hall, L. W., Jr.; Burton, D. T.; Margrey, S. L.; Graves, W. C. *J. Toxicol. Environ. Health* 1982, 10, 1017.
- (17) APHA, AWWA, and WPCF "Standard Methods for the Examination of Water and Wastewater", 14th ed.; American

- Public Health Association: Washington, DC, 1976.
- (18) Dixon, W. T.; Brown, M. B. "Biomedical Computer Programs P-Series"; University of California Press: Berkley, CA, 1979.
 - (19) Draper, N. R.; Smith, H. "Applied Regression Analysis"; Wiley: New York, 1981.
 - (20) Hall, L. W., Jr.; Margrey, S. L.; Burton, D. T.; Graves, W. C. *Arch. Environ. Contam. Toxicol.*, 1983, 12, 715.
 - (21) Terpin, K. M.; Wyllie, M. L.; Holmstrom, E. R. Ichthyological Associates Inc., 1977, Bulletin No. 17.
 - (22) Meldrim, J. W.; Gift, J. J.; Petrosky, B. R. Ichthyological Associates Inc., 1974, Bulletin No. 11.
 - (23) Hall, L. W., Jr.; Margrey, S. L.; Graves, W. C.; Burton, D. T. In "Water Chlorination: Environmental Impact and Health Effects"; Jolley, R. L.; Brungs, W. A.; Contruvo, J. A.; Cummings, R. B.; Mattice, J. S.; Jacobs, V. A., Eds.; Ann Arbor Science Publishers: Ann Arbor, MI, 1983; pp 983-991.
 - (24) Helz, G. R.; Hsu, R. Y. *Limnol. Oceanogr.* 1978, 23, 858.
 - (25) Gibson, C. I.; Tone, F. C.; Wilkinson, P.; Blaylock, J. W. *Ozone: Sci. Eng.* 1979, 1, 47.
 - (26) Sprague, J. B.; Drury, D. E. In "Advances in Water Pollution Research"; Jenkins, S. H., Ed.; Pergamon Press: Oxford, England, 1969; pp 169-179.
 - (27) Giattina, J. D.; Cherry, D. S.; Cairns, J., Jr.; Larrick, S. R. *Trans. Am. Fish. Soc.* 1981, 110, 526.
 - (28) Cairns, J., Jr.; Cherry, D. S.; Giattina, J. D. In "Energy and Ecological Modelling"; Mitsch, W. J.; Bosserman, R. W.; Klopatek, J. M., Eds.; Elsevier: Amsterdam, Netherlands, 1982; pp 207-215.
 - (29) Hose, J. E.; King, T. D.; Zerba, K. E.; Stoffel, R. S.; Stephens, J. S., Jr.; Dickson, J. A. In "Water Chlorination: Environmental Impact and Health Effects"; Jolley, R. L.; Brungs, W. A.; Contruvo, J. A.; Cumming, R. B.; Mattice, J. S.; Jacobs, V. A., Eds.; Ann Arbor Science Publishers: Ann Arbor, MI, 1983; pp 967-982.
 - (30) Cherry, D. S.; Cairns, J. *Water Res.* 1982, 16, 263.

Received for review July 11, 1983. Revised manuscript received December 27, 1983. Accepted February 1, 1984. This work was supported by the Maryland Power Plant Siting Program (Contract 83-81-04).

NOTES

Decay Rates of Nitrogen Oxides in a Typical Japanese Living Room

Shin'Ichi Yamanaka

Kyoto City Institute of Public Health, 1-2, Higashitakadacho, Mibu, Nakagyoku, Kyoto 604, Japan

■ Decay process of indoor-originated NO₂ and NO was surveyed in detail in a typical Japanese living room with a chemiluminescent autoanalyzer. It was demonstrated that the decay process of NO₂, being considered to comprise homogeneous and heterogeneous processes as well as air exchange, follows approximately first-order kinetics. Each contribution was determined tentatively from the CO decay rate and the variation of the NO₂ decay rate accompanying change of relative humidity (RH) or interior surface property. Under low RH (43.5-50%), the sink rate of NO₂ was 0.99 ± 0.19 h⁻¹ (air change) regardless of interior surface property. However, it increased in proportion to RH above 50% (~72.5%), depending on the interior surface property, too. The surface effect itself appeared to be dependent on RH. The parameters for the simple calculation of indoor NO₂ level were presented.

Introduction

Recent works showed that individual exposure to NO₂ is considerably attributed to indoor NO₂ since most people spend so much of their time indoors and NO₂ originates indoors as well as outdoors (1, 2). Many investigations have been undertaken on indoor NO₂, which involve the indoor-outdoor concentration ratio without any indoor NO₂ source and comparison of its level in homes with different types of heating or cooking appliances (3-8). Considering the adverse effect of low level NO₂ to a human being, it is essential to anticipate a probable NO₂ level in a room with some source by a simple calculation. It may be helpful also in the design of dwellings and selection or location of heating or cooking appliances. Although the

emission data for several domestic appliances have been presented (9), such calculation has still been impossible since the decay process of NO₂ has remained to be elucidated. NO₂ is rather reactive and can be removed indoors through a process other than ventilation. The overall decay rate of NO₂ had been determined in several previous works (10), and about the indoor decay of O₃ some comprehensive investigations have been carried out (11-13). The purpose of this study is to determine the dependency of the decay rate on relative humidity and interior surface property as well as air exchange separately in a typical Japanese living room and to approach a prediction method of indoor NO₂ level by a simple calculation. For in the environment without any other reactive pollutants like ordinary homes, relative humidity is considered to be a main factor in homogeneous gas-phase reaction of NO₂; another process contributing to the decay of NO₂ may proceed on the interior surface.

Materials and Methods

Characterization of Test Room. A typical Japanese living room generally consists of floor mats, i.e., *tatami* in Japanese, paper slide doors, i.e., *fusuma* and/or *shoji*, clay walls and a wood board ceiling. With respect to the interior surface property, little variation is found among the Japanese living rooms compared with that among the western styles which have a wide variety of surfaces such as carpet, curtains, clothed walls, painted boards, etc. The room studied here had 9.8 m² of floor mats (six pieces), 13.6 m² of clay wall, 12.9 m² of paper slide doors, and 10.1 m² of wood board ceiling, in all 46.4 m² of apparent surface area and also 23.4 m³ of air volume. Since there was almost

no other pollution source, the indoor level of other reactive pollutants such as O₃ and SO₂ may be extremely low.

Indoor NO₂ Source and Running. A gas-fired radiant or a kerosene-fired convective type unvented heater was used as a source of NO₂, and they also emitted NO and CO together. The former has 6.9 MJ/h fuel consumption rate, and the latter has 7.4 MJ/h.

One run took 3 h: for the first 70 min the heater was operating, and for the remainder of the time the heater was turned off with all the doors and windows shut. During that time, NO₂, NO, and CO concentrations, room temperature, and relative humidity (RH) were automatically recorded while a fan was operated at one corner of the room to mix the air. High RH (~60%) was achieved by a certain amount of hot water in a plate on an electric heater at the center of the room. In an other case, RH naturally varied according to meteorological condition, i.e., lower in clear days and higher in cloudy or rainy days. Air samples were introduced to the instruments through Teflon tubings from a point at 1.3-m height.

Modification of Interior Surface. It is presumable that the smoother and chemically stabler is the surface, to the less extent NO₂ removal on it may occur. In this study, the interior surface was covered with polyethylene film (0.3-mm thickness) in part or completely to alter the property with respect to NO₂ removal; in the preliminary experiment, polyethylene (PE) was found to be useful for this purpose. Infiltration rate was always monitored with the decay rate of inert gas, CO. In some runs, a carpet made of acrylic fiber was used to cover the floor mats.

Analytical Instruments. A chemiluminescent NO_x analyzer equipped with a recorder, ACL-14D (Yanagimoto Mfg. Co. Ltd.), which could record NO₂, NO, and NO_x (NO₂ + NO), was used; the efficiency of NO₂ converter had been confirmed to be more than 95% in the inspection just before use. An electrochemical CO analyzer equipped with the filter to eliminate interference, "Ecolyzer Model 2600" (Energetics Science Co. Ltd.), and a recorder, R-102 (Rikadenki Kogyo Co. Ltd.), were also used. They were calibrated once a day with 92 ppm of NO and 39.2 ppm of CO standard gas (Seitetsu Kagaku Kogyo Co. Ltd.), respectively.

The room temperature and RH recorded with a thermograph (Isuzu Seisakusho Co. Ltd.).

Results and Discussion

NO₂ Decay Rate in Polyethylene Bag. A total of 0.04 ppm of NO₂ in dried N₂ was packed into a PE bag (150 L volume, 1.58 m² of inner surface area), and the decay of NO₂ was followed regularly. Prior to use, this bag was washed out with dried N₂. In order to minimize penetration or diffusion of NO₂ out of the bag and the homogeneous gas-phase reaction, the concentration in dried N₂ comparable to the outer level was preferred, being stored in a dark room. NO₂ in this bag decayed only slightly (5%) after 2 h. Consequently, it was found that for about 1 or 2 h the heterogeneous reaction of NO₂ on PE film can be neglected. Hence, if the interior surface is covered with PE film completely, the decay attributable to it may be considered to be minimum in the room concerned.

Variation Pattern of NO₂, NO, and CO Concentrations. The typical variation patterns of NO₂, NO, and CO concentrations in one run with a gas-fired radiant type unvented heater are shown in Figure 1. NO₂ concentration continued to increase, reaching the peak level which is a steady state, while NO concentration initially rather decreased slightly and then exhibited little variation. NO did not appear to be oxidized in air as described later but appeared to be oxidized slightly through the flame of the

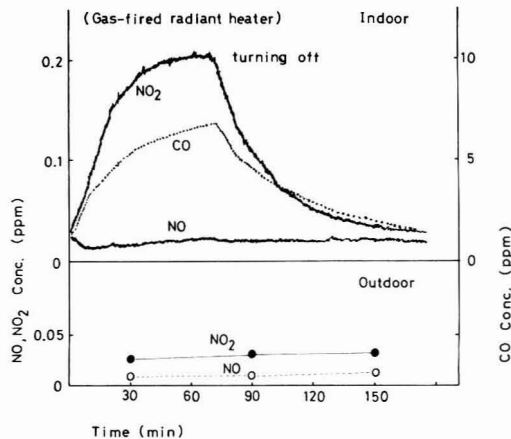


Figure 1. Variation patterns of NO₂, NO, and CO concentrations. Outdoor level was monitored once an hour.

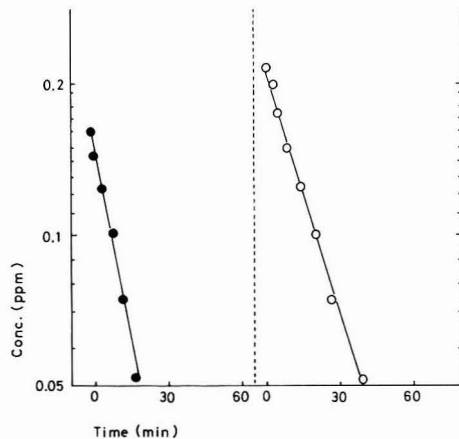


Figure 2. Decay curve of NO₂ in semilog space. (●) 57% RH, without covering the surface; (○) 45% RH, with covering all the surface.

heater. The initial slight decrease of NO concentration is presumably due to this thermal oxidation. CO concentration increased gradually until the turning off point. After that point, all of them except NO decreased in each its own way.

In a room under well-mixed conditions, NO₂ mass balance can be expressed as

$$V(dC_i/dt) = -qC_i - R + qC_o + E \quad (1)$$

where V is the air volume of the room (m³), C_i is the indoor level of NO₂ (ppm), t is the time (h), q is the flow rate of air exchange (m³/h), R is the sink rate of NO₂ (cm³/h), E is the NO₂ emission rate for the source (cm³/h), and C_o is the outdoor level of NO₂ (ppm), provided that oxidation of NO to NO₂ is neglected.

After the heater was turned off, that is, under $E = 0$, the variation of NO₂ concentration was also recorded on semilog graph paper, giving a straight line (Figure 2). This indicates that the overall decay process follows approximately first-order kinetics. This is considered to comprise homogeneous and heterogeneous processes as well as air exchange. Then by assuming that an additivity is valid

$$dC_i/dt = -(\alpha + \beta + \gamma S)C_i + \alpha C_o \quad (2)$$

Table I. Experimental Results

run	RH, %	temp, °C	decay rate of CO, h ⁻¹	sink rate of NO ₂ , h ⁻¹	peak level ^a of NO ₂ , ppm	covering and other remarks
1	43.5 ± 0.5 ^b	30.0 ± 3.0 ^b	1.49 ± 0.05 ^c	0.67 ± 0.11 ^c	0.220	all the surface
2	44.0 ± 2.0	28.3 ± 4.3	1.68 ± 0.04	1.15 ± 0.06	0.180	wall
3	45.0 ± 0	31.3 ± 2.7	2.04 ± 0.04	0.81 ± 0.12	0.185	
4	45.0 ± 2.0	29.3 ± 3.8	1.68 ± 0.04	1.02 ± 0.11	0.195	floor
5	45.0 ± 3.0	30.9 ± 3.3	1.46 ± 0.06	1.15 ± 0.06	0.195	wall
6	45.0 ± 3.0	28.3 ± 4.3	1.59 ± 0.04	1.27 ± 0.05	0.180	wall
7	45.5 ± 1.5	30.8 ± 3.3	1.55 ± 0.03	1.22 ± 0.05	0.190	floor
8	48.0 ± 2.0	29.5 ± 3.5	1.56 ± 0.04	0.98 ± 0.09	0.205	wall
9	49.0 ± 3.0	28.0 ± 4.0	1.54 ± 0.04	0.87 ± 0.07	0.215	wall
10	49.0 ± 2.0	29.5 ± 2.5	1.84 ± 0.06	0.94 ± 0.05	0.190	
11	46.0 ± 1.0	27.8 ± 3.8	1.29 ± 0.03	0.85 ± 0.04	0.220	all the surface
12	40.5 ± 3.5	31.0 ± 4.0	2.04 ± 0.03	1.04 ± 0.14	0.165	wall and floor (carpet)
13	43.0 ± 2.0	29.0 ± 3.5	1.44 ± 0.03	1.02 ± 0.06	0.205	wall and floor (carpet)
14	44.0 ± 2.0	27.0 ± 4.0	1.63 ± 0.06	1.35 ± 0.12	0.210	wall and floor (carpet)
15	51.5 ± 2.5	29.0 ± 3.5	1.98 ± 0.06	0.90 ± 0.07	0.190	floor
16	50.5 ± 3.5	30.8 ± 3.8	1.84 ± 0.03	0.67 ± 0.05	0.180	all the surface
17	52.0 ± 3.0	29.0 ± 4.0	1.79 ± 0.07	0.65 ± 0.10	0.180	all the surface
18	53.5 ± 3.5	30.0 ± 4.5	1.49 ± 0.09	0.80 ± 0.05	0.185	all the surface
19	57.0 ± 3.0	28.0 ± 3.0	1.62 ± 0.06	2.05 ± 0.13	0.155	
20	57.5 ± 3.5	28.3 ± 3.0	1.70 ± 0.07	1.72 ± 0.17	0.155	
21	61.5 ± 4.5	29.5 ± 4.0	1.51 ± 0.05	2.49 ± 0.07	0.140	
22	63.5 ± 4.0	31.5 ± 3.5	1.71 ± 0.10	1.40 ± 0.11	0.165	all the surface
23	67.0 ± 7.5	29.5 ± 4.5	1.50 ± 0.04	1.75 ± 0.08	0.160	all the surface
24	67.0 ± 5.0	30.5 ± 5.0	1.59 ± 0.02	2.69 ± 0.24	0.115	
25	69.5 ± 7.5	30.5 ± 3.5	1.36 ± 0.04	2.99 ± 0.15	0.110	
26	72.5 ± 7.5	28.5 ± 3.5	1.26 ± 0.04	2.81 ± 0.14	0.115	
27	72.5 ± 8.5	31.5 ± 3.5	1.31 ± 0.07	1.86 ± 0.09	0.140	all the surface

^aSubtracted the background level. ^bRange of variation. ^cMean ± standard error.

where $\alpha = q/V$ is a nonreaction term, i.e., infiltration rate in air change per hour (ach, h⁻¹), $\beta + \gamma S$ is the sink rate of NO₂ in ach (h⁻¹), β is a homogeneous process term (h⁻¹), γS is a heterogeneous process term (h⁻¹), and S is the interior surface area (m²). Hence

$$C_i = (C_p - \alpha C_o/k) \exp(-kt) + \alpha C_o/k \quad (3)$$

where C_p is the peak level of NO₂ (ppm), $k = \alpha + \beta + \gamma S$, and $\alpha C_o/k$ is the indoor background level of NO₂.

α can be obtained from the decay rate of CO. Then $\beta + \gamma S$ can be derived from the overall decay rate of NO₂ minus α or from the decay rate of the concentration ratio, i.e., (NO₂)/(CO).

Effect of Relative Humidity and Surface Property on the Sink Rate of NO₂. Decay process of NO₂ was followed with changing RH and interior surface property. Experimental results are shown in Table I. CO decay rate, i.e., the infiltration rate which was obtained from the CO decay curve using the linear least-squares method in semilog space, appeared to be independent of each experimental condition except that it was rather smaller at the highest RH (69.5–72.5%). Its mean value during this study was 1.61 ± 0.21 h⁻¹. This is a little higher than that found by NBS for a typical home in the U.S. (14). The sink rate of NO₂ was derived from the decay of the concentration ratio, (NO₂)/(CO), by using the same method as described above. Then they were plotted vs. RH in Figure 3 which includes only two surface conditions, i.e., covering the surface completely or not at all. Under low RH (43.5–50%), the sink rate showed some scatter, being regardless of surface property. Though carpet appeared to remove more NO₂ than other surfaces, it is obscure. In conclusion, below 50% RH the surface effect was as small as the experimental error; it could not be detected by this approach. The mean value obtained by using data from runs 1 to 11 was 0.99 ± 0.19 h⁻¹. However, above 50% RH, the sink rate increased in proportion to RH as shown in

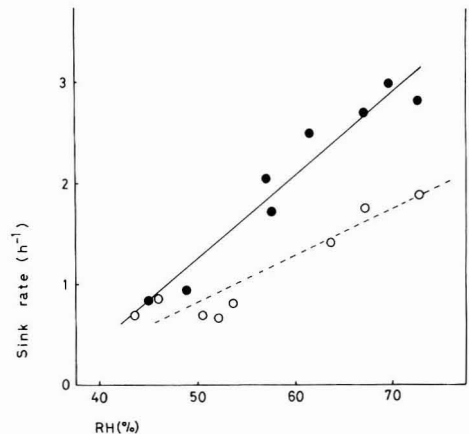


Figure 3. Sink rate of NO₂ vs. RH relationship. (●) Without covering the surface; (○) with covering all the surface.

Figure 3 in both conditions; there was an obvious difference of slope between these two conditions. Each regression equation was derived with the linear least-squares method, and this difference of slope was confirmed to be significant ($P_t < 0.01$) by statistical t test. On the assumption that $\gamma S = 0$ when the interior surface is covered completely with PE, the regression equations are given as eq 4 and 5. Thus γS was also found to be dependent on RH.

$$\beta + \gamma S = -(2.96 \pm 0.54) + (0.084 \pm 0.009)(RH) \quad (4)$$

$$\beta = -(1.49 \pm 0.40) + (0.046 \pm 0.007)(RH) \quad (5)$$

Although the sink rate of NO₂ must be also dependent on temperature, it was not considered in this study since the range of its variation was rather limited (±2% in K).

Table II. Sink Parameters of NO₂

RH, %	β , h ⁻¹	γS , h ⁻¹
50	0.81	0.43
55	1.04	0.62
60	1.27	0.81
65	1.50	1.00
70	1.73	1.19

Parameters for Simple Calculations of Indoor NO₂ Level. Tentative determination of β and γS for the room studied was undertaken with eq 4 and 5. Those results are summarized in Table II with each RH divided into five classes to be practically useful.

These parameters are usable to estimate the probable indoor NO₂ level for a similar room as follows. At a steady state, eq 1 and 2 give

$$dC_i/dt = -(\alpha + \beta + \gamma S)C_i + \alpha C_o + E/V = 0 \quad (6)$$

In a case without any indoor source

$$C_i = \alpha C_o / (\alpha + \beta + \gamma S) \quad (7)$$

Under ordinary condition with indoor source, $\alpha C_o \ll E/V$. Then

$$C_i = C_p = E / (\alpha + \beta + \gamma S) V \quad (8)$$

C_o may be obtained from the monitoring station concerned, and E is presented elsewhere (15, 16).

A γ , however, is not readily available since it varies depending on materials such as carpet, curtains, painted furnitures etc. If $\gamma = 0$, the α determined individually, and the β presented here are used to calculate C_p for a room, it would give the upper limit value of NO₂ level in that room.

For only a typical Japanese room of similar size, the probable maximum level can be estimated more precisely with α , β , and γ obtained in this study. For instance, from 10.7 NO₂ cm³/h as E for the current heater (unpublished datum), the C_p calculated with $\alpha = 1.61$ and eq 4 becomes 0.19 (45% RH), 0.14 (55% RH), and 0.11 ppm (65% RH), respectively, well corresponding to the observed.

Although from the eq 8 the peak level must have one to one matching with the overall decay rate, it was not always observed in Table I. It is probably due to a little variation of the emission rate and/or the thermal oxidation of NO emitted by the source and/or originating outdoors. Further investigation is necessary about this latter problem in order to improve the prediction accuracy.

Decay Process of NO. Variation patterns of the gases with a kerosene-fired convective unvented heater operated for 15 min are shown in Figure 4. Since it has a rather high emission rate of NO_x, NO₂ concentration reached the peak level only 10 min after turning on the heater, while NO concentration increased drastically to exceed 1.0 ppm by far.

Although a large amount of NO was consumed after turning off the heater, the sink rate of NO₂ was consistently unchangeable (1.34 ± 0.07 h⁻¹ at 50% RH) throughout one run, as the same order with a gas-fired heater. This indicates that the oxidation of NO to NO₂ does not appear to occur to a significant degree indoors as described earlier by Wade et al. (5).

Furthermore, in this case the overall decay rate of NO decreased gradually from 1.06 to 0.59 h⁻¹ according to its concentration; the outdoor level was so low that it could not cause such a retardation by getting indoors. Since it

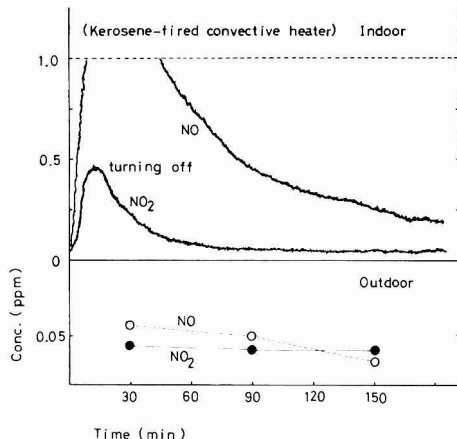


Figure 4. Variation patterns of NO₂ and NO concentrations. Outdoor level was monitored once an hour.

was smaller than the infiltration rate of this room, NO might be supplied freshly into the air by way of another process such as catalytic reduction, e.g., from NO₂ adsorbed on the "surface". However, this remains unclear.

Conclusions

The overall decay process of NO₂ was found to follow first-order kinetics in a typical Japanese living room. Since it is considered to comprise homogeneous and heterogeneous processes as well as air exchange, determination of these relative contributions was undertaken from NO₂ decay rate variation accompanying the change of relative humidity or the interior surface property. By use of this approach, the following have become evident: (1) Under low RH (43.5–50%), the surface effect could not be detected, and the sink rate of NO₂ was 0.99 ± 0.19 h⁻¹, (2) However, it increased in proportion to RH above 50% (~72.5%), depending on the surface property, too. (3) Surface effect itself appeared to be dependent on RH. The sink rate–RH relationship was derived with regression analysis, and the parameters essential for simple calculation of indoor NO₂ level were presented.

In the run where a kerosene-fired convective type unvented heater was used, a large amount of NO was emitted and consumed at a slower rate than the infiltration rate, while the sink rate of NO₂ remained unchanged. Two aspects are drawn from this fact. The one was that oxidation of NO to NO₂ is unlikely indoors; the other, on the contrary, was that NO appeared to be freshly supplied into the air through a catalytic reduction process from NO₂ adsorbed on the surface. However, the latter is not clear. Further investigation is necessary.

Acknowledgments

I express my appreciation to the members of Kyoto City Institute of Public Health and Environmental Protection Department of Kyoto Municipal Office for their aid in carrying out these experiments.

Registry No. NO, 10102-43-9; NO₂, 10102-44-0.

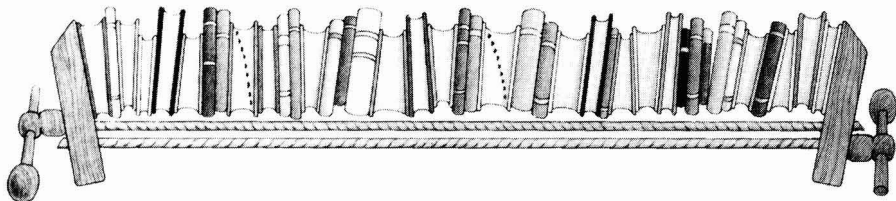
Literature Cited

- (1) Spengler, J. D.; Ferris, B. G., Jr.; Dockery, D. W.; Speizer, F. E. *Environ. Sci. Technol.* 1979, 13, 1276–1280.
- (2) Dockery, D. W.; Spengler, J. D.; Reed, M. P.; Ware, J. *Environ. Int.* 1981, 5, 101–107.
- (3) Thompson, C. R.; Hensel, E. G.; Kats, G. *J. Air Pollut. Control Assoc.* 1973, 23, 881–886.

- (4) Derham, R. L.; Peterson, G.; Sabersky, R. H.; Shair, F. H. *J. Air Pollut. Control Assoc.* 1974, 24, 158-161.
- (5) Wade, W. A., III; Cote, W. A.; Yocom, J. E. *J. Air Pollut. Control Assoc.* 1975, 25, 933-939.
- (6) Palmes, E. D.; Tomczyk, C.; DiMattio, J. *Atmos. Environ.* 1977, 11, 869-872.
- (7) Melia, R. J. W.; Florey, C. Du. V.; Darby, S. C.; Palmes, E. D.; Goldstein, B. D. *Atmos. Environ.* 1978, 12, 1379-1381.
- (8) Palmes, E. D.; Tomczyk, C.; March, A. W. *J. Air Pollut. Control Assoc.* 1979, 29, 392-393.
- (9) Yamanaka, S.; Hirose, H.; Takada, S. *Atmos. Environ.* 1979, 13, 407-412.
- (10) Yocom, J. E. *J. Air Pollut. Control Assoc.* 1982, 32, 500-520.
- (11) Mueller, F. X.; Loeb, L.; Mapes, W. H. *Environ. Sci. Technol.* 1973, 7, 342-346.
- (12) Sabersky, R. H.; Sinema, D. A.; Shair, F. H. *Environ. Sci. Technol.* 1973, 7, 347-353.
- (13) Shair, F. H.; Heitner, K. L. *Environ. Sci. Technol.* 1974, 8, 444-451.
- (14) Spengler, J. D.; Colome, S. D. *Technol. Rev.* 1982, 85, 32-44.
- (15) National Research Council "Indoor Pollutants"; National Academy Press: Washington, DC, 1981; pp 134-149.
- (16) Wadden, R. A.; Scheff, P. A. "Indoor Air Pollution"; Wiley-Interscience: New York, 1983; pp 52-78.

Received for review August 8, 1983. Accepted January 11, 1984.

WE'VE SQUEEZED DECADES OF RESEARCH INTO ONE CONVENIENT SUPPLEMENT.



Evaluated Kinetic Data for High Temperature Reactions, Volume 4: Homogeneous Gas Phase Reactions of Halogen- and Cyanide-Containing Species.

*D.L. Baulch, J. Duxbury, S.J. Grant, and D.C. Montague,
Department of Physical Chemistry, University of Leeds, U.K.*

For 10 years, *The Journal of Physical and Chemical Reference Data* has provided reliable, up-to-date data for scientists around the world.

And now, we're introducing a new supplement that brings together the results of years of research in 721 convenient pages.

Published jointly by the American Chemical Society and the American Institute of Physics for the National Bureau of Standards, this monograph presents kinetic data for 300 homogeneous gas phase reactions involving halogens, the cyanide radical, and their compounds.

Wherever possible, the data have

been critically evaluated to give the best estimates of reaction rate parameters and their associated error limits and temperature ranges.

The supplement also offers relevant thermodynamic data, discusses it thoroughly, and lists recommended rate constants for each reaction in tabular form. And a comprehensive bibliography provides an easy-to-follow roadmap to all pertinent literature in the field.

A valuable addition to any scientific library, this supplement is of critical importance in environmental, energy, and combustion research.

Fill out the form below and order your copy today.

American Chemical Society, Distribution Office
1155 Sixteenth St., N.W., Washington, D.C. 20036

Please send me _____ hardcover copies of *Evaluated Kinetic Data for High Temperature Reactions, Volume 4: Homogeneous Gas Phase Reactions of Halogen- and Cyanide-Containing Species* at \$80 each.*

Please send all three supplements listed below at the special package rate of \$123.25 hardcover, \$112.50 softcover (25% off the regular price of \$163 hardcover, \$150 softcover).

- First Supplement to Volume 2: *Physical and Thermodynamic Properties of Aliphatic Alcohols*, 420 pages (1973), R.C. Wilhoit and B.J. Zwolinski. (Data for 722 alcohols in the carbon range C₁ to C₅₀.)
- First Supplement to Volume 3: *Thermal Conductivity of the Elements—A Comprehensive Review*, 796 pages (1974), C.Y. Ho, R.W. Powell, P.E. Liley. (Recommended or estimated values for all 105 elements, information on 5,200 sets of raw data.)

- First Supplement to Volume 6: *Energetics of Gaseous Ions*, 783 pages (1977), H.M. Rosenstock, K. Draxl, B.W. Steiner, J.T. Herron. (Critically evaluated data information on ionization potentials, appearance potentials, electron affinities, and heats of formation of gaseous positive and negative ions.)

I enclose a check or money order for \$ _____, payable to American Chemical Society.

Please charge my Mastercard VISA.

Account # _____

Expiration date _____ Mastercard Interbank # _____

Signature _____

Name _____ Title _____

Employer _____

Address _____

City _____ State _____ Zip _____

* Foreign orders please add \$4.00 for each volume ordered for postage and handling. Effective January 1985, Supplement prices outside the U.S. and Canada will be increased by approximately 20%. California residents add 6% state use tax.

Please allow 4 to 6 weeks for delivery.

DuPont Environmental Services announces five new techniques to dispose of virtually all your wastewater and contaminated equipment

DuPont announces new and broader capabilities to safely and permanently dispose of your liquid industrial wastes and contaminated equipment. Using state-of-the-art techniques, DuPont Environmental Services offers new ways to treat wastewater and a unique method of equipment decontamination. Here's what Environmental Services is prepared to do for you:

- 1 Handling toxic contaminants—**DuPont can now treat wastewater with up to 2000 ppm of sulfides and 100 ppm of free cyanides. DuPont can also treat your heavy-metal sludges, wastewater from oil-bearing streams and selected waste pickle liquors.
- 2 Disposal of lagoon and Superfund wastes—**Through pre-treatment, DuPont can now handle liquids from most lagoon and Superfund sites.
- 3 On-off site treatment reduces bulk—**DuPont can reduce waste stream volume by membrane concentration, minimizing shipping costs to DuPont's disposal facilities.
- 4 Biosludge disposal—**DuPont can safely dispose of biological sludges generated by your treatment facilities.

- 5 Equipment decontamination—**Heating metal up to 750°C is a complete and sure way to decontaminate large pieces of equipment exposed to lead alkylates, carcinogens and other toxic materials. Thermal decontamination is more environmentally acceptable than landfill. It also bypasses burdensome legal problems: the decontaminated equipment is sold for scrap and recycled.

DuPont treatment and disposal facilities are located at Chambers Works, Deepwater, N.J., site of the world's largest "PACT" System (powdered activated carbon treatment).

Let DuPont ease your concerns about waste disposal. Contact DuPont Environmental Services by calling 800-341-4004 toll free. Or write for a detailed brochure to DuPont Company, Room G-40535, Wilmington, DE 19898.

 **DU PONT
ENVIRONMENTAL
SERVICES**



CIRCLE 1 ON READER SERVICE CARD